r&t report

GODDARD SPACE FLIGHT CENTER

Research and Technology

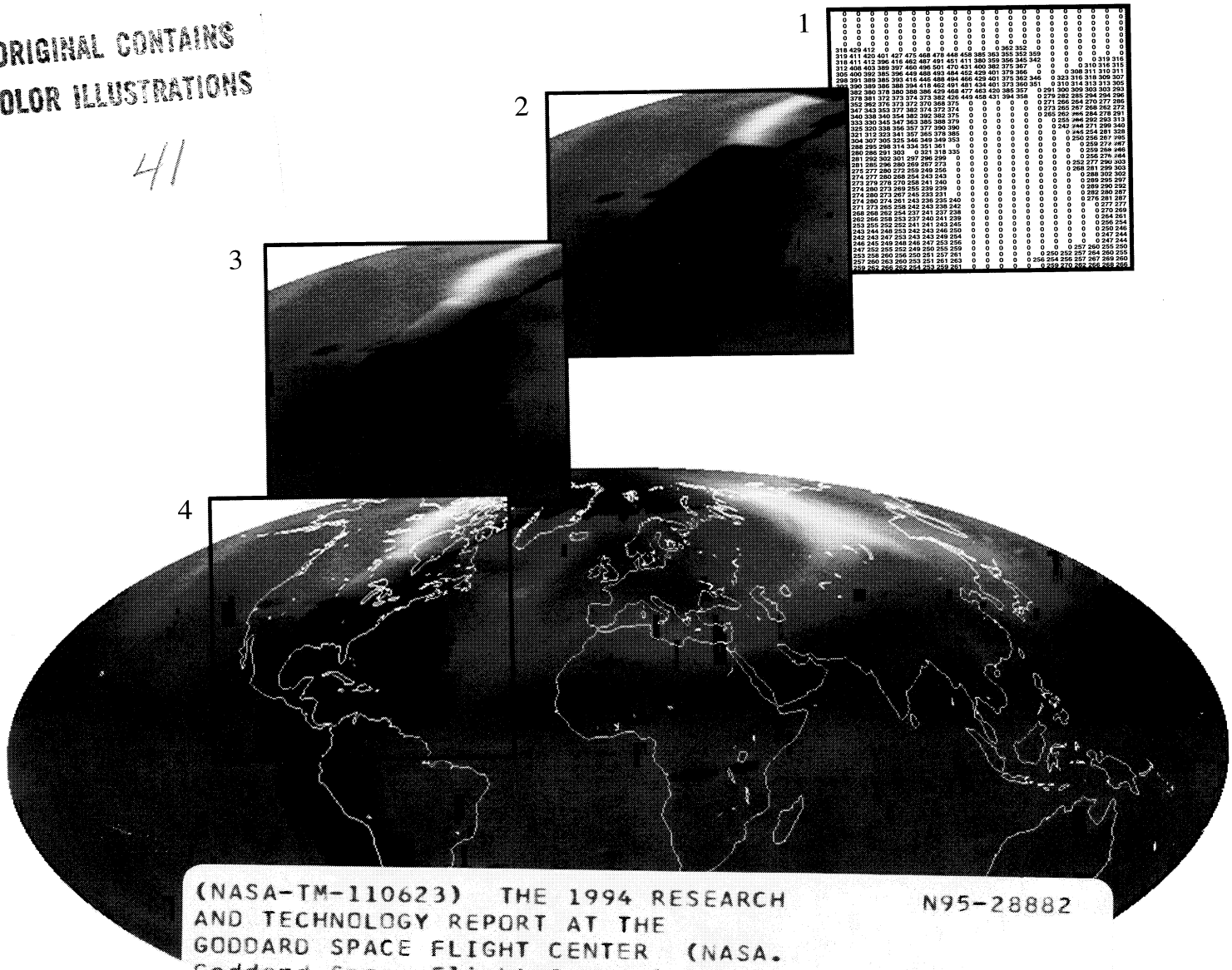

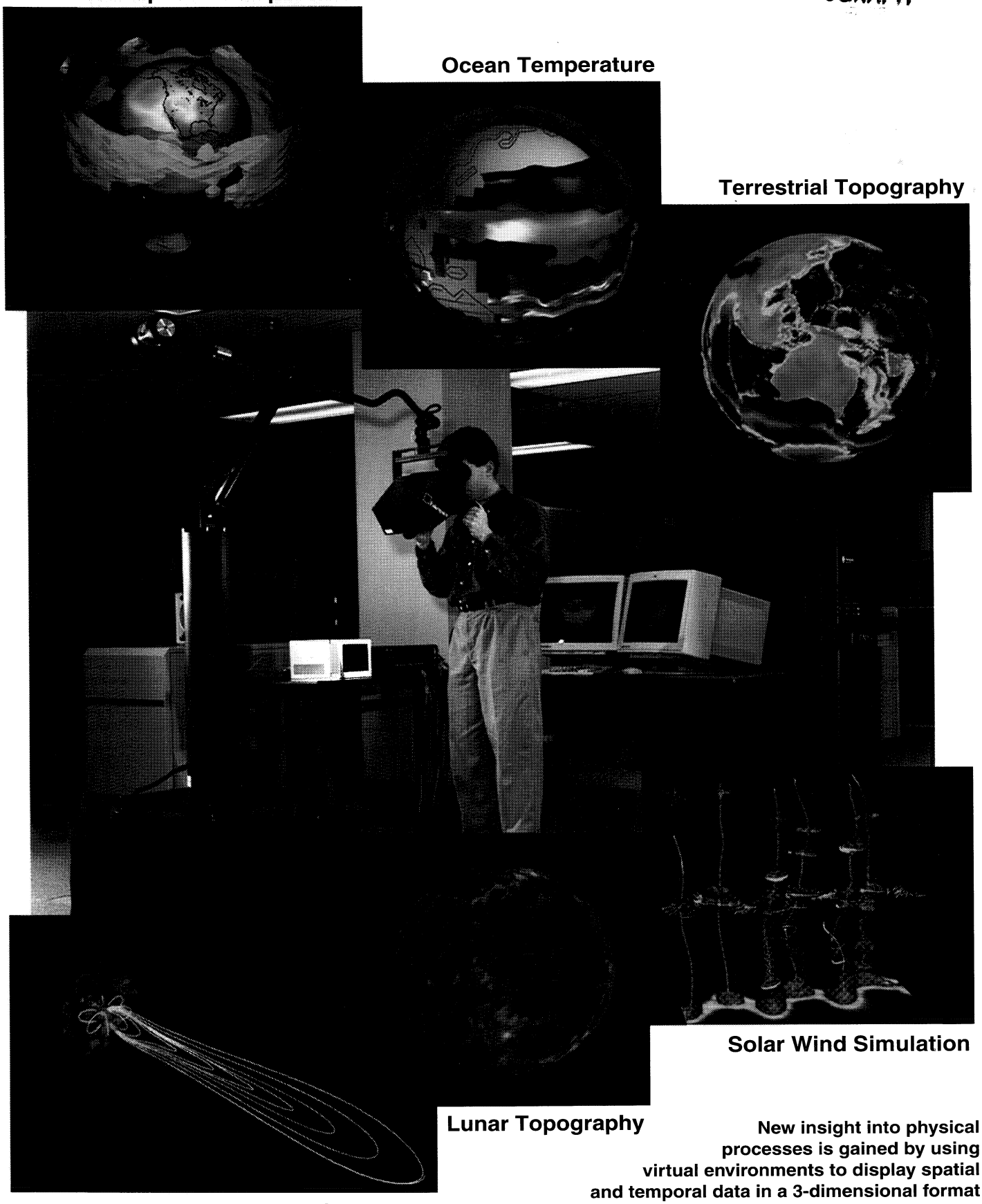

New insight into physical processes is gained by using virtual environments to display spatial and temporal data in a 3-dimensional format that the Investigator can manipulate.

RESEARCH AND TECHNOLOGY

R&T REPORT

Goddard Space Flight Center

FOREWORD

The breadth of subject material in this 1994 edition of the Research and Technology Report illustrates the broad scope of activities at the Goddard Space Flight Center. The numerous entries dealing with data processing and data visualization in the first section of this Report and the illustration of the stages of development of an information system on the front cover show our strong emphasis on data and its interpretation.

The past decade has seen brilliant successes in instrument and spacecraft hardware development, with data of central importance in the chain of events that lead to mission success. Now, as we focus more on understanding the data as an operational part of the mission, we must build the capability for data interpretation into the initial design of the mission. We are learning to present the data in many formats, to be able to combine different data sets, and to network these data around the world.

Moving from megabytes to gigabytes to terabytes, we see not only a quantitative but now a qualitative change in our ability to understand processes in both space and Earth sciences. In article after article, we see the wealth of ideas emerging. In Moseley's article on DIRBE, we use the motion of the Earth to help observe the Zodiacal light through the interplanetary cloud. In Parkinsons's article, we observe terrestrial sea ice over an 8-year period that indicates no major "hemispheric-scale increase or decrease" during the period of 1979 to 1986. This is an example of the role of one particularly important data set in our understanding of the rate of global change.

Besides the requirements in the space sciences, we have accepted the challenge for calibrated data sets created by the special long-term nature of the Mission to Planet Earth. This is an important and difficult mission, one that is critical to NASA's future.

John M. Klineberg
Director, Goddard Space Flight Center

PREFACE

The 1994 Research and Technology Report deals with new ways of processing and dealing with data. The cover depicts data processing from the time it is returned from the spacecraft until it is reduced so that a scientist can use it. Level 0 is unprocessed instrument data with the same format and time order as put on the spacecraft. Level 1 (cover) is the returned formatted data with full space/time coordinates radiometrically corrected. Level 2 is the data with retrieved environmental variables at the same location as the original source converted to geophysical parameters (in this case, total ozone concentration). In Level 3 averaging and compositing data from lower levels is performed. Level 4 model output and/or variables are added (e.g., missing data).

Controversy is the handmaiden of discovery; few scientists can thrive in an atmosphere free of discourse and opinion. Every new idea is ahead of its time. Recognition comes only after a healthy exchange of give and take. In selecting the frontispiece picture depicting "virtual reality," we anticipated that it would precipitate pro and con. Some see this as a toy, more for play than serious investigation. Some see this as a useful method of instruction for demonstration and instruction. Others believe this will lead to a new technology which will lead to discovery, to see new relationships not intuitively obvious from looking at static images.

Research within NASA has always endeavored to push beyond the comfort zone. Our thrust toward the stars, our exploratory missions, and our search for understanding have attracted the finest minds to this Agency. The computer power that we have now enables use to enter a new dimension. Machine memory and speed of computation allow us to overcome the impatient moments of "waiting for the results." We can now "see" in other regions of the electromagnetic spectrum and in space/time coordinates almost as fast as we can think.

We are at the beginning of this technology of virtual imagery; but, like other ideas of our time (lasers, CD-ROMS, microprocessors), we are starting to experiment with its benefits. Years to follow will determine the utility of these new tools; skeptics should watch, wait, and keep a wary eye.

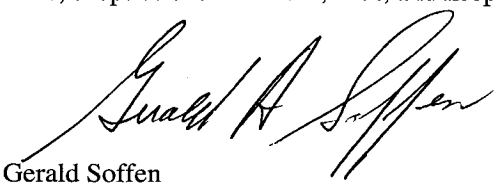

Gerald Soffen
Executive Editor

*FEDIX provides free access to its holdings. Follow the prompts to establish access to the system. To get to the GSFC material, at the first FEDIX menu, choose item (1) Comprehensive Agency Information. At the succeeding menus, choose item (3) NASA, item (5) Space Centers, then item (2) GSFC, respectively. The GSFC menu will present menu items that correspond to the major sections of the R&T Report.

CONTENTS

DATA PROCESSING AND VISUALIZATION

SPACE SCIENCES

High-Energy Astronomy

CONTENTS

Solar System

CONTENTS

New Techniques

EARTH SYSTEM SCIENCE

Atmospheres

Oceans and Ice

CONTENTS

Solid Earth

Soils and Vegetation

NETWORKS, PLANNING, AND INFORMATION SYSTEMS

Mission Scheduling and Operations

CONTENTS

Spacecraft Operation and Status

Software Engineering

CONTENTS

CONTENTS

Thermal Control

New Mechanisms

Testing and Evaluation

FLIGHT PROJECTS

CONTENTS

DATA PROCESSING AND VISUALIZATION

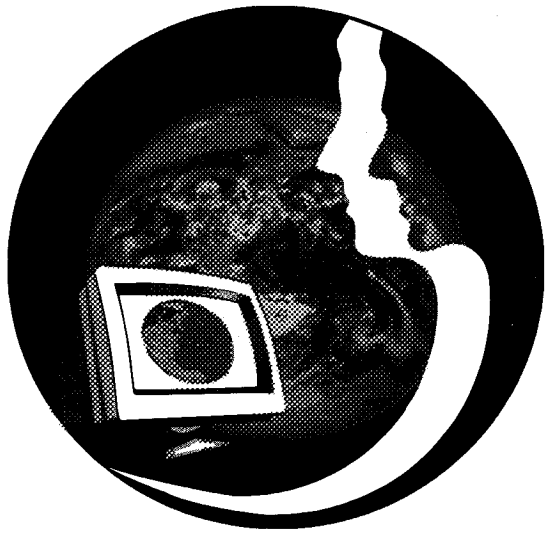

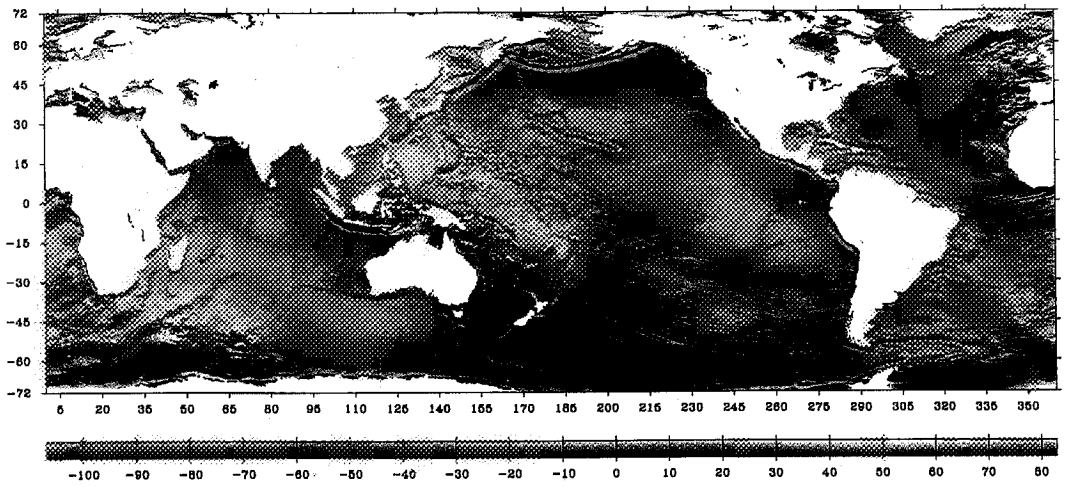

Top: Public access to Goddard Space Flight Center's scientific datasets is facilitated through the use of standard data formats, distribution media tailored to each mission, outreach to the user communities, and on-line information systems connected to the Internet.
Bottom: Mean sea-surface height (in meters) computed from 2.6 gigabytes of altimeter data from the TOPEX, Geosat, and ERS-1 satellites. The height is represented both by color and by elevation, which is shown in the shadows cast by the elevation irregularities. This combination of visualization techniques displays small-scale features much better than either technique would individually. (Image courtesy of M. Kim, University of Texas.)

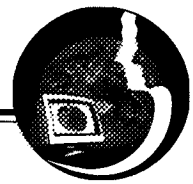

DATA PROCESSING AND VISUALIZATION

THE PAST FEW YEARS have witnessed a remarkable development spanning all disciplines of NASA Earth and space sciences, namely, direct visual representations of large volumes of satellite-acquired observational data and/or experimental data. This has been made possible because of advances in computation, mass storage, and communication technologies that are enabling the processing, rendering, and delivery of data volumes previously considered beyond one's practical computational capacity. Less than a decade ago, all GSFC data systems and archives produced data for distribution on magnetic tape or hard paper copy. Today, fully rendered scientific satellite data are electronically accessible over the Internet in seconds! This completely changes the way in which we deal with data and their delivery in support of our scientific community. The ready access to visually represented complex scientific data constitutes nothing less than an information revolution unparalleled in its implications for understanding ourselves and the environment in which we live.

This year's Research and Technology Report is devoted to the ways in which data and visualization of data are revolutionizing the space sciences, Earth sciences, mission operations, spacecraft planning, engineering, and current and future flight project programs. Illustrative of the revolutionary impact of national digital access to visual data are the articles on the worldwide campaign to observe the Comet Shoemaker-Levy's plunge into Jupiter, Solar physics data on the information superhighway, visualization of ISTP data, the final IUE archive, 3D simulation of the magnetosphere, visualization of the lunar surface, a virtual environment for Earth and space science data, the length of the sea-ice season in the Southern Ocean, numerical simulation of El Niño, TOVS pathfinder data set, potential impacts of climate change on world food supply, baseline measurements across the Pacific, and intelligent, agent-oriented approaches to autonomous mission operations.

Until very recently, a researcher's ability to find needed data depended largely on personal knowledge of the data holdings at an extensive number of often remote (and, at times, inaccessible) locations. Even if the data were known to be available, it often took weeks or months to acquire those data for local use, as the individual who owned the data had to make arrangements to copy it to tape for subsequent delivery by standard postal routes. One of the key technologies which has hastened the explosive growth of on-line information and archival data systems has been the rapid increase in the use of wide area computer-to-computer communications networks. These networks are providing transparent pathways to the computer systems all around the world, and especially at GSFC. With the use of on-line information and archival data systems, coupled with advances in computer network access tools, knowledge of and access to the contents of massive data archives are often only a few key strokes away. For example, scientists connected to the Internet have access to GSFC space and Earth science data bases, mission planning systems, information systems, scientific and technical library systems, and computational facilities for the purposes of facilitating correlative space data exchange, data analysis, and space research. As discussed in many of the articles in this year's R&T Report, GSFC has an extensive array of information, archival data, and computational systems that are being accessed by scientists at a phenomenal rate.

The use of the new computer-to-computer wide area networks, supporting such new approaches to data access as the World-Wide Web (WWW), is providing a new dimension for quick access to key GSFC data in the Earth and space science community. The WWW provides our developers at GSFC with the ability to combine images and data with text in a composed page or screen. The combination of text and images is called hypertext. The hypertext foundation of WWW allows researchers to access data holdings literally around the globe, with no foreknowledge of the location of those data, as the hypertext links connect these composed screens (homepages) with a mere click of a mouse button. The popularity of the WWW is demonstrated by recent data which show that WWW traffic is the fifth largest source of packets on the Internet. The utility of this approach is discussed in this year's Report in Gurman's article on the impact of the information highway on Solar physics data.

The sheer amount of data becoming available is, at least in part, due to the volume of data being acquired by increasingly complex sensors, supporting missions that now span several decades. The numbers are staggering: Telemetry rates for typical GSFC missions of the very early 1970s ranged in the few kilobits per second range; by the middle 1980s, this had increased to over 50 kilobits per second. And today, NASA is planning missions which will transmit to the ground over 1 megabit per second before the end of the decade. Even data that have already been acquired and processed are expanding, as older spacecraft data are getting a new lease on life by reprocessing. For example, as described in the article by Michalitsianos, reprocessing the IUE archive will increase the size of the archive from 90 gigabytes to well over 800 gigabytes, giving scientists all over the world a new and more detailed look at some of the older data sets. Clearly, we are in the midst of a space data explosion! Fortunately, technology advances in storage media and computer robotic mass storage systems are catching up with our ability to acquire or produce data. For the first time, scientists can search and manipulate terabytes of data in hours, instead of months to years. At the NCCS, a threshold was passed this past year, when the storage system was expanded to 30 terabytes exceeding by a factor of two all the existing data at GSFC. This is bringing about a new paradigm in computing where computer cycles are not the driving requirement, but rather data access.

Accompanying the storage and processing of data has been the development of intelligent data management systems with friendly user interfaces, visualization software, and on-line agents for discovering and retrieving information. NSSDC is providing rapid access to large amounts of data through implementation of a jukebox of 12-inch optical disks, each of which holds six or more gigabytes of data, as described by Behnke. It is important to note that currently only a fraction of the information of space and Earth science data that exist are truly accessible over these computer networks. But the rapid access to even the limited amount of data that are on-line is supporting an extensive amount of science research world-wide. New information and data systems are currently being developed that will allow users to access data from programs such as NASA's Earth Observing System (EOS) before this decade is over.

This stunning increase in data volume, storage capacity, and network connectivity and throughput is supporting an even more stunning change in the way data are being manipulated. The availability of high-power, individual workstations, often with multiple CPUs and gigabytes of memory, and improved coding techniques are giving researchers new ways of examining their data. The field of data visualization now allows scientists to interact with their data in ways that were not heretofore possible. The acquisition by the NCCS of a virtual reality boom allows a scientist to step into a three-dimensional dataset and look at—and manipulate—the numerous interactions between data from perspectives that could not even be dreamed of just a few short years ago. Given the complexities of, for example, the interactions between many of the Earth's subsystems, the ability to view these data from within will allow scientists to obtain new and, perhaps, revolutionary insight into the ways in which these subsystems interact to generate the geophysical and biogeochemical phenomena that give rise to and support the biosphere, as described by Mitchell. The possibilities are virtually endless, and will allow scientists world-wide to examine phenomena over temporal and spatial scales ranging from the molecular to the cosmological, with results that should surprise, delight, and, perhaps, shock us as we endeavor to understand ourselves, our planet, and the universe of which we are a part.

GSFC personnel are on the forefront in the conceptualization, development, and utilization of these new communications, computer, and visualization technologies in an integrated fashion, enabling rapid access to NASA's treasure house of scientific data and numerical simulations. These new technologies are revolutionizing the way we have traditionally managed, stored, manipulated, and archived NASA's most valuable space and Earth science data. A new information science discipline is emerging at GSFC. By providing rapid access to GSFC archives and supercomputers, and providing scientists the tools to better visualize their data, we are building a new alliance with our scientific communities. As demonstrated by this year's R&T Report, it is indeed an exciting time.

We are just beginning to see the information system revolution. It is hard to imagine what the future holds!

Milton Halem
James L. Green

SOLAR PHYSICS DATA IN THE CRASH LANE: THE SOLAR DATA ANALYSIS CENTER IN THE AGE OF THE INFORMATION SUPERHIGHWAY

EVEN IF THE NATIONAL Information Initiative (NII) had not been put forward, 1994 would still likely have come to be known as the "year of the Internet" (although we might have been spared some of the hype about the "Information Superhighway"), simply because this year saw the explosive growth of World-Wide Web (WWW) resources on the Net, and especially of the widespread use of the Mosaic WWW client. Given the appropriate (freeware or shareware) "viewer" applications, Mosaic can display color images, show movies, play sounds, and generally make the Web a reality on the desk of any user of a Macintosh, PC, UNIX, or OpenVMS workstation.

Astronomers have embraced the Web, and Mosaic in particular, with an enthusiasm bordering on the manic. In early September 1994, a Web-served listing of astronomical services on the Web numbered over 600 sources around the world. In the summer of 1994, Web servers at the Jet Propulsion Laboratory (JPL), the Space Telescope Science Institute (STScI), and Goddard Space Flight Center (GSFC) received thousands of requests per hour for imagery of Comet Shoemaker-Levy 9's impacts on Jupiter—and a PBS show about the impacts used a split screen to show the features available on the various Mosaic "home pages" around the world dealing with the comet. No earlier medium has made the imagery obtained by NASA spacecraft available to so many people, on demand, at high fidelity.

Astronomers, however, use the Web not only to impart to the general public and the serious amateur the beauty of what they do, but also to share information with each other over this novel medium. The Solar Data Analysis Center (SDAC) Web services at GSFC are good examples of the versatility and usefulness of the Web to astronomers and solar-terrestrial physicists (see the figure). At this writing, the SDAC top-level Web listing (home page) offers access to:

- Current solar imagery from space- and ground-based solar observatories, including both data archives at the SDAC and resources at NOAA's Space Environment Laboratory and the National Solar Observatory.

- The U.S. public data archive (consisting of all data more than 1-year old) for the joint Japanese-U.S.-U.K. *Yohkoh* solar mission.

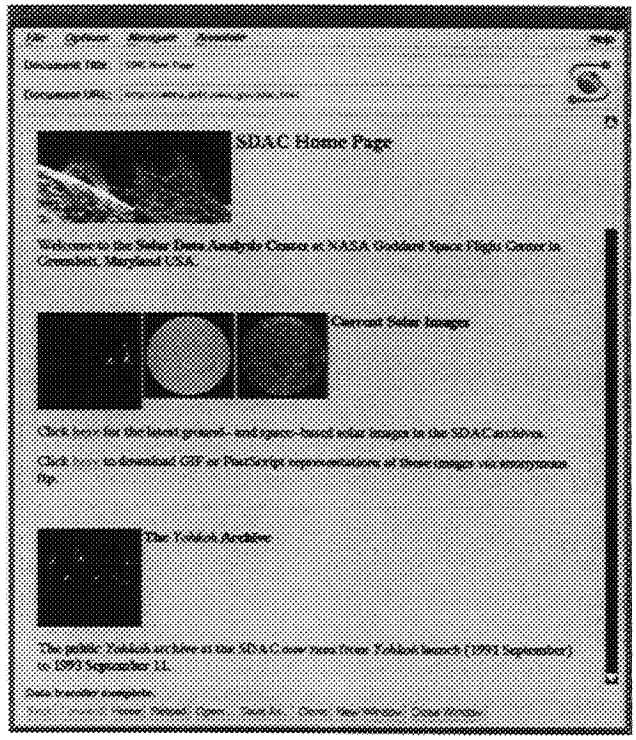

The Solar Data Analysis Center Web listing provides the public with easy access to solar data.

- NASA Eclipse Bulletins (prepared by Dr. Fred Espenak of the Laboratory for Extraterrestrial Physics and Jay Anderson of the Canadian Prairie Weather Center) and solar eclipse predictions.

- Science operations planning, scientific workshop, and public information resources for the ESA-NASA Solar and Heliospheric Observatory (SOHO) mission, including on-line access to scientific simulation plans and the prototype SOHO observing databases.

- Access to an on-line solar ultraviolet spectral atlas derived from the Naval Research Laboratory (NRL) High Resolution Telescope and Spectrograph (HRTS) rocket/Spacelab-2 payload (and served from Norway).

- Access to the *Compton Gamma Ray Observatory* (CGRO) Burst and Transient Source Experiment (BATSE) on-line catalog of solar flares at the SDAC,

including the option to plot light curves for any of the over 4,000 flares in the catalog.

- Information about the reflight of the SPARTAN 201 payload, including the White Light Coronagraph operated by GSFC.

- Access to miscellaneous resources available via anonymous file transfer protocol (ftp), from SOHO project documents to QuickTime movies of the rotation of the solar corona in soft x-rays.

As technically useful and aesthetically pleasing as these services are, these resources would be worth relatively little were it not for the most powerful feature of the World-Wide Web: the link. Information of related types can be listed as "hot links" on a Mosaic page, and a single click of a mouse button will take the user to the new page—regardless of whether the page is offered by the same server as the last page or by a machine half a world away. The SDAC Web services are cross listed, for example, in the GSFC home page, the Compton Observatory Science Support Center pages, the Space Physics Data System home page, solar physics and astronomy servers at the National Geophysics Data Center (NGDC), the NOAA Space Environment Laboratory, ESA, the University of Rennes (France), the STScI, and dozens—perhaps hundreds—of others around the world.

The Web is thus blind to geography; it knows only the limitations of bandwidth, and a server in Europe with a high-speed connection is always "closer" than one next door with a low-speed line. Astronomers already use the Web to make preprints of scientific articles available to the community; to publish job listings; to make available on-line an abstract search service; to make the latest "hot" images and spectra from space available to each other and to the general public. NASA uses the Web to let the public know the Shuttle launch schedule, the types and purposes of its payloads, and how to reach a variety of educational resources within the Agency. The SOHO mission will use the Web to make its latest synoptic observations available to the world scientific community—indeed, to the entire world of the Internet—within 24 hours of the acquisition of the data. As currently envisaged, the entire public SOHO archive itself will be accessible via database queries entered through Mosaic forms.

A brief glance at the variety of NASA information resources available on-line through the WWW (starting, say, at the NASA home page) shows how widespread use of the Web already is within the Agency to communicate technical as well as public affairs information. Nearly all NASA services are less than 1 year old, so it is not hyperbole to observe that the availability of NASA information resources to the technically capable public—and that now includes high school students and their teachers—has undergone a revolution in 1994. It is clear that, with the advent of the WWW, and NASA's enthusiastic adoption of it, the Agency is fulfilling its mission (as defined by the National Aeronautics and Space Act of 1958) to "provide for the widest practicable and appropriate dissemination of information concerning its activities and the results thereof" in ways the authors of the Act could only have imagined.

Contact: Joe Gurman (Code 682)
301-286-4767
gurman@uvsp.gsfc.nasa.gov

Sponsor: Office of Space Science

Dr. Joe Gurman is facility scientist for the Solar Data Analysis Center. He holds a PhD in Astrophysics from the University of Colorado, and has been at GSFC for 15 years, the last 9 of those as a civil servant in the Solar Physics Branch, where he is currently working as a coinvestigator on the Extreme Ultraviolet Imaging Telescope on the Solar and Heliospheric Observatory.

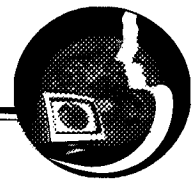

VISUALIZATION OF INTERNATIONAL SOLAR-TERRESTRIAL PHYSICS DATA

THE INTERNATIONAL Solar-Terrestrial Physics (ISTP) Program is a multispacecraft, multinational program whose objective is to promote further understanding of the Earth's complex plasma environment. Extensive data sharing and data analysis will be needed to ensure the success of the overall ISTP program. For this reason, there has been a special emphasis on data standards throughout ISTP. Each of the missions will contribute data in a common format. These data are key physical parameters, and their interrelationships will be important for the definition of major scientific studies in magnetospheric and solar-terrestrial physics. The most efficient and scientifically revealing way to combine these datasets is through visual means. In this article we will briefly describe the ISTP missions, the common format and guidelines for usage, and the numerous tools which have been developed with the ultimate goal of visualizing ISTP data and attaining meaningful scientific objectives.

The first ISTP spacecraft, the Japanese-U.S. (ISAS-NASA) Geotail spacecraft, is now in orbit. Wind, a NASA spacecraft, was lanunched on November 1, 1994. Another NASA spacecraft, Polar, is slated for launch in 1995. Several existing equatorial missions are being tapped to supplement these observations, including the GOES (NOAA) and LANL (DOE) spacecraft, and the larger-orbit IMP-8 spacecraft. Ground-based data from DARN, SESAME, CANOPUS, and Sondestromfjord, and theoretical studies and modeling complement the spacecraft data. In addition, NASA is collaborating with the European Space Agency (ESA) in two additional missions: SOHO and Cluster, with launches planned for 1995. The Russian Space Research Institute (IKI) is participating through the Inter-Agency Consultative Group, with the Interball mission.

One of the key tools will be the Common Data Format (CDF), which is a means of storing data and descriptions of the data in a standard, readily accessible format. CDF has a high-level programming and toolkit library, which provides functionality without excessive programming. Both the library and the datasets are transportable across a wide variety of platforms (VAX, Sun, SGI, IBM, HP, PC, and soon Macintosh). CDF was developed by, and is maintained at, the National Space Science Data Center (NSSDC).

A set of implementation guidelines was specially developed for space physics data by the Space Physics Data Facility, which is associated with the NSSDC. These ISTP guidelines were designed on top of, but separate from, CDF (i.e., they provide detailed information on how to structure data in CDF and what descriptions of the dataset are to be included). Sufficient descriptions are included so that standard labels, time tags, dependencies, uncertainties, and offsets can be explicitly defined for later searching, plotting, merging, and subsetting. The goal was to make the resulting dataset a useful and understandable data product, available for convenient research use with a standardized and automated set of retrieval and analysis software.

To compare and correlate ISTP CDF datasets efficiently, a number of smart tools have been developed. The tools are termed smart because they take advantage of the information contained within the CDF datasets themselves, with no programming or knowledge of the data format required of the end user. Smart tools isolate the scientific community from specific format issues so that users can concentrate on their scientific objectives. Computer software applications that are designed based on generic CDF datasets require user input to add much of the functionality available with the use of the smart tools.

Both generic and smart tools now exist or will be designed and implemented in the future for use with CDF; these are shown in the figure. This figure is divided into three sections: creation, visualization, and manipulation, with CDF at the center, and each succeeding layer building on those underneath. The CDF C and Fortran programming interface spans all three sections, and forms the basis of all of the applications. The ISTP guidelines, in the layer next to the C and Fortran programming interface in the figure, are used in several applications. The outer layer contains the recently developed applications, each of which is described briefly below.

CREATION. CDF datasets can be created using only the C or Fortran programming interface, although the process is simplified by using "skeleton tables"—specially formatted ASCII text files that contain the descriptions of the data. The CDF toolkit makes use of skeleton tables in the creation of CDFs. The creation process is made even easier through a smart tool called MakeCDF, which is also based on the ISTPguidelines. With a dataset in hand, a user describes the input format through a user interface, and the tool then creates the CDF dataset. No program-

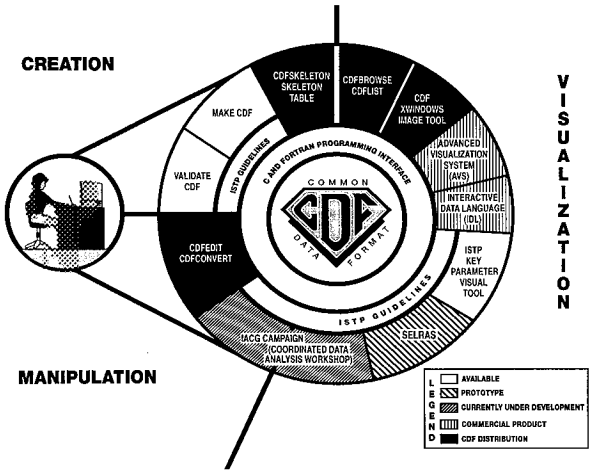

Associated tools and programs for creation, visualization, and manipulation of data in the common data format (CDF).

ming is required. Another tool built on top of CDF and the ISTP Guidelines is a package which validates whether or not a particular CDF meets the ISTP Guidelines (i.e., whether or not all of the required descriptions are included). This tool is included in the creation section because use of this tool must precede establishment of a multispacecraft, multinational database.

VISUALIZATION. The CDF toolkit includes tools to list and browse the data values and descriptions, and a CDF X-windows Image Tool for viewing image data. Other packages based on CDF include the Advanced Visualization System (AVS), a commercial package for plotting multidimensional data, and the industry-standard Interactive Data Language (IDL), which has a built-in CDF interface and access to the programming library. Three applications exist or are currently under development which use both CDF and the ISTP Guidelines: the ISTP Key Parameter Visualization Tool (KPVT), the Space Environment Laboratory System for Retrieval and Analysis of Scientific Data (SELRAS), and an application tool planned for the upcoming IACG Campaigns, which may be modelled somewhat after the Coordinated Data Analysis Workshops sponsored by NASA. The ISTP KPVT was developed at the ISTP Science Planning and Operations Facility (SPOF) for plotting approximately 1-minute-resolution survey (key parameter) data from the ISTP program; it is described in more detail in the article *ISTP Science Products and Tools,* also in this volume. SELRAS is a prototype system developed by NOAA to access solar-terrestrial geophysical data. Using this existing tool, a user can create time series plots and listings of selected GOES and NOAA satellite data. The ISTP KPVT and SELRAS tools were developed independently by different agencies. Expertise gained in the creation of these tools was incorporated into the design of the IACG Campaign tool, which is based on a dynamic working list. Variables can be added, deleted, listed, or plotted from any of the datasets included in the IACG campaign database.

MANIPULATION. The CDF toolkit includes tools to edit and convert CDFs. The IACG Campaign tool is designed to include facility to create and/or modify variables in a user's working environment. These variables are added to the working list, and can be listed or plotted.

The authors would like to thank the many people who contributed to this work including R. E. McGuire, W. H. Mish, G. Goucher, R. Burley, R. Candey, and S-Y. Hsieh, with thanks also to R. Kilgore for the artwork.

Contact: Ramona Kessel (Code 632)
301-286-6595

Richard Burley (Code 632)
301-286-2864

Sponsor: Office of Space Science

Dr. Ramona Kessel is an astrophysicist at the SPDF of GSFC. She earned both an MS and a PhD in Physics from the University of Kansas and has been at GSFC for 3 years. Dr. Kessel serves as the acquisition scientist for ISTP and developed the Implementation Guidelines for ISTP usage of the CDF. She assists ISTP scientists and programmers with CDF implementation, represents NSSDC and particularly the CDF effort to ISTP investigators in various countries, and takes part in the Inter-Agency Consultative Group Science Campaigns. Dr. Kessel is presently involved in several research studies.

Mr. Richard Burley is a systems engineer at the SPDF of GSFC. He earned a BS in Computer Science from Bowling Green State University and has been at GSFC for 10 years. Mr. Burley's efforts at the SPDF have revolved around developing an improved toolkit for CDF including makeCDF, a flat data file to CDF file translator; makeSFDU, a CDF to SFDU translator; and generalized plotting and graphics software for CDF data files.

INTERNATIONAL SOLAR-TERRESTRIAL PHYSICS SCIENCE PRODUCTS AND TOOLS

THE ISTP PROGRAM is now providing simultaneous coordinated scientific measurements from most of the key areas of geospace. This is currently being done with spacecraft instrumentation that is in geosynchronous, circular, and deep magnetosphere tail orbits, along with instrumentation at high-latitude ground stations. These data will be augmented with data from spacecraft instrumentation on the to-be-launched NASA Wind and Polar spacecraft, the ESA SOHO and Cluster spacecraft, and the Russian Interball spacecraft. This combined database, available on-line over the NASA Science Internet and distributed on computer platform-independent (ISO 9660) CD-ROM, is being used to obtain a more complete understanding of how mass, momentum, and energy from the solar wind are transported across geospace boundaries, stored and energized in the magnetosphere, and subsequently dissipated into the Earth's atmosphere.

The instrumentation associated with the ISTP Program is capable of producing measurements on a variety of time scales. To effectively survey this large suite of measurements and identify important scientific events, all instrumentation must produce summary parameters called key parameters at approximately 1-minute time resolution for each operational day. Most of these are fields and particle time series, but SOHO, Polar, and the CANOPUS ground-based investigation will provide images of the Sun, auroral regions, and all-sky images, respectively, at a variety of wavelengths.

Starting in September 1992, and on an almost continuous basis, fields and particle key parameter time series have been computed from five geosynchronous satellites (GOES 6/7 and LANL 89/90/91), IMP-8 (in an approximately 35 Earth-radius (R_e), near-circular orbit), Geotail (in a deep magnetosphere tail orbit), and radar, magnetometer, radiometer, and other measurements from four ground-based investigations located in the northern and southern hemispheres at high latitudes. Thus, these key parameters simultaneously cover geospace from 35 R_e in front of the Earth to over 200 R_e behind. The ISTP Central Data Handling Facility (CDHF) located at GSFC is the place where these key parameters are either computed or ingested. For example, the ground-based key parameters are computed locally and are electronically transferred to the CDHF; the Geotail key parameters are computed from the Geotail telemetry in the CDHF. The key parameter CD-ROMs are made and distributed by GSFC's Information Processing Division (IPD) Data Distribution Facility (DDF).

The table presents the missions and instruments currently contributing key parameters. All of these key parameters are encapsulated in the ISTP CDF that has been developed by the NSSDC at GSFC. The CDF is described elsewhere in this volume, under "Visualization of ISTP Data."

Tools have been developed by the ISTP Science Planning and Operations Facility (SPOF) to display these key

Instrumentation, Both Space and Ground Based, Currently Providing Key Parameters for the ISTP Project. These Key Parameters Are Available Via Internet and on CD-ROM

Investigation	Instrument	Principal Investigator
Geotail Spacecraft	Plasma (CPI)	L. A. Frank
	Energetic Particles (EPIC)	D. J. Williams
	Magnetic Field (MGF)	S. Kokubun
	Electric Field (EFD)	K. Tsuruda
	Plasma Waves (PWI)	H. Matsumoto
	Energetic Particles (HEP)	T. Doke
	Plasma (LEP)	T. Mukai
LANL Geosync Spacecraft 89/90/91	Magnetospheric Plasma Analyzer (MPA)	D. J. McComas
	Synchronous Orbit Particle Analyzer (SOPA)	R. D. Belian
GOES GEOSYNC Spacecraft 6/7	Energetic Particle Sensor (EPS)	R. Zwickl
	Magnetic Field (MAG)	R. Zwickl
IMP-8 Spacecraft	Plasma Investigation (PLA)	A. Lazarus
	Magnetic Field (MAG)	R. Lepping
CANOPUS Ground-based Investigations	Bistatic Auroral Radar (BARS)/Allsky Imager (ASI)/Magnetometer and Riometer Array (MARIA)/Meridian Photometry Array (MPA)	G. Rostoker
Dual Auroral Radar Network (DARN and Super DARN) Ground-based Investigations	PACE/GOOSE BAY/SASKATOON	R. A. Greenwald
SONDRESTROM Ground-based Investigations	Radar	J. D. Kelly
Satellite Experiments Simultaneous with Antarctic Measurements (SESAME) Ground-based Investigations	Advanced Ionospheric Sounder (AIS)/ELF-VLF Logger/Fabry Perot Interferometer (FPI)/Magnetometer (MAG)/Riometer (RIO)	J. R. Dudeney

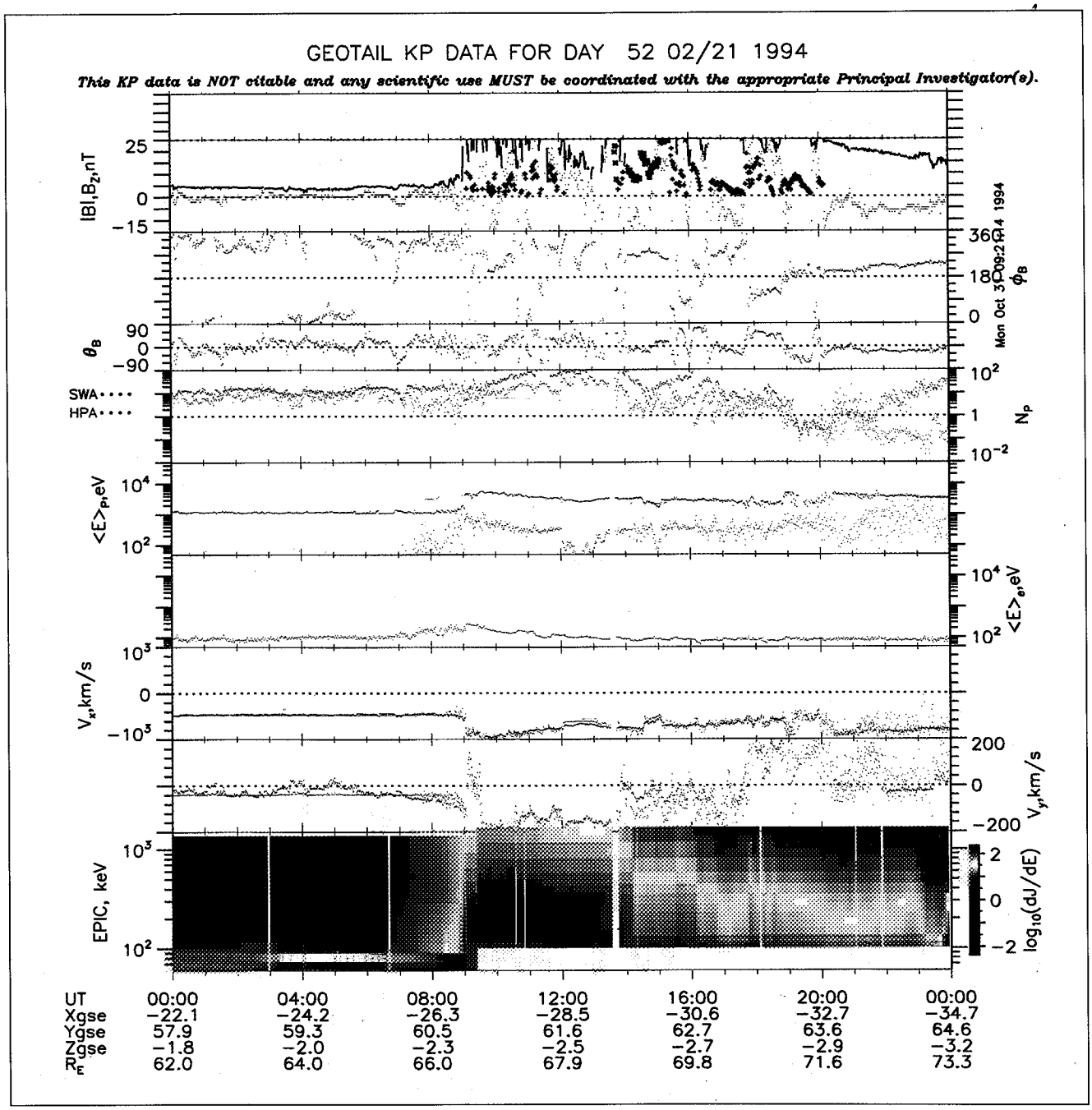

Key parameter data from instruments on the Geotail spacecraft showing the February 21, 1994, strong interplanetary shock that impacted the Earth, producing the kind of global changes to the geospace environment that ISTP was organized to explore.

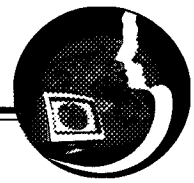

parameters. These tools read the ISTP key parameter CDF files and use the associated metadata for proper data display. In addition, the SPOF produces "custom" displays of key parameters from Geotail, IMP-8, geosynchronous satellites, and ground-based instrumentation. For important scientific periods, these plots are available over the WWW (http://lepmp.gsfc.nasa.gov/). An example of the available data is shown in the figure for an event on February 21, 1994.

The SPOF uses the Satellite Situation Software (described in the *1993 GSFC Research and Technology Report,* page 164) to generate information used in planning instrument operations for the Wind and Polar spacecraft, and for coordination of science operations with other missions. These coordination efforts involve science campaigns sponsored by ISTP and the Inter-Agency Consultative Group for Space Science (IAGC) initiatives. Coordination also takes place between the SPOF and the Solar-Terrestrial Energy Program (STEP) coordination office.

Contact: William Mish (Code 694)
301-286 5444
wmish@istp1.gsfc.nasa.gov

Sponsor: Office of Space Science

Mr. William Mish is ISTP Deputy Project Scientist for Data Systems and Head of the Information Analysis and Display Office of the Laboratory for Extraterrestrial Physics. He holds a BME from George Washington University.

A DATA PROCESSING SYSTEM FOR THE GGS/WIND PLASMA EXPERIMENT

THE SOLAR WIND Experiment (SWE) on the Wind spacecraft is an integrated set of instruments designed to investigate outstanding problems in solar wind physics. These instruments consist of two Faraday cups and electron and ion spectrometers. The electron-ion spectrometer is a set of electrostatic analyzers that measure solar wind particle velocity distributions in three dimensions over the energy/charge range 7 V to 24.8 kV. The strahl detector is a toroidal electrostatic analyzer configured to detect the electron beam often observed coming from the direction of the Sun and aligned with the magnetic field. Together, these two instruments measure the particle flux at 912 distinct points in phase space during a single 3- second rotation of the spacecraft, where each point in phase space corresponds to a particular particle energy and direction in space. Electrons and ions may be measured during alternate spacecraft rotations, or a single species may be measured for an indefinite period.

The most basic plasma measurements are those of the velocity distribution function of a given particle species (e.g., electrons or ions) and the distribution of particle velocities about the direction of the magnetic field. Data are collected at the rate of one particle velocity distribution every other rotation when the spacecraft is in the high-bit-rate telemetry mode. Given the velocity distribution of electrons, for example, the density, plasma flow speed, average thermal speed and anisotropy, and heat flux can all be deduced, and the stability of the distributions to electron-induced plasma wave emission can be assessed.

The general requirements for the electron-ion spectrometer and the "strahl" detector data processing system are as follows:

- Data over an extended time period (months to years) must be available by rapid, random access, and then graphically displayed for the purpose of surveying the data. The types of phenomena of interest in a survey include spacecraft crossings of magnetospheric boundaries (such as the Earth's magnetopause and bow shock, which have characteristic plasma signatures) and the occurrence of energetic particles streaming away from the bow shock, observable when the spacecraft is in the solar wind and magnetically connected to the bow shock.
- More detailed data, such as single 3-second measurements of particle velocity distributions selected from examination of the survey data, must be available by rapid, random access for graphical display alongside the survey data.
- Other correlative data, such as measurements from other experiments, must also be accessible for display in time-association with the plasma measurements.
- The data system must allow user-supplied analysis procedures to be easily and quickly implemented.

Although in the recent past, several passes through the data on a mainframe computer were necessary to meet these requirements, they can now be fully met by currently available workstations and associated software.

The SWE data processing system consists of a set of programs in a computer workstation managed by a single interactive graphical interface between the user (usually a scientist analyzing the data) and various applications which read, process, and display the data. The first figure is a block diagram of the current data system, which will be used for the SWE after its launch in November 1994. Input data are shown on the left and may be studied via the various outputs on the right. The input data to the system are the raw telemetry data, referred to as level zero (LZ) data; data products that have been derived from the LZ data for the purpose of surveying extended time intervals to gain an overview of the data; and other correlative data, such as magnetic field data and key parameters from other experiments onboard the spacecraft. These data may be displayed on the screen of the monitor, as hard copy, or written to a file for future reference.

The LZ data, normally supplied on CD-ROM, are assembled into the 912-point matrices characterizing a single velocity distribution function, as shown in the second figure. The plasma parameters such as density, plasma flow speed, etc., are computed from velocity space moment calculations using distributions such as that shown in the second figure. One such set of velocity moments (density, flow speed, thermal speed, and anisotropy) are plotted as a function of time in the upper panels of the third figure. Also

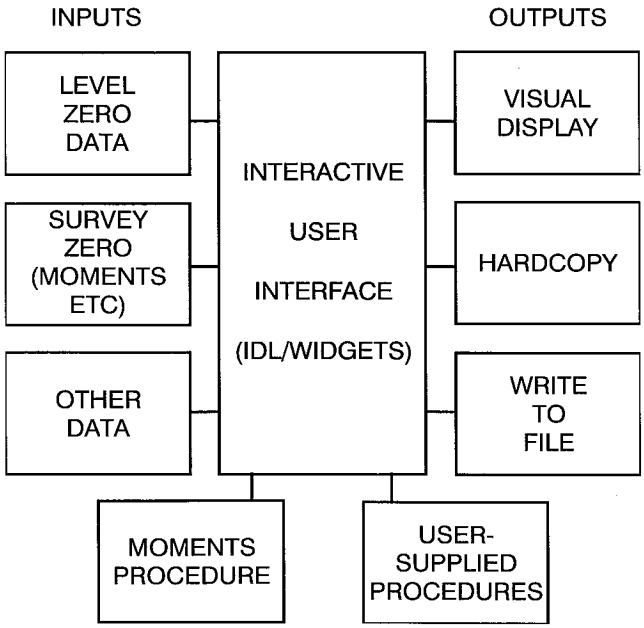

Solar Wind Experiment ground-based data analysis system.

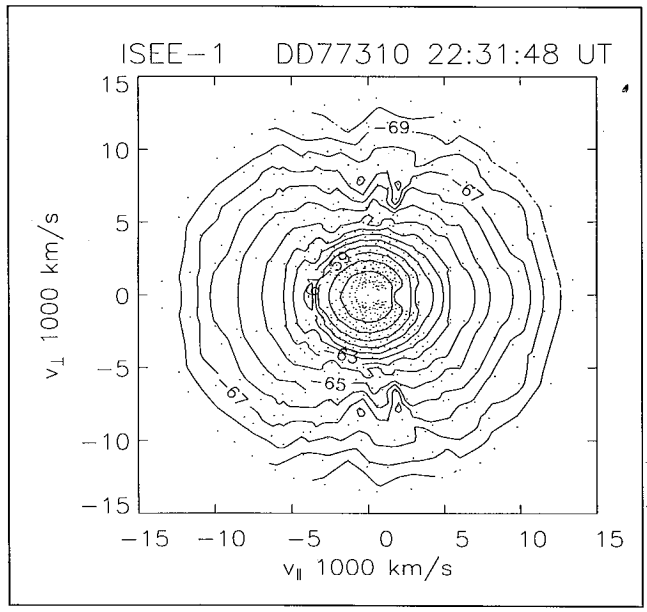

The fundamental plasma measurements by SWE are velocity distribution functions, similar to the ISEE-1 measurement shown here. Iso-contours of phase space density are shown as a function of electron velocity, parallel and perpendicular to the magnetic field.

shown in that figure are color-coded plots of particle flux as a function of energy, pitch angle of particle velocity relative to the magnetic field, and time. Many months of such data may be stored on a single hard disk or CD-ROM. Displays of this type of survey data have been found to be very revealing of new phenomena.

A typical interactive analysis session may involve a scientist scanning the survey data (such as those in the third figure) and selecting intervals of detailed data, such as velocity distributions, which may be read in the raw telemetry format, processed, and displayed (as shown in the second figure), along with the survey data. The process of conversion from LZ data to displays of calibrated physical quantities such as the phase space density in the second figure is sufficiently fast that standard approach is to calculate quantities as they are required, rather than retain them in data files for future reference. This latter approach would entail considerable overhead for data storage and management. Interpretive operations on the displayed data may be performed with user-supplied procedures using interactive graphics and analysis software. This is where the "science" is done.

In addition to scientific processing, the system uses programs derived from those used during instrument development and integration to display and make statistical records of the instrument "housekeeping" quantities included in the raw telemetry data. Trend analysis can be carried out to support this activity. This single system can, therefore, keep up with routine data processing, interactively perform what used to be called data analysis, and monitor the condition of the instrument over the lifetime of the spacecraft.

Contact: Richard Fitzenreiter (Code 692)
301-286-6825

Keith Ogilvie (Code 692)
301-286-5904

Sponsor: Office of Space Science

Dr. Richard Fitzenreiter, a member of the data evaluation team for the SWE investigation with responsibility for data analysis development, received his PhD from Catholic University in 1972. He is interested in solar wind and boundary layer research and has been at GSFC since 1962.

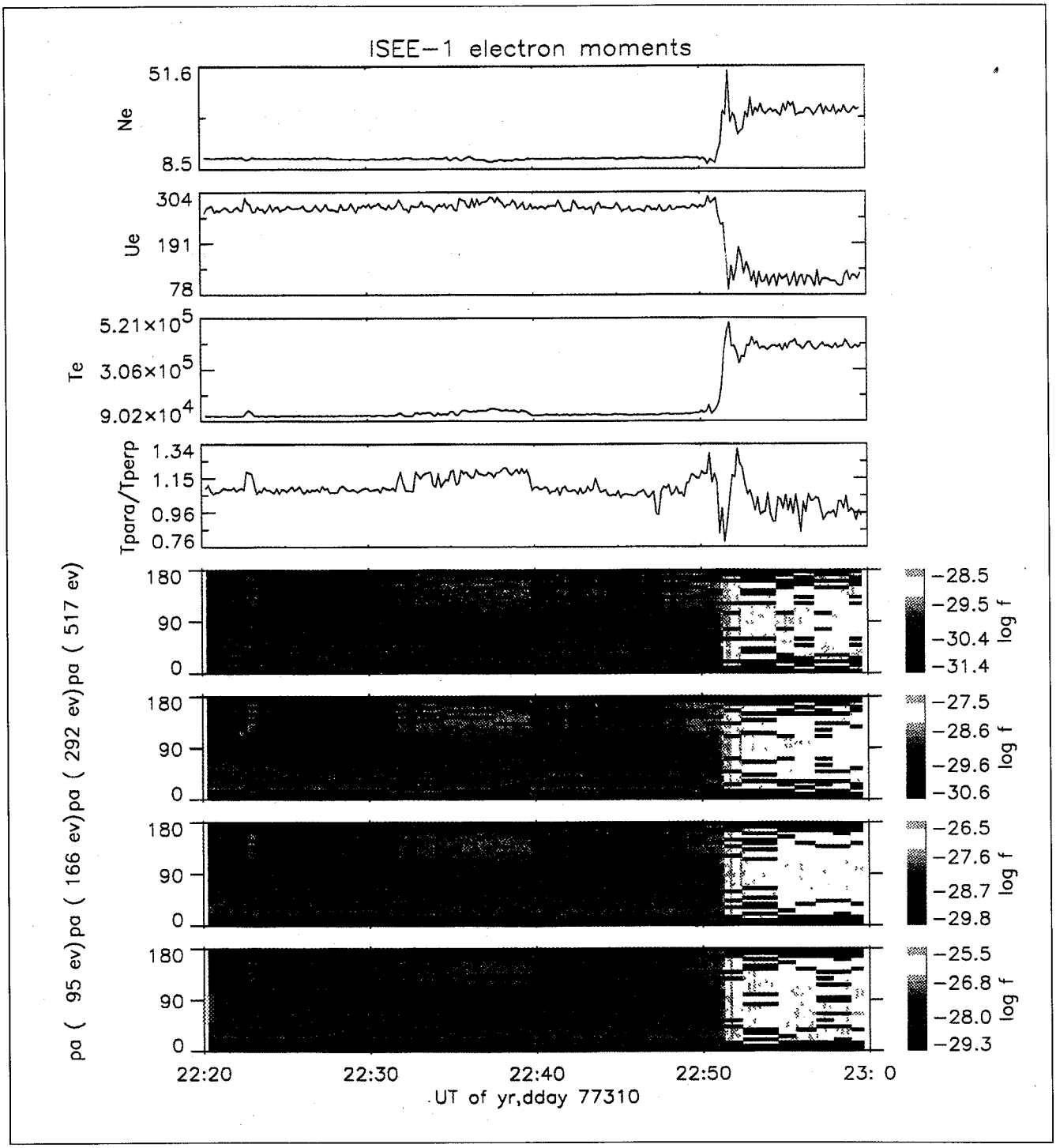

An example of the type of data to be used for surveying the SWE data. Shown is a crossing of the Earth's bow shock (22:51 UT) from the solar wind into the magnetosheath. Prior to the shock crossing, electron heat flux from the Sun shows up as green in the color-coded pitch angle images near the angle 0° . The sporadic yellow spikes extending from approximately 135° to 180° are the electron foreshock, an upstream solar wind precursor of the bow shock.

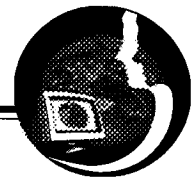

Dr. Keith Ogilvie is Head of the Interplanetary Physics Branch and Principal Investigator for SWE. His interests include solar wind physics and the interaction with the planets. Dr. Ogilvie received his PhD from the University of Edinburgh in 1954 and has been at GSFC since 1960.

THE NATIONAL SPACE SCIENCE DATA CENTER PROVIDES NETWORK ACCESS TO KEY DATA VIA THE NSSDC DATA ARCHIVE AND DISSEMINATION SERVICE

THE NATIONAL SPACE Science Data Center (NSSDC) is making a growing fraction of its most customer-desirable data electronically accessible via both the local and wide area networks. NSSDC is witnessing a great increase in its data dissemination because of this network accessibility. To provide its customers the best data accessibility, the NSSDC makes data available from a nearline mass storage system, the NSSDC Data Archive and Dissemination Service (NDADS). The NDADS, developed in January 1992, is a customized system of hardware and software that provides user access to the nearline data via anonymous ftp, an e-mail interface (ARMS), and a C-based software library. In January 1992, the NDADS registered 416 requests for 1,957 files. By August of 1994, the NDADS registered 2,006 requests for 51,470 files, amounting to some 32 gigabytes.

The focal point of NDADS is the mass storage components of two Cygnet jukeboxes, each configured with two 6.5 gigabyte Sony optical disk drives. The two jukeboxes provide the NSSDC with 1.2 terabytes of nearline optical disk storage. A VAX cluster computer configuration drives the two jukeboxes and provides network connections to the NASA science community, which includes NSI-DECnet, Internet, and U.S. SprintNet. At present, there are about 0.5 terabytes of science data resident on NDADS. Although the numbers of datasets in the space physics and astrophysics areas are comparable, about 90 percent of the NDADS data, by byte count, are astrophysics data. NSSDC expects to increase its rate of NDADS data ingestion to about 1 to 2 terabyte/year in the next few years.

These incoming data include a mix of data currently arriving at NSSDC, plus selected data being promoted from NSSDC's offline archives to NDADS. To date, NSSDC has focused on loading space physics and astrophysics data to NDADS. Key space physics datasets presently available from NDADS come from the IMP-8, ISEE-3, DE-1 and 2, Hawkeye, and Skylab missions. Key NDADS-accessible astrophysics datasets typically include the basic observation data files and accompanying ancillary files (calibration, etc.). The astrophysics missions with data in NDADS are IUE, ROSAT, IRAS, Ginga, VELA5B, HEAO-1 and 2, OAO-3 and the Astronomical Data Center Source Catalogs. For specific dataset information on the NDADS collection, users can send an e-mail request to the archives account at the node nssdca.gsfc.nasa.gov. On the subject line of the e-mail message, users can enter HELP or HOLDINGS for further information.

The NSSDC developed the NDADS to support the following requirements:

- Loading of data files to nearline storage and of associated metadata files to an inventory database.
- User access to the (relational) inventory database.
- User access to and retrieval of data.
- Data security.
- User understanding of the system (through on-line user guides, etc.).
- Aggregation of files according to individual project needs.
- Capability to support additional types of mass storage devices as acquired.

File aggregation is a special concept, whereby related files are grouped into predefined "granules" or "entries." Users are thereby able to request, for example, an astrophysical observation by unique entry ID and have the system retrieve and stage all the relevant files without the user having to specify each one. This makes NDADS more than a typical file management system.

NSSDC developed a specialized software system for NDADS to achieve the needed requirements and to provide the needed evolvability. The current software system is written on a VAX VMS™ 5.5-2 platform and relies on the SYBASE relational database management system for locating and mapping the files/granules. The system was developed as a server to support network clients and as a direct applications interface to support NSSDC operations. The direct applications interface allows the staff better access and control over the system in support of data

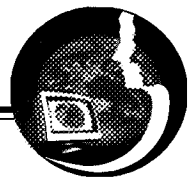

ingestion. The client/server approach is required for several user interfaces, for example, anonymous ftp.

The system architecture has four primary functional components: external interface, metadata management, data management, and the application toolkit/server. The external interface provides users an interface to issue data storage and staging requests, processes the request, and informs the user of the status of his or her request. The metadata management component interfaces with the SYBASE database management system to ingest, retrieve, and update the metadata in the database. In particular, it provides the mappings between data granules and actual files residing on the nearline archive. The data management component interfaces with the application toolkit/server to actually transfer data to and from the storage devices. The application toolkit/server is the heart of the system, interfacing with the external interfaces component, the metadata management component, and the data management component.

The system is designed to enable the NSSDC to add additional storage devices transparently to the external users without modification of the base software system. The development of the "fetcher" modules or specific device drivers allows a new storage device to be integrated into the data management system. Each fetcher module is expected to provide a certain small set of services to the "master fetcher," such as mounting the device, copying a file onto the device, copying a file out of the device, etc. Currently, the NSSDC has fetchers for the Cygnet-Sony WORM jukebox and on-line magnetic disk devices, and there are plans to include several other mass storage devices. Another important feature is the high level of security and recovery applied to the storing and staging of data from the NDADS storage devices.

The NDADS has been developed to serve the specific needs of the NASA science community. It combines specialized hardware with customized software to significantly enhance the power of the NSSDC scientific database system. The success of this facility can be measured in several ways: the number of requests for data, the turnaround time, capacity, and convenience to the community. Available 24 hours a day every day, NDADS currently satisfies in excess of 1000 requests per month in an average of less than 10 minutes. The NDADS service represents three-quarters of all NSSDC data requests. NSSDC believes its NDADS nearline data management environment can evolve to exploit future changes in both hardware and software. By providing a well-constructed and secure infrastructure, NSSDC will be able to meet the future requirements of managing terabytes of data, cooperatively supporting NASA missions, and supporting user interfaces that rapidly change to best meet the needs of scientists and others on the information superhighway.

Contact: Jeanne Behnke (Code 633.1)
301-286-8340
behnke@nssdca.gsfc.nasa.gov

Sponsor: Office of Space Science

Ms. Jeanne Behnke has been with the NSSDC since 1985 and is the systems manager. Jeanne Behnke earned a BS and MLS in Information Systems Management/Science from the University of Maryland.

THE NATIONAL SPACE SCIENCE DATA CENTER COMMON DATA FORMAT

WHEN ONE FIRST hears the term Common Data Format (CDF) one intuitively thinks of data formats in the traditional (i.e., messy/convoluted storage of data on disk or tape) sense of the word. Although CDF has its own internal self-describing format, it consists of more that just a data format. CDF is a scientific data management package (known as the CDF Library) which allows programmers and application developers to manage and manipulate scalar, vector, and multidimensional data arrays. The irony of the term "format" is that the actual data format which CDF utilizes is completely transparent to the user and is accessible through a consistent set of interface routines, the CDF Interface. Therefore, programmers are not burdened with performing low-level I/Os to physically format and unformat the data file.

The CDF software has been critical in the success of many NASA-related activities, such as the NSSDC Coordinated Data Analysis Workshops (CDAW) and the NASA Climate Data Systems (NCDS) activities, and has become the standard for storing the ISTP Project key parameter data. The CDF package is used by government agencies, universities, and commercial organizations, as well as independent researchers on an international level. For example, CDF has been adopted as the de facto standard among many international space physics programs that are participants in the IACG campaign. Among them are NASA's ISTP, ESA's SOHO and Cluster missions, and the Russian Space Research Institute (IEU) INTERBALL mission. The CDF software is also supported and distributed as part of Research Systems Inc. (RSI) Interactive Data Language (IDL) and the International Business Machines (IBM) Data Explorer (DX) commercial software packages. In addition, there are numerous free tools, utility programs, and applications based on the CDF software available across the network.

The principle idea upon which the CDF model was designed was to facilitate the storing and manipulation of data ensembles from a wide variety of scientific disciplines (oceanography, solar-terrestrial physics, Earth science, planetary astronomy, and astrophysics) in a generic fashion. The hallmark of the CDF concept is its dataset independence. This independence is achieved by means of an internal format containing its own data dictionary (metadata) as well as the data. This self-describing property makes it possible for the CDF to be used for data from a wide variety of disciplines. The CDF files contain two types of data: the data values themselves, and user-provided metadata. Both are accessible via the CDF interface. Using an internal data dictionary to describe the contents of a data file to achieve a data-independent transportable standard is not new. However, the CDF differs from earlier formats by being oriented toward the researcher's view of the data. Traditional data management packages do not support multidimensional structures and are limited to sequential access of multiple variables.

The CDF library is a flexible and extensible software package which allows the novice user to easily and quickly generate a CDF by taking advantage of the high level capabilities, while providing more advanced and sophisticated features for the experienced user. The CDF interface permits access to more than one type of variable and multiple CDFs simultaneously, so that applications can work with multiple CDF datasets with disparate structures as easily as with a single CDF dataset.

The interface routines provide the programmer with an abstract view of the contents of a CDF, while relieving them of the burden of having to physically unpack or pack the contents (data and/or metadata) of a file. These routines are analogous to that of conventional database management package Host Language Interface (HLI) routines. Although CDF is callable from a number of programming languages (e.g., C, Fortran, C++, Pascal, etc.), the library directly supports two interfaces, C and Fortran, to make programming easier and more attractive to the scientific user community. When creating a CDF, the user can specify the manner (C/row vs. Fortran/column) in which their data are to be stored.

The CDF library is written in C and is portable across several computational platforms and operating systems, as are the CDF data files that are produced via the software. Internally, the CDF library supports two physical encoding schemes, native (host) and network formats. The native encoding scheme allows the data to be stored in the CDF, consistent with the physical data representation on the machine from which the CDF Library is running. The network encoding scheme physically stores data in the IEEE-754 format. Therefore, when a user accesses the data, the data are transparently converted between the native and IEEE-754 formats. This option gives the

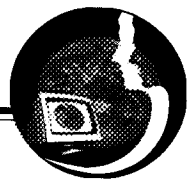

programmer the ability to transfer CDF files to other environments from which the CDF Library runs and to read the data without having to be concerned with data conversion, which, between disparate platforms, is performed internally by the CDF library with little impact on performance.

The data and metadata values in a CDF also can be accessed (decoded) in a scheme other than that of the host computers. For example, a CDF application running on a Sun can access CDF files that are physically stored on a VAX in VAX encoding and can request the data in the Sun (IEEE-754) encoding. This provides the foundation for client/server applications in which the client and server reside on disparate platforms.

The library provides random access to data elements from within a CDF in one of two methods, either single-element or hyperplane access. Single-element access allows a user to uniquely access any specific element from within a CDF. The hyperplane technique provides aggregate access to single- or multidimensional structures propagated across contiguous or noncontiguous array and/or record boundaries, allowing application software to perform uniform subsampling and/or dimensional-slicing of data.

The user has the option of selecting from one of two filing systems in which the data and metadata are stored. The first is the traditional CDF multifile system, which is the default filing system. Its simplistic organization makes it extremely powerful for storage efficiency, access speed, and updating. A file is maintained for each variable separately, and an additional file is maintained for the metadata (e.g., a CDF that consisted of 5 variables would maintain 6 files (5 variable files + 1 metadata file)). The single filing system consists of only one file, which contains all metadata and actual data for each variable. Both filing systems can be sequentially or directly accessed, facilitating quick access to large disk-resident datasets.

The software employs its own internal high-speed caching algorithm, similar to that used by virtual memory operating systems, to move data in and out of memory. This provides higher data throughput to application software. Although default values are maintained for the size of the cache, the user or application can change these values through the interface to enhance the performance of his or her application. In addition, the software provides extensive error-checking and -reporting capabilities that assist the applications programmers in writing and debugging CDF-based applications.

The figure provides an illustration of a CDF Windowing Imaging Tool (CWIT) for IBM PCs. CWIT is a two-dimensional imaging tool based on the CDF. Among its features are a flexible look and feel style interface, three standard projections (orthographic, azimuthal, or mollweide) in geographic coordinates with mapped overlays, pseudo-color variables, magnification, rendering style, projection type, pallets selection, and others. There exist similar tools for the Macintosh (CMIT) and Sun (CXIT; X is for X-windows) computers. The image on the right was generated by mapping sea level pressures ranging from 960 to 1,040 millibars onto an orthographic-mapped projection. The left image represents the luminosity of the solar corona in the x-ray band from 2 to 60 Angstrom units wavelength taken from the Skylab S-054 X-ray Spectrographic Telescope. The data values of photometric film density are scaled to the range from 0 to 511.

Although the CDF software has been in existence since 1986, its popularity has grown significantly over the past couple of years, due largely to the contact the CDF Support Office maintains with its user community. As with most successful products, the process of adding new features, capabilities, and porting of the software to new environments is a continuous one. The requirements for future releases of the CDF software are solicited from the user community on a continuous basis. The requirements are prioritized at the CDF Steering Committee meetings and implemented in future releases based on the priority rankings. Version 2.4 of the software was released in February of 1994, and we are currently working on an incremental release, 2.5, which is scheduled for the fall of 1994. CDF 2.5 will consist of the Macintosh port. Releases beyond 2.5 are scheduled to consist of data compression, merging and subsetting, sparse matrices, bit data types, possibly client/server implementations, other ports (Cray, 32-bit compilers for the PC, others as requested), and more documentation.

The CDF Support Office is physically located at the NSSDC at GSFC. The support office is responsible for providing CDF programming assistance, on-line help, release notes, distribution memos, and documentation. The Internet address for the CDF support office is: cdfsupport@nssdca.gsfc.nasa.gov.

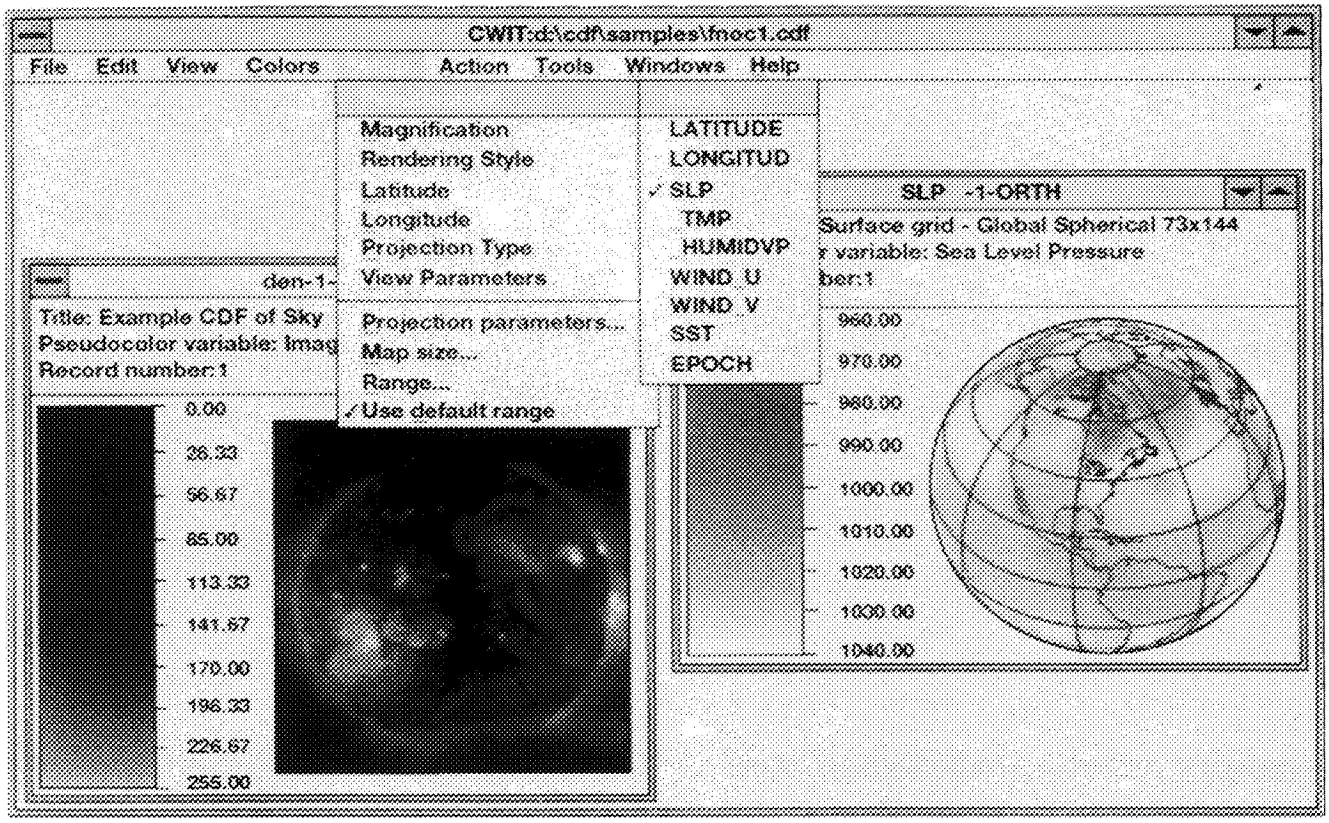

An illustration of a CDF windowing imaging tool for IBM PCs.

Contact: Gregory Goucher (633.2)
301-286-2341
goucher@nssdca.gsfc.nasa.gov

Jason Mathews (633.2)
301-286-6879
mathew@ncgl.gsfc.nasa.gov

Sponsor: Office of Space Science

Mr. Gregory Goucher is a computer scientist at the NSSDC Interoperable Systems Office (ISO) of GSFC. He has earned a BS in Information Systems Management from the University of Maryland at Baltimore County (UMBC), an MS in Computer Science from The Johns Hopkins University, and has been with GSFC 11 years. Mr. Goucher is the ATR for the CDF task and provides technical support for the development and implementation of advanced scientific software applications.

Mr. Jason Mathews is a computer engineer at the NSSDC Interoperable Systems Office (ISO) of GSFC. He earned a BS in Computer Science from the Columbia University, an MS in Computer Science from the George Washington University, and has been at GSFC for 4 years. Mr. Mathews provides technical support for the development, implementation, and testing of advanced scientific software applications.

ARCHIVE OF WIDE-FIELD ULTRAVIOLET ASTRONOMICAL IMAGES

THE ULTRAVIOLET IMAGING Telescope (UIT), which flew on the Space Shuttle Columbia in 1990 as part of the Astro-1 payload, returned over 800 wide-field images of astronomical objects. Fully reduced and calibrated versions of these valuable data were made available to the astronomical community through the NSSDC in December 1993. An improved final archive will be delivered in early 1995.

The UIT data provide a new view of many of the most historically important and interesting objects of large angular size and brightness. The field observed by the UIT is wide, with a diameter of 40 arcminutes. The spatial resolution is moderate, at about 2 arcseconds. The UIT is complementary to the instruments on the HST, which observes small fields of view (2.5 arcminutes or less) at very high resolution. Observations in the ultraviolet are important for isolating hot stars, since cool ones do not have significant ultraviolet emission. The dataset returned by the UIT shows the largest total sky area yet covered by any imaging instrument at ultraviolet wavelengths of 120 to 300 nm. The UIT archive is thus a unique resource supporting the detailed targeting of future astronomical observations.

Early in the UIT project, it was realized that a comparable archive of images at conventional visible wavelengths (400 to 600 nm) would be important to obtain the full scientific value of the UIT data. Large-format charge-coupled device (CCD) detectors were just coming on line at ground-based observatories, making such a set of calibrated, wide-field, high-resolution images possible. UIT team members undertook several observing runs at Kitt Peak National Observatory, Cerro Tololo Inter-American Observatory, and Mount Laguna Observatory to obtain these data, which are comparable in volume to the UIT data themselves.

The UIT images are recorded on photographic film. Ultraviolet photons are both amplified and converted to blue light by two-stage image tubes. The photons reach the film by way of a fiber-optic coupler. The film is removed from the Space Shuttle after landing and returned to GSFC for processing. The developed film is digitized using a Perkin-Elmer 1010m microdensitometer. The resulting digital images are processed by computer.

The software used to reduce the UIT data is called Batch Data Reduction (BDR). Originally intended to be run on a batch-oriented mainframe of early 1980s vintage, this software now runs on high-performance desktop workstations. BDR has been affected by two kinds of change: migration from one computing platform to another and evolution in the scientific understanding of the instrumental attributes of the UIT. Through it all, the underlying design of BDR has needed very few amendments, and the detailed codes have become ever more machine-independent. As a result, the UIT team is confident of its ability to incorporate new processing steps, to change instrumental parameter values, and to keep up with new computing technology within a stable, reliable structure.

Products generated by BDR are linearized, flat-fielded images with astrometry; north-up versions of the images; point-source photometry tables; and box-averaged quick-look versions of the images. All of these data are available in the archive and may be requested through the NSSDC.

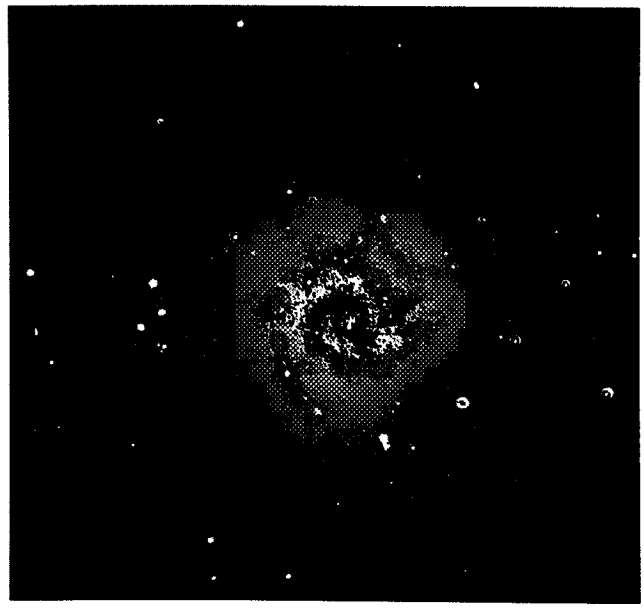

The giant Sc spiral galaxy M74, which resembles our galaxy, the Milky Way. Ground-based visible data are shown in red, and UIT ultraviolet data are shown in blue-white. The prominent ultraviolet knots are large associations of young stars.

The UIT ground-based image archive is currently being organized for release to the astronomical community on CD-ROM.

The accompanying figures are examples of UIT ultraviolet data combined with the ground-based visual data. They also represent research areas studied by UIT science team members.

The first figure shows the galaxy M74, a giant spiral galaxy seen nearly face-on. In this composite image, the visible-light emission is represented in red, while the UV emission is shown in blue-white. Newborn hot stars and associated reflection nebulosity dominate the UV emission. The concentration of this activity along the spiral arms is indicative of global dynamic processes at work on time scales of about 10 million years, which is the approximate time for gas to traverse an arm. The regularity of M74's spiral windings has prompted astronomers to regard it as a "grand design" spiral galaxy. Much of the UV emission from the spiral arms in M74 is concentrated in knots measuring hundreds of light years across. At an estimated distance of 24 million light years, M74 is comparable to the Milky Way galaxy in size and mass. M74 and the Milky Way are also similar in terms of their tight spiral windings, the moderate size of their bulges, and their total star-formation rates.

The second figure shows the globular cluster M79 in the Milky Way galaxy. Globular clusters, which are the oldest stellar groups observed within galaxies, are used to study the life histories of low-mass stars. Each of the million or so stars in a given globular cluster is the same age. However, the speed of the aging process depends on the mass a star has when it is formed. The higher a star's initial mass, the faster it evolves. Many stages of the stellar lifetime are observed simultaneously in M79 because a range of initial masses is represented. In the figure, the picture on the left is a visible-light image crowded with thousands of stars that are relatively cool like our Sun. The picture on the right is a UIT image showing that the ultraviolet light is produced by a mere 200 stars with surface temperatures from two to ten times that of the Sun. These stars are in an interesting late phase of their lives. UIT images permit the measurement of each star's ultraviolet brightness for comparison to the results of theoretical calculations.

M74 and M79 are examples of two types of objects for which the UIT is well suited, namely, nearby galaxies and globular clusters, respectively. Other nearby galaxies in the UIT dataset are M31, M81, and M33, as well as fields within the Magellanic Clouds. Other globular clusters are Omega Centauri and NGC 1851. Among the other types of objects represented are reflection nebulae (e.g., NGC

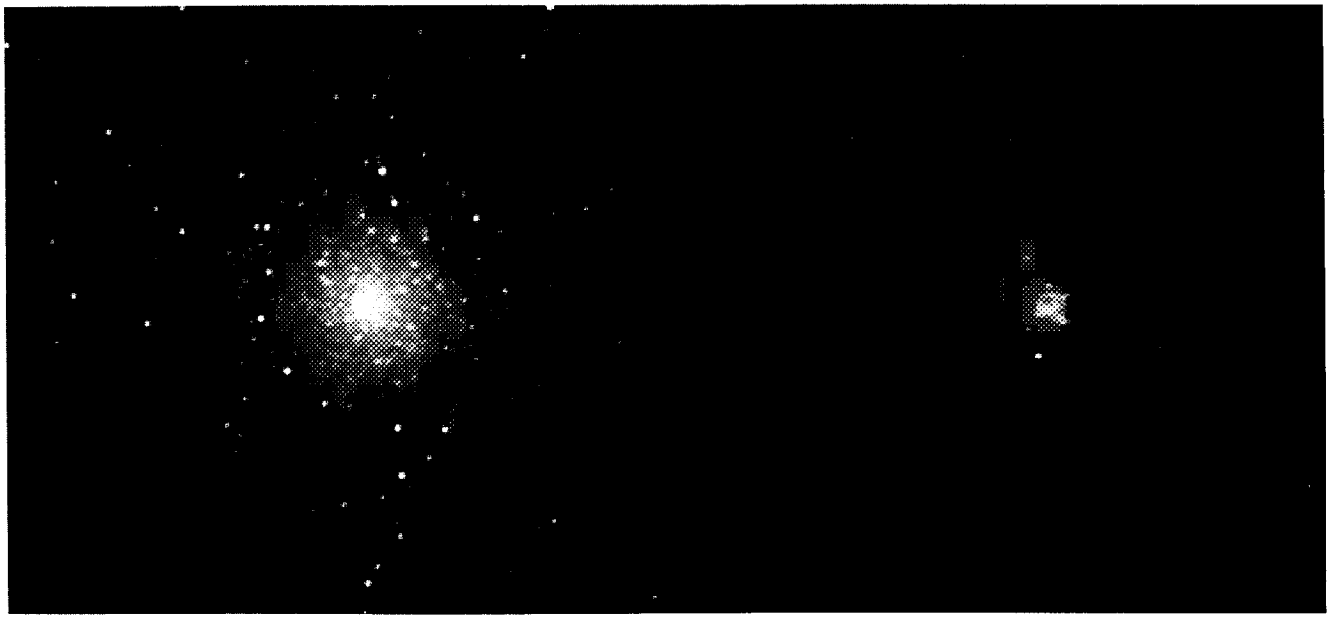

The globular cluster M79 in the Milky Way galaxy. Globular clusters are the oldest stellar groups observed. Left: ground-based image taken in visible light. Right: UIT space-based image taken in ultraviolet light. The UIT image selects hot stars whose temperatures are several times that of the Sun.

7023), and supernova remnants (e.g., the Cygnus Loop and the Crab Nebula). From this list, it can be seen that the UIT space-based ultraviolet images, together with the associated ground-based images, form a resource valuable not only for research, but for education. An example such as M74 quickly shows a student the difference between the ultraviolet view and the visual one, and it leads easily to the consideration of such important ideas as stellar populations, stellar evolution, and galactic structure.

The second flight of the Astro payload, manifested for 1995, is expected to produce over 1,800 more UIT images, which will be processed and made available in the same manner as the Astro-1 UIT data.

The figures were produced by Joel Offenberg and William Waller of Hughes STX Corporation.

Contact: Susan Neff (Code 681)
301-286-5137

Robert Hill (Hughes STX)
301-286-3624

Sponsor: Office of Space Science

Dr. Susan Neff is the Head of the Astronomy Branch in the Laboratory for Astronomy and Solar Physics. She is a coinvestigator for UIT. She received a PhD in Astronomy from the University of Virginia in 1981 and has been at GSFC since 1985. Her research interests include active galaxies and star formation.

Mr. Robert Hill is the group leader for UIT Batch Software and Data Production within the UIT task at Hughes STX Corporation. He holds a BA from Harvard University. His professional interests include software design, data archiving, and research on irregular galaxies.

REPROCESSING OLD DATA TO OBTAIN NEW RESULTS: THE FINAL IUE ARCHIVE

THE INTERNATIONAL Ultraviolet Explorer (IUE) Project has developed the New Spectral Image Processing System (NEWSIPS) to improve the threshold sensitivity of IUE data, expanding the observing potential of the instrument. When applied to the archive, NEWSIPS will also create a homogeneous dataset with optimal signal-to-noise (S/N) ratio, accurate calibrations, and thorough documentation as the final product of the IUE mission. The final archive will allow future investigators to directly compare data from different epochs of IUE operation and to use archived data with minimal assistance. The final archive is being developed while IUE is still an operational spacecraft to take advantage of the expertise of scientists who actively use IUE and to determine what new calibration data are needed from the satellite.

NEWSIPS significantly improves the quality of the spectral data compared to the original processing system for IUE data (IUESIPS). (See the 1993 GSFC Research and Technology Report, page 49, for an example of the results of applying NEWSIPS to existing IUE data.) Data quality improvement comes from more-accurate photometric correction of the raw data values; single, flux-conserving resampling of the data, weighted-slit extraction technique for low dispersion data; global background removal technique for high dispersion echelle data; and more-accurate flux calibrations.

The new processing algorithms exploit the presence of fixed pattern noise (pixel-to-pixel sensitivity variations in the cameras) as a reliable fiducial to register the raw science image with the raw Intensity Transfer Function (ITF) image. Proper registration of IUE images is crucial to accurate photometric correction because the variability of the geometrical distortions introduced by the SEC Vidicon cameras ensures that the raw science images are never perfectly aligned with the ITF. While reseau marks etched on the faceplates of the cameras were intended to be used to geometrically rectify the science images, they cannot be detected at the low exposure levels usually found in the background of IUE images. Therefore, the IUESIPS method of processing images uses predicted reseau positions to align the science images with the ITF images. Unfortunately, these mean positions are poorly known, and the application of a misregistered ITF (by more than 0.2 pixel) manifests itself as systematic noise in the photometrically corrected image, and, ultimately, in the spectrum.

To achieve proper alignment of the ITF images with each science image for the final archive reprocessing, the fixed pattern inherent in IUE images is used as the fiducial. Small patches of the science image are cross-correlated against corresponding areas on the appropriate ITF image to determine the spatial displacement between these two images. The displacement of each pixel in the science image from its corresponding pixel in the ITF can thus be determined to sub-pixel accuracy. Such an approach has several advantages: a large number of fiducials can be found everywhere on the image, the fixed pattern can be detected even at the lowest exposure levels, and fiducials are available near the edge of the image, where distortion is greatest. In the IUESIPS processing of IUE data, the ITF images have been resampled into geometrically correct space, significantly smoothing the calibration data. In the NEWSIPS system, the ITF images are retained in raw space.

Only one resampling of the data is performed in the new processing system, minimizing the smoothing inherent in such an operation. The linearized pixel values are resampled into a geometrically rectified and rotated image, such that the spectral orders are horizontal in the image, and the dispersion function of the spectral data within an order is linear. The resampling algorithm preserves not only the flux to 1 to 3 percent (as opposed to 5 to 7 percent in IUESIPS), but also the spectral line shapes.

The low-dispersion spectral data are extracted by a weighted-slit extraction method. The advantages of this method over the IUESIPS boxcar extraction are that the S/N ratio of the spectrum is improved while flux is conserved, most of the cosmic rays are automatically removed, and the output includes an error estimate for each point in the flux spectrum.

High-dispersion data in the final archive will have two additional major improvements. One of the most significant problems with the analysis of high-dispersion IUE data has been the proper determination of the background in the region where the echelle orders are crowded and overlap. The new processing system includes a global

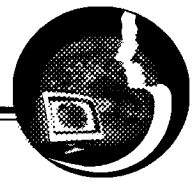

background removal algorithm that determines the background level of each high dispersion image by fitting, in succession, one-dimensional Chebyshev polynomials, first in the spatial and then in the wavelength direction. This technique effectively compensates for the effects of electron back-scattering (halation) that leads to an artificial increase in the background. Another enhancement is an entirely new data product for high-dispersion data: a geometrically rectified and rotated image with horizontal spectral orders. The new data product will allow future investigators to perform customized extractions on specific, high-dispersion echelle orders.

A fundamental improvement in the final archive is the use of more-accurate calibration techniques. All absolute flux calibrations are being rederived. The new calibrations use white dwarf models to determine the relative shapes of the instrumental sensitivity functions, whereas previous UV satellite and rocket observations of the white dwarf star eta UMa and other standard stars are used to set the overall flux scale. The IUE final archive-extracted spectral data are also corrected for sensitivity degradation of the detectors over time and with temperature, a calibration not previously available with IUESIPS processing.

Properly exposed low-dispersion data processed with the final archive software have been shown to have 10 to 50 percent greater S/N ratios than data processed with the original IUESIPS. Underexposed and high-background data can show improved S/N ratios of 100 to 300 percent high-dispersion data processed with NEWSIPS generally have increased S/N ratios of 50 to 150 percent. Signal-to-noise ratios of 50 or greater can be realized in a single high-dispersion IUE spectrum.

In addition to the new image processing techniques developed for the final archive, diagnostic output parameters have been developed which provide the future investigator with a measure of the quality of the spectral data for each image. These parameters, such as S/N characteristics, continuum and background flux levels, and use of a default profile in the extraction algorithm when needed, are stored in the FITS header and in the IUE Final Catalog as searchable keywords. These keywords will allow investigators to assess the quality of each image without actually examining the data, thereby saving considerable time for large studies. The value of the final archive to future investigators will depend largely on the accuracy and ease of use of the Final Catalog. Both NASA and ESA IUE Observatories have verified the accuracy of the data items necessary to process correctly the image and/or are crucial for scientific analysis.

The NEWSIPS production processing system which incorporated the new image processing algorithms and calibrations was developed by the IUE Project to be fully automated, with minimal human resources required for production. The goal is to develop an efficient, inexpensive production system with maximum scientific gain. This has been achieved in several ways:

- A database-driven production system automatically queues images for processing and generates the necessary input information file, ingests the output information file, and tracks processing status of each image.

- Thoroughly tested, robust algorithms ensure minimum failure rate for the diverse IUE archive of 100,000 images without human interaction during the processing. The failure rate for images in NEWSIPS to date is less than 0.5 percent; virtually all of these images contain corrupted raw data.

- Automated quality control techniques monitor the processing of each image and flag an image for output diagnosis if any critical parameters fall outside of the normal thresholds. This tool has virtually eliminated the need to spot-check the output by personnel and is a significant cost saver.

- Electronic request capability for NEWSIPS data allows an investigator to request—via e-mail—specific images to be processed immediately by the NEWSIPS production system. Images of greatest interest to the scientific community will thus be processed first for the final archive. The investigator will be informed by return e-mail when the requested images have been processed and archived for retrieval.

Currently, the 100,000 spectral images that populate the IUE archive are being reprocessed and archived on optical disk, and electronic access to NEWSIPS-processed data are available through the GSFC NSSDC. More than 8,000 spectral low-dispersion images have been reprocessed; by

late 1997 the entire NEWSIPS archive should be available for general use by the scientific community.

Contact: Andrew Michalitsianos (Code 684.1)
301-286-6177

Sponsor: Office of Space Science

Dr. Andrew Michalitsianos has been Deputy Project Scientist for IUE since 1990. He received his PhD in Astrophysics from the University of Cambridge, England, in 1973. He received the NASA Medal for Exceptional Scientific Achievement in 1993 for his work with IUE in understanding the nature of interacting binary stars (symbiotic stars).

ULTRAVIOLET SPECTROSCOPY WITH THE GHRS: FROM DATA PACKETS TO MODELS

AFTER THE FIRST Servicing Mission of the Hubble Space Telescope in December 1993, each instrument team made one or more observations to demonstrate that the space observatory had indeed been repaired. For this demonstration, the Goddard High Resolution Spectrograph (GHRS) team selected a star called R136a5, which lies in a dense young star cluster in a neighboring galaxy, the Large Magellanic Cloud. This cluster has been called a unique laboratory for studying massive-star evolution and the "Rosetta Stone" for interpreting starbursts in distant galaxies.

The observations of R136a5 were made in early April 1994. The telemetry data were received by the Data Capture Facility at GSFC and forwarded to the Space Telescope Science Institute in Baltimore for preprocessing and formatting. A few days later, the GHRS data-analysis center at GSFC received the formatted data on an 8-mm Exabyte tape, acquired the data, made a thorough quality-check on the data, and updated the GHRS observation catalogue. GHRS scientists then reduced the data (i.e., transformed the data array to a spectrum). The first figure shows a segment of the reduced GHRS spectrum of R136a5 both in photographic form and as a plot of flux versus wavelength. The major features of the spectrum are formed in the outflow from the star. The features are identified as C IV 1550 (triply ionized carbon at a wavelength of 1550 Angstroms), He II 1640, and N IV 1718.

To interpret the spectrum, we built a numerical model of the star proper and its surrounding wind. The model is based on a solution of five equations: an equation of continuity, a momentum equation, an energy equation, a general state equation, and a radiative transfer equation. We assumed a velocity law in the wind specified a priori, so we did not have to solve the momentum equation. The continuity equation then yields the density as a function of distance from the star. In solving the energy balance equation, we assumed that all energy is transported by radiation (i.e., no shocks in the wind). To solve the equation of state for the excitation and ionization state of the gas, we solved a set of statistical equilibrium equations for all important excitation and ionization states of all important atoms, including 162 energy levels of various ions of H, He, C, N, O, and Si. Because of the low density the dominant atomic-level transitions are radiative transitions, so we had to solve the state equation simultaneously with the radiative transfer equation.

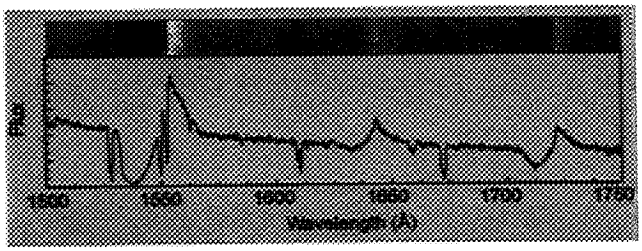

Spectrum of the star, R136a5, obtained by GHRS after the HST Servicing Mission.

The second figure shows an example of the results. The 3D plot shows the density of the ground state of triply ionized carbon (Z-axis) as a function of X-Y location in the wind. The colors represent the velocity of the outflow as seen by an observer stationed to the lower right (red = receding material, blue = material coming toward the observer). The third figure shows the corresponding theoretical profile of the C IV 1550 spectral feature. Again, the colors identify the region of the wind contributing to the feature. By comparing spectral line profiles calculated

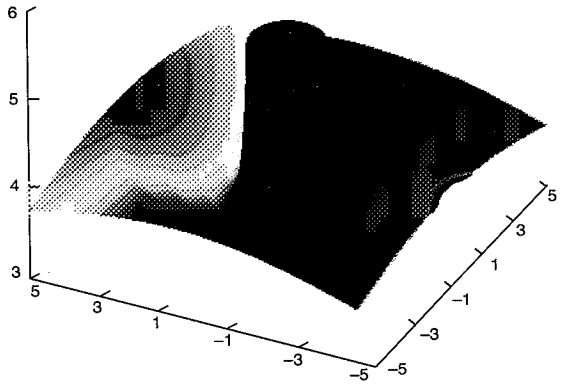

A 3D plot of the C^{+++} density of the wind. The X-Y axes show distance from the star in units of the stellar radius, R_* ($\pm 5\ R_*$). The Z-axis shows the logarithm of the density in particles per cm^3. The plot has been clipped at the location of the star, giving the plot a flat top. The radial velocity of the wind, denoted by the colors, ranges from -3000 km/s^{-1} (purple) to +3000 km/s^{-1} (bright red).

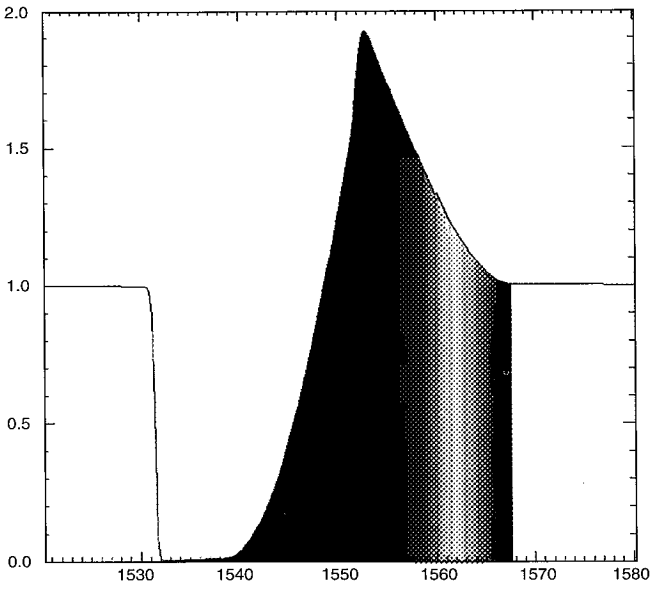

Predicted profile of C IV 1550, shown as normalized flux vs. wavelength in Angstroms. The colors identify the region of formation (c.f. figure 2).

from a model with the observed spectrum, we have determined that R136a5 is a hot (T_{eff} ≥42,500 °K), massive (60 solar masses, $M_\odot$) star, still on the main sequence. To our surprise, it has a very high rate of mass-loss, ≥1.8×10^{-5} $M_\odot$ yr^{-1}, which is much higher than is assumed by modern evolutionary models for stars like R136a5. As a consequence, its evolutionary track should differ qualitatively from these models. We suggest that evolutionary models that assume a mass-loss rate enhanced by pulsational instability may be more appropriate for stars in this young star cluster.

Contact: Sally Heap (Code 681)
301-286-5359

Sponsor: Office of Space Science

Dr. Sally Heap is the Co-Principal Investigator of the GHRS and works in the Laboratory for Astronomy and Solar Physics. She has 25 years of service at GSFC. She earned a BA in Astronomy at Wellesley College and a PhD in Astronomy at UCLA. In 1992, she received a NASA Scientific Achievement award for her contributions to the HST program.

VISUALIZATION OF THE LUNAR SURFACE

THE CLEMENTINE MISSION, sponsored by the Ballistic Missile Defense Organization with participation from NASA, mapped the Moon from late February through May 1994. The Clementine spacecraft carried a laser ranging instrument that measured the distance of the spacecraft from the lunar surface at spacecraft altitudes of 640 kilometers (km) or less. The instrument consisted of a diode-pumped Nd:Yag laser transmitter, a silicon avalanche photodiode detector, and a 130 nanosecond resolution time interval unit that provided a single shot vertical ranging precision of 40 meters (m). Approximately 66,000 valid measurements were made between lunar latitudes of ±75°. Previous far-side topographical measurements of the Moon were made with the Apollo laser altimeter and limited to equatorial swaths.

The Clementine instrument sampled at a rate of 0.6 pulses per second, which corresponds to an average spacing on the surface of 20 km between samples. To display the sampled data, Greg Neumann and Maria Zuber of The Johns Hopkins University, working with the Geodynamics Branch at GSFC, have applied an interpolation algorithm based on curvature of maximum tension to map the sampled data onto a uniform latitude and longitude grid. The resolution of the grid is 2° in latitude and longitude, corresponding to about a 60 km square at the lunar equator. The first figure shows these elevation data, where black values correspond to 9 km below the mean lunar radius of 1,738 km, and white values, to 8 km above. Various circular depressions can be seen which match the large lunar craters seen in the image of the lunar surface shown in the second figure. The relatively uniform elevation of the mares can also be seen. A large depression is evident in the lower-left and -right corners of the first figure, which shows no corresponding feature in the surface image in the second figure.

While these 2-dimensional images are useful, they do not convey the spherical nature of the Moon's surface, nor do they show the relationships between the highs and lows of the elevation and the lunar surface features. To provide a more intuitive view of the dataset, a 3-D perspective visualization of the Moon was made by the Scientific Visualization Studio (SVS). In this visualization, the lunar elevation data modulated the radius of the Moon. The radius was computed as $R(long,lat) = r_o + S * e(long,lat)$, where r_o is the mean lunar radius, S is a scaling factor and e(long,lat) is the elevation value at a particular longitude and latitude. A lighting model was employed to produce shading to aid in visualizing surface variations. In one visualization using this technique, the paths along which the elevation measurements were

Surface elevation of the Moon with respect to latitude and longitude (ranging from -180° to +180° longitude and -75° to +75°). Elevation ranges from 9 km below mean lunar radius (black) to 8 km above the mean lunar radius (white).

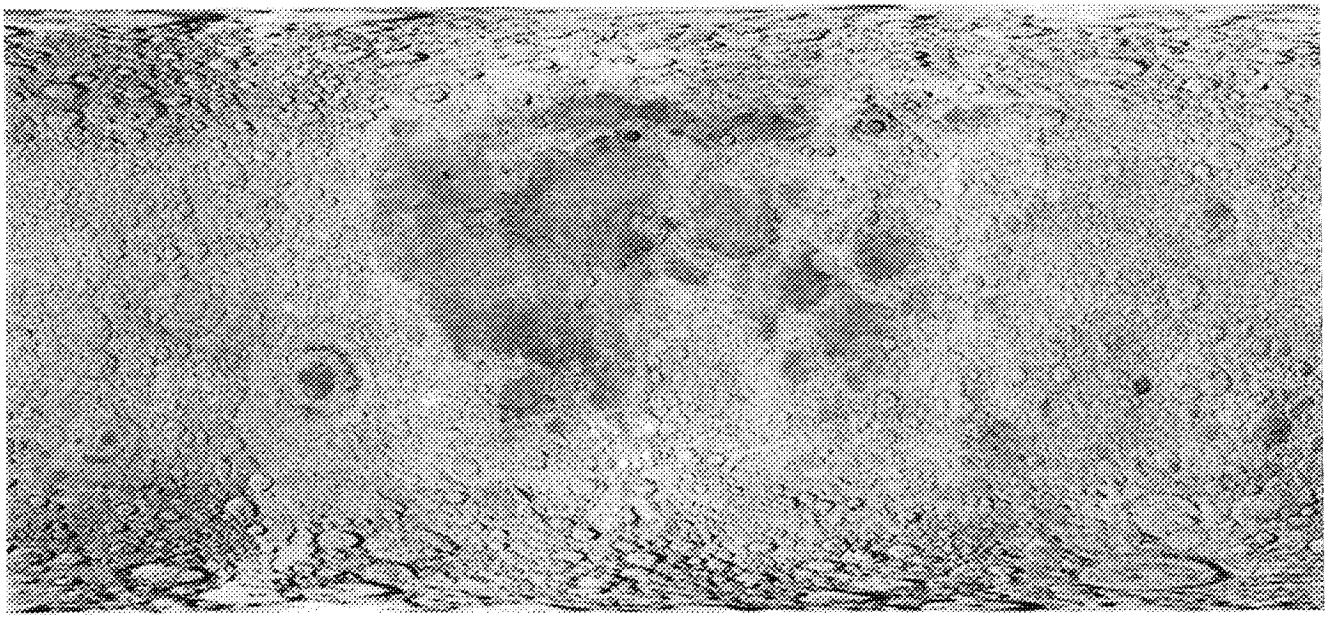

Lunar surface image with respect to the latitude and longitude (ranging from -180° to +180° longitude and -90° to +90° latitude).

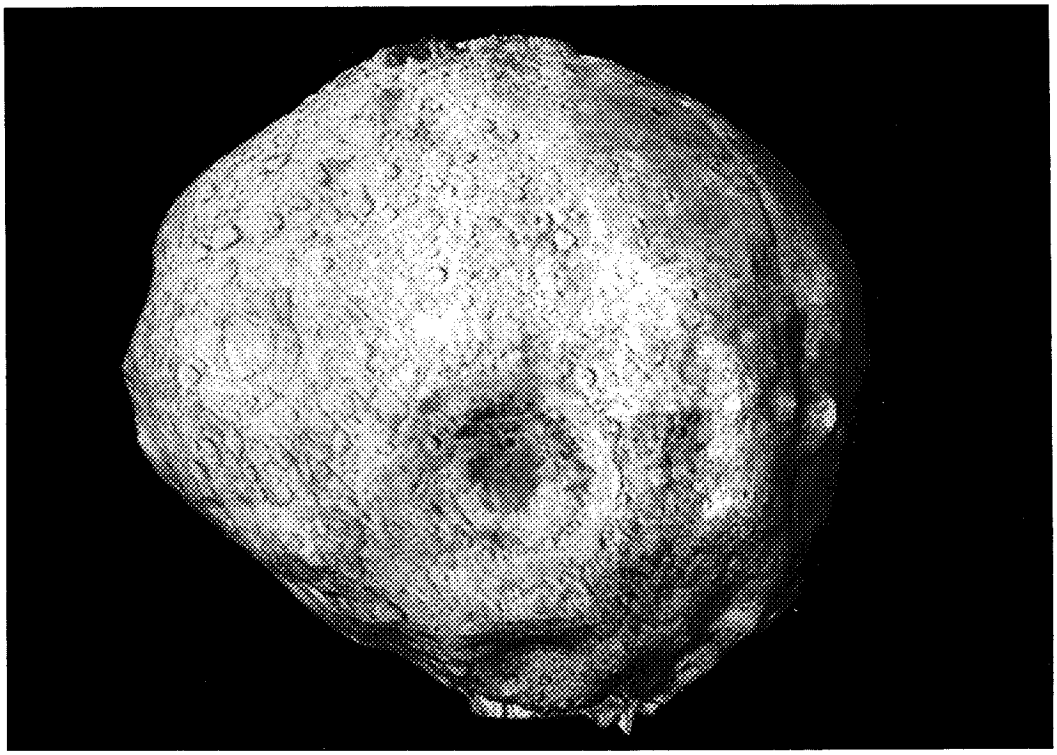

The 3-D perspective view of the Moon where the radius is a function of the elevation and the surface image is superimposed onto the lunar surface. The elevation variation is exaggerated by a factor of 20.

made became immediately visible as "bumpy" ridges, indicating the problems that occur when trying to do interpolation over large areas. In addition, obviously invalid data values became quickly apparent. This is an example where a 3-dimensional visualization greatly aids the human visual system to fully understand and interpret datasets.

Another example of this type of visualization is shown in the third figure, where the lunar surface image in the second figure is superimposed on the Moon's surface. A scale factor of 20 exaggerates (and thus emphasizes) the surface flattening effect of the depressed region in the lower-left and -right corners of the first figure. It is also obvious that the major craters are depressed, a clear indication that the elevation data matches the surface features.

Four animations of the Moon were made, each with the Moon rotating through 360° on its polar axis and employing scale factors of 1, 5, 10, and 20, respectively. The Moon's elevation variations show up most readily at scale factors above 5. Animation is an important aid to visualization. In this case, the rotation helps the eye to catch various features and follow them as they go from profile at the edge to full view in the center. Software for generating these animations was developed by Dave Pape of the SVS in Scientific Applications and Visualization Branch.

Contact: James Strong (Code 932)
301-286-9535
strong@leaf.gsfc.nasa.gov

Sponsor: Office of Mission to Planet Earth

Dr. James Strong is a mathematician/engineer working in the SVS. He earned a PhD in Electrical Engineering and Computer Science at the University of Maryland in 1971. He has been at GSFC since 1963, working in spacecraft telemetry systems, optical computing, massively parallel computers, image processing, and, currently, in computer graphics and scientific visualization.

VIRTUAL ENVIRONMENT VISUALIZATION OF EARTH AND SPACE SCIENCE DATA

RESEARCHERS INVESTIGATING large-scale natural phenomena face the problem of analyzing ever-increasing amounts of data, both from remote-sensing instrument observation and from computational simulations. It is clear that visualization of these data is key to understanding the underlying structure and principles of the phenomena represented by the data and that new and innovative visualization methods will be required as the data volume increases. One such method is virtual environment visualization, the creation of three-dimensional models or structures from the data that a researcher can investigate "naturally," as if these objects were real, physical entities that can be seen and manipulated. The Scientific Applications and Visualization Branch has set up a testbed virtual environment for scientific visualization to investigate the usefulness of virtual environment methods for understanding large datasets.

Since computers have grown in power and capacity and remote-sensing instruments have expanded their resolution and bandwidth, scientists involved in the Earth and space sciences are facing the problem of analyzing and understanding vast amounts of data. For example, the NASA Center for Computational Sciences at GSFC currently sees tens to hundreds of gigabytes per day of computational and assimilation data move through its computers and mass storage systems, and the as-yet-to-be-launched EOS instruments are expected to gather and archive terabytes of data per day. Certainly, there are many approaches to analyzing such data, but one of the most effective is visualization, the creation of visual images and animations from the data. Despite the fact that scientists explain their results in terms of equations and principles, many researchers understand their results in terms of mental visualizations. Effective scientific visualizations created from data are a form of "experiment" whose results, both images, and animations, can be compared to the researcher's mental image, either to validate that image or to reveal new features of the physical situation.

Scientific visualization done by computer involves several steps. Data are first read into the visualization software, and then a computer model of a particular feature of the data is created. For example, if the data are from global ozone density measurements, the model might be a globe whose surface is colored at each point to represent the ozone density above that point on the Earth. Finally, the visualization is "rendered" (i.e., a picture or image of the model is created to represent what a person would see if that person were looking at the model). Several difficulties can arise with this process if the dataset is large or complex. First, the image may be so complicated that the researcher cannot sort out spatial relationships or identify key features from the monoscopic, two-dimensional image. Second, to find an effective model that reveals physical features, the user may have to manipulate the model extensively, in terms of both viewpoint (turning or zooming in on the model) or detail (colors used or features chosen). Each piece of visualization software has its own unique interface for viewing or manipulating such models, some of which are complex and require experience to use well.

In virtual environment visualization, the user interacts with a visualization model as if it were a real object. Separate images are rendered for each eye to produce a three-dimensional effect. The motion of the user's head and body are tracked by sensors, and the image is moved in response to this motion to allow the user to naturally investigate the model as if it were real. Sensors may also track hand movements and gestures so that the model can be manipulated and changed "by hand" just like a real object. In some virtual environments, the most important aspect is "immersion," the feeling of reality. For example, a virtual car interior should accurately represent the spatial feeling and instrument layout of the real car to judge comfort and convenience. In a scientific virtual environment, the most important aspect is control, so that manipulation and movement of the model are natural, and physical insight comes more rapidly.

As part of the High Performance Computing and Communications (HPCC) Earth and Space Science Applications Project, the Scientific Applications and Visualization Branch is setting up a virtual environment system for the scientific visualization of Earth and space science data. In collaboration with GSFC and HPCC researchers, this system will be used to investigate the utility of virtual environment methods for such researchers and what developments are necessary in computer hardware, software, and peripherals to fully realize the promise of such methods for scientific visualization. To minimize the development time for this system, we

decided to build the system from an existing scientific visualization package, the Flow Analysis Software Toolkit (FAST), that had been developed for NASA by Sterling Software. This package could be distributed to our researchers for prototyping on their own computers, because it already contains a full set of tools to build models from scientific data, and both the source code and the developer were available to perform the virtual environment modifications.

Starting in 1992, Sterling software began modifications to FAST to create a version, VR-FAST, which would utilize virtual environment peripherals to control the visualization process. A large Silicon Graphics computer with four central processors and two graphics processors was placed at Sterling, along with a Virtual Research Flight Helmet and a Virtual Technologies Cyberglove (both pictured in the figure). One graphics processor would control each eye of this medium-resolution (320x200) color helmet for a stereoscopic display, and both the helmet and glove would have their positions tracked electromagnetically by an Ascension Flock of Birds tracker. During 1993 and early 1994, VR-FAST interfaces to the helmet and glove were completed and used in preliminary tests on three-dimensional datasets from a computer simulation of the Earth's magnetosphere. In addition, development work at GSFC was performed to add geographic mapping to FAST so that datasets could be registered with the Earth's geography when visualized. During this period, Sterling also acquired a Fakespace 3C Boom for evaluation testing with this system. The boom is a very-high-resolution (1280x1024) stereo color display device which is tracked mechanically rather than electromagnetically.

In June 1994, a series of demonstrations and tests were performed with the virtual environment system at GSFC. Among the prototype datasets visualized in these tests were (1) a Clementine lunar topography dataset and a lunar image from the Laboratory for Terrestrial Physics, (2) a full-Earth topography dataset, (3) an ocean temperature dataset from the Laboratory for Hydrospheric Processes, (4) a full 3-D simulation dataset of the Earth's magnetosphere from the Space Data and Computing Division, (5) a global atmospheric temperature dataset from the Laboratory for Atmospheres (illustrated in the figure), and (6) a simulation dataset of instabilities in the solar wind from the Laboratory for Extraterrestrial Physics. Among the results of this test series was the determination that the

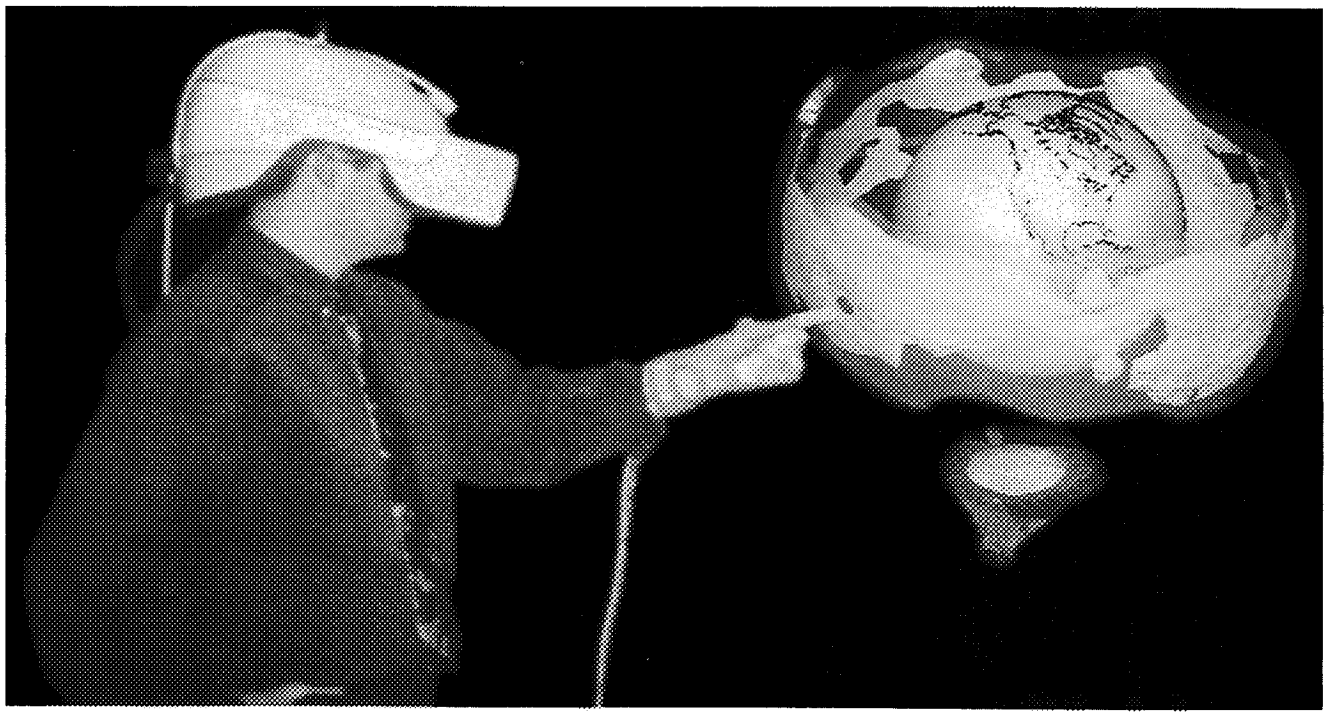

A composite image, superimposing a user wearing a virtual environment helmet and cyberglove on top of the visual model of the temperature of the Earth's atmosphere being viewed by the user.

boom configuration is more useful for scientific visualization than the helmet due to its higher resolution and the precision of the mechanical tracking. Also demonstrated was a virtual instrument, a control device which appears to the user within the visualization, allowing interactive feature control during viewing.

Beginning in October 1994, the VR-FAST virtual environment facility will be operational at GSFC as a test facility of the Space Data and Computing Division. GSFC and HPCC researchers will be able to work with their own data within the system as evaluations are performed on the utility, features, and techniques of the virtual environment system for scientific analysis and understanding.

Contact: Horace Mitchell (Code 932)
301-286-4030
Horace.Mitchell@gsfc.nasa.gov

Sponsor: Office of Aeronautics
Office of Mission to Planet Earth

Dr. Horace Mitchell is Head of the Scientific Applications and Visualization Branch. Dr. Mitchell earned a PhD in Physics from Rice University in 1978. He has been at GSFC for 3 years directing user support and scientific visualization services for the NASA Center for Computational Sciences.

SPACE SCIENCES

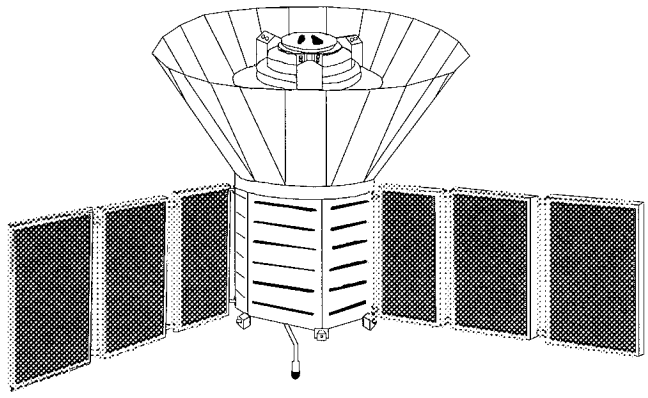

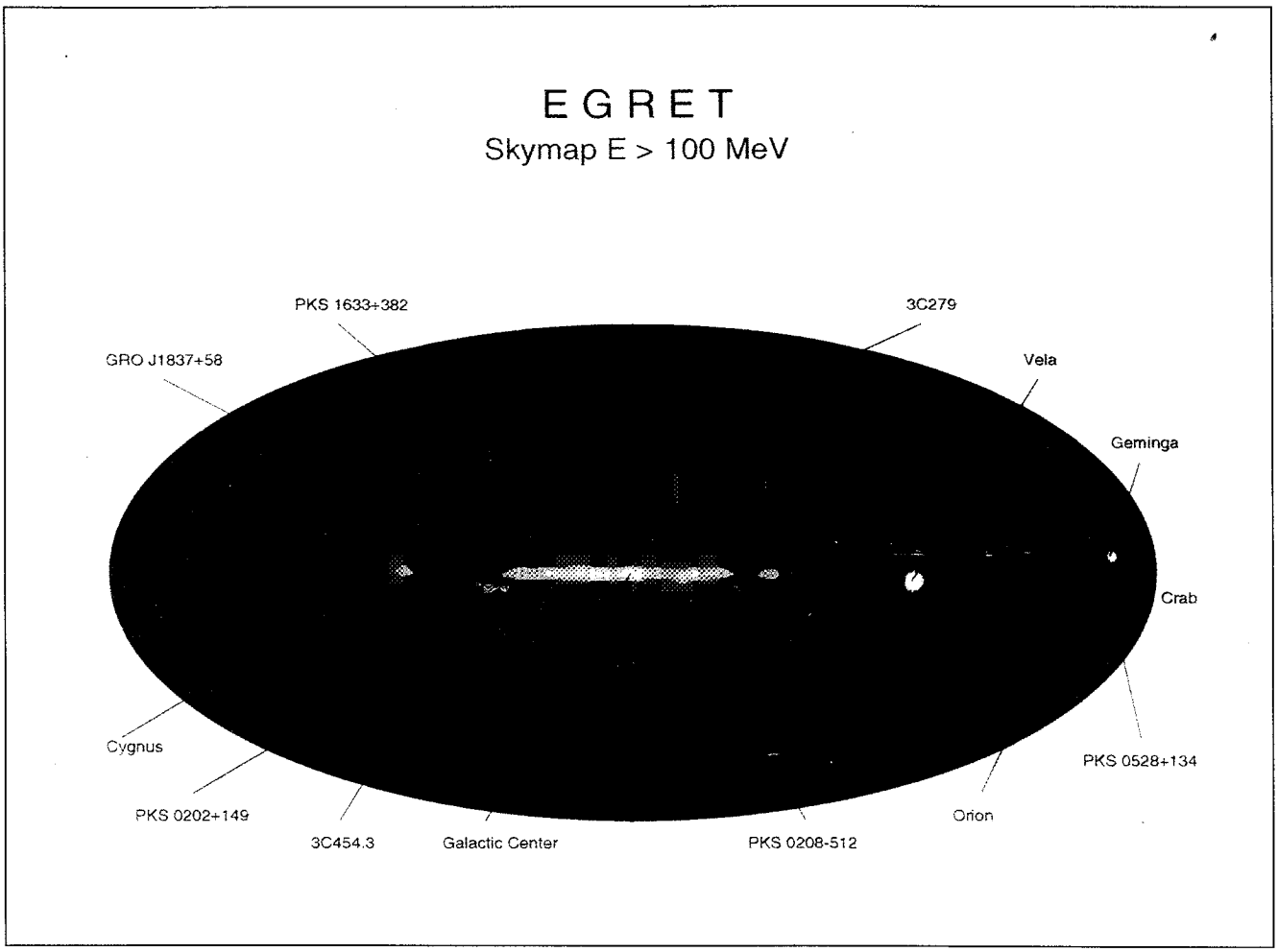

EGRET All-Sky Map—This remarkable image of the entire sky is the culmination of the first all-sky survey in gamma rays. This map, made by the Energetic Gamma Ray Telescope (EGRET) at energies above 100 MeV, shows the diversity of the gamma-ray sky. The diffuse emission from the galactic plane is the most prominent feature along with bright sources like the Crab Pulsar and the quasar 3C 279. EGRET's discovery that the quasars sometimes emit most of their energy in gamma rays has challenged theories of how these objects are powered.

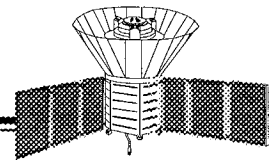

SPACE SCIENCES

THE SPACE SCIENCES DIRECTORATE at Goddard Space Flight Center conducts a vigorous program in astrophysics and space physics through unique instruments and sensors operated at high altitudes in the terrestrial atmosphere and in interplanetary space. The resulting data and conclusions are shared widely with the scientific community and are published or archived for the permanent record and the benefit of future users.

Hubble News

In January, 1994, NASA announced the successful checkout and initial scientific findings from the optically corrected Hubble Space Telescope (HST). The GSFC Space Sciences Directorate provides the staff of project scientists who assisted in the First Servicing Mission and oversees science aspects of the development of future instruments for the HST, including a Goddard Space Flight Center experiment, the Space Telescope Imaging Spectrograph.

Many highly regarded observations and discoveries from the repaired Telescope were reported during 1994 on "Space Astronomy Update," a series of televised briefings that originate at NASA Headquarters and occasionally at this Center, and which are produced and presented in part by scientists of the Directorate. The announced findings represent the work of many accomplished scientists throughout the United States and abroad who conduct research programs with the HST.

The reported Hubble findings included the observation of two glowing rings surrounding the debris from Supernova 1987A, and imaged by HST's new Wide Field and Planetary Camera-2. The rings are much larger than, and not coaxial with, the inner and brighter ring that is centered on the supernova. The three-ring phenomenon is unlike anything previously detected in space, and awaits a coherent general explanation.

Another major announcement came after two HST instruments, the WFPC-2 and the Faint Object Spectrograph (FOS), were focused on the central region of the giant elliptical galaxy M87. The camera imaged a small disk of glowing gas, showing apparent spiral structure, at the center of M87. The FOS observed several locations in the new-found disk and measured large Doppler shifts which indicate that the disk is revolving so rapidly that only the gravitation of an enormous unseen mass at its center could prevent the disk from flying apart. The conclusion appears almost inescapable that there is a black hole with a mass of two to three times the mass of the Sun at the center of M87.

Observations of the Orion nebula with the WFPC-2 showed that what may be a majority of the very young stars in the nebula are surrounded by flattened, dusty clouds. These clouds, dubbed "proplyds," may be protoplanetary nebulae, the potential birth sites of future planetary systems, like our own solar system. However, further work is necessary to establish this interpretation. In addition, it is possible that environmental conditions in the Orion nebula may dissipate or disrupt the proplyds in some or many cases before planets can form.

A fundamental benchmark in surveys of the universe was established as part of the Hubble Space Telescope Key Project on the Extragalactic Distance Scale, an ongoing program to determine an accurate value for the Hubble constant. The latter quantity is the present rate at which the universe is expanding, a parameter that is widely in dispute among astronomers. The benchmark measurement is the distance to the Virgo cluster of galaxies, the nearest large cluster of galaxies to our own Milky Way. The discovery and monitoring of twenty Cepheid variable stars in M100, a Virgo cluster galaxy, enabled the measurement. Cepheid variable stars are pulsating objects that change rhythmically and reproducibly in size, temperature, and brightness. They obey a well known period-luminosity law, according to which the longer the interval between peak brightnesses, the brighter the median magnitude of the star.

Comparing the true magnitudes of the 20 Cepheid variable stars as determined from the period-luminosity law with the apparent brightnesses as recorded by the HST, and making necessary allowance for other known factors, the investigators established that the Virgo cluster is located 17.1 Megaparsecs (about 56 million light years) from the Earth. A likely conclusion is that the Hubble constant is about 80 kilometers per second per Megaparsec. If so, the time since the Big Bang may be as small as 8 billion

years or as large as 14 billion years, depending on the average density of the universe. The seeming conflict of these quantities with the ages previously determined for the oldest known stars (up to about 16 billion years) needs to be resolved through further determinations of the Hubble constant and careful examination of the theory of stellar evolution, from which star ages are estimated.

According to earlier observation and theory, the lower the mass, the more stars are formed. Thus, stars 100 times more massive than the Sun are relatively rare, but stars with half the mass of the Sun are numerous. However, observations of a globular star cluster with the WFPC-2 suggested that the star formation process begins to cut off at masses below about one-fifth the mass of the Sun. The WFPC-2 images showed that there are many fewer of the smallest hydrogen burning stars (red dwarfs) with 0.2 solar masses or less than expected.

Observations of very distant galaxies with the WFPC-2 showed that elliptical galaxies are present in seemingly aged condition, with the red colors and smooth shapes characteristic of old stellar systems, at an era only about two billion years after the Big Bang. This may cause astronomers to reexamine theories of how long it takes a galaxy to form and develop to its final state.

The repaired Hubble Space Telescope contributed mightily to the study of the solar system, through superb and timely visible light and ultraviolet images of the impacts of fragments of the split comet Shoemaker-Levy 9 on the planet Jupiter in July, 1994. The HST also obtained spectrograms indicating significant changes in the chemical composition of regions of Jupiter's atmosphere after the impacts. HST also obtained what appear to be the first images of the surface of Saturn's large moon, Titan, whose substantial hazy atmosphere defeated earlier attempts to glimpse its surface by the interplanetary space probes Pioneer 10, Pioneer 11, and Voyager 2. In addition, HST images of Neptune showed that Neptune's Great Dark Spot, discovered by Voyager 2 in August, 1989, had vanished from the planet, although the Great Red Spot on Jupiter has persisted for at least three centuries.

Cosmology and High-Energy Astronomy

Investigations of conditions in the early phases of the universe draw major support from the huge store of systematic data collected by instruments onboard the Cosmic Background Explorer (COBE). In recent work, COBE scientists are systematically analyzing measurements from COBE's Diffuse Infrared Background Experiment, to identify the changing signature of the zodiacal dust cloud through which the Earth moves in its orbit around the Sun, and to likewise account for other "foreground" emissions from sources such as the interplanetary dust of our Milky Way galaxy. Eventually, this work might lead to the discovery of a theorized cosmic background of infrared radiation from the early epoch at which vast numbers of galaxies first formed through the universe.

Recent findings from the Compton Gamma Ray Observatory (CGRO) include the detection of gamma ray bursts at energies 100 times greater than previously observed. These extremely high-energy gamma-ray emissions are found to persist much longer than the associated gamma ray bursts with lower energy photons. And, in studies of so called blazars with the Energetic Gamma Ray Experiment Telescope on CGRO, astronomers found that some are highly variable, with huge changes in energy emission on very short time scales, although blazars are identified with the nuclei of distant galaxies. Many gamma ray emissions were detected with characteristics resembling those from one class of blazars, the "optically violently variable quasars," although no associated quasars are found in telescopic records. This may mean that there exists a previously unknown class of quasars that are very dim in ordinary visible light, but which shine brightly in high-energy gamma rays.

Solar System

Space physicists investigated related problems of the Earth's magnetosphere (the huge region surrounding our planet that is filled with lines of force from the Earth's magnetic field), and the solar wind, which streams out from the Sun and disturbs the magnetosphere. Studies of the solar wind inward to about one-third of an astronomical unit from the Sun showed that a significant class of known disturbances in the solar wind do not arise from circumstances as it travels outward through space, but rather originate very near the Sun itself. Observations in the magnetotail, the portion of the Earth's magnetosphere that extends far from the Earth in the direction opposite the Sun, and which responds to major disturbances in the solar wind were subjected to careful analysis and modeling with advanced three-dimensional magnetohydrodynamic

techniques. The measurements were gathered by the GEOTAIL spacecraft. Surprisingly, structures in the magnetotail called flux ropes, which were generally thought to be oriented parallel to the long dimension of the magnetotail, were found to extend perpendicular to it, or across the tail. Research in this area will contribute to a better understanding of the relationship between phenomena in the solar wind, the magnetotail, and the magnetic substorms that occur on Earth.

Some Space Sciences investigations extended downward to the ionosphere, the region of the Earth's atmosphere that reflects lower frequency radio waves, which enabled radio communications across the seas before the advent of communications satellites. It was found that significant electric field disturbances of a type usually associated with thunderstorms occur on numerous occasions at altitudes well above 100 km. Previous theory held that the stimulus of the electric field disturbance cannot propagate upwards from the thunderstorm region to beyond this altitude. Investigators are following up this discovery from the San Marco D satellite by examining the possibility that heating events from thunderstorms alter the electrical properties of regions near the 100 km layer, allowing the storms to trigger the disturbances at higher altitudes that were detected by San Marco D.

The lowest layer of the Earth's atmosphere is the troposphere, which is frequently subject to pollution from the activities of human beings. A new computer modeling method, developed by planetary scientists to study the chemistry of the atmospheres of the giant planets Jupiter, Saturn, Uranus, and Neptune, can also be applied to allow students in the classroom to examine the consequences to the troposphere of various kinds of pollution releases on the Earth.

New Techniques

New technologies developed to support forefront investigations in space science often lead to applications in industry. For example, a new technique to bond advanced ceramics, composite materials, and other substances to unlike materials has been used to construct laboratory apparatus to study particulate matter under the conditions that may have applied when the solar system formed. (This apparatus has been successfully tested onboard NASA's Reduced Gravity Research Aircraft.) The related new bonding technologies are now being pursued in industry to develop equipment to monitor emissions from industrial smokestacks, and for developing improved processes for fabricating automotive components and jet aircraft brake pads.

Kenneth J. Frost
Stephen P. Maran

HIGH-ENERGY ASTRONOMY

TWO PARAMETERS FROM A BILLION DATA SAMPLES: COSMOLOGY FROM SPACE DATA

IS IT POSSIBLE for us to understand the large-scale properties of the Universe using data collected from the vantage point of our tiny Solar System? How did the Universe begin and how did it evolve? What is the Universe made of? What data can answer these key questions of modern cosmology (the study of the origin and evolution of the Universe)? While there are only a handful of observable phenomena available to help answer these cosmological questions, it is surprising how much we can conclude about the Universe as a whole. Indeed, the Cosmic Background Explorer (COBE) satellite, the National Aeronautics and Space Administration's (NASA's) first space mission dedicated to cosmology, has been successful in its attempt to find the proverbial needle in a haystack. Using the Differential Microwave Radiometer (DMR) instrument aboard the COBE spacecraft, two cosmological parameters were determined from a billion data samples, but only with the use of additional fake "data" samples from computer-simulated Universes.

The 1929 discovery that our Universe is expanding led to the Big Bang theory of cosmology. This theory allowed specific predictions to be made about the material content of the Universe that were later verified by observations. The Big Bang theory also allowed the prediction that there should be a cold faint relic glow in the sky remaining from the hot Big Bang that began the Universe 15 billion years ago. The glow, called the cosmic microwave background radiation, was discovered in 1964. The glow is a fossil record of the history of the Universe, and much can be gleaned by measuring its properties (see the first figure). There are many impediments, however, to conducting these difficult measurements. The atmosphere of the Earth is a major obstacle to observational attempts to study the afterglow of the Big Bang from the ground, so NASA launched the COBE satellite in 1989. The satellite completed its observations in December 1993. The Far Infrared Absolute Spectrophotometer (FIRAS) instrument on COBE was successful in measuring the relic glow, and determined that the radiation temperature is only 2.726 Kelvin (degrees Celsius above absolute zero).

One aspect of cosmology that causes some puzzlement is the origin of structure we see in the heavens. We see galaxies and we see patterns of galaxies that stretch across the sky. We know that these structures came about by fluctuations in gravitational attraction, but we do not know the source of these fluctuations. However, the same fluctuations that allowed structures to grow via gravity should also cause tiny variations in the temperature of this afterglow radiation from the Big Bang. After unsuccessful

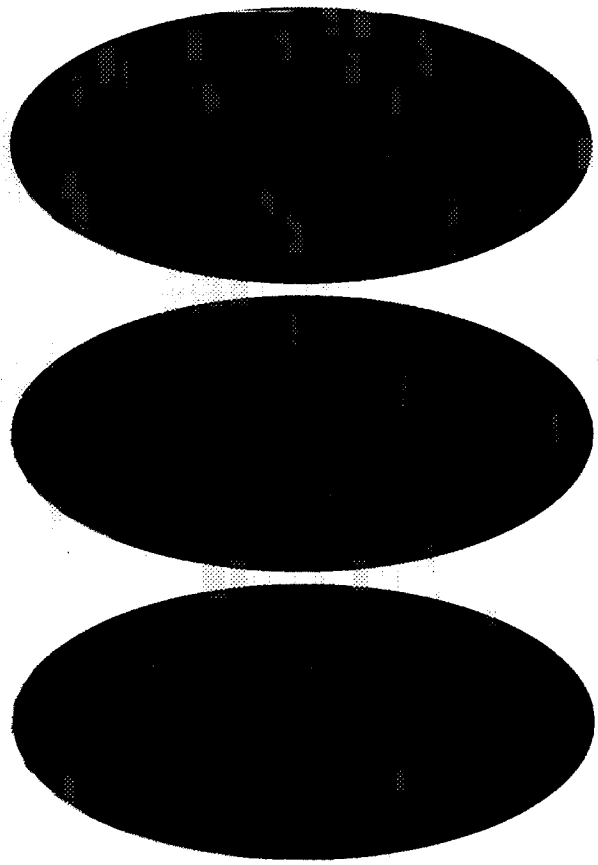

(top) The real COBE Differential Microwave Radiometer projected full sky data showing red band of microwave emission from our Milky Way galaxy. (middle) The Milky Way microwave emission was modeled and subtracted to give the middle oval sky projection. The black region near the center of the picture is due to uncertainty in the microwave emission model. (bottom) Simulated microwave anisotropy data. Note the general similarity between the real data in the middle oval and the simulated data in the lower oval.

searches for these fluctuations over the course of several years, even the DMR instrument on COBE determined that the temperature of this afterglow radiation from the Big Bang is uniform across the sky to a part in a hundred thousand. But, at this faint level the DMR investigation discovered cosmic temperature fluctuations for the first time—a major success for modern cosmology. Several steps in the data analysis were required, however, to reach this important conclusion.

The first step in determining whether the data really show faint fluctuations in the cosmic microwave background temperature was to eliminate nonrandom contaminating signals in the data arising from the DMR instrument itself, since not all of the signals made by the instrument were separated easily from the data (see the second figure). The second step was to average the billion data points available to seek out faint signals. At that level, the DMR instrument detected tiny temperature fluctuations despite the fact that the DMR instrument itself generated noise that was 10 million times greater than the cosmic signal. It was only by virtue of averaging together the billion data samples received that such a sensitive level could be reached. After the data were averaged, the results were compared with the range of results obtained by performing the same analysis on Monte Carlo-simulated data. Ironically, a billion real data samples could only be understood with the inclusion of these simulated "data." The result of the comparisons was strong evidence that the observed temperature fluctuations were real, and not simply due to noise or other instrumental effects.

Yet another impediment to determining the validity of the measurements arises from our location in the Milky Way galaxy, which contributes its own radiation signal to the measurements. The local Milky Way radiation had to be modeled and removed from the data to allow study of the underlying cosmological signal. Even so, separating the cosmic fluctuations from the noise, other instrumental effects, and the Milky Way emission with the billion data samples was not enough. The final step was to assess what this particular observed level and pattern of temperature fluctuations across the sky teaches us about our Universe. The data were therefore examined relative to the expected cosmological models, which are specified by two free parameters: the fluctuation amplitude and a parameter that summarizes the fluctuation pattern. All of the billion data points were included to derive these two parameters. Thus the COBE DMR data points undergo true data reduction—from a billion numbers to only two!

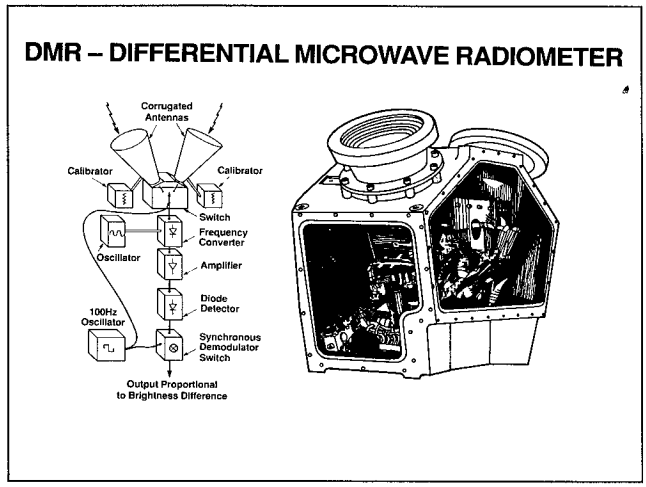

The Differential Microwave Radiometer instrument with a schematic diagram of the signal flow.

We must recognize that we are at a specific (although not special) location in the Universe and that what we measure about the Universe would be somewhat different if observed from a different vantage point. We would like to launch space probes that travel around the Universe, making measurements from many locations, so we could determine the average properties of the Universe and how much variance there is from one spot to another. That, of course, is not feasible. Instead, we attempt to understand the meaning of our data by simulating data. We ask the computer to give us pictures of what the sky would look like from thousands of different vantage points for specified ranges of cosmological models. We then compare our actual sky data to the fake sky "data" and pose the question of how likely it would be for us to have obtained our real data for each cosmological model. It so happens that the uncertainty in the two final cosmological parameters determined by the experiment depend more on the fake computer-simulated data than on measured sky data. In other words, the experiment tells us as much as it possibly could have about cosmology. We are limited in our knowledge not by the apparatus, but rather by our limited vantage point in the Universe.

COBE data are available through the National Space Science Data Center (NSSDC) and have been used and referenced by hundreds of scientists around the world.

Contact: Charles Bennett (Code 685)
301-286-3902

Sponsor: Office of Space Science

Dr. Charles Bennett is the Deputy Principal Investigator of the DMR experiment on the COBE mission. Dr. Bennett received his PhD in Physics from the Massachusetts Institute of Technology in 1984. He has been at GSFC for 10 years, where he is Head of the Infrared Astrophysics Branch.

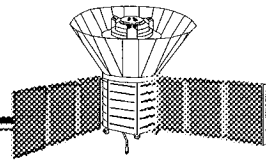

THROUGH THE PRESENT TO THE PAST: THE DIFFUSE INFRARED BACKGROUND EXPERIMENT SEARCH FOR LIGHT FROM THE EARLY UNIVERSE

IF WE LOOK AT THE clear night sky on a summer evening, far from the lights of cities, we see individual bright stars and a hazy glow, stretching from north to south. We now know that this glow is the combined light of the millions of distant stars of our home galaxy, the Milky Way. Our galaxy is a flattened disk, with its center visible in the southern summer sky for U.S. observers. As we look beyond our own celestial neighborhood, the combined light of millions of galaxies like our own further contribute to the light of the night sky. The light we receive from the very distant parts of the Universe has been on its way to us since the Universe was very young. The measurement of this light from the distant Universe provides us with a way to directly observe the Universe when it was young, to see light from the first generation of galaxies to form after the Big Bang. This insight into the early history of our Universe does not come easily. There are many interfering sources of emission which make the detection and identification of this light from the early Universe difficult. Sources of such interference include the Earth's atmosphere, the telescope, and all the intervening celestial sources.

The Diffuse Infrared Background Experiment (DIRBE) on the COBE satellite was designed to answer the question: "How bright is the night sky, and what does knowledge of the sky brightness tell us about the origin and evolution of galaxies and the Universe?" The experiment was designed to operate in the infrared part of the spectrum, with wavelengths just longer than the visible, to the submillimeter region, a factor of 30 in wavelength. (Recall that our eyes are only sensitive over a factor of two in wavelength, from the violet to the red.) DIRBE measured half the sky each day, scanning a swath which ranged from 60 to 120 degrees from the Sun. Using these scans over the 10 months of operation of this experiment, we have made complete maps of the brightness of the sky.

In the near infrared, as shown in the first figure, the sky is dominated by light from stars in the disk and bulge of our galaxy, with an additional diffuse glow from sunlight scattering off the dust particles in the Solar System like dust motes in a sunbeam. The plane of our galaxy, the Milky Way, is the horizontal swath bisecting the map. The S-shaped band follows the plane of the Solar System. This is the

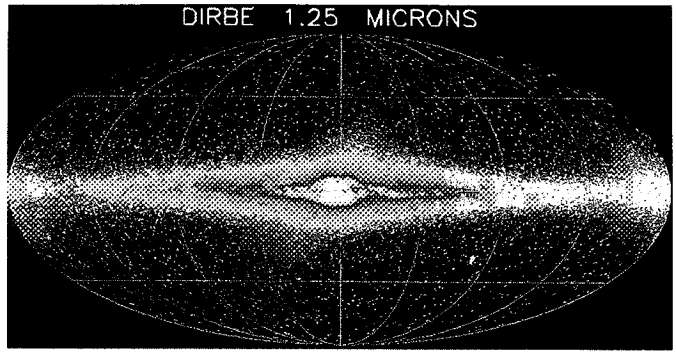

A map of the sky at a wavelength of 1.25 μm.

Zodiacal light. At this wavelength, we see the distribution of stars in our galaxy, and scattered sunlight in our Solar System. Note the bands of interstellar dust absorbing some of the starlight near the Galactic Center. Models of the Galactic stellar distribution and the Zodiacal light are developed from this and other DIRBE near infrared measurements to provide an accurate estimate of their total contributions to sky brightness.

As we move to longer infrared wavelengths, we encounter new sources of emission. At long infrared wavelengths, as shown in the second figure, the sky brightness is dominated by emission from the Galactic plane. This emission arises from small interstellar dust particles which are

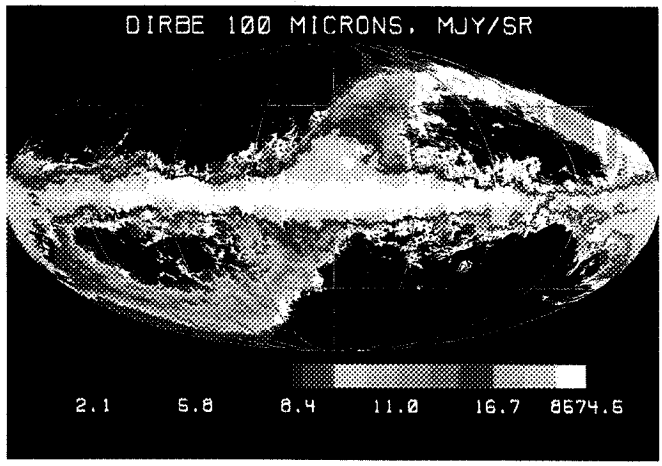

A map of the sky at a wavelength of 100 μm.

heated by starlight to temperatures where they emit strongly in the far infrared (about 20 degrees above absolute zero). At this wavelength, the light we see is re-processed sunlight; the interplanetary dust grains absorb some of the incident solar radiation and re-emit it in the far infrared. The Galactic plane stretches across the image as in the near infrared map, but the familiar stellar emission is gone. The intense far infrared emission arises from circumstellar and interstellar dust heated by the starlight and from dust clouds in regions of recent star formation. The Zodiacal light is again apparent as an S-shaped band across the map. In both figures, part of the emission may arise from distant, early Universe sources.

The removal of the bright emission from the nearby Universe requires detailed mathematical modeling of both the Zodiacal light from our Solar System and of the Galaxy. The modeling of the Zodiacal light is particularly challenging, since we are measuring from inside the interplanetary cloud. Inferring the distribution of dust and infrared emissions in the Solar System from our measurements is a little like doing a CAT scan from inside your body. It is computationally challenging, but we have excellent prospects for producing accurate models because of the large amount of high-quality data extending over the 10-month mission. The motion of the Earth during the mission provided us with a variety of perspectives from which to analyze the cloud. The Galaxy is somewhat easier to model. It is basically a flat disk, and relatively simple models fit the observed distributions well. After developing these models for the nearby "modern day" Universe, we can subtract their contributions, peeling away these layers to reveal the light from the distant early Universe.

In this measurement, we are checking the final numbers on the balance sheet of the Universe. Existing measurements provide very weak constraints on the amount of infrared light in the Universe because of the contamination of the measurements by the bright nearby sources. The light from tremendously energetic processes in the early Universe may be hidden behind these bright "present day" sources. Very soon, the DIRBE experiment with its improved measurements and modeling will lift away the foreground sources, allowing us a view into the infancy of our Universe and a new insight into its evolution.

Contact: Harvey Moseley (Code 685)
301-286-2347

Sponsor: Office of Space Science

Dr. Harvey Moseley is a senior astrophysicist in the Infrared Astrophysics Branch of the Laboratory Astrophysics at GSFC. He is a coinvestigator on COBE and the x-ray spectrometer experiments. He received his PhD in Astronomy and Astrophysics from the University of Chicago in 1979. Dr. Moseley has been at GSFC for 15 years, where he has worked on studies of infrared emission and has developed detectors and instrumentation for infrared and x-ray astronomy.

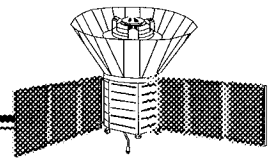

LONG-DURATION, HIGH-ENERGY GAMMA-RAY BURSTS

A GAMMA-RAY BURST occurs approximately once each day and can last from a fraction of a second to several minutes. The direction to the source of each burst is unpredictable. Bursts were first discovered in the 1970s, yet their origin is still unknown. We do not even know if they originate within the Milky Way or at the far reaches of the Universe. The mysterious origin of gamma-ray bursts is further deepened by the data obtained from the Energetic Gamma Ray Experiment Telescope (EGRET) on the Compton Gamma Ray Observatory (CGRO). EGRET is sensitive to the highest energy gamma rays, and has detected photons from gamma-ray bursts of energy up to 100 times greater than data obtained from earlier instruments. These high-energy photons are observed not only at the same time as the lower-energy flux, but also after. While the EGRET observations severely constrain the possible sources of the emission, no candidate source can easily meet all of the requirements imposed by all of the observations of these enigmatic flares of gamma-ray emission.

In the 3 years of operation of the satellite, a half dozen bursts have been intense enough to allow EGRET to detect high-energy gamma rays. These high-energy photons

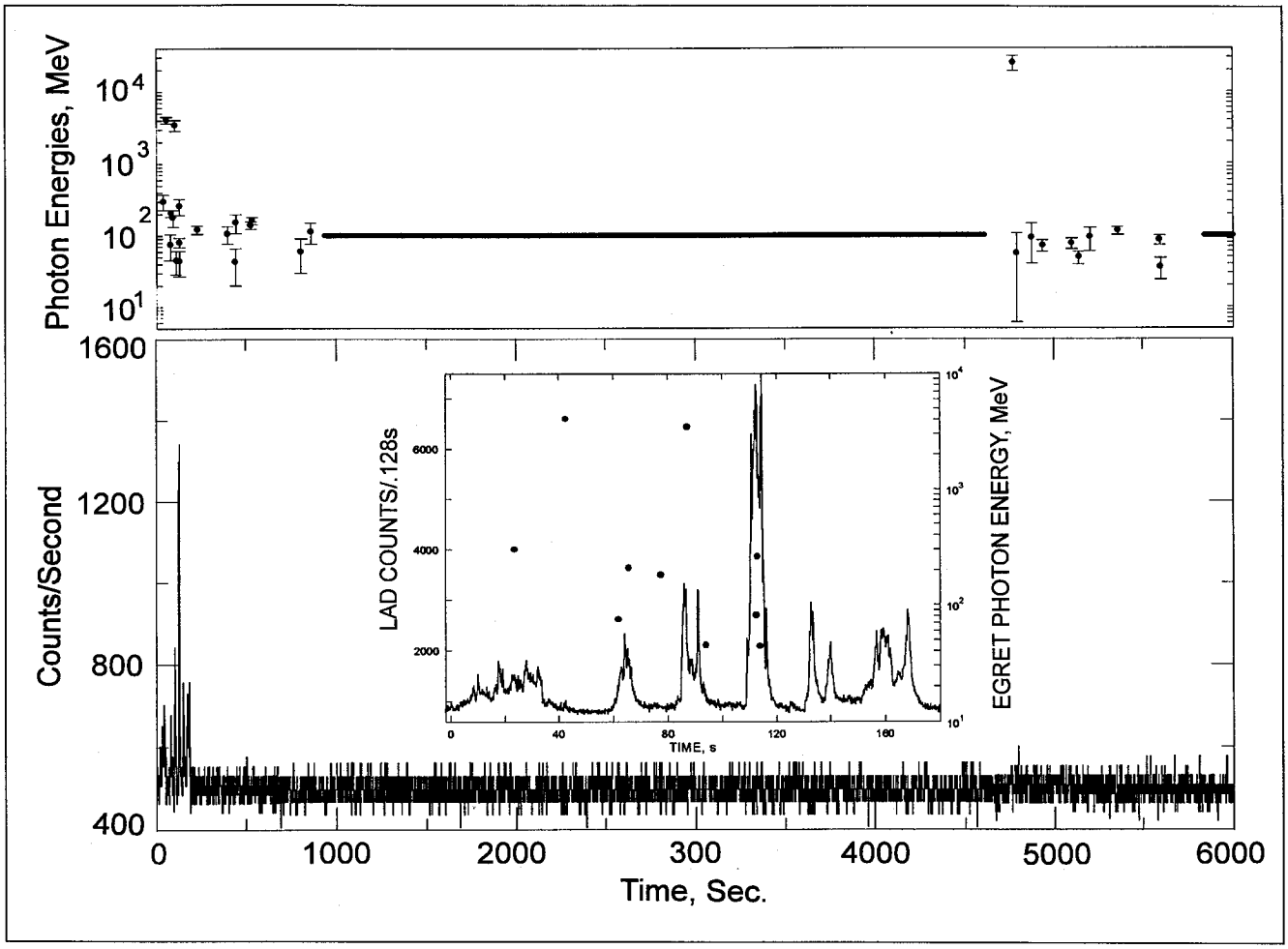

The energies and times of the gamma rays detected by EGRET are shown in the top plot. In the bottom plot is the low-energy, gamma-ray intensity as detected by the Ulysses detector over the same time interval. (The horizontal lines in the top plot indicate when the Compton Observatory view of the burst was blocked by the Earth.)

are considerably fewer than lower-energy gamma rays, partly because they are difficult to produce. On Earth, a particle accelerator is required to attain these energies; by inference, the sources of gamma ray bursts must also have some type of accelerator. It is difficult for high-energy gamma rays to escape the area around the source, because they are easily destroyed by interactions with more plentiful, lower-energy photons. While it is difficult to postulate the reasons for the very existence of high-energy gamma rays, the facts are that EGRET data demonstrates no indication of a cut-off in emission at even the highest energies.

In all of the bursts observed by EGRET, the duration of the high-energy emission is as long or longer than the emission observed for that same burst at lower energies. The longest-duration burst observed to date was on February 17, 1994. It lasted for more than an hour, as compared to 5 minutes for the lower-energy emission. The timing of the observations of the individual photons detected by EGRET and the low-energy gamma-ray intensity as a function of time is shown in the first figure. The highest-energy gamma ray is over 100 times the energy of emission observed in a gamma-ray burst prior to EGRET's measurements. The direction to the source of this gamma ray is shown in the second figure and is consistent with the direction to the source of the gamma-ray burst as determined by several other independent methods, which are also indicated in the figure. The energy of the photon was ~20 GeV (about a billion times the energy of a photon observable by the eye). The photon was detected more than 70 minutes after the lower-energy emission of the burst had disappeared.

Such high-energy emission with such extreme delay had not been predicted by any of the model mechanisms which might produce a gamma-ray burst. Several proposed thermal models are eliminated by the distribution of the energies of the high-energy gamma rays, especially when considered in conjunction with the low-energy gamma rays. The highest energies exclude models involving annihilation at rest. The long duration of the bursts eliminates several models that involve a very short catastrophic event. With these eliminations, what type of origin is still possible? There must be a mechanism that is capable of efficient, very rapid acceleration of particles to relativistic energies and can last over an hour, or there must be a mechanism that allows relativistic particles to interact for that long once created. A sudden release of energetic particles is also possible, but it must be very sudden indeed.

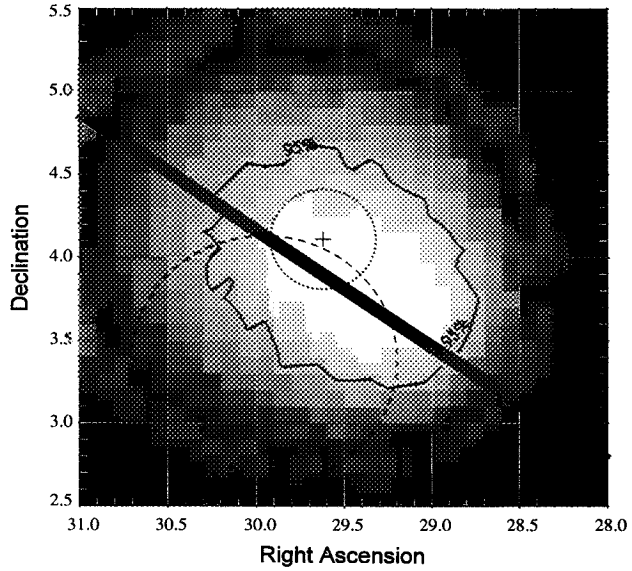

The small dotted circle with the cross in the center is the direction of the highest-energy gamma ray detected in a gamma-ray burst. This photon was detected over an hour after the lower-energy emission had diminished. The brightest colors and the corresponding jagged contour line indicate the most probable direction of the gamma-ray burst as determined from the high-energy photons detected by EGRET during the time interval of the low-energy emission. The dashed circle is the most probable position determined by COMPTEL, another instrument on the CGRO. The narrow green arc gives the position of the burst from the relative time of arrival of the burst at the Ulysses and Compton spacecraft.

There are other theoretical constraints, resulting from observations of the Burst and Transient Source Experiment (BATSE), also on the CGRO. The BATSE results indicate that the distribution of gamma-ray burst sources in space is very nearly a spherical, symmetric distribution when viewed from the Earth. All of these constraints provide a significant challenge for theorists trying to determine the origin of these mysterious bursts.

Contact: Carl Fichtel (Code 662)
301-286-6281

Brenda Dingus (USRA)
301-286-6617

Sponsor: Office of Space Science

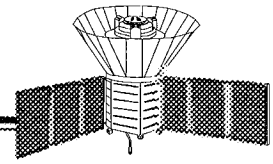

Dr. Carl Fichtel is chief scientist in the Laboratory for High Energy Astrophysics, Acting Head of the Gamma Ray Astrophysics Branch, and a Senior Goddard Fellow. Among other awards, he has received the John C. Lindsay Memorial Award and the NASA Exceptional Scientific Achievement Medal. He holds a PhD from Washington University in St. Louis.

Dr. Brenda Dingus began working at GSFC 5 years ago. She is now a research scientist with the Universities Space Research Association (USRA) and a member of the EGRET scientific team. Her research interests include gamma-ray bursts, as well as detector development. She holds a PhD from the University of Maryland and a BS from Harvey Mudd College.

NEW INFORMATION ON GAMMA-RAY BLAZARS

DURING ITS FIRST 2 years of operation, the EGRET on CGRO discovered 44 gamma-ray sources which have been identified with radio-loud, optically violently variable (OVV) quasars, or with related objects known as BL Lac objects. The OVV quasars and the BL Lac objects are sometimes collectively called blazars.

Although gamma-ray emission had been anticipated from such objects, it is remarkable that some of the detected objects are at very great distances, while similar objects which are much closer are not detected as gamma-ray sources. Indeed, a detailed analysis of the objects shows that the gamma-ray sources at larger distances tend to be brighter than those which are closer. Since an object observed at a great distance from us is younger than a closer one (because of the fixed velocity of light, the light we see now from very far objects was emitted when they were relatively young), this means that the gamma-ray sources are bright when they are young and become dimmer when they age.

A comparison of the energy output in the different wavelength bands shows that the maximum energy emitted in the gamma-ray regime is much larger than in any other wavelength band except for those objects generally called BL Lac objects. For these objects, the energy output is about similar to that in the optical region. This distinction could provide another criterion for distinguishing between OVV quasars and BL Lac objects, as portrayed in the accompanying figure.

Most of the detected quasars are also highly variable in their gamma-ray emission: a quasar that is seen to be gamma-ray bright in one observation may be completely invisible a month later. Several have been seen to change intensity by a factor of 3 to 5 over a few days' time. Although the analysis is not yet completed, intensive monitoring of the gamma-ray blazars at different wavelengths— from radio through gamma ray—indicates that the variability is highest in the gamma-ray portion of the spectrum.

Several dozen sources have been seen by EGRET for which there is no clear identification with objects known at other wavelengths, although their gamma-ray properties appear to be quite similar to those for which identification has been possible. Since the gamma-ray measurements are generally less sensitive than those at

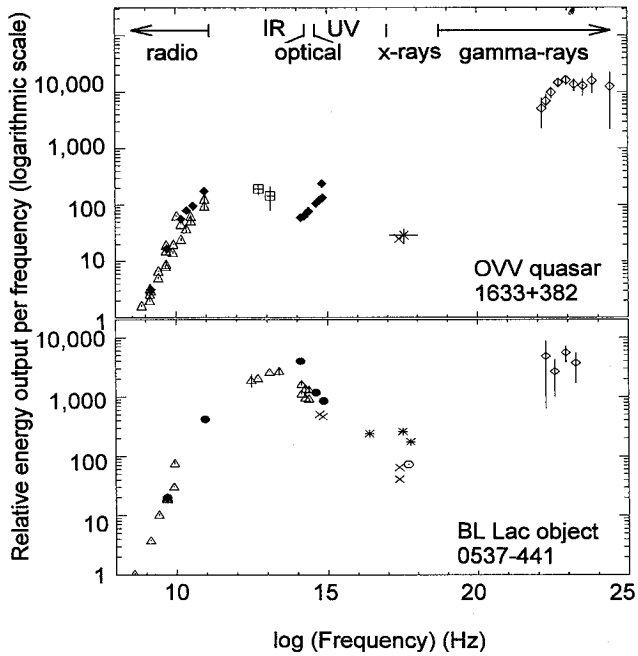

Examples of two multiwavelength spectra, showing an OVV quasar whose luminosity appears to be dominated by the gamma-ray output, and a BL Lac object whose gamma-ray luminosity is comparable to that at infrared wavelengths.

radio and optical frequencies, this might suggest that there are some quasars which are bright in the gamma-ray regime, but surprisingly dim in other bands.

Based on the similarities to those detected by EGRET, a number of blazars already known from observations at other wavelengths have been predicted to also emit gamma radiation, but have not been detected by EGRET. This may be explained by the general variability of these objects. It may be that those which are as yet undetected just have not "blazed" while EGRET was looking. Another possible explanation is that the gamma-ray radiation from these blazars is not emitted in our direction. Gamma radiation is very likely emitted from jets found associated with these objects. Such jets are well-known features of active galactic nuclei, and are seen in the optical, as well as in the radio, bands. This could mean that the gamma radiation is more narrowly beamed than the radio and optical radiation. Further observations should provide more complete answers on how general gamma-ray emission is among blazars and related objects.

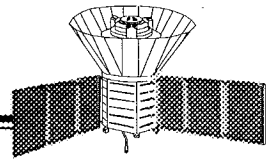

Contact: Robert Hartman (Code 662)
301-286-7178

Corinna von Montigny (NRC)
301-286-6396

Sponsor: Office of Space Science

Dr. Robert Hartman is a coinvestigator for the Energetic Gamma Ray Experiment Telescope on the Compton Gamma Ray Observatory. He earned a PhD in Physics from the University of Chicago, and has been at GSFC for 25 years, where he works in the Gamma Ray Astrophysics Branch developing detector systems for high-energy gamma-ray astronomy.

Dr. Corinna von Montigny came to GSFC in January 1994. She is now a Resident Research Associate with the National Research Council and a member of the EGRET scientific team. Before coming to GFSC, she participated in the software development for EGRET at the Max-Planck Institute for Extraterrestrial Physics in Germany. She received a diploma in Physics from the University of Tuebingen and her PhD in Physics from the Technical University of Munich.

THE COMPTON GAMMA RAY OBSERVATORY: NEW RESULTS FROM COMPTON DATA

THE ARTHUR HOLLY CGRO is the second in NASA's series of Great Observatories. Its complement of four experiments, designed to detect celestial gamma rays, represents a dramatic increase in sensitivity, angular resolution, and energy coverage over previous gamma-ray missions. Carried into orbit on April 5, 1991 by the Space Shuttle Atlantis, it has been in continuous operation since then, providing the scientific community with an unprecedented wealth of gamma-ray data. The observing program carried out in the early phases of the mission has resulted in the first all-sky surveys in medium- and high-energy gamma rays. The data for the survey at high energies is now available through the Compton Observatory Science Support Center (COSSC) at the Goddard Space Flight Center (GSFC) on CD-ROM. The COSSC organization is also responsible for maintaining the public archive of Compton Observatory data products and for providing Guest Investigator support.

Compton Observatory data continue to provide fuel for the debate over the origin of the mysterious gamma-ray bursts. Early Compton results demonstrated that these brief (typically 1 to 100 seconds in duration), intense flashes of gamma rays were isotropically distributed on the sky and cast substantial doubt on the previously held theories identifying burst sources with known populations of galactic neutron stars. The Compton Observatory has now recorded and cataloged over 1,000 of these events, and researchers are combing these data for clues to the burst origins. Recent results, based on public domain data for burst durations, suggest that faint bursts last longer than bright bursts, a result consistent with a general relativistic time dilation expected if the bursts are located at cosmological distances. Other workers have also shown from public domain data that dim bursts contain relatively fewer high-energy gamma rays than bright ones. This result may also be due to time dilation causing a softening or redshifting of burst energy spectra if they originate at cosmological distances.

Still other workers have used Compton Observatory data for the object Mrk 421 in conjunction with other satellite- and ground-based observations to question recent theoretical models for the production of gamma rays in the active galaxies known as blazars. The models predict that variations in the gamma-ray flux of the blazar Mrk 421 measured by the Compton Observatory should correlate with flux variations observed at other wavelengths. The first figure shows that the gamma-ray flux levels recorded by Compton during previous observations of this galaxy have remained fairly constant. Observations at other energy bands, however, have indicated significant flux variations. Most dramatically, this source was observed to flare by an order of magnitude in x-rays and very high-energy gamma rays during the most recent period of Compton observations. The first figure shows that no increase of corresponding magnitude was seen in medium-energy gamma rays. The COSSC organization has supported this research by providing software, analysis facilities, and archival data.

The continuing operation of the Compton Observatory instruments has given scientists the opportunity to monitor many transient sources of high-energy radiation in our own galaxy, studying changes in these sources over time scales ranging from seconds to several years. One group of researchers has undertaken an ambitious long-term project to use Compton data to monitor an exotic class of binary star systems. These systems, also known as accretion-driven pulsars, produce x-rays and gamma rays

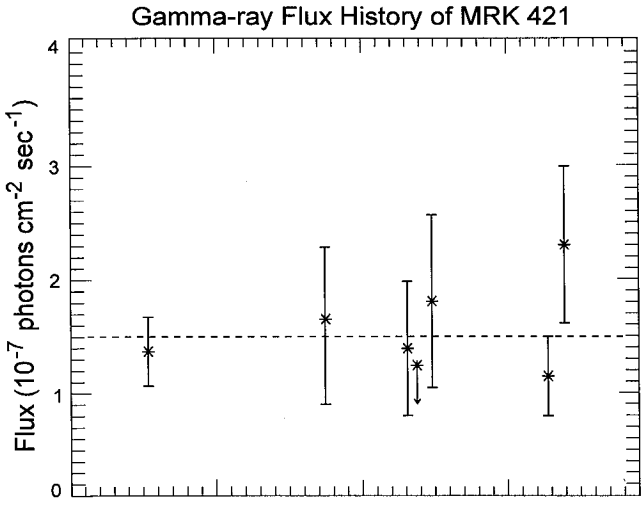

Archival Compton data combined with recent observations of the blazar Mrk 421 illustrates that the gamma-ray flux has remained relatively constant during Compton observations beginning in 1991. The vertical bars on the data points indicate the error in the flux determinations.

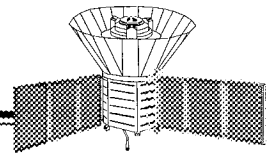

when mass is transferred from the primary star (a giant star with an extended envelope) to the secondary star, a rotating neutron star. The data collected in this monitoring program for the system known as A0535+262, along with a recent intense outburst from this system, has led to a solution for the binary star orbits allowing improved mass estimates for the components. The outburst also revealed the existence of "quasi-periodic" oscillations (QPOs) in the system's x-ray and soft gamma-ray flux. The general increase in flux from A0535+262 over the period from February to March 1994, based on CGRO data, is shown in the second figure. A detailed analysis of these data revealed the regular oscillations that are evidence of the neutron star's rotation and the QPOs, which are interpreted as evidence that the mass transfer to the neutron star occurs as "blobs" of stellar material falling through the neutron star's magnetic field and onto its surface. Researchers noted that both the regular oscillations and the QPOs showed an increase in frequency during the outburst, providing observational linkage between the mass transfer rate of the system and the rotation and magnetic field characteristics of the neutron star.

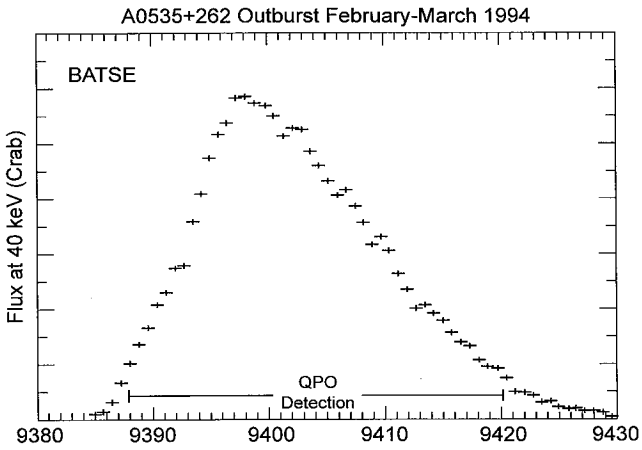

The soft gamma-ray flux level in units of the Crab Nebula flux for the accretion-driven pulsar A0535+262 is seen to rise dramatically during the period from February through March 1994. A more detailed analysis of the data shows the onset of "quasi-periodic oscillations" (QPOs) during the outburst over the period indicated.

Archival research using the Compton data archives, along with the continuing operation of the satellite observatory, is providing increasingly exciting opportunities and many new results for the astronomical community.

Contact: Neil Gehrels (Code 661)
301-286-6546

Jerry Bonnell (Code 661)
301-286-1579

Sponsor: Office of Space Science

Dr. Neil Gehrels is an astrophysicist in the Nuclear Astrophysics Branch, the Project Scientist for the Compton Observatory, and coinvestigator for the balloon-borne Gamma Ray Imaging Spectrometer (GRIS) and the Transient Gamma Ray Spectrometer (TGRS) on Wind. Dr. Gehrels' research includes gamma-ray studies of active galaxies, supernovae, and the center of our galaxy. He has 11 years of experience at GSFC and holds a PhD in Physics from the California Institute of Technology.

Dr. Jerry Bonnell has been at GSFC since 1987 and is presently with the USRA organization under contract to the Laboratory for High Energy Astrophysics. He has had the pleasure of working on the COBE and IUE projects and is currently a staff scientist with the COSSC. His research interests include gamma-ray bursts and multi-wavelength studies of active galaxies. He received his PhD in Astronomy from the University of Maryland.

WHAT DO HIGH-RESOLUTION X-RAY SPECTROSCOPY OBSERVATIONS TELL US ABOUT CONDITIONS IN PHOTOIONIZED ASTROPHYSICAL PLASMAS?

PHOTOIONIZED PLASMAS are important in a large fraction of cosmic x-ray sources. These include some of the brightest sources in the sky, and the most extensively studied, in addition to some of the faintest and most exotic. X-ray binaries are likely to contain a collapsed degenerate star such as a neutron star, a white dwarf, or possibly a black hole. Active galaxies may be associated with massive black holes, the remnant of the coalescence of a dense cluster of stars. Such objects are intrinsically difficult to study, owing to their relatively small size and the intense radiation and gravitational fields in their vicinity. Study of the reprocessed radiation can provide information which is not available from any other technique. Since the spectrum we observe depends on the conditions in the reprocessor, fitting of observed spectra can constrain the temperature, density, and element abundances. X-ray line spectra from photoionized objects have been observed with several experiments, including the solid state and grating spectrometers on the Einstein (HEAO-2) satellite, and the Broad Band X-ray Telescope (BBXRT) flown as part of the ASTRO-1 mission in the space shuttle in late 1990.

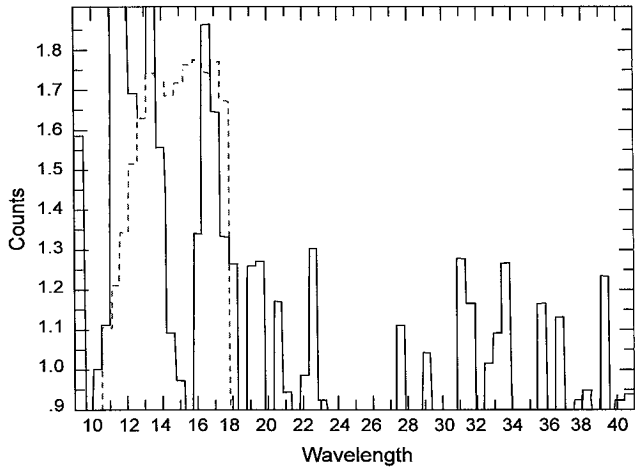

Spectrum of the x-ray binary Cygnus X-2 as observed by the grating spectrograph on the Einstein (HEAO-2) satellite. Vertical axis is logarithmic counts, and the horizontal axis is the photon wavelength in A. Dashed curve is model fit to the observed spectrum. Continuum has been subtracted.

Photoionized plasmas differ in several important ways from the coronal plasmas which are more familiar in many laboratory and astrophysical applications, such as Tokamaks and supernova remnants. Line emission is predominantly by radiative recombination cascades and dielectronic recombination rather than by electron collisional excitation. This leads to distinctly different emission spectra from individual ions. Recombination also leads to free-bound continuum emission, and the continua may be sufficiently narrow to mimic line emission when viewed with the limited resolving power of most past instruments. In a gas which is photoionized by hard x-rays the innermost electrons of ions can be preferentially removed. As this vacancy is filled by less tightly bound electrons, one or more fluorescence line photons may be emitted, producing an additional distinctive signature of photoionization; the most abundant ions capable of emitting these lines are the ions of iron.

The solid curves in the first figure show a spectrum from a bright binary x-ray source, Cygnus X-2, as observed by the grating spectrometers on the Einstein (HEAO-2) satellite. The underlying continuum has been subtracted from the spectrum shown here. The spectrum is as notable for the lines which are absent as for those which are seen. The ions most likely to contribute to the spectrum at these energies are the most cosmically abundant: oxygen and iron. However, the strong 15 A line of Fe XVII, and the La line of O VIII near 19 A are weak or absent. The dashed curve in the first figure represents an attempt at modelling this spectrum using a photoionized plasma consisting of pure iron with a superposition of components of various ionization parameters and emission measures. Clearly, although the positions of the strongest observed features can be reproduced by the model, the contrast between these features and the gaps between them are not reproduced. In spite of this, it is most likely that the emitting gas is photoionized and that oxygen is underabundant relative to iron.

An illustration of the utility of iron fluorescence lines in diagnosing photoionized gases is given by the observations of the Seyfert 2 galaxy NGC 1068. Objects of this class have active nuclei, as evidenced by strong emission lines in the optical and ultraviolet. The first panel in the second figure shows the spectrum of NGC1068 taken with

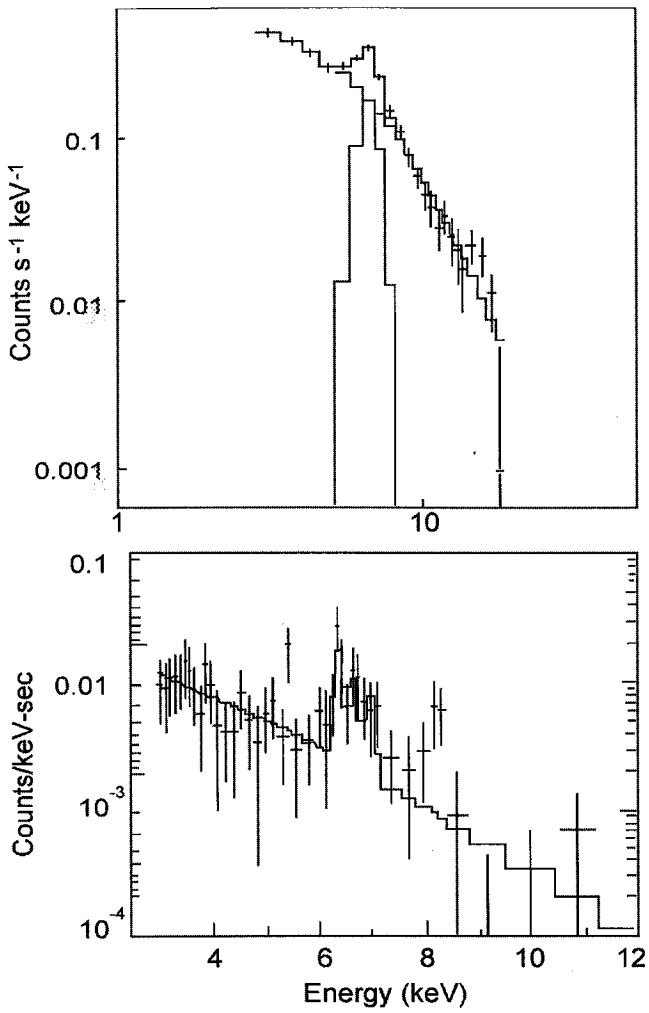

Spectra of the Seyfert galaxy NGC 1068 as taken by the Ginga satellite (top panel) and BBXRT experiment (bottom panel).

the Japanese x-ray astronomy satellite Ginga, showing a strong broad iron line with energy 6.6 KeV and equivalent width 2 KeV. More recently, NGC 1068 was observed at higher spectral resolution by the BBXRT instrument. The spectrum, shown in the second panel in the second figure, reveals that the iron K line can be modelled by 3 narrow components at 6.4, 6.65 and 6.97 KeV. The 6.4 KeV line can only be emitted by fluorescence in neutral or nearly neutral gas, and so is indicative of photoionization. From this measurement we can constrain the column density of this new component of fluorescing gas to be greater than any other known component of gas in this system by approximately an order of magnitude, and we conclude that this gas must nearly surround the active nucleus.

All astrophysical x-ray spectra are affected by photoelectric absorption by material along the line of sight to the photon source. Such material may be quite far from the source and thus unaffected by the radiation from the source. If so, the opacity distribution in the x-ray band can be characterized as an approximately e^{-3} energy dependence. This universal shape has served as an adequate description of the data from many objects.

If, on the other hand, absorbing gas is close enough to the source to be appreciably heated and ionized, then the opacity can be considerably affected. Measurements of the opacity then can serve to constrain the ionization state of the absorbing gas and hence, via modelling, the conditions in the absorber. The opacity distributions from partially ionized absorbers resemble the neutral absorber at the highest energies where absorption is detected, typically near 1 KeV, but have reduced opacities at lower energies. This is interpreted as being due to preferential ionization of the more fragile lighter elements responsible for opacities at low energies—H, He, and C—while heavier elements which dominate the opacities at high energies—O, Ne, and Mg—are more nearly neutral.

An example of the use of photoelectric absorption in diagnosing photoionized plasmas comes from the BBXRT observations of the Seyfert 1 galaxy NGC 4151. This object is thought to contain an active nucleus which is not hidden from our direct line of sight. The third figure shows the count spectrum observed with BBXRT together with fits to a neutral absorber (panel a) and to a photoionized absorber (panel b). It is clear that there is an excess of counts below 1 KeV above the best fit model shown in panel a, while the ionized absorber adequately fits the data at these energies. Together with a luminosity estimate based on extrapolating that observed in the x-ray band the fits shown in panel (b) require that the absorber have a density approximately $30/cm^3$ and a distance from the continuum source of 8×10^{19} cm. This is approximately consistent with the expected position of the gas responsible for the emission of UV lines. However, the gas which

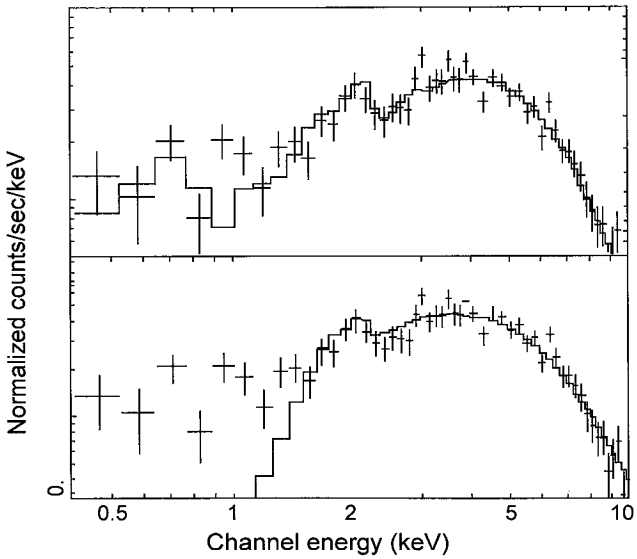

Spectrum of the Seyfert 1 galaxy NGC 4151 as observed by the BBXRT experiment (crosses) fit to models of absorption by neutral (solid curve, upper panel) and partially ionized gas (solid curve, lower panel).

absorbs the x-rays has very much higher ionization; its existence could not have been inferred in the absence of x-ray spectral observations.

Contact: Timothy Kallman (Code 665)
301-286-3680

Sponsor: Office of Space Science

Dr. Timothy Kallman is an astrophysicist in the theoretical office of the Laboratory for High Energy Astrophysics. He earned a PhD in physics from the University of Colorado in 1980. Dr. Kallman has been at GSFC for 12 years, where he works on the development of plasma diagnostics for use in x-ray astronomy.

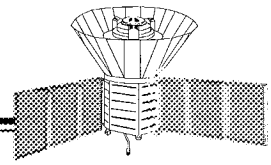

ONBOARD DATA PROCESSING FOR A CALORIMETER X-RAY SPECTROMETER

OUR TEAM, AT GSFC and the University of Wisconsin-Madison, has been developing a new type of x-ray spectrometer using the technique of calorimetry, which involves measuring the heat associated with some process. In our devices, the x-ray to be measured is absorbed in a small mass, and we observe how much the temperature of this mass increases in order to estimate the energy of the incident x-ray. Our ability to do this for individual x-ray photons is noteworthy, since the amount of energy in one of the photons we study (around 1 keV) corresponds to 10^{-19} of the calories a nutritionist would use. To sense such a small amount of energy, we require that the absorber have a very small "thermal mass"—more properly referred to as heat capacity—so that the tiny amount of energy will correspond to a perceptible temperature rise. To achieve such low values of heat capacity, we keep the detectors at a tenth of a degree above absolute zero. At low temperatures, the heat capacities of many materials become quite small, since additional heat is shared among the very few things left to excite, and other degrees of freedom have been "frozen out."

The signature of an x-ray falling upon the detector is a rapid change in voltage followed by an exponential decay. In our present devices, this decay has a time constant on the order of tens of milliseconds. These signals are very slow compared to those produced by more conventional x-ray counters. These pulses appear above a baseline which varies due to several types of noise in these systems. Some of the noise signals, such as those due to electromagnetic pickup or mechanical vibrations in the refrigerator, can be reduced by careful design, while others are intrinsic to the components used to read out the temperature, and will always be present. Our task is to extract the best possible estimate of the pulse in the presence of this noise. Conventionally, this estimation would be performed by analog circuitry, which would pass through a range of frequencies in which the signal-to-noise ratio was relatively high, and use the output of this filter. But it is difficult to design such filters so that they are optimal and so that they can be adjusted for changes in the signal-to-noise function. Since we want to construct the most precise pulse height estimates, we have chosen to implement our filter digitally.

A digital version of a filter is fairly easy to implement, especially for such relatively slow signals as we would encounter. In practice, an analog-to-digital converter (ADC) is used to produce a string of samples from the waveform at the output of the amplifier. In our laboratory experiments, we store these "sweeps," which always include a fair number of samples from before the arrival of an x-ray, and perform the filtering later, using a general purpose computer. The sweep record is examined to make sure that it contains no more than one pulse. We then sum the products of each sample with the corresponding sample of the filter template. Since the x-rays arrive asynchronously with respect with our sampling, and since our trigger does not always place the peak of the pulse into the same bin, we perform this multiply-and-accumulate cycle several times, slipping the alignment of the data with respect to the template by one bin each time. A simple function is then fitted to the sum-versus-alignment phase. Our estimate of the pulse height is the interpolated peak of the fitted function.

For an x-ray spectrometer aboard a satellite observatory, we will not be able to transmit enough data to the ground to represent all the information contained in a complete sweep, so we want to perform the pulse height estimation in the satellite itself. We employ special microprocessors, called digital signal processors (DSPs), with features to support such filtering calculations. These features usually include the ability to perform a multiplication and an addition in one machine cycle, so that the basic calculations underlying our filtering can be performed very rapidly. Systems to be used on spacecraft must be fairly compact, must not use much power, and must not be damaged or upset by the radiation encountered in orbit. This eliminates the commonly available DSP chips, and led us instead to choose a slightly unusual microprocessor. The Harris RTX-2010 is available in a radiation-resistant version, and has relatively low power requirements. The RTX family has an architecture unlike most microprocessors, as it is intended to be used as a "Forth-engine": a processor efficiently executing programs written in the computer language Forth. It has two hardware stacks, one for arguments and one for subroutine return addresses. A subroutine call (within the current 64-k segment) requires only one 16-bit instruction word. The hardware implements only fixed-point operations, so care must be taken to scale our calculations to keep all results in range.

To minimize the number of components needed for each channel, and to maximize performance and flexibility, we decided to not have circuitry look for pulses in the output of the amplifiers, but to instead use the microprocessors

to inspect the sampled data stream to determine when to trigger the pulse height estimation algorithm. By implementing this trigger function in software, we are able to set the trigger thresholds very low; if the in-flight noise turns out to be different from expected values, the software thresholds are much easier to adjust than would be possible with a hardware trigger.

Each channel has an amplifier, some anti-aliasing filtering, and an ADC. The output of the ADC goes to the digital filtering stage, which consists of an RTX chip, some memory, and a semi-custom logic array in which we implement all the various functions needed to interface the parts. After we take measurements of what fraction of time the processors are busy in our breadboard system, we will know whether we can multiplex the data from several channels into one microprocessor.

One of the reasons for adopting digital filtering was that the software solution is much more amenable to adjustment to reflect actual in-orbit instrument performance; as a result, we must be able to vary the filter coefficients. And, since our planned satellite instrument has 32 channels, each with its own filter template, to transmit these coefficients from the ground would require a prohibitive amount of up-link telemetry. Therefore, we have decided to implement the filter template generation process onboard (i.e., the software includes the ability to generate the optimal filter template). This involves collecting an average pulse and an average power spectrum of the noise. The power spectra are formed by applying a fast Fourier transform (FFT) to sweeps taken when no x-rays are present. The optimal template is formed by performing an FFT for the average pulse, calculating the signal-to-noise ratio as a function of frequency, using that ratio to weight the transform of the average pulse, and transforming the result back into the time domain.

We are currently building a breadboard data system to verify this design. This system, which includes detectors, front-end electronics, and cryogenics, will implement full processing chains for two groups of eight channels each. This system will probably evolve into the flight electronics for a calorimeter spectrometer to be flown on the Japanese/U.S. mission, Astro-E, in 1999.

The development of the calorimeter data processing system is the work of a large team. We would like to acknowledge contributions from Richard Kelley, Caroline Stahle, Robert Baker, Jeff Dumonthier, Phong Le, and George Winkert.

Contact: Andrew Szymkowiak (Code 666)
301-286-3528

Kevin Boyce (Code 663)
301-286-3036

Sponsor: Office of Space Science

Dr. Andrew Szymkowiak has worked as an astrophysicist in the X-ray Astrophysics Branch since receiving his PhD in Physics from the University of Maryland in 1984.

Dr. Kevin Boyce has been an electronics engineer in the Electronics Systems Branch since receiving his PhD in Physics from the Massachusetts Institute of Technology in 1992.

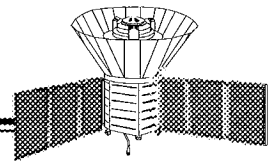

CAUGHT IN THE ACT

IN ASTRONOMY, a star whose brightness is not steady but changes with time is a common observational target. The signals in astronomical data obtained from these stars can reveal much about the stars themselves. Many different mathematical techniques have been used to detect such signals. Often, periodicities were sought because they implied that something regular was occurring in or near the star—an eclipse of one body by another, or a steady pulsation in the star itself. In these cases, the Fourier transform (representing the data as the sum of many different sine curves) is especially useful because it provides clear information on the constant frequencies present in a dataset.

More recently, a number of different analysis tools are being applied to data in an effort to uncover frequencies that themselves change with time. One such tool is the Gabor transform, which is based on the concept of the short-time windowed Fourier transform, using a time interval (or "window") that is usually much smaller than the length of the entire dataset. A small segment of the data is viewed through this window, and the Fourier transform tells us which frequencies are present for that segment of time. The position of the window on the data is then changed, so that we see a different region of the data through the window, and another Fourier transform is computed. Continuing to slide the window along the entire dataset results in a graphical representation of which frequencies are present in the short segments and whether they change from one segment to the next. In the Gabor transform the window is moved by only one data point each time, so that the evolution of the frequencies can be viewed continuously in time. The Gabor transform is the analysis method of choice when the data contain frequencies which change significantly over the duration of the observation.

In the last decade, a class of star has been identified called rapidly oscillating peculiar A-type spectrum (roAp) stars. These stars exhibit cyclical changes in their brightness on very short time scales, typically between 4 and 15 minutes. (The Sun is also known to experience oscillations on this time scale, but of a much smaller amplitude than is observed in the roAp stars.) The strength, or amplitude, of the pulsation has also been observed to oscillate regularly in many roAp stars. There are a number of possible causes for this behavior, according to a theoretical model that has been developed to explain roAp stars. In the model, the material in the star oscillates along the direction of the magnetic field lines of the star. Just as is the case with the Earth, the rotational pole of the star is not aligned with the magnetic pole. As we view the star from Earth, the magnetic pole comes into and out of our line of sight, depending on our viewing angle and the distance separating the two poles on the star. Because of this, the rotation modulates the oscillation, making it appear first stronger and then weaker to observers on Earth. In addition, most roAp stars do not oscillate with only one frequency; in general, several frequencies are active at once. If the oscillations are close to each other in frequency, the result will be a more complicated pulsation called a beat frequency. This is the same effect that can be heard when two violins that are slightly out of tune with respect to one another attempt to play the same note. The sound apparently gets louder and softer periodically; this beating period is determined by the degree to which the two instruments are out of tune. Both rotational modulation and the beating of nearby frequencies produce frequencies that evolve smoothly in time.

The High Speed Photometer (HSP), a first-generation instrument aboard the HST, was designed to record very rapid variations in the brightness of astronomical objects. We used the HSP to observe the roAp star HD 60435 in the ultraviolet region of the electromagnetic spectrum. During our observation, there was an oscillation with an 11.6-minute period present in the data. This oscillation was strong at the beginning of the dataset, but weakened later in the observation. We used the Gabor transform to study the variation of the frequency of the oscillation over time.

The figure presents the results of the Gabor transform applied to the HD 60435 observation. Here we have used color to indicate the relative strengths of the frequencies present in the data. A deep red color corresponds to the strongest frequency present. A black value corresponds to the weakest frequency. The color pallet changes smoothly between the extremes to represent all possible strengths for the frequencies present: red is stronger than yellow, which is stronger than green, while black is weaker than gray, which is weaker than purple. Time is shown along the horizontal axis. Displayed in this way, the Gabor transform is a data visualization tool that provides significant insight. It is immediately apparent from the figure that the 11.6-minute period is very strong in the first ~200 minutes of data, and weakens considerably thereafter. In fact, the rather abrupt "switch-off" observed

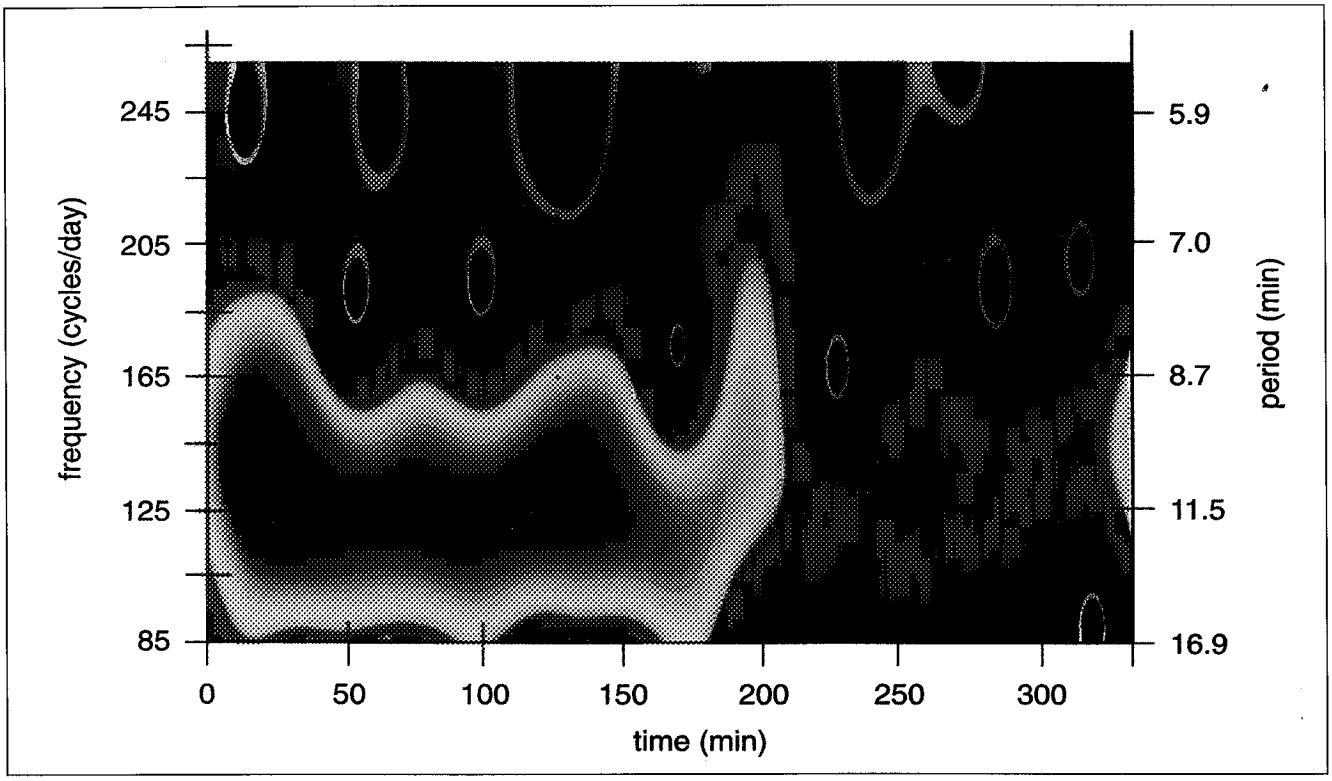

The Gabor transform of HD 60435. Time increases from 0 to 334 minutes along the x-axis; the period ranges from 16.7 to 5.5 minutes on the y-axis. Black corresponds to low power (weak frequency) and red, to high power (strong frequency). At early times, the 11.6-minute period is clearly dominant. There is an episode where the frequency abruptly rises sharply near 200 minutes. After this event, the 11.6-minute period is evident again, but with significantly less power than it had prior to the event.

is surprising, in that it is not consistent with either the beating or the rotational modulation explanation of the frequency evolution. Each of these causes would give a gradual decline with time, from red to blue.

To our knowledge, this is the first observation of a roAp star in any wavelength which has demonstrated such rapid frequency evolution. As a result, we do not yet understand why the oscillation periods in such an roAp star should change so suddenly. However, such an observation testifies to the utility of the Gabor transform in providing graphical insight into systems whose behavior is neither periodic nor well-understood.

Contact: Joseph Dolan (Code 681)
301-286-5920

Patricia Boyd (USRA)
301-286-6493

Sponsor: Office of Space Science

Dr. Joseph Dolan has been studying neutron stars and black holes, the end states of stellar evolution, for 15 years in the Astronomy Branch of the Laboratory for Astronomy and Solar Physics at GSFC. A coinvestigator on the HSP Team on the HST, he is also interested in astronomical polarization. Dr. Dolan holds a PhD in Astrophysics from Harvard University.

Dr. Patricia Boyd is involved in the analysis of HSP data as a GSFC Visiting Scientist with the Universities Space Research Association (USRA), working in the Astronomy Branch of the Laboratory for Astronomy and Solar Physics. Her research interests include binary stars and chaotic evolution in astrophysical systems. Dr. Boyd holds a PhD in Physics and Atmospheric Science from Drexel University.

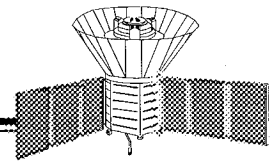

ENERGETIC PARTICLES AND ELEMENT ABUNDANCES IN THE SOLAR CORONA

THE ELEMENTAL ABUNDANCES in a sample of material provide a powerful tool to identify the origin of that material and to understand the physical processes that have formed it. The basic clay which these processes mold is the cosmic or universal abundance (i.e., 90 percent H, 10 percent He, 0.08 percent O, 0.06 percent C, 0.01 percent Ne, etc). The elements other than H and He are trace elements from the abundance standpoint, but they carry most of the information of the nuclear or atomic processes undergone by the specimen. The Sun was originally formed from material having universal abundances; except for the region near its center where nuclear reactions occur, the bulk of the Sun, including the photosphere, still has its original abundances.

High-energy particles, with velocities of ~10 percent of the velocity of light, are accelerated from many different sites in the heliosphere and beyond. Different sources and acceleration mechanisms produce particle populations with different patterns of element abundances. We measure these abundances by simply counting the number of particles of each element of a given velocity that enter detectors flown on spacecraft outside the Earth's magnetosphere. This tool is so powerful that, given the abundance of only a few elements, we can easily distinguish energetic particles from impulsive solar flares, coronal and interplanetary shock waves, the anomalous component from the shock at the heliopause, or galactic cosmic rays.

The most intense sources of energetic particles we have seen are the large gradual solar events. In these events, large filamentary structures of magnetized plasma that often stand motionless above the solar surface erupt suddenly to produce coronal mass ejections. These eruptions drive shock waves out through the corona and solar wind, sweeping up ambient material, and accelerating particles to high energy. On average, these shock waves accelerate particles democratically, providing a direct sample of material from the solar corona. Elemental abundances in these energetic particles provided the first evidence that the composition of the corona was different from that of the photosphere, and they continue to provide our most complete information on coronal abundances. When the ratio of coronal and photospheric abundances of an element is plotted as a function of the element's first ionization potential (FIP), an organized pattern appears, affectionately known as the FIP effect. A sample pattern, from a recent analysis of measurements accumulated by the ISEE 3 spacecraft over the last 15 years, is shown in the accompanying figure. Elements with FIP < 9 eV are clearly enhanced in the corona, by a factor of about 4 relative to those with higher FIP.

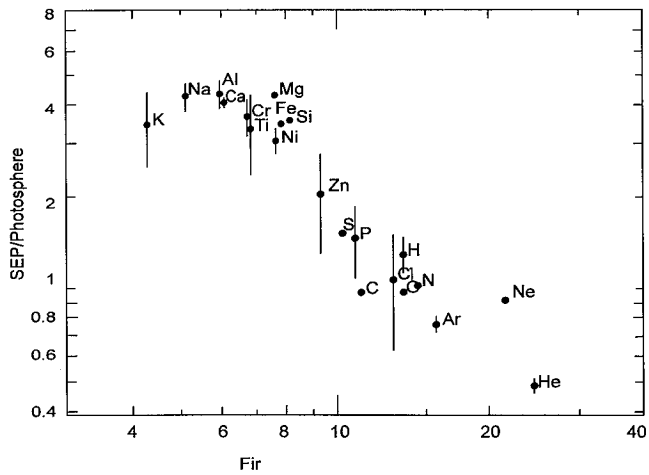

Ratio of element abundances in the solar corona to those in the photosphere as a function of FIP (based upon energetic-particle measurements on the ISEE 3 spacecraft).

At first sight, the FIP effect is surprising, since we know that elements in the hot corona are highly ionized. How could the energy required to remove the outermost electron matter to a coronal Fe ion that typically has had 10 to 16 electrons already removed? The answer lies in the way atoms are transported up into the corona from the photosphere. In the cooler photosphere, low-FIP atoms remain ionized by the abundant 10 eV Lyman-α photons from H, while the high-FIP elements remain neutral. As elements move upward along magnetic flux tubes, the ions are constrained to move along the field lines, while the neutral atoms can leak out of the tube. Thus, more of the ionized, low-FIP elements are delivered to the corona at the top of the flux tube, where they become highly ionized. This qualitative understanding of the ion-neutral behavior is undoubtedly correct. However, the quantitative

understanding of the effect, and especially its variation in different structures throughout the corona, remain active areas of investigation.

Contact: Donald Reames (Code 661)
301-286-6454

Sponsor: Office of Space Science

Dr. Donald Reames is an astrophysicist in the Nuclear Astrophysics Branch. He received his PhD in Physics from the University of California at Berkeley in 1964 and has since specialized in observations of energetic particles, their abundances, and the physics of particle acceleration at the Sun, in the heliosphere, and in the galaxy.

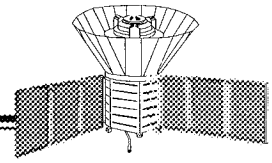

SIMULATION OF THE MAGNETOSPHERE WITH THE FIRST THREE DIMENSIONAL MAGNETOHYDRODYNAMIC CODE WITH ADAPTIVE MESH REFINEMENT

THE CONTINUOUS, high-speed flow of conducting fluid from the Sun, the solar "wind," and its subsequent interaction with the Earth's dipole, bar-magnet-like magnetic field leads to the existence of "boundary layers," such as Earth's bow shock, which represent a sharp transition from one physical state to another. The scale sizes that characterize these boundary layers are usually many orders of magnitude smaller than the scale sizes that characterize the Earth's magnetic field or the solar wind itself. The existence of these boundary layers makes it nearly impossible to simulate the fully coupled solar-wind Earth system globally using standard numerical algorithms without enormous computational expense. Previously, modelers had to be content to model a particular boundary layer separate from the global environment in order to provide a spatial grid adequate to resolve the phenomena. An example of this approach in space physics is the localized modeling of the magnetotail. All of these efforts have improved our understanding of the phenomenon on a local scale. However, as the models used boundary conditions that did not accurately reflect the global evolution of the environment surrounding the boundary layer and could not account for the feedback from the boundary layer during its evolution, the resulting physical picture of how the boundary layer actually affected the global evolution was not satisfactory. The lowest-order physical approximation that permits realistic modeling of a global system plus boundary layers is the magnetohydrodynamic (MHD) approximation.

MHD models of the magnetosphere have been in existence for well over a decade, and have dramatically contributed to our understanding of how the solar wind couples with the Earth's magnetic field to produce the magnetosphere. Heretofore, the spatial resolution of these global models was limited by a combination of processor speed, memory size, and the availability of systems. However, other approaches can help ameliorate the situation. One of these approaches is adaptive mesh refinement (AMR). AMR permits a fine numerical mesh where needed, and nowhere else. In addition, the resolution of the mesh can be as high as one desires consistent with the physical approximation represented by the equations being solved. Finally, any physical parameter or combination of parameters can be used to determine the regions where refinement or de-refinement is desired. For these reasons, AMR is ideal for modelling the complex flows that result when the solar wind forces the coupling of the interplanetary magnetic field (IMF) with the Earth's magnetic field and the resultant boundary layers.

Just as our approach differs from previous approaches to the global modelling of the magnetosphere in that we utilize AMR, our numerical scheme differs as well. Without exception, all previous approaches have used finite volume or finite difference approximations, while we utilize a finite element approach together with dynamic adaptive refinement of an unstructured mesh. (The finite element approach differs from the finite difference approach in that finite elements use a nonorthogonal basis function to represent the transported variables, while the finite difference approach uses a Taylor series expansion to approximate the partial differential equations.) The combination of finite element and AMR on an unstructured mesh provides an extremely powerful tool for modeling the complex dynamics associated with the Earth's magnetosphere, as well as irregularly shaped boundaries common to systems such as the Jupiter-Io system. In addition, the ability of the code to automatically make the mesh finer or coarser in response to the formation and movement of fine features in the flow field is an extremely powerful tool, allowing one to compute very accurately a variety of physical phenomena, such as the current systems that result from the solar wind-magnetosphere interaction. In particular, the boundary layers, such as the bow shock, the magnetopause, the magnetotail, and the polar cusp regions that characterize and, to some degree, control the global dynamics of the magnetosphere, can be resolved in a manner heretofore not possible in global models of the magnetosphere, thereby permitting greater insight into the dynamics of the solar wind-magnetospheric coupling.

The figure illustrates the mesh generated utilizing the 2D version of our MHD code by AMR. Two views are shown: the entire computational domain, comprising an area 1,000 Earth radii square; and an extreme blow-up of the area near the 10-Earth-radii inner-boundary of the domain. The triangles in the most refined regions have a characteristic width of 1.3 Earth radii. Approximately 6,000 nodes

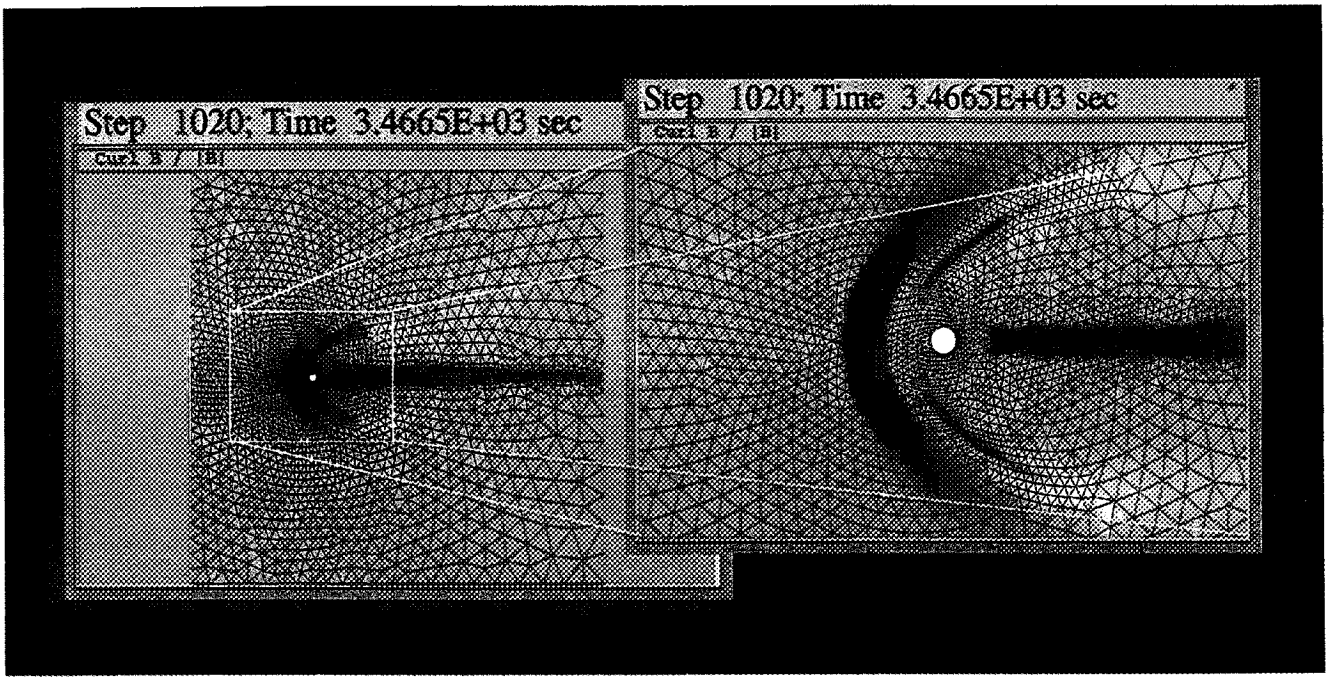

2D representation of the magnetosphere, calculated using AMR techniques. The magnetotail is evident.

comprise the entire grid. Note that if we had been forced to use the grid size corresponding to the most refined regions over the entire domain, 600,000 nodes would have been required, a penalty of a factor of 100 in computer time and memory. Here we clearly see the power of AMR. The detailed structure of the magnetotail is quite evident in the figure. Results from our 3D version of the MHD code show similar results, but, more importantly, illustrate the truly 3D character of the magnetotail in the form of flux ropes.

This work was a collaboration between the ISTP Program and the High Performance Computing and Communications Program.

Contact: Steven Curtis (Code 695)
301-286-9188

Daniel Spicer (Code 930)
301-286-7334

Steven Zalesak (Code 934)
301-286-8935

Rainald Lohner (GMU)
703-993-4075

Sponsor: Office of Space Science
Office of Aeronautics

Dr. Steven Curtis is Head of the Magnetospheric Physics Branch of the Laboratory for Extraterrestrial Physics and deputy Project Scientist for Theory for the ISTP Program. His research interests are primarily in space plasma physics. His PhD is from the Department of Physics at the University of Maryland.

Dr. Daniel Spicer is a senior scientist with the Space Data and Computing Division. His research interests are primarily in space plasma physics. His PhD is from the Department of Physics at the University of Maryland.

Mr. Steven Zalesak works within the High Performance Computing Branch. His research interests are in computational fluid dynamics.

Prof. Rainald Lohner is a Head of the Computational Fluid Dynamics Group at George Mason University. His primary research interests are in computational fluid dynamics.

MULTISPECTRAL IMAGING OF SOLAR SYSTEM OBJECTS USING THE STARFIRE OPTICAL RANGE 1.5-M ADAPTIVE OPTICS TELESCOPE

A NEW CLASS OF highly compact, two-dimensional imaging spectrometer was employed to collect data from the comet Shoemaker-Levy/Jupiter crash events in July 1994. Data were also taken from measurements of Saturn. This imaging camera, which currently operates in the shortwave infrared (600 to 1000 nm), has as its enabling technology an acousto-optic tunable filter (AOTF) cut from a single crystal of TeO_2. This spectral imager operates with high spectral and spatial resolution and with no moving parts. The operating principals were highlighted in the 1993 GSFC Research and Technology Report.

The first figure is a layout of our AOTF camera, showing the key optical elements. This configuration was designed to be used with ground-based telescopes for astronomy at large image scales. It can also be operated as a stand-alone camera by simply attaching a commercial camera lens at the front end. The field is imaged at focal ratios greater than f/13 onto a 3 by 4-mm rectangular field stop positioned at the entrance to the AOTF (marked "Image Plane" in the figure). This position is one focus of a 13-cm diameter elliptical mirror. Orthogonally polarized beams exit the AOTF with a mid-band deflection angle of 7.5°. In this observing run, only one polarization was used. Since the field image is placed near the AOTF, small color-dependent changes in the deflection angle do not result in translation of the final images along the array. Relay lenses place the orthogonally polarized images side-by-side on an elongated (586 by 384) Thompson CCD array.

The experiments reported here were performed on the 1.5-m telescope at the Starfire Optical Range (SOR), which is operated by the Phillips Laboratory, Kirtland Air Force Base, in Albuquerque, New Mexico. The telescope was operated in a laser-guide-star adaptive-optics mode, capable of continuous compensation at 130-Hz closed-loop bandwidths. A copper-vapor laser, focused at a 12-km range, was used as the guide star, and a range-gated sensor operated a continuous-facesheet-deformable mirror that was controlled by 241 actuators. A separate, novel, full-aperture image correlator and a steering mirror was employed to remove overall tilt.

The second figure shows some of the data collected at the SOR. The six panels on the left show some of the S-L9 comet fragment collision sites in two different wavelengths: 890 nm, a strong methane band, showing high altitude plumes formed in the stratosphere, and at 760 nm in the continuum, where one can see down to the cloud tops. Pair (a) was taken at UT 7/20, 03:00, while (b) was taken 40 minutes later, and (c), 1 hour after (b). One can see the collision sites rotate from left to right. The Great Red Spot is marked to identify the central meridian. The trio of images of Saturn on the right was taken at three

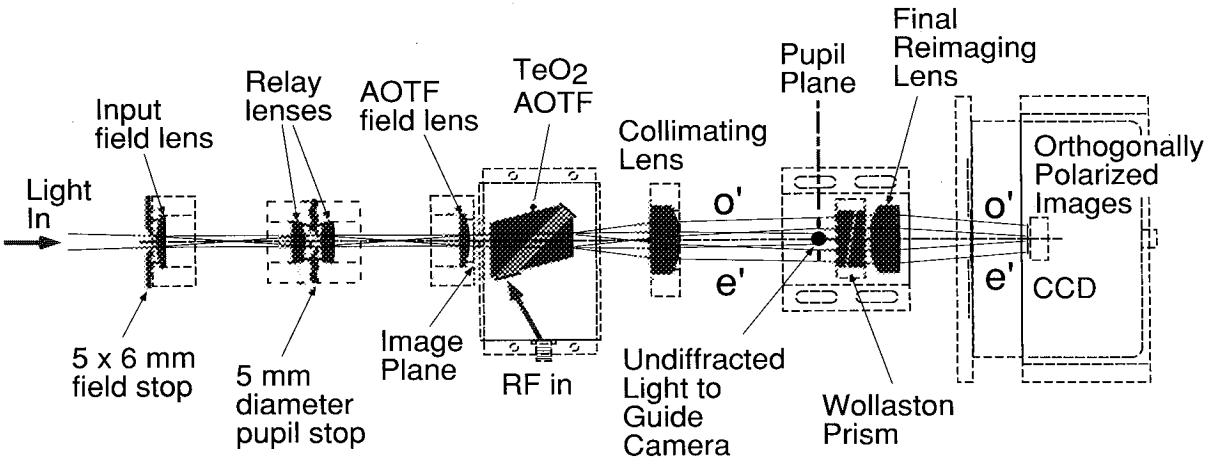

AOTF Camera schematic layout.

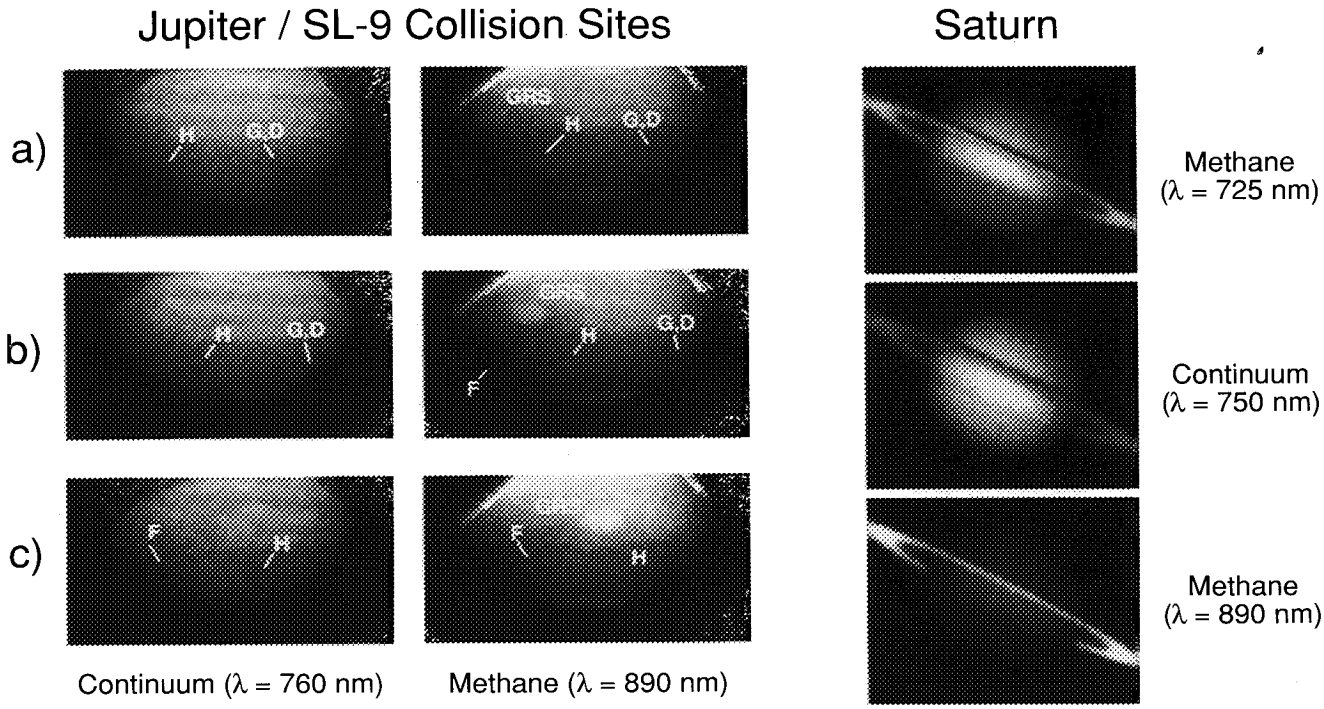

Jupiter and Saturn as seen at SOR. GRS is Jupiter's Great Red Spot.

different wavelengths: in two methane bands of differing strengths, and one continuum wavelength. In these Saturn images, as the reflectivity decreases due to stronger absorption by the atmospheric methane, the rings seen in reflected sunlight, appear much brighter than the planetary disk.

Contact: John Hillman (Code 690)
301-286-7974

David Glenar (Code 715)
301-286-3354

Sponsor: Office of Space Science Directors Discretionary Fund

Dr. John Hillman is Associate Chief of the Laboratory for Extraterrestrial Physics. He has been at GSFC since 1969 working in research related to planetary atmospheres and astrophysics. He earned his PhD in Physics from The American University.

Dr. David Glenar holds a PhD in Astronomy from the Pennsylvania State University. In 1990, he moved to the Engineering Directorate from the Planetary Systems Branch, and is presently Head of the Remote Sensing Section.

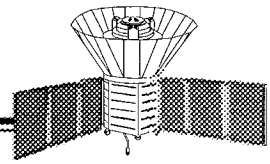

SPACECRAFT OBSERVATIONS OF INTERPLANETARY TURBULENCE

THE SUN INTERACTS with the Earth not only through its light but also through a continuous "wind," composed primarily of hydrogen that has been fully ionized into its constituent protons and electrons by the hot solar corona. Because the particles in the wind are charged, they stretch the Sun's magnetic field—which would otherwise be like the Earth's familiar dipolar field—into a spiral pattern with fields pointing towards the Sun in the northern heliospheric hemisphere and away from it in the southern, over half of the 22-year solar cycle. This ionized wind (a plasma) and associated magnetic field are not quiescent, but rather are continually disturbed by gusts and activity in the Sun's lower atmosphere. What we finally observe with spacecraft is, then, a turbulently evolving medium in which large-scale twists and turns are continually being bent into smaller structures, until finally the scales become small enough for the kinetic energy of the plasma to be dissipated in heating the wind itself. The study of the dynamics of this easily measurable system provides us with information on turbulent systems in general, and with insights on how fluctuations in plasmas play a role in such processes as the heating of solar flare loops or the acceleration of the wind itself.

Our group has studied the solar wind using observations from Helios, Mariner, ISEE, Voyager, and other spacecraft, as well as with computer simulations of magnetized plasmas. Of particular recent interest has been the evolution of the region near the solar equator, across which the average magnetic field changes from inward-pointing to outward-pointing. This "current sheet" region is often seen to be embedded in slower solar wind streams in which the density, temperature, and magnetic field undergo sudden variations, suggesting that each bundle of field lines is associated with very different conditions at its base. The Helios spacecraft probed the inner heliosphere to within one-third the distance between the Sun and the Earth. Our analysis of the data from this mission has shown conclusively that the origin of these variations is indeed in conditions near the Sun rather than in the subsequent evolution of the fields. However, we also find evidence that the structures are eroded as they move farther out. Further analysis and simulation of these regions should help us to understand the sources near the Sun of both the slowly flowing wind and the fluctuations in the fields.

In conjunction with the above studies, we have begun experimenting with novel ways of viewing the spacecraft and simulation data. Particularly as the quantity of data increases with multiple, high-time-resolution spacecraft missions and ever more powerful computers, there will be an increasing need for compact visual ways of seeing qualitative relationships between measured quantities. Our approach has been to exploit increasingly available stereographic technology to move into three dimensions to see vectors and volume-filling fields in their true geometry. This is most easily done on a special computer screen where the images can be manipulated. The figure shown here is a stereoscopic pair of images which illustrates the basic concept. The figure shows the magnetic field vectors along the Helios spacecraft trajectory in the region of the current sheet. Temperature is indicated by the colors; the density is represented by symbols along the axis. Note that the region where the average field flips direction is generally cool and dense but with strong variations, and that the field is much more complex than the simple picture of spirals would suggest. These techniques are in their infancy, but we expect that they will lead to more rapid and new insights into the data and the phenomena which they represent.

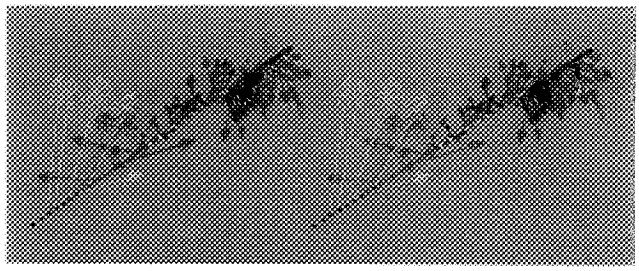

A stereo view of the interplanetary magnetic field (arrows) with the temperature indicated by the color of the arrows (red, hot; blue, cool), and the density indicated by the symbols on the axis (red, dense; blue, rarefied).

Contact: D. Aaron Roberts (Code 692)
301-286-5606

Melvyn Goldstein (Code 692)
301-286-7828

Sponsor: Office of Space Science

Dr. D. Aaron Roberts has 8 years of experience at GSFC and holds a PhD in Physics from the Massachusetts Institute of Technology. He is coinvestigator on the Space Physics Theory Program grant to GSFC, and Principal Investigator on a Director's Discretionary Fund grant to study stereoscopic analysis methods.

Dr. Melvyn Goldstein, Principal Investigator for the Solar-Terrestrial Theory Program grant to GSFC and NASA Deputy Project Scientist for the Cluster Mission, has 22 years of experience at GSFC. Dr. Goldstein, who holds a PhD from the University of Maryland, has received a NASA Exceptional Scientific Achievement Medal for his work.

A NEW LOOK AT VENUS' THERMOSPHERE H DISTRIBUTION

THE NEUTRAL HYDROGEN distribution in the upper reaches of Venus' atmosphere was initially studied using Pioneer Venus Orbiter (PVO) observations obtained during the spacecraft's first 3 years of operation (1978 to 1981). Neutral hydrogen (H) was not directly sampled on the mission. Its abundance was derived using a technique that was applied originally to the Earth's ionosphere.

Given in situ ion spectrometer measurements of O^+ and H^+, neutral spectrometer observations of O, (and CO_2 on Venus), and measured ion and neutral temperatures, the H concentrations could be determined at altitudes where H^+ is in chemical equilibrium. The ruling chemical processes are:

$$H^+ + O \Leftrightarrow O^+ + H$$
$$H^+ + CO_2 \Rightarrow HCO^+ + O$$

where the rates of the reactions are known functions of the ion and neutral temperatures.

The early Venus studies focused on "nondisturbed" data emphasizing the dawn-midnight quadrant. The analysis was restricted to data at altitudes below conservatively fixed upper boundaries in order to ensure that chemical equilibrium was a valid approximation to the H^+ distribution. We have extended the H database by including periods of time which did not appear in the earlier studies. Also, to ensure the inclusion of all valid H concentrations, the appropriateness of the chemical equilibrium

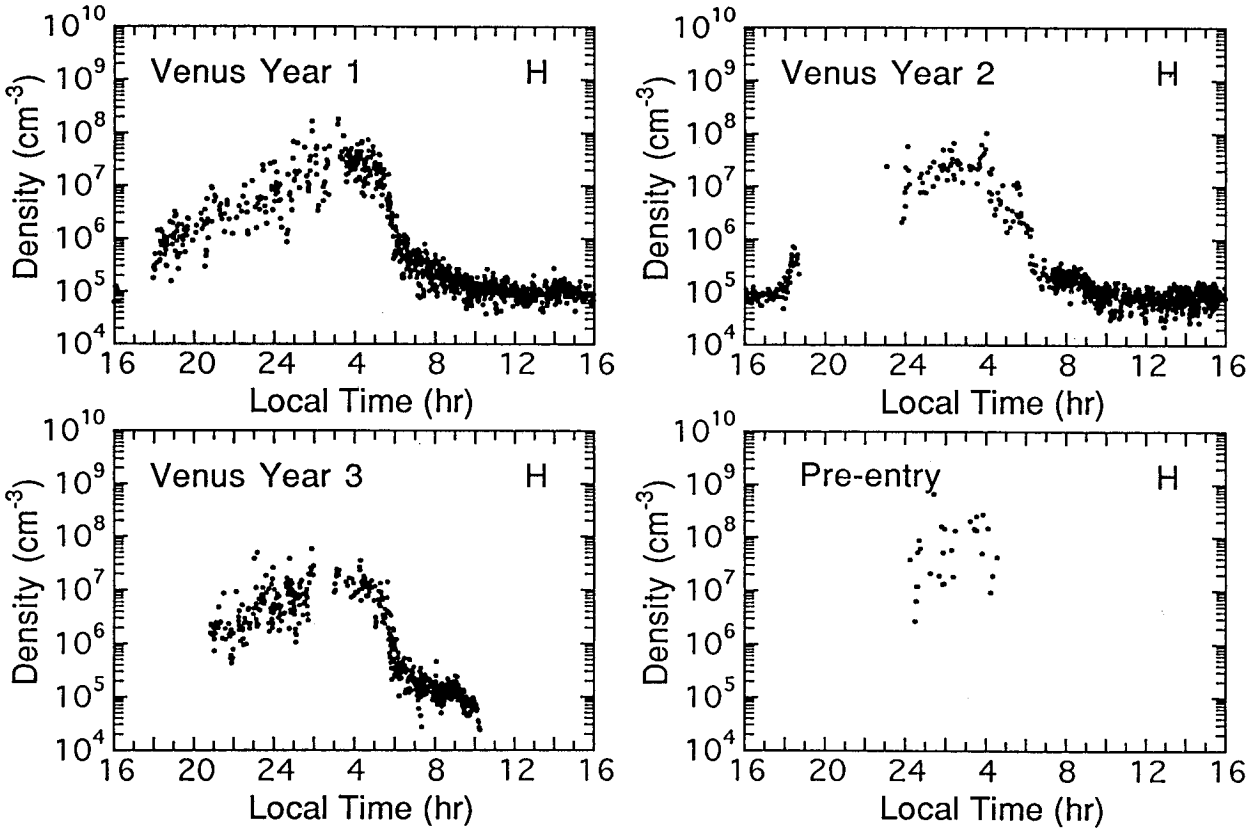

H concentrations around Venus for the first 3 years of the Pioneer Venus mission beginning in December 1978, and ending with the final partial ionosphere coverage just prior to spacecraft atmospheric entry in October 1992.

assumption on a point-by-point basis was verified through actual computation of the characteristic H^+ chemical and diffusion times. Only when the chemical reaction times of H^+ were shorter than the transport time is the assumption of chemical equilibrium applicable. The computed H concentrations provide a database that will be used to expand the empirical neutral atmosphere models, and to examine solar cycle and local time variations that were not singled out in the earlier studies.

The computed H concentrations for the 4 years that the PVO sampled the lower ionosphere, are shown in the figure. The altitudes of the plotted points range from approximately 180 to 270 km during the day, whereas at night the altitude range is reduced to approximately 160 to 180 km because the atmospheric density drops at the higher altitudes, allowing less hindrance to the diffusion of the ions.

This is the most complete dataset of the local time distribution of H about Venus that is now available. In addition to the characteristic H bulge in the midnight-dawn sector attributed to the superrotation of the Venus upper atmosphere, the small-scale variations and year-to-year changes in the H distributions provide valuable clues to the dependence of the atmosphere on solar wind dynamic pressure changes, and variations as a function of solar activity. The first 3 years of observations were made during a maximum in the solar cycle activity, whereas the preentry ionosphere encounters were during a period approaching a minimum in solar activity. The observations indicate a yet-to-be-understood increase of the nighttime H concentration with decreasing solar activity.

Contact: Joseph Grebowsky (Code 914)
301-286-6853

Sponsor: Office of Space Science

Dr. Joseph Grebowsky has 26 years of experience at GSFC in the Laboratory for Atmospheres. He is particularly experienced in the study of low energy plasma populations about the planets. Dr. Grebowsky holds a BS in Physics from Manhattan College and an MS and PhD in Physics from the Pennsylvania State University.

DIRECT MEASUREMENT OF ZONAL WINDS ON TITAN

ETHANE EMISSION WAS first detected on Titan in 1973; subsequent observations were made from the Infrared Interferometer Spectrometer (IRIS) on the Voyager spacecraft. These measurements were able to identify the band of ethane near wavelength λ=12 μm, and to retrieve ethane mixing ratios; however, the relatively low spectral resolution permitted a probe only of the lower stratospheric regions. Very-high-resolution 12 μm ethane measurements, as can be obtained with the Goddard Infrared Heterodyne Spectrometer (IRHS), can be used not only to further constrain the mixing ratios, but to trace the zonal winds on Titan by measuring the resultant Doppler shift of ethane emission lines. The infrared heterodyne technique is uniquely suited to this type of investigation due to its high spectral resolution (5 MHz) and frequency stability (~1 MHz). The instrument provides spectral resolving powers ($\lambda/d\lambda$) on the order of ~10^7, and diffraction-limited spatial resolution at the NASA Infrared Telescope Facility (IRTF) on Mauna Kea, Hawaii, of ~1 arcsec. At this resolution, the shape and position of individual lines of ethane can be measured, and the line-of-sight velocity of the source can be retrieved from the Doppler shift of the line frequency. This technique has provided a preliminary measurement of the direction and limiting magnitude of the stratospheric circulation on Titan.

These and other improved measurements of Titan's circulation will enable the retrieval of the mean magnitude of the wind fields, and provide constraints on dynamical theories of slowly rotating bodies (the cyclostrophic regime). The results will significantly enhance the planning for and science return from the Cassini mission and the Huygens probe of Titan. The latitudinal temperature gradients in Titan's stratosphere derived from Voyager IRIS data imply cyclostrophic circulation with zonal velocities of 75 to 100 m/sec. Knowledge of the direction and magnitude of the circulation is important for planning the release of the Huygens probe, to ensure the maximum period of communication during descent. Because the direction of the circulation cannot be determined theoretically, IRHS provides a possible technique for direct measurement of these parameters. Such measurements are a natural extension of our successful program to measure wind velocities on Venus, another slowly rotating body, and hydrocarbon emission from the outer planets.

The first attempt at this investigation was made in August 1993 at the NASA IRTF using the IRHS. Titan's small size dilutes the signal, as it is only 0.87 arcsecond in diameter versus our 1 arcsecond field-of-view with a 3 m telescope, as shown in the first figure. A technique of positioning the field-of-view on different areas on Titan yielded promising results. Vital to the success of these observations were the calibration measurements, taken prior to observing Titan, of differential refraction between the visible image used for guiding and the infrared image. Measurements were made on the east and west hemispheres and disk center of Titan. These were compared to determine the direction and magnitude of the Doppler shift resulting from the circulation. The direction of circulation (frequency shift of the ethane lines) was determined directly by comparing the spectra. The accuracy of the wind speed magnitude will depend on modeling the contribution of the wind fields within the field of view (FOV). Software to perform similar modeling and retrievals exists and has been used in dynamical studies on Venus.

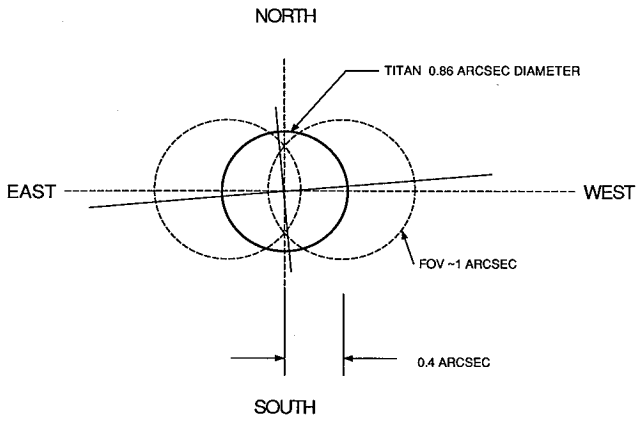

Observing geometry on Titan.

The second figure summarizes our measurements on the disk center and west limb positions; the spectra are offset for clarity. An apparent shift in the line positions is observed, indicating a prograde direction of the circulation in the 2 to 0.2 mbar pressure region on Titan, where the ethane emission lines originate. A mean magnitude for the circulation velocity of ~100 m/s was derived, but with uncertainties of comparable or greater magnitude, limited

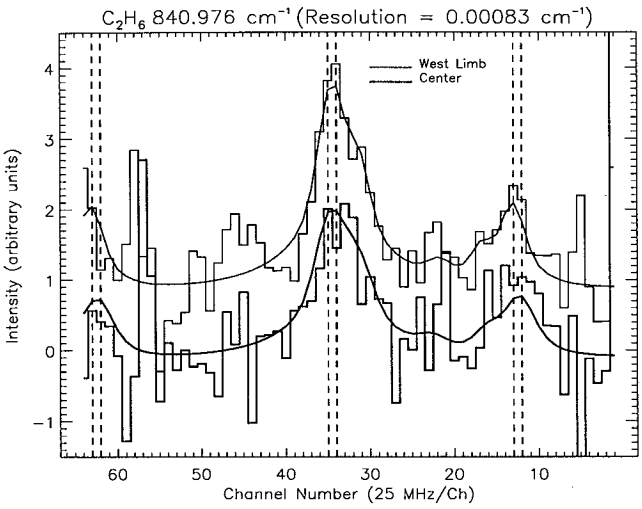

Ethane spectra on disk center and west limb of Titan. Both data and model fits are shown. The line Doppler shift is indicated by the vertical dashed lines. The direction of shift corresponds to prograde circulation.

mainly by the achieved signal-to-noise ratio on the spectra. The ethane abundance (mixing ratio) was determined to be ~$1x10^{-5}$ in Titan's stratosphere.

This first attempt at measuring the circulation on Titan revealed ways of improving this promising technique. Increased integration time at each aperture position will improve the signal-to-noise ratio. Tracking errors cause intensity differences since small drifts can take the field of view off Titan, diluting the measured signal. Integrating on more than three positions would establish, with greater precision, the region of contribution for each spectrum acquired. The ethane lines in the spectra were strong and at Titan ethane abundances were saturated, therefore, decreasing our ability to determine the ethane abundance and line positions accurately. Choosing less saturated ethane lines would allow us to obtain more accurate ethane abundances on Titan, as was done for Jupiter, and thus improve line position determination. The spectral region chosen for the 1993 observations contained multiple lines. Since the spectra are actually folded about the laser local oscillator frequency (double sideband spectra), the brightest spectral feature is in fact an overlap of two spectral lines from opposite sidebands. By choosing a spectral region with fewer, widely spaced lines, this overlap can be eliminated, reducing the complexity of the analysis and increasing its accuracy. For instance, to greatly enhance our velocity retrieval, we can measure dual line pairs originating in opposite sidebands of our instrument, as shown in the third figure. This is equivalent to making two simultaneous measurements. Since the two doublets appear separated and are in opposite sidebands, they will move relative to each other as the line-of-sight velocity changes. The magnitude of this motion will be twice as great as the differential Doppler shift and thus simpler to measure accurately. Only the heterodyne technique can make such observations possible by resolving individual lines and detecting small shifts in those lines.

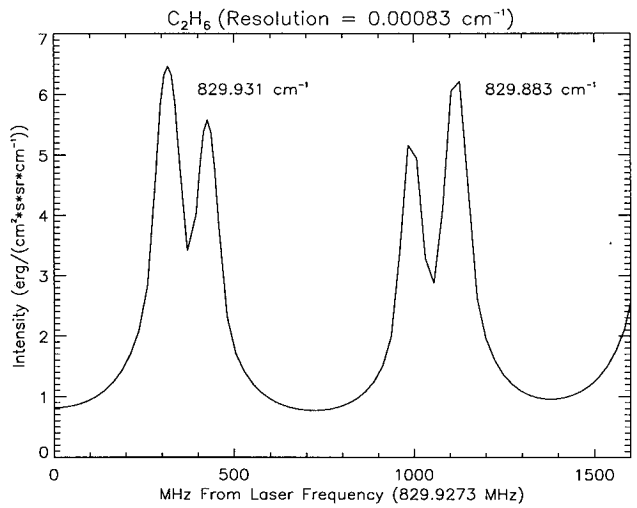

Model of proposed ethane lines on Titan which will enhance the measurement of circulation. The simultaneous measurement of these two lines will double the effective sensitivity to velocity shifts.

Contact: Theodor Kostiuk (Code 693)
301-286-8431

Kelly Fast (University of Maryland)
301-286-1544

Timothy Livengood (NRC/RRA)
301-286-1552

Sponsor: Office of Space Science

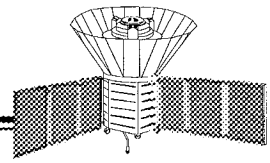

Dr. Theodor Kostiuk is an astrophysicist in the Planetary Systems Branch of the Laboratory for Extraterrestrial Physics and Chief Scientist for Exploration Programs in the Space Sciences Directorate. Dr. Kostiuk earned a PhD in Physics from Syracuse University and has 20 years of service at GSFC. His interests include composition, thermal structure and dynamics of planetary atmospheres, infrared spectroscopy and development of advanced instrumentation. He is currently on part-time detail to NASA Headquarters working in the Solar System Exploration Division managing the Planetary Instrument Definition and Development Program.

Ms. Kelly Fast is a faculty research assistant at the University of Maryland, working with members of the Planetary Systems Branch. She received her BS in Astrophysics from UCLA and an MS in Astronomy from the University of Maryland. Her scientific interests include ionospheric research and infrared imaging and spectroscopy of the outer planets.

Dr. Timothy Livengood received his PhD in Physics and Astronomy from The Johns Hopkins University in September 1991 and has been an NRC Resident Research Associate at GSFC for the past 3 years. His primary research interests are in infrared and ultraviolet observations of planetary aurorae and atmospheric emissions.

SHAPE, SIZE, AND DISTRIBUTION OF PARTICLES IN METEORITE CHONDRULES: CORRELATIONS WITH MAGNETIC PROPERTIES

CHONDRULES ARE millimeter-sized spheroids of once-molten droplets, present in the most-abundant class of meteorites, the chondrites. The chondrules, composed mostly of silicate minerals but containing other minerals and metal particles, are believed to be melting products of preexisting solids in the early solar nebula. Magnetic fields present in the early solar system have imprinted the chondrules with magnetic characteristics which are now observable in the laboratory. Magnetic properties provide important clues to the nature of the magnetic fields present during early phases of solar system evolution. These magnetic records of the formation processes undergone by the chondrules are contained mainly in the metal particles in the chondrules. Magnetic data, measured by Dr. Peter Wasilewski of this Laboratory, of individual chondrules from various different meteorites show a broad range of values for their magnetic properties. This information suggests that several different magnetic recording scenarios may have occurred. In addition, there is evidence that some chondrules have been exposed to relatively strong magnetic fields, possibly those associated with high electromagnetic energy fields from lightning discharges in the solar nebula.

A question of particular interest is whether the different magnetic recording scenarios and different field strengths are associated with different shapes, sizes, distributions, and compositions of the metal particles in chondrules, since this would have direct bearing on our understanding of solar nebula processes. This question is addressed by a recently initiated study that uses a scanning electron microscope (SEM) to provide high-resolution images of the shape, size, and distribution of metal particles within individual chondrules.

The initial SEM work involved study of ten individual chondrules from the Bjurbole meteorite, selected to cover a wide range of values of measured magnetic properties. These chondrules, consisting of a variety of different textural types and being generally spherical in shape, ranged in size from approximately 1.0 to 2.0 mm diameter. These sizes also represent a reasonable sampling of the narrow size distribution of chondrules present in the Bjurbole meteorite. After mounting in thermoplastic media, cutting to expose the interior of the chondrule, polishing, and carbon-coating, the chondrules were examined with the SEM (see the figure).

Results from this first phase of the SEM study, comparing some of the chondrules' microstructure with their specific magnetic properties, indicate possible patterns of metal particle distributions and potential correlations with magnetic properties. All of the chondrules examined are found to contain small metallic particles (on the order of $\leq$1 micron) typically distributed along crystal boundaries. Many of these particular particles, to within the resolution of the SEM, generally appear roundish in shape. Somewhat larger, metallic, irregularly shaped particles ($\leq$10 microns) are also abundant in all of the chondrules. There is a tendency for chondrules having increasing saturation remanence magnetization (SIRM) values to contain increasing abundance of the largest observed sizes (up to approximately 200 microns) of irregularly shaped metallic particles. In addition, these large particles tend to occur at or near the outer edge of their respective chondrules. In addition to having metallic particles distributed around portions of the edge of the chondrule, a few of the chondrules have metallic particles present in clumps within the chondrule. Furthermore, there appears to be a tendency for the metallic particles to have some degree of directionality to their distributions within some of these areas. It is noteworthy that only these few chondrules have another high-value magnetic property, known as REM, defined as the natural remanence magnetization divided by the SIRM. This is an indicator of the strength of the magnetic field to which the chondrule material was exposed during its process of formation. The REM values of these few chondrules are distinctly greater than the REM values of the other chondrules examined to date with the SEM, and indicate that these particular chondrules had been exposed to strong magnetic fields during their formation.

Future work to be undertaken includes elemental mapping and chemical analyses using the x-ray spectrometer attachment to the SEM to determine chemical compositions of the metal particles as well as of other ferromagnetic phases (e.g., iron sulfide) present in the individual chondrules; petrographic characterization of the metal particles, other magnetic minerals, and the silicate mineralogy of

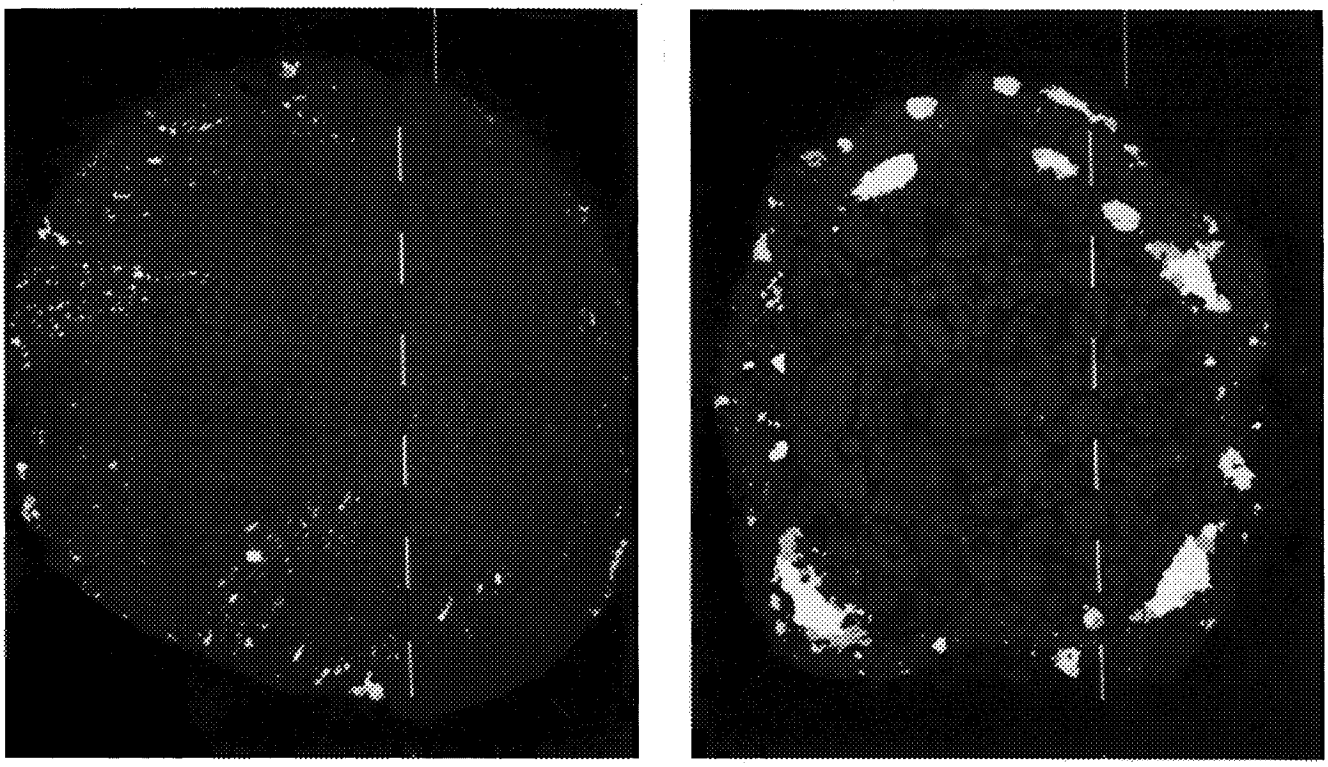

Photomicrographs of SEM backscattered electron detector images of two chondrules from the Bjurbole meteorite, each taken at 80 X magnification, showing examples of the diversified morphology and distribution of metal particles (the white areas) present in individual chondrules from the same meteorite. Each scale bar represents 100 microns.

the chondrules; and similar examinations of individual chondrules from other chemical-petrologic classification types of meteorites.

The goal of this SEM study is to determine which magnetization scenarios are associated with which textural and petrologic types of meteorite chondrules in order to be able to help elucidate the physical conditions and processes which have imprinted the observed magnetic characteristics during chondrule formation in the early solar system. The significance of this study, once completed, is that new information will be provided that will identify petrographic correlations of metal particle morphology, distribution, and chemical composition in meteorite chondrules with the wealth of magnetic property data which already exists for these same chondrules. This information perhaps will include constraints on our understanding of the prevalence of lightning discharge in the solar nebula.

Contact: David Nava (Code 691)
301-286-5483

Sponsor: Office of Space Science

Dr. David Nava is an astrophysicist with the Astrochemistry Branch of the Laboratory for Extraterrestrial Physics. He is a coinvestigator for the Upper Atmosphere Research Program and for the Planetary Atmospheres Program, and he was a Principal Investigator for NASA's Returned Lunar Sample Program. Dr. Nava's research involves chemical reaction kinetic studies of atmospheric systems and geochemical studies of meteorites. Dr. Nava, who received a PhD in Chemistry from Arizona State University, has worked at the GSFC for 26 years and has received two NASA Special Achievement Awards and a NASA Exceptional Performance Award.

MODELLING MAGNETIC FLUX-ROPES IN THE EARTH'S MAGNETOTAIL

MAGNETIC FIELD and plasma measurements of ten moderately large and dynamic plasma structures in Earth's distant magnetotail were made by the Japanese spacecraft GEOTAIL in early 1993. These structures were shown to have helical magnetic field configurations similar to those of magnetic clouds, which are very large magnetic structures seen in the solar wind. Such a transient signature is shown to be well-approximated by a model representing a special equilibrium state of a moving magnetic configuration, known as a force-free flux-rope. Surprising, for this set of magnetotail events, the rope-axes were estimated, on average, to lie close to the "east-west" direction that extends across the magnetotail, and not parallel to the tail-axis, as had been suggested earlier for such possible structures. This cross-tail orientation has special implications for the related generation mechanism and for the pattern of electrical currents that flow during these active periods. Similar structures have been observed in the Earth's tail by other spacecraft, but this is the first time that comprehensive helical field modelling has been successfully attempted. Also, this is the first study to provide empirical evidence that cross-tail orientations for flux-ropes are probably not uncommon in the tail.

This study is part of an ongoing effort to better understand Earth's active magnetotail, which plays an important role as a region for storage and spontaneous release of energy during a magnetic substorm (i.e., a global geomagnetically active period). For years, a central region of the tail during at least some of these dynamic periods had been described in terms of a signature that had a marked northern to southern variation of the north-south component of the magnetic field, and then a return to low-latitudinal directions. The signature has been named a plasmoid, which was viewed as having effectively a two-dimensional structure. That is, to first approximation, the signature was assumed to have no cross-tail spatial variation. Our investigation started mainly as an attempt to search for such classical plasmoid signatures in GEOTAIL magnetic field and plasma data obtained for the period when the spacecraft was in the distant tail between about 90 and 130 Earth-radii (R_e = 6,378 km) from Earth, a region in which the ISEE spacecraft had observed such signatures.

It was immediately recognized, however, that the candidate GEOTAIL field signatures that were found, although plasmoid-like in some respects, showed strong central fields rather than the relatively weak central fields consistent with a plasmoid. In fact, they had strikingly similar field structural characteristics to those of fields in magnetic clouds, as mentioned, which are cylindrically symmetric structures when observed over a small part of their extent (i.e., locally), and, at 1 AU, are larger than plasmoids by a factor of about 500 to 1000! Because such clouds are fairly well approximated locally by a mathematical formalism employing the force-free flux rope assumption and a related magnetic field fitting-technique, it seemed possible that the tail structures might also be so approximated, regardless of the vast difference in their sizes.

The analysis of these events consisted of the following steps: (1) a variance analysis of the magnetic field was performed to find the maximum, intermediate, and minimum fluctuation-directions. This is done to help determine an approximate coordinate system in which to describe the tilt of the rope's axis; (2) for the kind of equilibrium configuration state that we are considering, it can be shown that the field components are given in terms of Bessel-functions of the zeroth order (axial component), and first order (azimuthal component), and that the radial component (normal to the rope axis) is zero everywhere in the rope; (3) the choice of sign (±) for the azimuthal component determines the helicity of the flux rope (i.e., whether the twist is right- or left-handed); we fit the observed field to these equations after first checking the sign of helicity for reasonableness; (4) finally, B_o, the intensity of the field along the axis, is fitted as a simple scaling factor for all components.

These equations tell us that the field is strictly along the rope's axis when at the axial position and it is perpendicular to it (in a circular geometry) at the boundary. The first figure shows a sketch of what such a flux-rope might look like in relation to a passing spacecraft, and displays some of the parameters that the model attempts to obtain. All ten measured events were at least reasonably well-fit by these functions, and seven were quite well-fit by them. However, for some events, in relatively small central regions, the (near-axial) fields were surprisingly more intense than the nearby tail-lobe fields; the example shown below will be such a case. The associated electrical current densities, which are field-aligned in this model and therefore also helical in structure, can be estimated directly from the model. When the current density is integrated throughout the cross-section of an average size flux rope

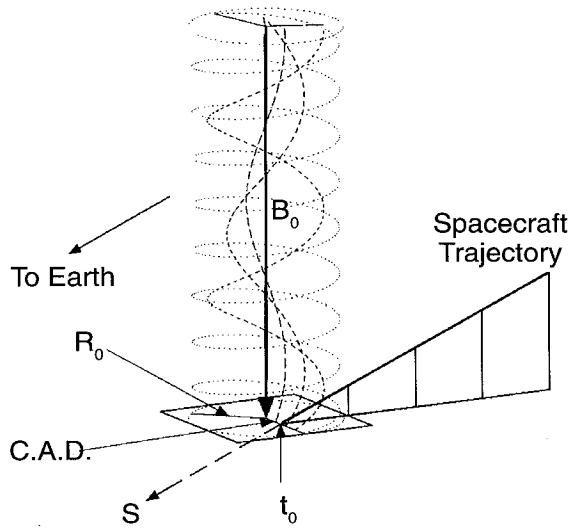

A model magnetic flux rope showing a nested set of field lines of different pitch angles according to their distance from the axis, shown in relation to a trajectory of a visiting spacecraft. B_o is the magnetic field on the axis of the flux-rope, R_o is the rope's radius, t_o is the time of closest approach of the spacecraft, C.A.D. is the closest approach distance, and S is the spacecraft trajectory vector.

of about 15 R_e in diameter, we obtain about 5 million amps across the tail! The tail itself is only about 60 R_e in diameter at this distance.

The second figure shows an example of one of the more successful attempts to fit the actual field of one of the candidate flux-ropes to the modelled field. In the lower panels we show the model-estimated longitude (ϕ_A) and latitude (θ_A) the axis of the flux-rope. Since ϕ_A of 77° is near 90°, this indicates an axis that is pointed nearly cross-tail. Since the study yielded generally successful results upon employing the technique to these tail signatures, it is argued that they are, indeed, part of a family of force free flux-rope structures with this intriguing cross-tail proclivity. We expect to use this technique in the re-analysis of some of the ISEE-3 data, which represents a very large dataset.

This work was done in collaboration with colleagues at the University of Iowa (Prof. L. A. Frank and Dr. Bill Paterson), Nagata University (Prof. S. Kokubun) and ISAS (Dr. T. Yamamoto). We are grateful for the use of their

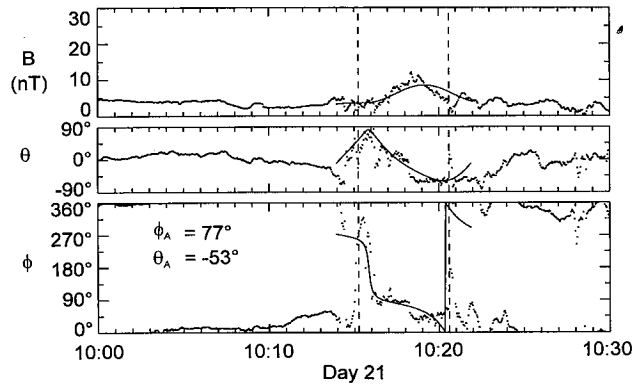

Thirty minutes of vector magnetic field data (3-s averages) for January 21, 1993, in terms of field magnitude (B), field latitude (θ), and longitude (ϕ) and the overlaid flux rope model-curve (solid line), that holds only for the interval which is shown between the vertical dashed lines.

GEOTAIL magnetic field and plasma data. We were joined in this study also by Mr. Jeff Jones of Hughes/STX.

Contact: Ronald Lepping (Code 696)
301-286-5413

Donald Fairfield (Code 695)
301-286-7472

Sponsor: Office of Space Science

Dr. Ronald Lepping, a 25-year resident of the Laboratory for Extraterrestrial Physics, specializes in magnetohydrodynamics and magnetospheric and interplanetary physics. He participates in magnetometer investigations on IMP-8 (Principal Investigator), Voyagers 1 and 2 (coinvestigator), and Wind (Principal Investigator). Ron holds a PhD in physics (1969) from Rensselaer Polytechnic Institute.

Dr. Donald H. Fairfield studies magnetospheric and magnetic fields at the Laboratory for Extraterrestrial Physics. He specializes in magnetospheric physics, and has received several NASA achievement awards during his 27 years at GSFC. Don holds a PhD (1965) from the Pennsylvania State University.

OBSERVATIONS OF IONOSPHERIC ELECTRIC FIELDS ABOVE ATMOSPHERIC WEATHER SYSTEMS

IT IS COMMONLY believed that quasi-DC (i.e., those well below 1 Hz) electric fields from thunderclouds remain confined to regions below about 100 km, due to the shielding effects of the highly-conductive ionosphere. In the simple global circuit model, the ionosphere is considered a highly conductive plate which effectively "shorts" the thundercloud electric field at the ionosphere base. Compared to the resistive atmosphere, the ionosphere is indeed highly conductive. Because of this isolation, ultra-low-frequency (ULF) atmospheric electricity was thought to have little effect on the upper ionosphere and magnetosphere. Of greater significance is that the converse was also considered true.

However, the ionosphere is not a perfect conductor. The reaction of the ionosphere to external electric fields, like those created by thunderstorms, is a complicated function depending upon diurnal effects, incident frequency, external solar activity, etc. Because the conductivity values are finite, quasi-DC electric fields could conceivably "leak" to higher altitudes. Unfortunately, theory predicts that the field strength from such leaking fields should be very small in the ionosphere, being attenuated by as much as 140 dB from their original values. Such weak fields, theorized to be on the order of 0.1 mV/m in the ionosphere, would be very difficult to measure directly via electric field experiment.

Despite such theorized difficulties, the double probe electric field experiment onboard the equatorial-orbiting San Marco D spacecraft detected over 20 electric field events originating from underlying active weather systems. The first figure is an example of an electric field event measured at 190 km above an active weather system as detected by San Marco in 1988. Originally, such electric field events were considered an anomaly, since they did not possess any corresponding density perturbation which typifies ionospheric electrical activity (i.e., like the spread-F phenomenon). Recent analysis shows that, as a group, the events displayed a number of unusual properties.

First, the events tended to cluster over the Indonesian Basin, northern South America, and the west coast of Africa, all known sites of atmospheric activity, and the events tended to recur when the spacecraft passed over certain

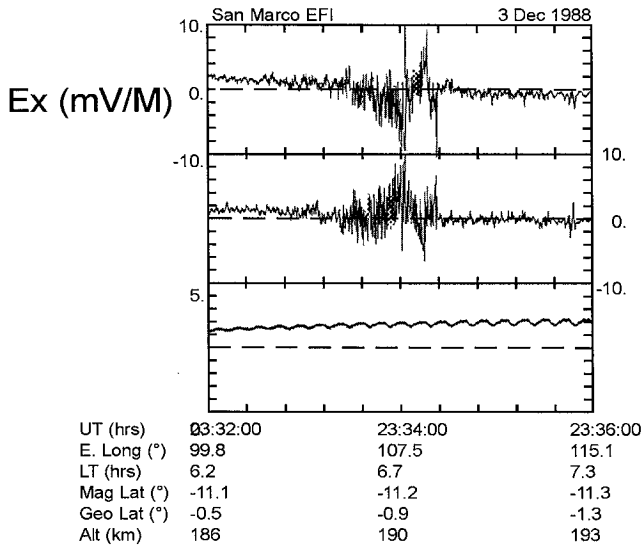

The San Marco quasi-DC electric field measured on December 3, 1988, over a storm system in Indonesia. The top panel of the figure contains the E_x measurements, where x is directed in the nadir direction. The middle panel displays the E_y measurements, where y is directed in the geographic east direction. The bottom panel shows the measured ion density obtained from a biased, axially symmetric ring collector mounted on top of the spacecraft about the +Z axis.

large weather convection features. For example, a number of events recurred in association with spacecraft passages near Hurricane Joan in mid-October of 1988. Of all the Atlantic cyclones in 1988, Joan extended most southerly (i.e., nearest to the spacecraft trajectory), had the lowest pressure (932 mb), and had very high sustained wind speeds (143 mi/hr). In two cases, the San Marco electric field observation of the cyclone occurred within a few hours of the north-south passage of the Special Sensor Microwave/Imager (SSM/I) onboard DMSP F-8. In these cases, the SSM/I image indicated the presence of significant atmospheric convective cells observed within 5° of the E-field observation point. The convective features were associated with clusters of storms that extended south of the cyclone.

The second figure shows a composite of an SSM/I image of the weather features in Indonesia. The line in the figure is the footprint of the magnetic field lines directly connected from the San Marco spacecraft down to 100 km during the occurrence of the December 3 electric field event shown in the first figure. Note that a large weather feature lies just south of the mapping point, and is considered the inducer of the electric field event.

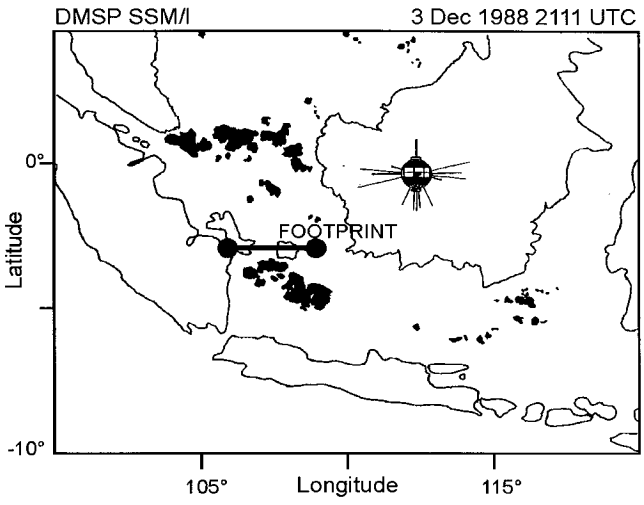

A composite of an SSM/I image showing intense convective storm systems over Indonesia. This system maps directly to the San Marco spacecraft during the observation of the anomalous DC E-field event on December 3, 1988.

Why are the observed electric field strengths larger than predicted by theory? Theoretical calculations assume a fair-weather ionospheric conductivity profile above a single charged thundercloud. However, the a priori assumption in the models of a fair-weather conductivity profile may not be accurate. Thunderstorm emissions at higher frequencies (i.e., very-low-frequency emissions) may heat the ionosphere, thereby making it more resistive. Any reduction in the conductivity as compared to its fair-weather value would enhance the ULF field strengths above theorized levels. Also, in a large weather system, there may be multiple convection cells operating as coherent ULF wave generators. This coherency would also enhance the field strengths above theorized levels. In any case, the observations of relatively strong ionospheric electric fields above active weather systems suggest an electrical coupling between the atmosphere and ionosphere, which was previously thought to be insignificant.

Contact: William Farrell (Code 695)
301-286-4446

Thomas Aggson (Code 694)
301-286-5726

Edward Rodgers (Code 912)
301-286-4131

Sponsor: Office of Space Science

Dr. William Farrell is a coinvestigator of GGS Wind/MFI and Cassini/RPWS. He earned a PhD in physics at the University of Iowa in 1987. His professional interests include the study of natural radio wave generation in planetary atmospheres and magnetospheres, and magnetic receiver design.

Dr. Thomas Aggson is a principal investigator on the San Marco D electric field instrument. He earned a PhD in physics at the University of California/Berkeley in 1960. His research interests involve ionospheric electricity, including the study of the Spread-F phenomenon and ionospheric modification via atmospheric electrical events.

Dr. Edward Rodgers is a Principal Investigator of a project designed to examine the distribution of rainfall in tropical cyclones using the DMSP SSM/I images. He earned his PhD in atmospheric science at Colorado State University in 1992. His research interests include the remote sensing of atmospheric systems from space-based platforms.

INNOVATIONS IN ATMOSPHERIC PHOTOCHEMICAL MODELING

PHOTOCHEMICAL MODELS of planetary atmospheres are attempts to use a computer to simulate the chemistry and transport of trace species in a planetary atmosphere. The chemical reactions are initiated by solar ultraviolet photons which break apart the molecules in the atmosphere to form reactive species. The end products of the subsequent photochemistry often include new stable molecules which are not in thermodynamic equilibrium with the atmosphere and hazes. Even though the initial and final species are frequently very minor components of the atmosphere, they are often far more important than their low relative abundance might suggest. The classic example of this is ozone in the Earth's atmosphere, where its parts-per-million abundance belies its importance to life.

Atmospheric photochemical models must be responsive to two very different types of data. The first type comes from laboratory measurements of photochemical processes: reaction rates (and branching ratios, if more than one set of products is possible), photoabsorption cross sections, quantum yields, etc. The second type comes from observational (remote sensing) data, which reveal the presence in the atmosphere of species predicted by the model. However, what the model predicts—the mole fraction distributions of chemical species—is not what is observed directly. What is observed is either emission features in the infrared (IR), or absorption features in either the IR or the ultraviolet (UV) regions of the spectrum. To interpret these observations, the photochemical-model-predicted distributions must be used to generate synthetic spectra that can be compared directly against the observational data. Thus, an ideal photochemical model would have a flexible structure, so that updates to the photochemical reaction scheme would be effortless, and would allow easy comparison to observations. A prototype of such a model was developed at GSFC this past year.

For the prototype (see figure), the methane (CH_4) photochemical chemical system on the outer planets (Jupiter, Saturn, Uranus, and Neptune) was chosen for several reasons. Methane is an important trace species in outer-planet stratospheres. Its photolysis leads to the production of stable C_2 hydrocarbons (e.g., acetylene (C_2H_2), and ethane (C_2H_6) and more complex hydrocarbons that can produce hazes. Methane, along with acetylene, ethane, and the resultant hazes, absorb the planetary infrared emission, and are thus important in controlling the thermal structure of the stratosphere. Modeling the observed distributions of these species can provide information on the strength of vertical mixing and dynamics, if we know their chemical production rates well enough. Many of the relevant reaction rates and quantum efficiencies are poorly known, and new and better laboratory measurements of these parameters are being made, so updates on a nearly continuous basis are required if the data analysis is to remain timely. Also, the laboratory measurements are often not at the desired low temperatures ($T < 150$ K) and pressures ($100 > P > 10^{-3}$ mbar) relevant to the outer planet stratospheres where CH_4 photolysis takes place. Thus, parametric studies must be done to determine the sensitivity of model results to the unknowns in the reaction scheme.

There are numerous datasets available for model comparison and validation. Methane, acetylene, and ethane all emit in the IR and absorb in the UV. The highly successful Voyager mission has observations of these compounds on the outer planets, and there are ongoing, NASA-supported ground-based observations of these species. Also, model results can be used for planning the joint ESA-NASA Cassini mission to Saturn and its large moon Titan. Finally, the flexibility of the model could be tested by altering the photochemical scheme to analyze observations of the Comet Shoemaker-Levy 9 impact on Jupiter.

The prototype was constructed from an existing 1-dimensional photochemical model. Flexibility was introduced into the model by use of FORTRAN 77 structures, a common extension in FORTRAN compilers for UNIX workstations. The structures are used to establish a "map" between the reactants and reaction pathways at run-time. Furthermore, a graphical user interface (GUI) for the flexible model was developed via the Interactive Data Language (IDL). The GUI greatly increases ease of use, and allows the users to focus on data analysis rather than on programming details. The use of FORTRAN structures and IDL creates a very network-friendly environment; the code can reside on a workstation while users can access the model via other workstations, X-terminals, or personal computers running an X-terminal emulator.

The user creates all of the input data required to run the model by either mouse clicks or by filling in dialog boxes within the GUI. First, the planet and background atmosphere

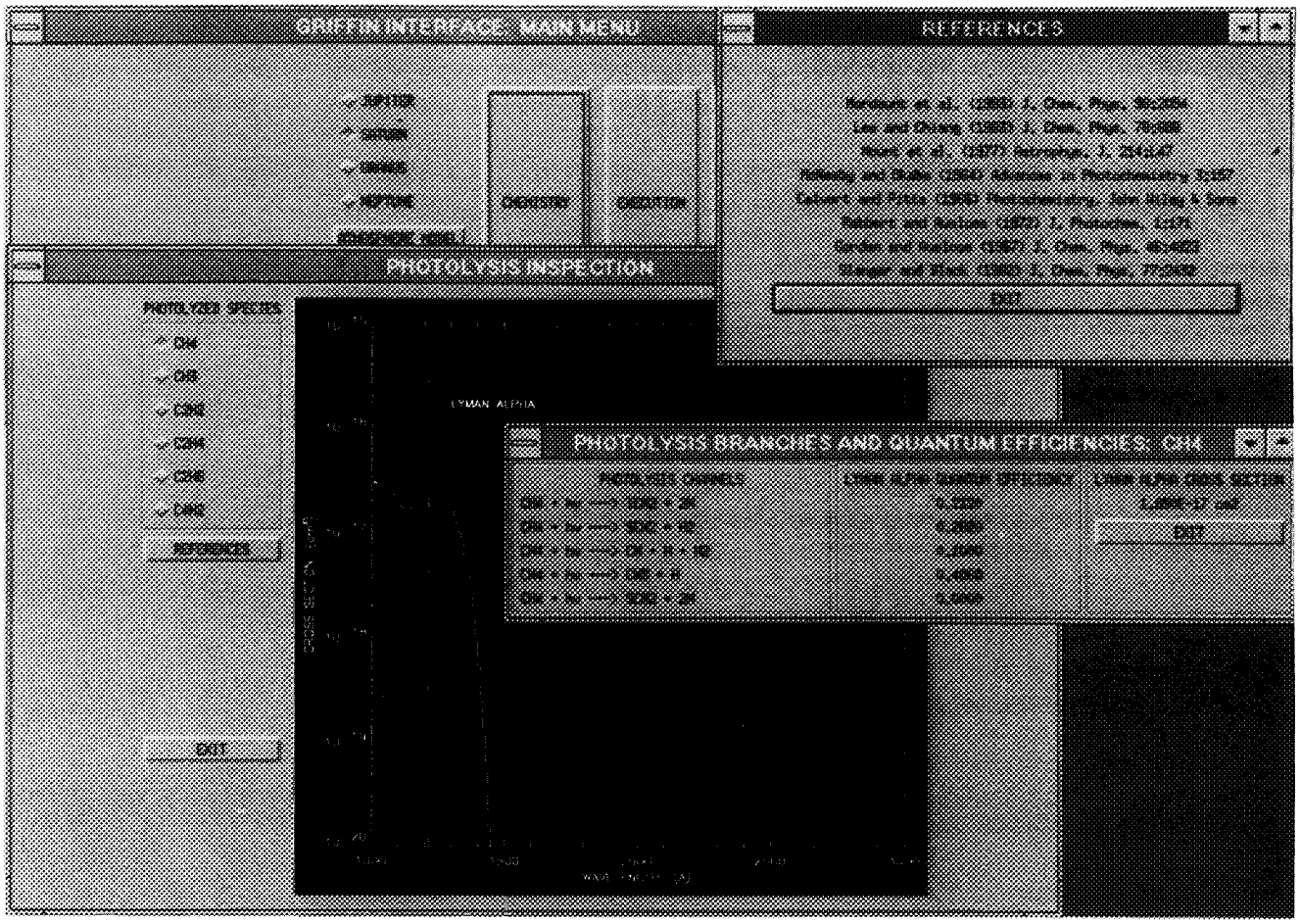

Shown in this figure are various windows and subwindows of the photochemical model (code name GRIFFIN). In this particular case, the user is inspecting the information in the model concerning the photolysis of CH_4 by the solar UV. The user has opened windows; displaying the photolysis branches and quantum efficiencies, a graph of the methane absorption cross section, and the references that the information in the model is based upon. The wavelength for Lyman-α is highlighted since in the region methane absorbs 80 percent of the photons are at Lyman-α.

are selected. Next, the UV solar spectrum is chosen, thus changing the level of solar activity. Then aaltitude profile for the eddy diffusion coefficient (K) is constructed. In a one-dimensional model, all of the dynamics collapse into a single parameter, the ed diffusion coefficient. The strength of K is representative of the amount of vertical mixing in the atmosphere from whatever source: waves or mass motion. An integral part of this process is the graphical display of the atmospheric thermal structure, solar flux, and eddy mixing profile for inspection by the user before the choices are confirmed. The reaction scheme is then constructed from a fixed list of species (prototype limitation). There are 64 separate reactions in the default list. A new reaction can be added, an existing reaction deleted, or a existing reaction rate changed via the GUI. If the user chooses to alter a reaction rate, dialog boxes displaying the relevant literature reference and for user notes pop up. In addition, the rate can be compared graphically against the collisional rate in the selected model atmosphere. The final preexecution step is to tell the model to compile the map between the reactants based upon the user-created reaction scheme. The model is then executed. It presently uses a Newton-Raphson technique to iterate from the initial guess to the final equilibrium solution. The user can either accept the default initial conditions, boundary values, and convergence criteria, or supply others. Upon completion, selected results (mole fraction profiles, reaction rate profiles, etc.) can be displayed graphically on the screen, printed out, or saved to a file.

The next step in model development will be to remove the limitations of the prototype model in updating and altering the photochemical scheme via the GUI, and increase the scope of the analysis package. This will make the model useful for analyzing other photochemical systems on other planets, and will help interpret data returned from previous NASA missions and to plan future ones. Later, an existing IR synthetic spectra generator will be adapted to take the photochemical model output directly as input, compute the predicted spectra and compare the results to a selected observation. This will enable comparison of the photochemical model against data in one seamless step.

In addition to research use, the model has high educational potential. For example, the photochemistry in the model could be altered to simulate tropospheric smog production on the Earth. Students could adjust the emission rates of various precursor species to see their effect on the final composition and amount of air pollution. Students could explore various ways of controlling air pollution without having to learn the intricacies of numeric computation.

This work was largely performed as a result of a Small Business Innovative Research contract with Computational Physics Inc. (CPI). The code was developed with the assistance of John Roberts, Pat Marsden, and Carolyn Biczel.

Contact: Paul Romani (Code 693)
301-286-1525
Internet: romani@gsfc.nasa.gov

James Bishop (CPI)
703-204-1301
Internet: Jbishop@euler.cpi.com

Sponsor: Office of Space Science

Dr. Paul Romani currently works in the Planetary Systems Branch of the Laboratory for Extraterrestrial Physics. He is a coinvestigator for the Composite Infrared Spectrometer on the joint NASA-ESA mission. His research interests during his past 6 years at GSFC include photochemistry, photochemical production of hazes, and cloud physics on the outer planets. He received a PhD in Atmospheric Science at the University of Michigan.

Dr. James Bishop is currently a senior physicist with Computational Physics, Inc. He is involved in remote sensing modeling of the terrestrial middle and upper atmosphere, kinetic and radiative transport modeling of exospheres, and outer planet stratospheric photochemistry. He received a PhD in Space Physics and Astronomy at Rice University.

NEW BRAZING TECHNOLOGY OPENS WAY FOR IMPORTANT LABORATORY DATA AT HIGH TEMPERATURE

TO GENERATE CLOUDS of refractory particulates for studies of the properties of large fractal aggregates similar to those that must have been present in the primitive solar nebula, we require a rugged, compact, highly-reliable evaporator, capable of reaching temperatures in excess of 1,500 K and suitable for flight on manned spacecraft. Advances in Intragene-based bonding technology (described below) to date have been sufficient to assure us that we can build the highly efficient, light-weight evaporator capable of repeatedly generating the clouds of very small (~20 nanometer) refractory particles necessary to study grain-grain coagulation in zero gravity. Such processes are similar to those which must have occurred in the primitive solar nebula during the earliest stages of the planetary accretion process. We expect to be able to determine not only the particle coagulation rate but also the structure and physical properties of the resulting aggregates. Since the Intragene-bonded furnace system should be capable of achieving very high temperatures, these experiments can make use of more realistic materials, such as iron or silicate grains, rather than the less refractory analog materials we had initially expected to settle for when using a less-capable evaporator system. Use of these more-realistic materials will greatly enhance the data obtained in microgravity experiments and certainly make the results easier to apply to both conditions in the primitive solar nebula and to processes occurring today in protostellar environments.

High-temperature furnace systems designed for use on manned spacecraft must be compact, efficient and extremely reliable, yet remain easy to install, and safe to handle. Reasonable efficiency can be achieved with conventional designs; but to satisfy safety, weight, and volume constraints, components fabricated from graphite, advanced carbon-carbon composites and ceramics are needed. Unfortunately, use of such materials has been extremely difficult until recently, due to lack of a reliable technique for bonding such materials to one another to allow them to endure repeated thermal cycling to temperatures in excess of 1,000 °C. Conventional active-metal brazes are not capable of such repeated, high-temperature excursions, although they have been used successfully for applications closer to room temperature where the light weight, structural stiffness, or chemical resistivity of the ceramic has been a key design factor and mechanical fasteners could not be used. We envision the basic design for our evaporator as an alumina crucible (containing the material to be vaporized) enclosed in a graphite heater coil encased in a titanium/zirconium/molybdenum (TZM) sheath, and surrounded by an alumina heat shield. Each component should be rigidly bonded to the others without the use of mechanical fasteners of any kind.

Through the GSFC Small Business Innovative Research (SBIR) program we developed a technique capable of bonding virtually any advanced ceramic, carbon-carbon composite, metal, or graphite component to another (see the figure). Furthermore, the bond can be made stable to temperatures just below the melting point of the lowest melting temperature material in the joint. As an example, a copper-graphite joint was repeatedly cycled to 1000°C from room temperature with no ill effects, yet copper melts at 1,083°C. Similarly, TZM-mullite joints can withstand repeated cycling to ~1,500°C, approximately 100°C below the working temperature of the ceramic mullite. Prior to the advanced development of the Intragene process, an evaporator such as that described above would have been impossible, and any resulting evaporator would have been both less reliable and considerably larger because of the need for screws, bolts or other fasteners.

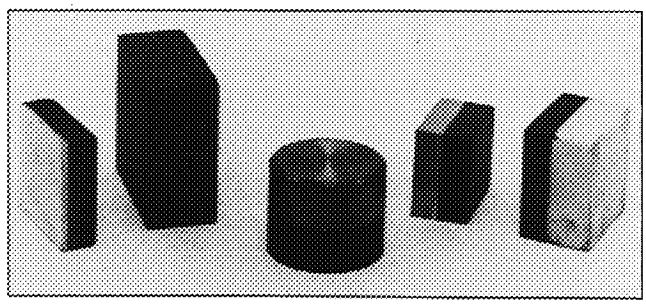

Five examples of Intragene bonded test pieces. From left to right: thin alumina ceramic bonded to graphite using a thick silver interlayer, two carbon-carbon composites bonded using a nickel interlayer, graphite bonded to copper using a thick TZM interlayer, TZM bonded to graphite and graphite bonded to alumina. The copper-graphite bond (center) can withstand repeated cycling between room temperature and 1,000°C.

TUNABLE 9- TO 12-MICRON MICROWAVE MODULATED LASER SYSTEM

GAS LASERS CAN provide a very stable source of infrared radiation whose frequency stability is $\sim 10^{-7}$, although there are techniques available to increase the stability to $\sim 10^{-9}$, or <100 kHz. The principal problem with using a gas laser for laboratory or astronomical spectroscopy is that it is not tunable, except to precise wavelengths corresponding to specific transitions in the molecular gas. The laser system we are developing, which is described here, creates sidebands on the beam by modulating the laser with a microwave signal in the 8- to 20-GHz region. Since the sidebands are at a frequency of the laser plus or minus the microwave frequency, they can be tuned with the microwave signal. By using a stabilized microwave source, the sidebands will have the same frequency stability as the laser. The laser system uses a Fabry-Perot etalon to filter out the main laser radiation and the unwanted sideband, leaving a single, tunable infrared beam.

The laser system is shown in the first figure, where the infrared beam is shown being modulated and then filtered to produce the tunable infrared source. The principal components are the laser, a microwave modulator, and a Fabry-Perot etalon. A spectral diagram at each point illustrates the effect of the modulator and filter on the spectrum of the infrared beam. The Fabry-Perot etalon is set up to tune with the microwave frequency, thereby tracking the sideband output of the source. A detailed diagram of the laser system is shown in the second figure, where the infrared beam is the dotted line. A Macintosh computer is used to control the microwave source, the laser, the Fabry-Perot etalon, and a lock-in amplifier that detects the output beam. A traveling wave tube (TWT) microwave

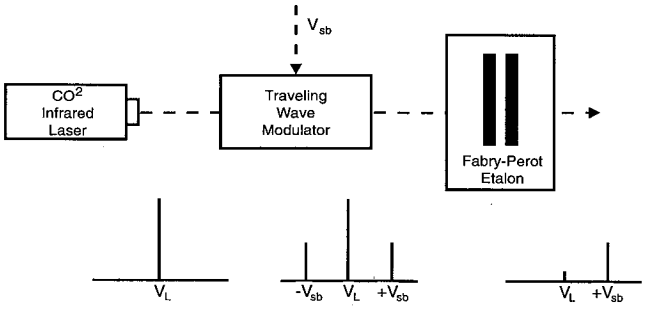

Functional diagram of the tunable laser system. The spectrum illustrations are for the upper sideband tuning of the Fabry-Perot etalon.

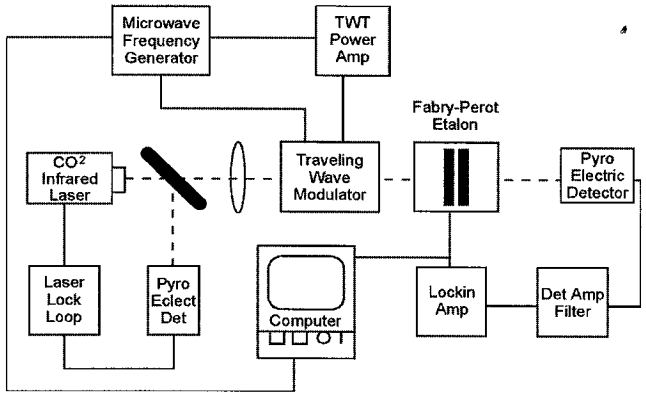

System diagram of the tunable laser.

power amplifier is used to provide a 20 Watt microwave signal to the modulator. The infrared beam is coupled into a GaAs waveguide modulator, where a traveling wave interaction with the microwave field produces the modulation. The modulation is only 1 to 2 percent of the main beam, producing the sideband pattern shown in the third figure. The pedestal under the sidebands is the leakage of the main laser beam through the Fabry-Perot etalon. With a power out of the laser of 1 Watt, the modulator output consists of 200 milliwatts of main laser beam and 2 milliwatts in each sideband. This power is adequate for laboratory spectroscopy, and also for use as a local oscillator in an infrared heterodyne receiver.

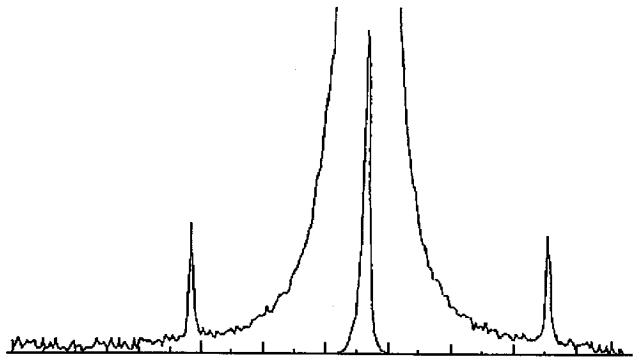

The output spectrum of the laser modulator showing the two 14 GHz sidebands produced by the microwave modulation of the laser. The vertical scale was expanded (X100) because the sidebands are only 1 to 2 percent of the main laser beam.

A prototype of the tunable infrared source was used to measure the spectrum of ethylene. The spectrum obtained is shown in the fourth figure for two different gas pressures. The spectrum spans 11 to 15 GHz from the center of the 626 10P12 CO_2 laser line, and has a resolution of 10 MHz. Pressure broadening of the lines is evident at 3.4 Torr. A number of other transitions were also studied.

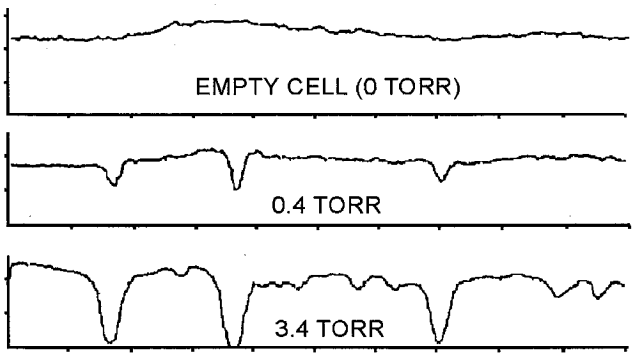

Infrared spectrum of ethylene in the range of 11 to 15 GHz from the 626 10P12 CO_2 laser line at 10.513 μm. Pressure broadening can be seen in the 3.4 Torr spectrum. The resolution of this spectrum is ~10^{-6}, or 10 MHz.

A beam-imaging system was developed to display the infrared beam of the laser source. The system has the sensitivity to see both the main beam and the sideband beam coming from the modulator, which allows us to evaluate the effectiveness of the Fabry-Perot filtering in rejecting the main laser beam. An illustration of this beam-imaging is shown in the fifth figure, in which the main laser beam pattern is mapped. The beam is elongated because it has been passed through the optical waveguide in the modulator. The sideband beams show a similar pattern. Some cylindrical optics may be needed to match these beam patterns to a detector or mixer in the case of the infrared heterodyne receiver.

The use of this tunable laser source in a laser heterodyne receiver is the next step and will eliminate the problem of limited spectral coverage in these receivers. At present, CO_2 laser receivers using all isotopes of CO_2 only cover 10 percent of the 9- to 12-micron spectrum. The microwave modulated tunable laser source would cover the entire spectrum and would also simplify the problem of Doppler tracking an astronomical source. The prototype infrared source is being developed for use with our laser heterodyne receiver at the NASA IRTF telescope on

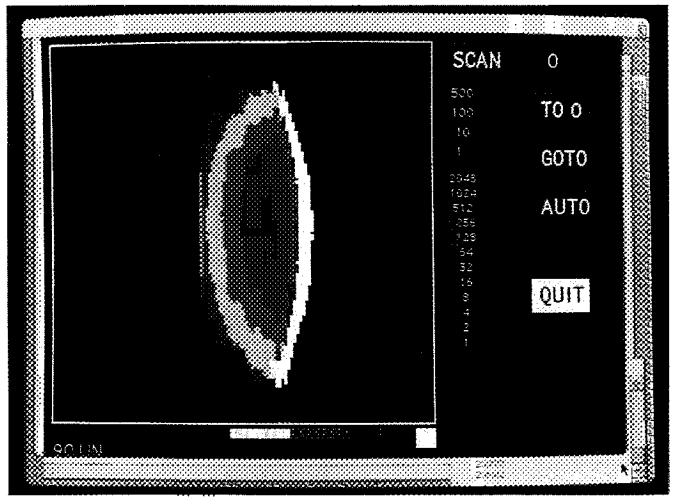

Image of the laser beam cross section at the output of the modulator illustrating the elongation of the beam caused by the optical waveguide in the modulator.

Mauna Kea in Hawaii. This receiver has already been used for the study of ethane and ethylene on Jupiter and Titan as well as for measuring the winds of Venus by Doppler techniques.

This work was done in collaboration with Zhiping Chu and Peter Cheo of the University of Connecticut.

Contact: David Buhl (Code 693)
301-286-3942

Theodor Kostiuk (Code 693)
301-286-8431

Sponsor: Office of Space Science

Dr. David Buhl is a research astronomer in the Planetary Systems Branch developing infrared receivers for astronomy and atmospheric experiments. He has also worked on techniques for using the Doppler shift of molecular lines to study the winds in planetary atmospheres, particularly the radio lines of CO. He was responsible for the detection of a number of molecules in the giant dust clouds of the galaxy, and for proposing that there is a direct link to molecules in Comets and the Origin of Life. David Buhl has degrees in Electrical Engineering from MIT and University of California at Berkeley and has been at GSFC for 20 years.

C-2

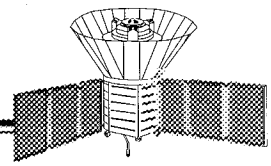

Dr. Theodor Kostiuk is an astrophysicist in the Planetary Systems Branch of the Laboratory for Extraterrestrial Physics and Chief Scientist for Exploration Programs in the Space Sciences Directorate. Dr. Kostiuk earned a PhD in Physics from Syracuse University and has 20 years of service at GSFC. His interests include composition, thermal structure and dynamics of planetary atmospheres, infrared spectroscopy and development of advanced instrumentation. He is currently on part-time detail to NASA Headquarters working in the Solar System Exploration Division managing the Planetary Instrument Definition and Development Program.

EARTH SYSTEM SCIENCE

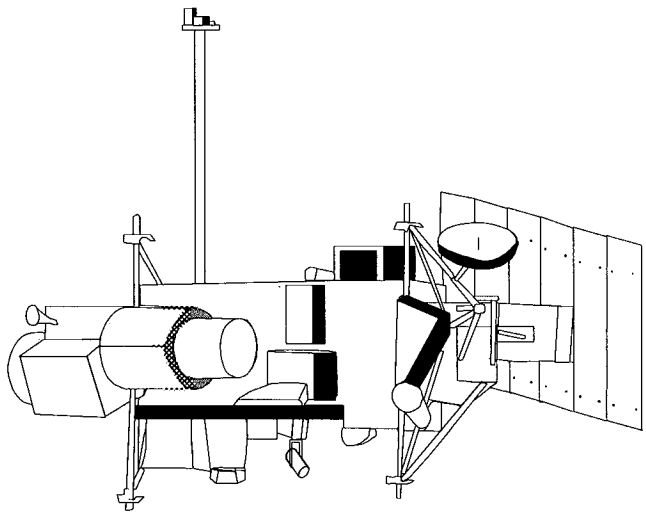

Goddard Space Flight Center's Earth Sciences Directorate plays a leadership role in the development of satellite and aircraft instruments and science algorithms to facilitate the study of the Earth as a system. In this example, an advanced prototype cloud retrieval algorithm uses narrowband visible, near-infrared, and thermal-infrared spectral information to differentiate between high cirrus clouds (purple and white), lower-level marine stratocumulus (greenish), and cirrus cloud shadows (purple in lower left of image). This algorithm will be employed on a global basis later this decade when Goddard's Moderate Resolution Imaging Spectroradiometer (MODIS) is flown as part of Mission to Planet Earth and the Earth Observing System.

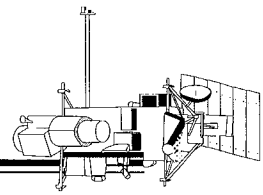

EARTH SYSTEM SCIENCE

THE SCIENTISTS AND ENGINEERS associated with research in Earth Science at GSFC continue to focus their efforts on defining the way the Earth works as an interactive system. The major motivation for this effort lies in NASA's goal of assessing the environmental effects of human activity and development, especially in terms of the possibilities for global warming and ozone depletion. Activities are continuing across a broad front: understanding the fundamental processes involved, modelling components of the system, building toward a comprehensive Earth system model, and developing the global observing systems needed to monitor the phenomena and make the measurements needed to understand the processes and to develop and test the models.

The novel and fundamental requirement of the Mission to Planet Earth (MTPE) enterprise is to understand the Earth in its entirety as a system. Our work in this area, as reflected in the papers selected for publication here, can be divided into several categories: atmospheres, oceans and ice, solid Earth, and soils and vegetation. Although it is convenient to present the work in this way, the reader should bear in mind that the ultimate goal is to link our understanding of these phenomena into a single, cross-disciplinary, comprehensive model of the Earth system.

Radiant transfer through the atmosphere is a major variable controlling the temperature of the Earth. In previous Research and Technology Reports we have presented the results of work on the amount, type and distribution of clouds. In this volume, two papers (Susskind; Whiteman et al.) describe efforts to measure relevant atmospheric variables such as water vapor and temperature. Another important factor concerns the energy involved in the evaporation and precipitation of water as a major driving force of the climate "engine." The paper by Adler et al. describes some results of studies of precipitation. Finally, the work by Heaps and Burris describes the measurement of those trace atmospheric constituents that can affect ozone balance.

Efforts to encapsulate the Earth processes into a comprehensive system description have already shown that ocean and ice components must be included to gain useful and predictive understanding of the system. Just as the evaporation-precipitation cycle acts as an engine that transfers energy between the atmosphere and the Earth's surface, ocean currents act as an engine transferring energy from one area of the globe to another. This is the basis for the work presented in the papers by Sanchez, Suarez, and Walsh. Conversely, polar ice cover acts as a valve controlling the absorption of solar radiation, so its extent must be monitored in order to determine the energy input to the engine. Observations of relevant phenomena are presented in papers by Parkinson and Gloersen.

The Earth system also operates on time scales much longer than the decadal scale phenomena described in the above-mentioned papers. Precise geodetic observations have enabled our scientists to study both contemporary, very slow motions across the Pacific-North American plate boundary (Sauber et al.), as well as the ancient tilting of lake shores during the creation of the Andes mountains (Bills).

The amount of global vegetation cover is a controlling factor in both the Earth's radiation balance and its moisture balance. Although our earlier research has allowed us to estimate the extent of the global biomass, we must understand the vegetation structure itself to determine the sensitivity of this biomass to climate change. Novel techniques for obtaining such information are described in papers by Harding and Blair, and by O'Neill and Petrella. The paper by Rosenzweig and Rind discusses the potential impact of such changes on the world's food supply.

These papers should be read individually to appreciate the significant advances in science and technology involved. However, they should be considered as separate parts of a larger, integrated picture which portrays the Earth as a comprehensive system, with the objective of providing accurate assessments of the environmental impact of external (and generally anthropogenic) forcings.

Louis S. Walter

ATMOSPHERES

THE TIROS OPERATIONAL VERTICAL SOUNDER PATHFINDER PATH A DATASET

THE TIROS OPERATIONAL Vertical Sounder (TOVS) consists of three sounding instruments which were designed primarily to produce global fields of the three-dimensional temperature-moisture structure of the atmosphere. The High-resolution Infrared Radiation Sounder 2 (HIRS2) is a 20-channel, infrared radiometer with a spatial resolution of 18 km at nadir. Radiances in these channels are influenced by a number of surface and atmospheric parameters, including atmospheric temperature up to about 20 mb. The Microwave Sounding Unit (MSU) is a four-channel microwave radiometer with a spatial resolution of 100 km at nadir. The radiances of MSU are mostly sensitive to atmospheric temperature between the surface and about 50 mb. The Stratospheric Sounding Unit (SSU) is a three-channel, infrared, pressure-modulated radiometer with 147 km spatial resolution, whose radiances are sensitive to atmospheric temperature primarily above 20 mb, extending to about 0.4 mb. These instruments were first launched on TIROS N at the end of 1978. Similar instrumentation has flown on NOAA operational polar orbiting satellites to the present day; another is scheduled to fly on NOAA J, to be launched in the near future. In general, two satellites, with 2:30 a.m., p.m. and 7:30 a.m., p.m. local time equator crossing times are flying simultaneously. Because similar TOVS instrumentation will have flown on operational satellites for a 16-year period between 1979 and 1995, the TOVS data provide an excellent capability to monitor natural climate variability and possibly identify global or regional trends during this time period. To do this, it is essential that data for the entire time period be processed in an identical manner, bearing in mind slight changes in instrument characteristics on the different satellites.

Pathfinder is a joint NASA/NOAA project to produce multiyear climate datasets from reanalysis of satellite data from NOAA operational satellites using a consistent processing scheme. Because of the variety and complexity of methods of analysis of TOVS data, a number of different processing methodologies, or Paths, were selected for use in analysis of the data. Our methodology, referred to as Path A, is called model-dependent, because a 6-hour forecast from a general circulation model is used as an initial guess for atmospheric temperature and moisture profiles in analysis of the data. Using a frozen processing system, we have analyzed NOAA 10 data (7:30 a.m., p.m. local time) for the period from December 1986 (the first month on NOAA 10) to December 1988. In addition, NOAA 9 data (2:30 a.m., p.m. local time) was processed for the period from December 1985 to December 1986 (the last month of NOAA 9). This gives a 3-year dataset, which includes the TOVS benchmark period from April 1987 to November 1988, and also contains a 1-month overlap between NOAA 9 and NOAA 10 data.

The Pathfinder Path A dataset contains a total of 45 retrieved quantities, gridded into 1° x 1° latitude/ longitude bins on a daily, 5-day, and monthly basis, with a.m. and p.m. orbits gridded separately. Gridded values include the mean value of each parameter, the standard deviation, and the number of cases in the sample. Among the retrieved quantities are: atmospheric temperatures at the surface and 11 mandatory pressure levels up to 30 mb; four coarse pressure layer mean temperatures; specific humidity at five mandatory levels up to 300 mb; total atmospheric precipitable water vapor above the surface and above four mandatory levels up to 300 mb; total integrated atmospheric O_3 amount; land or ocean surface skin temperature; fractional cloud cover, cloud-top pressure and cloud-top temperature; precipitation estimate; and outgoing longwave radiation (OLR).

Path A Product Error Assessment Monthly Mean Interannual Difference

	RMS	Bias
4-Coarse Layer Temperatures	0.7° to 1°	Bias <0.1°
Point Temperatures	1° to 2°	Bias <0.3°
Total Precipitable Water	0.2	
Precipitable Water Above Levels	25 to 40%	
Specific Humidity	25 to 40%	
Sea Surface Temperature	0.5°	
Land Surface Temperature	2°	
Total Ozone	5	
OLR	5 W/m^2	1 W/m^2
Cloud Fraction	0.1	
Cloud Top Pressure	50 mb	
Precipitation Estimate	3 mm/day	

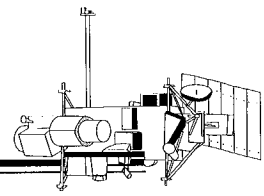

We have attempted to validate the accuracy of as many of these parameters as possible by comparing results with other collocated observations, such as radiosonde reports for atmospheric temperature and moisture profiles, ship and buoy reports for ocean surface skin temperature, Total Ozone Mapping Spectrometer (TOMS) observations for total ozone amounts, Earth Radiation Budget Experiment (ERBE) for OLR, and rain gauge reports for precipitation estimate. Because the Pathfinder data will be used to study interannual variability and possibly trends, it is important to assess the errors of the interannual monthly mean retrieved quantities compared to monthly mean differences of the validation data. Typical validation statistics for the interannual differences of NOAA 10 retrievals between the 12 months of the years 1987 and 1988 are given in the table. Bias refers to the error of the interannual difference averaged over all collocation areas for a typical month, while root-mean-square (RMS) errors indicate the RMS difference of the error over all collocation areas. The validation statistics for land surface skin temperature and cloud parameters are estimates. Comparisons were also made for interannual differences between months in 1986 (NOAA 9) and 1987 (NOAA 10), with comparable results. This indicates that the methodology produces retrieved quantities which are useful for studying climate variability even when years monitored by different satellites are compared.

The years 1987 and 1988 are particularly interesting because 1987 was a modest El Niño year, marked by anomalously warm ocean surface temperatures in the eastern equatorial Pacific Ocean, while 1988 had the reverse phenomenon of anomalously cold ocean temperatures in the same region. The first figure shows seasonal

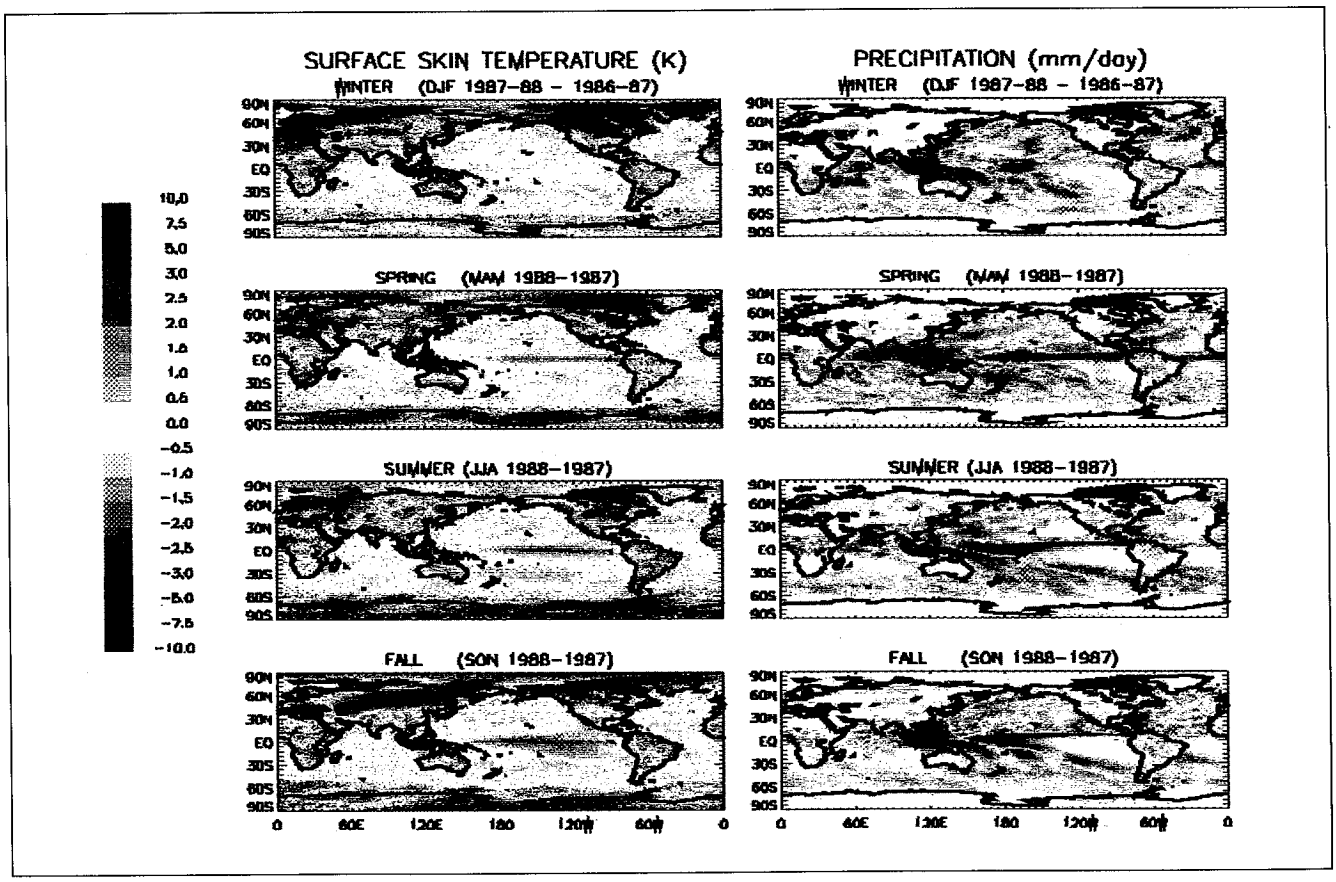

Interannual differences in surface skin temperature (K) and precipitation (mm/day) between each of the four seasons of 1988 and 1987. Red indicates increased temperature (precipitation) in 1988 compared to 1987 while blue indicates decreased values. The color scale is the same for both temperature and precipitation and is included in the figure.

mean differences of surface skin temperature (SST), and precipitation between 1987 and 1988 and 1986 and 1987 for the winter, spring, summer and fall seasons. The outstanding feature of the figure is that the SST differences between 1986 and 1987 and 1987 and 1988 are quite significant and show remarkable seasonal evolution. In the winter season, the SST differences are negligibly small along the equator. Significant differences appear first in spring, starting near the west coast of South America, with the spring of 1988 colder than 1987. In summer, the SST differences are as large as 2 to 4 K over a much larger area, moving westward from the South American coast. During fall, the westward propagation and expansion continues, and the SST differences are found over almost the entire equatorial Pacific Ocean between the dateline and 120°W. In addition to the equatorial Pacific Ocean, large coherent surface temperature differences can also be seen over the continental regions. For example, the temperatures over most of North America are much warmer during the summer of 1988 compared to 1987. It is well known that 1988 summer was a hot, dry year over North America.

The precipitation differences between 1988 and 1987 shown in the figure are also significant in all four seasons. In general, over the central and eastern equatorial Pacific Ocean, these differences are in phase with the SST differences, but with the maximum precipitation differences extending westward between 150°E to180. The precipitation over these regions in 1988 is lower compared to 1987 by 5 to 10 mm/day during all four seasons. Over the Maritime continent, South China Sea, Indian Ocean, Bay of Bengal, Arabian Sea, and Indian subcontinent, on the other hand, precipitation during 1988 is higher by 4 to 8 mm/day compared to 1987, although the SST differences over these regions are small. The precipitation differences found over the Indian and Pacific Ocean domains are most likely due to changes in local evaporation due to SST anomalies and changes in the atmospheric circulation, referred to as the southern oscillation, which is associated with anomalous SSTs in the Pacific Ocean.

While we feel the current 3-year dataset is useful for gaining some insights into interannual variability, as shown above, we have identified some shortcomings in the dataset. Therefore, an improved processing system has been developed to process the entire 16-year dataset (1979 to 1995), with completion expected in 1996. The original three-year dataset is currently available from the GSFC DAAC.

Contact: Joel Susskind (Code 910.4)
301-286-7210

Sponsor: Office of Mission to Planet Earth

Dr. Joel Susskind is Head of the Satellite Data Utilization Office and METSAT Project Scientist. Dr. Susskind earned a PhD in Physical Chemistry at Berkeley in 1968, where he did theoretical and experimental microwave spectroscopy, and has been at GSFC since 1977. His research interests involve atmospheric infrared and microwave radiative transfer, remote sensing, and analysis of climate variability.

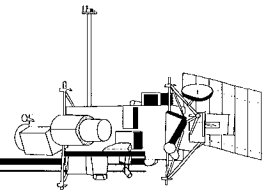

REMOTE MEASUREMENTS OF TEMPERATURE AND TRACE GASES USING A RAMAN LIDAR

MEASUREMENTS OF METHANE, temperature, and water allow the investigation of a number of interesting processes involving atmospheric transport. Using the instrument described in this report, it will now be possible to monitor the filamentary structures generated by the polar vortex, material that is peeled off the vortex edge, as it is carried into midlatitudinal regions. These regions have suffered unexpectedly low ozone levels in winter, raising questions as to whether this is primarily due to mixing of low-ozone air transported from the poles or whether chemistry within this region is making a significant contribution. Methane, a minor atmospheric constituent with a long residence time (>10 years), is an ideal tracer to identify the origin of an air parcel since levels within the polar vortex will be measurably lower than those found in midlatitudinal air.

Observations of water and temperature provide an opportunity to investigate the stratosphere's water budget. The oxidation of methane and other hydrocarbons are the major source of stratospheric water. Storms over the equatorial region of Southeast Asia are believed able to loft large quantities of water into the stratosphere, but precise values are not known. Water, an important greenhouse gas, can have a significant impact upon stratospheric temperature because of its strong infrared absorption.

Another transport process involving the tropics concerns a recently discovered barrier to the movement of air parcels poleward of ~20° latitude until the early fall. This barrier restricts the transport of volcanic aerosols and pollution—generated by high-flying aircraft—to the tropics for much of the year. Volcanic aerosols, such as those produced by eruption of the Philippine volcano, Mt. Pinatubo in 1991, can contribute to the destruction of ozone and to a decrease in stratospheric temperature as well. Measurements of methane, temperature, and water can help provide information on this phenomenon and can lead to estimates of the total mass of aerosols involved.

GSFC is developing a methane lidar (light detection and ranging) instrument, to remotely measure methane, temperature, and water vapor from an aircraft platform. The basic idea behind lidar is quite simple: a short and very intense pulse of light is produced (the instrument described here generates light at ~351 nm, in the near ultraviolet) which is scattered by the species of interest. Some of the scattered light is then collected by a telescope, detected by a photomultiplier tube, and counted by special electronics. The lasers, two xenon fluoride excimers, are among the most powerful lasers ever flown onboard an aircraft, with a combined output of 60 watts in the UV. The detector is built around filters to provide the spectral resolution and sensitivity required for the five data channels, with photon-counting photomultiplier tubes used as detectors. The complete package weighs ~1,500 kg, and measures ~6 by 1.5 by 1.5 m.

This instrument made a series of test flights from NASA's Wallops Island Flight Facility earlier this year. The simultaneous measurement of methane, water, and temperature provides the opportunity to study stratospheric and tropospheric dynamics on a scale not previously accessible by either satellite- or aircraft-based in situ instruments. A total of five test flights were made, including an 11-hour mission from Bangor, Maine, to Baffin Island and back, during which methane profiles up to 10 km above the aircraft were obtained. Temperature profiles to 60 km have also been demonstrated.

Contact: William Heaps (Code 916)
301-286-5106

John Burris (Code 916)
301-286-7473

Sponsor: Office of Mission to Planet Earth

Dr. William Heaps received his PhD in Physics from the University of Wisconsin in 1974. He has been at GSFC for 18 years where his primary interest has been in the optical detection of small molecules.

Dr. John Burris received his PhD in Physics from the University of Maryland in 1982. His primary research interests are the spectroscopy of small molecules and remote sensing.

SCANNING RAMAN LIDAR MEASUREMENTS OF ATMOSPHERIC WATER VAPOR DURING A COLD FRONTAL PASSAGE

THE GSFC SCANNING RAMAN Lidar (SRL) was successfully deployed at the Department of Energy's Cloud and Radiation Testbed (CART) Site in Billings, OK during April 1994 for the first Intensive Operation Period (IOP) hosted there. During the IOP, the SRL operated from just after sundown to just before sunrise for all declared evenings of operation. The lidar acquired more than 123 hours of data over 15 nights, with less than 1 hour of data lost due to a minor system malfunction. The SRL acquired data both on the vertical and in scanning mode toward an instrumented 60 m tower during various meteorological conditions, such as the intense cold frontal passage on April 15 described here.

The SRL uses a XeF excimer laser to transmit light at 351 nm. Return signals from four wavelengths are measured: the direct backscatter at the laser wavelength, and the Raman shifted returns due to water vapor (402 nm), nitrogen (383 nm) and oxygen (372 nm). The signals are gathered by a 0.76-m diameter telescope, and detected with photomultiplier tubes. The system includes a large 1.1-m by 0.8-m scan mirror, which allows the full aperture of the telescope to be scanned from horizon to horizon in a single scan plane. During normal operations, over 23,000 laser pulses are averaged to form 1-minute profiles of water vapor mixing ratio and aerosol scattering ratio, with 75-m range resolution.

The Raman lidar is uniquely capable of revealing the structure within complex frontal systems. The scanning capability of the SRL was used on the evening of April 15 to provide much higher vertical resolution than given by vertical data alone. The surface analysis for 0500 UT showed a cold front extending from the upper midwest through north central Oklahoma and toward west Texas. The flow in advance of the front was moist and southerly, while winds behind the front were northerly and considerably dryer.

The first figure represents the water vapor mixing ratio as measured by the SRL pointing vertically during the night of April 15. The cold front is clearly evident; it extends from the surface at 0430 UT to about 3.8 km at 1100 UT. The moist air due to the southerly flow in advance of the front is evident at 0400 UT, with mixing ratios exceeding 12 g/kg. The oscillation in the leading edge of the cold front is expanded in the second figure. The first two oscillations resulted in cloud formation, which is indicated

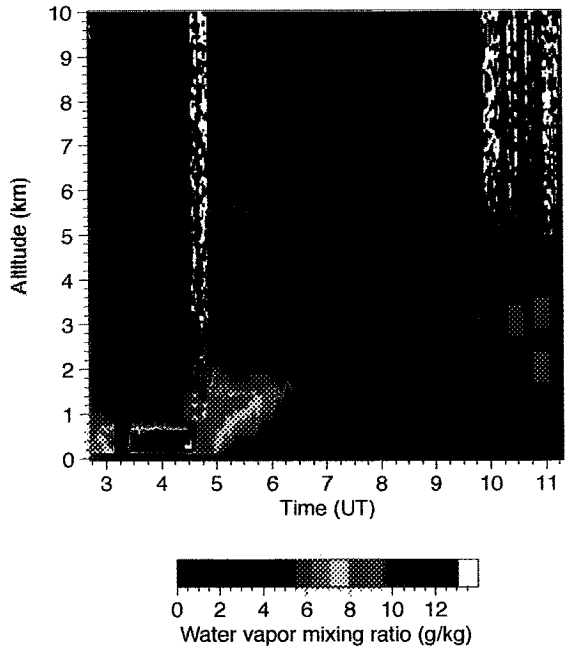

Lidar-derived water vapor mixing ratio at the DOE/CART site near Billings, OK during a cold frontal passage on the night of April 15, 1994. Vertical data.

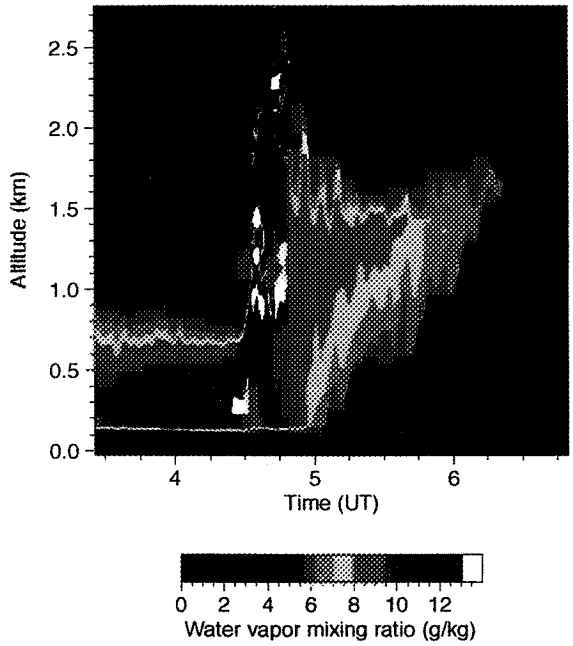

Expanded view of the oscillating leading edge of the cold front displayed in the first figure.

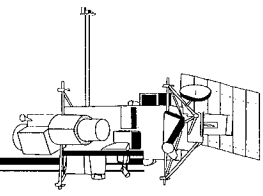

in the lidar imagery by the two vertical stripes at about 4.5 and 4.7 UT. The oscillations continued, but no further clouds were formed. The oscillations stopped after about 2 hours. These vertical lidar data provide striking detail of the complex structure of this frontal event.

The unique scanning capability of the SRL is demonstrated in the third figure. During the night, the SRL was acquiring data on the vertical as well as at 5° and 10° up from the horizon. The scanned data can be used to look at the same frontal passage with much higher vertical resolution assuming horizontal homogeneity. The third figure represents the water vapor mixing ratio as measured by the lidar while pointing at 10° above the horizon. The similarity between the second and third figures is immediately obvious. Due to the 4-minute temporal resolution of these scanned data, the oscillations in the front are not resolved but, for example, the vertical structure of the moist field in advance of the front is better resolved due to the equivalent 15-m resolution of these scanned data.

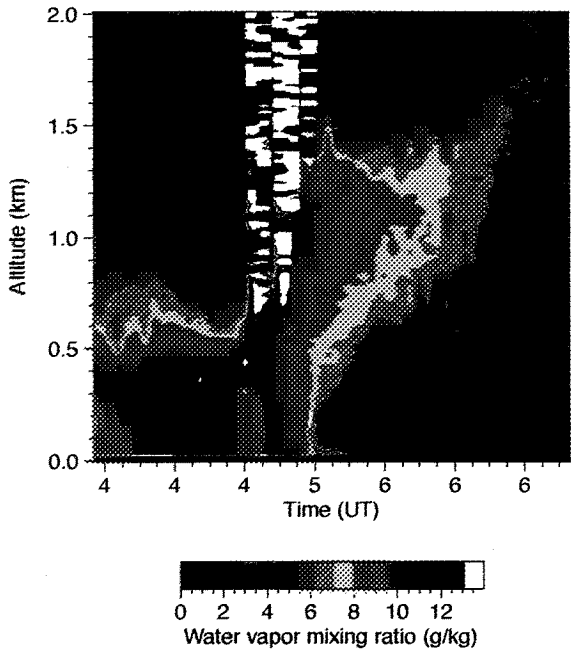

Lidar-derived water vapor mixing ratio at the DOE/CART site near Billings, OK using scanned data at 10° above the horizon during a cold frontal passage on the night of April 15, 1994. Note the improved vertical resolution as compared with the first figure.

The scanned data provide a valuable additional source of information in the study of the complex dynamics of this frontal passage. In addition, the excellent array of supportive data provided by the CART site, along with the Oklahoma mesonet data should allow this frontal passage to be studied in greater detail, and provide new insight into the dynamics of cold frontal passages.

Contact: Dave Whiteman (Code 924)
301-286-3115
dave@eib1.gsfc.nasa.gov

Harvey Melfi (UMBC)
410-455-2186
melfi@umbc.edu

Rich Ferrare (Hughes STX)
301-286-9089
ferrare@agnes.gsfc.nasa.gov

Keith Evans (Hughes STX)
301-286-9113
keith@raman5.gsfc.nasa.gov

Sponsor: Office of Mission to Planet Earth

Mr. David Whiteman joined NASA/GSFC in 1979. He is a physical scientist in the Experimental Instrumentation Branch of the Laboratory for Terrestrial Physics. Mr. Whiteman has concentrated on the design, development, and operation of lidar systems measuring stratospheric ozone and tropospheric water vapor and aerosols. He holds a BA in Physics from Williams College in Massachusetts.

Dr. Harvey Melfi earned his PhD in Physics from the College of William and Mary in 1970. He worked for over 20 years with both NASA and the EPA in the use of lasers in monitoring the atmosphere. He is currently a professor of Physics at the University of Maryland, Baltimore County.

Mr. Richard Ferrare is a principal scientist with Hughes STX. Mr. Ferrare earned a BS in Physics from the Pennsylvania State University and an MS in Meteorology from the University of Wisconsin- Madison. For the last 6 years, he has worked in the field of lidar remote sensing, developing algorithms for the retrieval of atmospheric water vapor, aerosols, temperature, and ozone using lidar data.

Mr. Keith Evans is employed by Hughes STX as a senior scientist. He holds an MS in Physics from American University in Washington, D.C. Mr. Evans began working in the field of lidar remote sensing over 3 years ago, developing algorithms for the retrieval of atmospheric number density and temperature and for statistical analyses including the spectra of the atmospheric water vapor mixing ratio.

ATMOSPHERIC MODEL SIMULATIONS OF A NARROW COLD FRONT RAINBAND

MESOSCALE ATMOSPHERIC models have been used to understand the physical processes in studies of tropical and extratropical cyclones, mesoscale convective systems, midlatitude fronts, sea-breeze circulations, and terrain-driven circulations. With a better understanding of mesoscale processes, we can derive better subgrid parameterizations for General Circulation Models (GCMs) and, therefore, have a better opportunity to correctly predict global climate changes. The Mesoscale Dynamics and Precipitations Branch recently acquired a Mesoscale Modeling System (MM5) from NCAR and Pennsylvania State University. The purposes for use of this system are: (1) to support Tropical Rainfall Measuring Mission (TRMM), Earth Observing System (EOS), and TOGA/COARE research; (2) to develop data assimilation techniques using NASA satellite datasets; (3) to explore cumulus parameterization schemes in conjunction with GSFC's cloud model; and (4) to study scale-interactive processes between global scale-, mesoscale-, and cloud-scale models. At GSFC, the MM5 model has been used in the simulation of a midlatitude Narrow Cold Front Rainband (NCFR) case, a squall line case, a South American Mesoscale Convective System case, and a case to assimilate Hurricane Florence using the Special Sensor Microwave/Imager (SSM/I) satellite dataset. In this report, we summarize the recent results from analysis of the NCFR case.

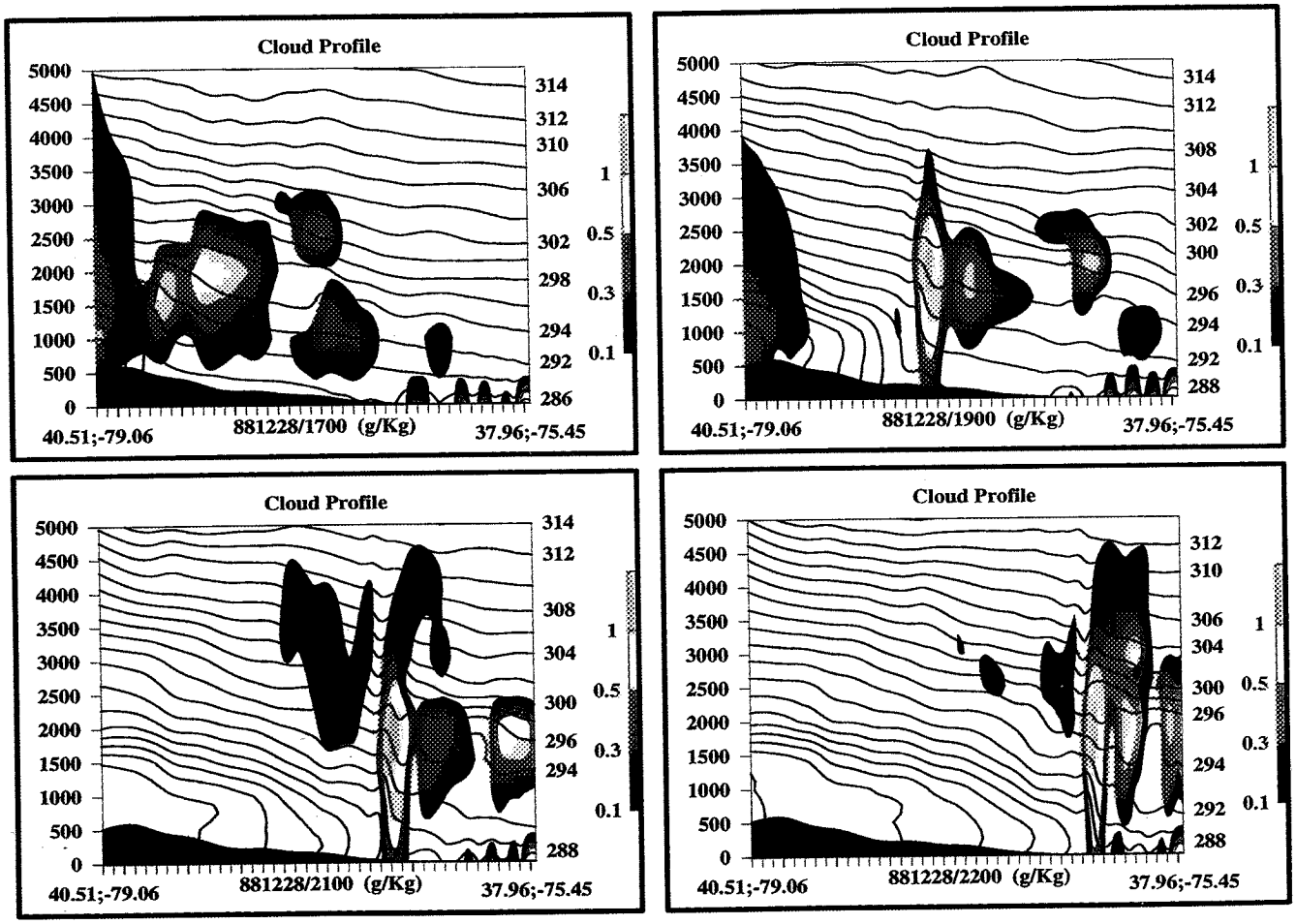

The xz cross section of cloud profile at hours from 1700 UTC to 2200 UTC. The color shading represents hydrometeor contents (g/kg), while the solid lines represent the contour of potential temperature (K).

A cold frontal rainband which occurred in the afternoon of December 28, 1988 was numerically simulated using MM5. A storm, which was associated with the frontal passage, caused considerable damage throughout a large region extending from central Virginia to Connecticut. The severity of the storm was not predicted in official weather forecasts issued that day. The storm was characterized by a line of severe convection with gravity-current-like structure along the leading edge of a strong surface cold front. One popular hypothesis asserts that such gravity-current-like structure is associated with the cold air outflow generated by evaporative cooling associated with the precipitation systems in the postfrontal region. This hypothesis was not supported by our model sensitivity tests. To be specific, turning off the moist processes in the model did not significantly affect the gravity-current-like structure of the front.

In our numerical experiments, three nested domains were constructed with grid resolutions of 45, 15, and 5 km, respectively. The innermost grid domain covers the entire Maryland, Virginia, and Washington, D.C. metropolitan areas. The model-simulated precipitation pattern, which showed a two-band structure, was found to be in close agreement with satellite observations of the temporal and spatial characteristics of the rainband. The modeled area of maximum precipitation was also in close agreement with radar observations of the area of maximum

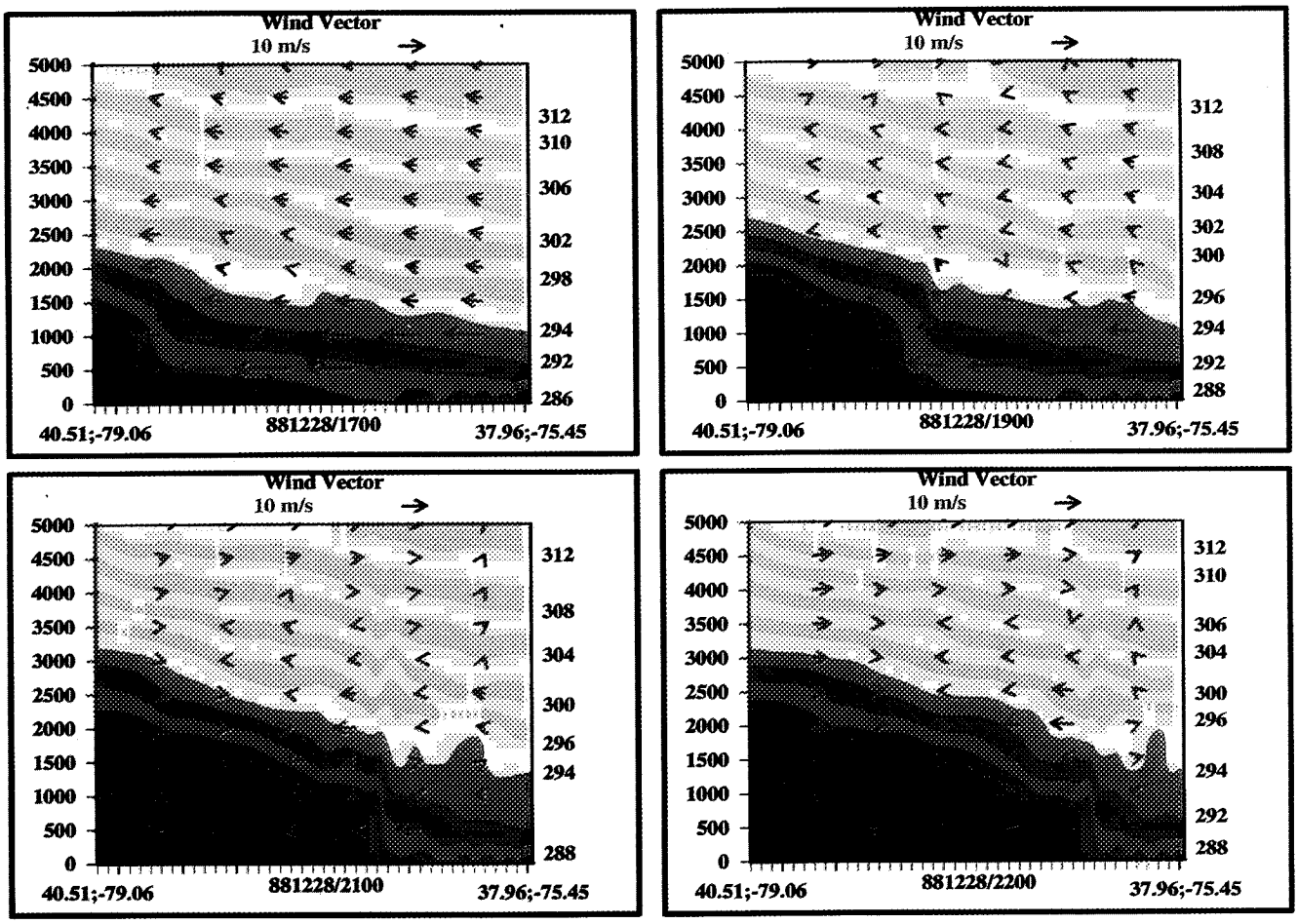

As in the first figure, except for the profile of wind vector (red arrows) to show the existence of low-level wind shear in the prefrontal environment. The contour of the potential temperature is shown by shaded colors, in which the main body of the cold front is manifested by light and dark blue colors.

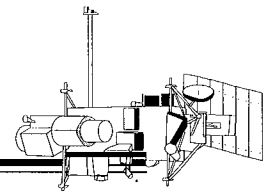

precipitation. The success of the model application in this case illustrates the great potential of MM5 as an effective metropolitan forecasting system.

We also investigated the role of terrain in affecting the rainband structure. This was done by comparing a no-terrain simulation with the control simulation. The comparison indicated that the observed rainband is organized by terrain features (as seen in the first figure), and associated downslope winds. In general, the case without terrain produced a wider rainband with a weaker precipitation rate. Note however, that while the terrain did affect cloud structure, it had little effect on the formation of the gravity-current-like structure.

To explain the gravity-current-like characteristics of the front, we suggested that the gravity-current- like feature is closely linked to the sign of the along-front, near-surface wind, both ahead of the front and at the front itself. Imagine that an eastward moving front lies parallel to a longitude line; then, if the prefrontal wind is southerly, Ekman-like boundary layer structure leads to low-level shear (as shown in the second figure), which tends to make the front more vertical. If the flow is southerly at the front itself, frictional processes create negative potential vorticity; this tends to reduce the resistance of the atmosphere to vertical motion. Thus, we expect more intense squall lines when the wind both at and ahead of the front is southerly.

Contact: Robert Adler (Code 912)
301-286-9086

Chaing Chen (SSAI)
301-286-5948

Craig Bishop (USRA)
301-286-4058

George Lai (SSAI)
301-286-3026

Sponsor: Office of Mission to Planet Earth

Dr. Robert Adler is Head of the Mesoscale Dynamics and Precipitation Branch of the Laboratory for Atmospheres. He holds a PhD in Atmospheric Science from Colorado State University.

Dr. Chaing Chen has 3 years of experience at GSFC. His main interests are cloud/mesoscale modeling and studies of mesoscale circulations interacted with cloud convections. He earned his PhD in Atmospheric Science from Colorado State university.

Dr. Craig Bishop joined GSFC as a visiting scientist in March 1994. He received his PhD from Monash University, Australia. His main interests are frontogenesis, cyclogenesis, the stability of time dependent flows, tropical cyclone bogussing, potential vorticity diagnostics and the effect of boundary layer potential vorticity production on climate.

Mr. George Lai has been working on mesoscale modeling at GSFC for 2 years. His special interests are mesoscale modeling, scientific visualization, and adjoint modeling. He received an MS in Atmospheric Science and an MS in Electrical Engineering from the University of California, Davis.

OCEANS AND ICE

OCEAN TIDES AND CIRCULATION MODELS BASED ON TOPEX/POSEIDON ALTIMETRY DATA

THE MOVEMENT OF WATER in Earth's oceans has many important implications for all life on the planet. For example, the oceans play important roles in global climate and its fluctuations by transferring heat from the equator to the poles. Further, the rate at which the burning of fossil fuels produces a rise in atmospheric temperature is dependent on the rate of absorption of CO_2 by the oceans and the amount of ocean warming produced by interactions with the atmosphere. Transfers of heat and momentum between the atmosphere and ocean are responsible for such events as El Niño, which affect global weather patterns. Other important phenomena are the movement of wastes and pollutants in the oceans on long time scales, and the oceanic flows which influence the relatively small areas where the world's fisheries are located.

Satellite systems can provide the global, synoptic datasets to describe global scale ocean circulation. Satellite observations of the oceans include such variables as color, temperature, ice cover, and the roughness and topography of the sea surface. From the latter, it is possible to derive information about the wave height, wind speed and direction, surface currents, and astronomically forced ocean tides. The roughness and topography of the sea surface are measured by means of specialized radars such as scatterometers and altimeters. Scatterometers are used to measure surface wind direction; they illuminate the sea surface at nonvertical angles. Altimeters use vertical illumination to measure wind speed, wave height, and the height of the satellite above the sea surface. If the position of the satellite with respect to the center of the Earth is known, then it is possible to compute the height of the sea surface with respect to the geocenter. Satellite altimetry measurements yield sea surface topography (SST) on a global basis. The SST represents the response to a sum of forces, with gravity (gravitational force plus centrifugal force due to the rotation of the Earth) predominating. The Earth's gravitational field also plays a dominant role in the determination of the satellite orbits. In the absence of other forces, the sea level would be an equipotential gravity surface called the geoid. The departure of the ocean surface from the geoid is due to the near-surface ocean circulation, the ocean tides, and a variety of other signals, including orbit error. To accurately determine ocean circulation, it is necessary to have precise models of the ocean tides as well as precisely determined satellite orbits.

Advances in computer technology and numerical techniques allowed the development of global tidal models during the late sixties, seventies, and early eighties, and the advent of satellite altimetry introduced a new era in the development of tidal models. Specifically, the success of the TOPEX/Poseidon mission is providing a new level of accuracy in the models based on satellite altimetry. TOPEX/Poseidon is a joint mission involving both NASA and the French Centre National d'Etudes Spatiales (CNES), cooperating in space and in oceanographic studies. The mission is designed to enhance the present understanding of global ocean dynamics by making precise observations of oceanic topography over a period of several years, using radar altimeters on an Earth satellite placed on a very accurately determined orbit.

Global tidal modeling has become an interdisciplinary subject, as tidal effects are important in better determination of gravity fields and satellite orbits, Earth rotation studies, and studies of the evolution of the Earth-Moon system, to name a few. The tidal potential is decomposed into a series of harmonic constituents, whose frequencies are determined by the rotation of the Earth and the motion of the Sun and the Moon. The principal constituent, the semidiurnal lunar tide, is called M2, which has a period of 12 hours, 25 minutes. An M2 solution, based on TOPEX altimetry data, is shown in the first figure. The solution was obtained by means of an expansion in terms of Proudman functions, which are defined in the ocean basins alone, and exhibit a number of desirable characteristics, such as mass conservation and orthogonality.

The determination of the large scale ocean circulation from satellite altimetry traditionally involves two distinct steps: (1) the determination of the sea surface topography, and, (2) the determination of the flow field associated with it. The balance of pressure forces (due to surface topography) and the Coriolis force (due to water flow and Earth rotation) predominates over most of the ocean surfaces, except in areas close to the equator where the Coriolis force vanishes. We have developed a new technique to

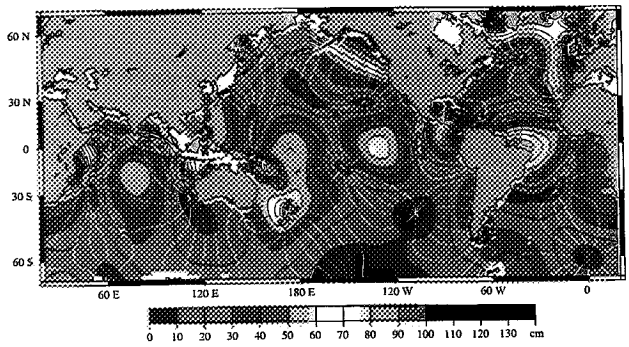

The amplitude (in color) and cotidal phase lines (in white) of the principal semidiurnal lunar tide M2. The thickest white lines connect locations experiencing high water at the time when the mean Moon passes the Greenwich meridian. Altimetry data used in the solution is from the first year of the TOPEX/Poseidon mission. Proudman functions were computed on a 2 by 2 spherical coordinate grid.

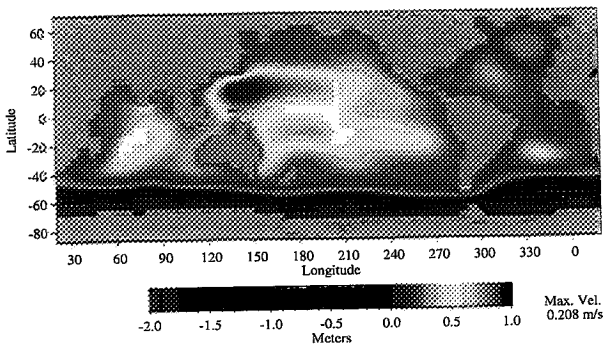

The SST (in color) and the circulation (white arrows) based on the first year of TOPEX/Poseidon altimetry data. Surface height functions and stream functions were computed on a 4 by 4 spherical coordinate grid. Maximum velocity locations are indicated by black arrows.

obtain the SST and associated flow field from TOPEX altimetry; those results are shown in the second figure. The new method allows the ocean currents to be computed over the entire ocean basins, including the equatorial regions. The functional representation is defined on the ocean basins alone, avoiding the difficulties encountered when using functions defined over the entire sphere.

Dr. Nikolaos K. Pavlis, Mr. William J. Cunningham, Jr., and Mr. Richard Ray, all from Hughes STX, and Dr. Dennis Morrow, of Cray Research Inc., made significant contributions to this project.

Contact: Braulio Sanchez (Code 926)
301-286-6741

Sponsor: Office of Mission to Planet Earth

Dr. Braulio Sanchez, who has been at GSFC for 16 years, works in the Space Geodesy Branch of the Laboratory for Terrestrial Physics. He is a principal investigator in the TOPEX/Poseidon project. His main interests include space geodesy, oceanography, and geodynamics. He received a BS from Northrop Institute of Technology, an MS from Iowa State University, and a PhD from the University of Texas at Austin.

THE LENGTH OF THE SEA ICE SEASON IN THE SOUTHERN OCEAN

BECAUSE SEA ICE is a strong insulator between the ocean and the atmosphere and a strong reflector of solar radiation, the length of the sea ice season has important direct impacts on polar climates. Other things being equal, a longer sea ice season results in less absorption of solar radiation by the ocean, less heat exchange between the ocean and the atmosphere, and less evaporation from the surface. There is also less momentum transfer from the winds to the liquid ocean, because some of the momentum is transferred to ice instead of to water.

Prior to the 1970s, the length of the sea ice season could be examined only for restricted individual locations. Long-term records exist primarily for the north coast of Iceland and for Laurie Island in the South Atlantic. With satellite technology, the variable can now be examined and mapped throughout the polar and subpolar regions. Satellite passive-microwave observations in particular are able to obtain sea ice information on a routine basis, due to the sharp contrast in microwave emissions of sea ice and sea water, and the ability of passive-microwave instruments to obtain global or near-global observations every few days. Satellite passive-microwave observations were used to examine the length of the sea ice season throughout the Southern Ocean for the period from 1979 to 1986, in the ocean regions mapped in the first figure.

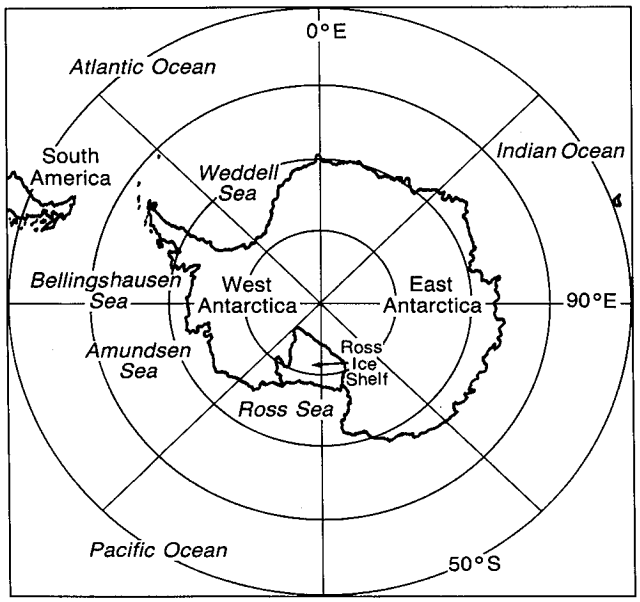

Location map for the south polar region.

The data used are from the Nimbus 7 scanning multichannel microwave radiometer (SMMR), a 10-channel, passive-microwave instrument that operated, generally on an every-other-day basis, from the launch of Nimbus 7 (October 24, 1978), until the SMMR scanning mechanism was turned off (August 20, 1987). The resulting dataset is the longest single-source data record for large-scale sea ice coverage, and includes year-round data from 1979 to 1986. Three of the ten SMMR channels are used in the calculation of sea ice concentrations (percent areal coverages), which are obtained to a spatial resolution of approximately 55 km and an estimated accuracy of ±7 percent. These gridded sea ice concentrations are then used to determine the length of the sea ice season, calculated at each grid point for each of the years from 1979 to 1986 by counting the number of days in the year having ice concentrations greater than 30 percent. Alternative ice concentration cutoffs of 15 and 50 percent were also tested, and both yielded the same conclusions as those found with the 30 percent cutoff, indicating a desired insensitivity of the results to the particular choice of ice concentration cutoff. By counting day-by-day, temporary advances and retreats of the ice cover are automatically taken into account in the length of the sea ice season, as are temporary openings and closings within the ice cover.

Spatial mapping of the results reveals that the length of the sea ice season in the Southern Ocean varies from a few days or a few weeks in the outer reaches of the wintertime ice pack, to a full year in sizeable regions of the southernmost portion of the Bellingshausen Sea, the westernmost portion of the Weddell Sea, and the southern but noncoastal Amundsen Sea, equatorward of the region of coastal polynyas (open-water regions within an ice cover). Considerably smaller regions of perennial or near-perennial ice exist at scattered locations along the Antarctic coast.

As indicated in the second figure, showing the average results over the period from 1979 to 1986, the length of the ice season, in general, decreases northward away from the Antarctic continent. Notable exceptions to this generality occur in two major regions (within the Weddell and Ross Seas) and in one lesser region (within the Amundsen Sea). In the Weddell Sea, a prominent east/west component to the spatial variability exists in addition to the north/south component, with season lengths decreasing from southwest to northeast. This can be explained by the cold

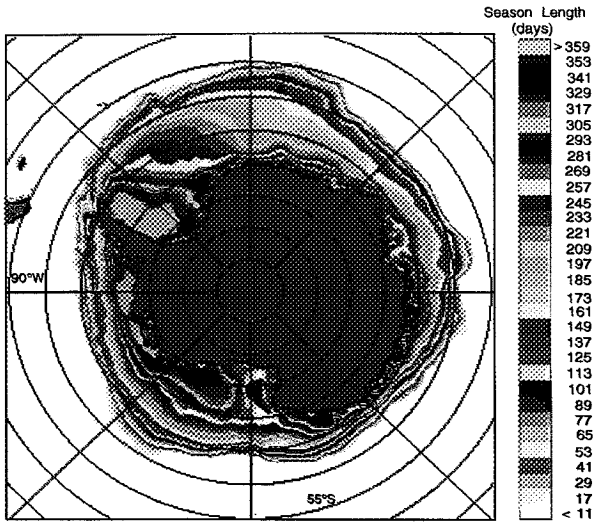

Average length, in days, of the sea ice season in the Southern Ocean over the years 1979 to 1986, calculated from the data of the Nimbus 7 SMMR. A grid element is considered to have sea ice if the ice concentration in that grid element exceeds 30 percent. (Nonocean colors appearing just off the coast of South America and the Falkland Islands to its east are due to land contamination of the microwave signal and should be ignored. This is true also for the third figure.)

waters and clockwise circulation patterns in the Weddell Sea. In the Ross Sea, directly north of the Ross Ice Shelf the patterns show a relative minimum in the midst of the sea, reflective of the frequent wintertime polynyas and consistent early opening of the ice cover in this region. Both the polynyas and the early opening are due, in part, to upwelling of relatively warm, salty water, and, in part, to strong south winds from off the Ross Ice Shelf, pushing the ice northward. In the Amundsen Sea, the frequent coastal polynyas off the many small ice shelves bordering the sea result in shorter season lengths adjacent to the coast than are found 2° to 3° latitude further equatorward. Although the basics described in the two preceding paragraphs are consistent for each year of the dataset, considerable interannual variability occurs in the details of the mapped ice-season lengths for the individual years (data not shown). For instance, at many locations the season length differed in consecutive years by over 50 days. Among the prominent regional interannual differences are the generally longer ice seasons in the Weddell and Bellingshausen Seas in the early part of the 1979 to 1986 period than in the later part, and the generally longer ice seasons in the Ross Sea in the later part of the period than in the early part. These and some of the other interannual differences can be summarized through the mapping of temporal trends.

The trend in the length of the sea ice season over the course of the 8 years (1979-1986) was calculated at each grid point as the slope of the line of least-squares fit through the yearly ice season lengths. The results, shown in the third figure, provide a strong visual depiction of basic patterns of change over the course of the 8-year record. As was the case with similar calculations earlier done for the northern hemisphere (see the *1992 GSFC Research and Technology Report,* page 77), the trends in the season lengths in the Southern Ocean show considerable spatial coherence and large regions with trends toward longer ice seasons, as well as large regions with trends toward shorter ice seasons. More specifically, the general trend over the 1979 to 1986 period was toward longer sea ice seasons in the Ross Sea, the south central Weddell Sea, and in much of the noncoastal pack off East Antarctica,

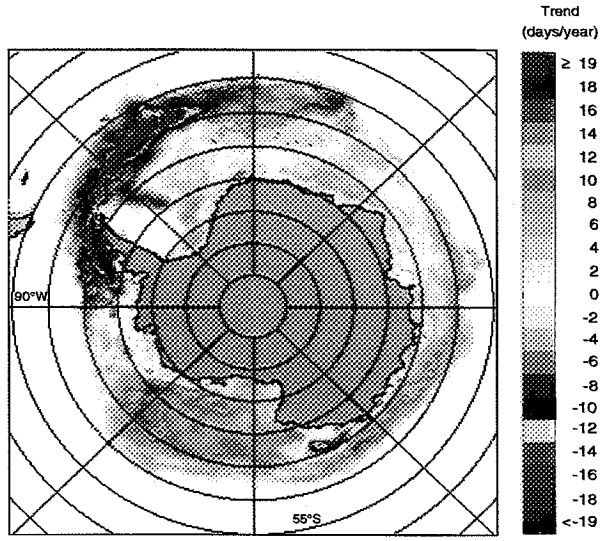

Trends in the length of the sea ice season in the Southern Ocean over the period from 1979 to 1986, calculated from the data of the Nimbus 7 SMMR using an ice concentration cutoff of 30 percent. Positive values indicate that the sea ice season tended to lengthen over the period, negative values that it tended to shorten.

and toward shorter sea ice seasons in the northern Bellingshausen Sea, the northern and eastern Weddell Sea, and the near-coastal waters off East Antarctica from about 95°E to about 160°E.

Previous analyses of time series of sea ice extents (areal coverages) in the Southern Ocean over the course of the SMMR dataset revealed no significant trends in Southern Ocean ice extent as a whole. The present study, through the roughly even distribution of positive and negative trends shown in the third figure, confirms the lack of major hemispheric-scale increases or decreases over the SMMR period and adds considerable spatial detail. The results are spatially very coherent and are not strongly dependent on the choice of the ice concentration cutoff used in the definition of the length of the sea ice season.

Contact: Claire Parkinson (Code 971)
301-286-6507

Sponsor: Office of Mission to Planet Earth

Dr. Claire Parkinson is a climatologist in the Oceans and Ice Branch and Project Scientist for the EOS PM mission. She has been employed at GSFC for 16 years, with her research centering largely on satellite data analysis of sea ice and its relevance to climate. She has also authored a book on the history of science and coauthored a book on climate modeling. She has a BA in Mathematics from Wellesley College and a PhD in Climatology from Ohio State University.

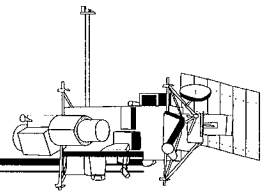

EL NIÑO-SOUTHERN OSCILLATION FREQUENCY COMPONENTS IN THE GLOBAL SEA ICE COVER

SEA ICE MARGINS in both the Arctic and the Antarctic have been used as a means of monitoring global climate changes on decadal and greater time scales. On shorter time scales, there are strong interannual variations evident in the time series of sea ice covers of the north and south as well as in localized regions. Removal of the strong seasonal cycle from the sea ice extents (essentially the area enclosed by the ice margin), obtained from the 9-year record produced from the SMMR on board the NASA satellite Nimbus-7, reveals undulations with periods greater than annual in the residual, but their spectral composition is not well defined. An improved view of the spectral composition is obtained by a multiple-window tapered-spectral analysis of this time series, revealing statistically significant periodicity with quasi-biennial and quasi-quadrennial components similar to those found in the El Niño/Southern Oscillation (ENSO) Index.

Quasi-biennial and quadrennial periodicities attributed to the ENSO appear as significant spectral components in the time series of the length-of-day (LOD) parameter, as determined from very long baseline interferometer, space geodetic, satellite laser ranging and Global Positioning Satellite (GPS) data. These spectral components also appear in the atmospheric angular momentum arising from zonally averaged global winds. With such clearly implied global aspects of ENSO effects, one might suspect that evidences of the ENSO should also clearly appear in the global sea ice covers. Yet, a clear observation has eluded investigators to date because of the strong seasonal signal in sea ice coverage and from localized weather events, which most certainly affect the nearby sea ice coverage.

To clarify comparisons of this sort, I utilized a technique developed by others for investigating seismic, atmospheric carbon dioxide, and other time series records to examine the time series of ice extents and ice areas (the ice extent less the amount of open water within the ice margin) in a 9-year record obtained from the SMMR on board the NASA Nimbus 7 satellite. I have also applied the technique to the LOD parameter, which has been suggested as a proxy for the ENSO events. This technique entails Fourier analysis of the data, including the use of eight different window filtering functions. It permits investigation within a narrow spectral range to exclude interfering events, with the result that the ENSO spectral components are more clearly seen than before in the LOD and, for the first time, in the sea ice cover. To obtain narrower spectral lines than result from the model solution amplitudes, I have utilized an F-test statistic, which is the ratio of the explained to unexplained variance within the spectral bandwidth.

The first figure shows plots of some results of this analysis. A quasi-quadrennial (QQ) component is the strongest line in the Arctic spectrum (panel a, first figure) with an F-statistic of about 4.5, well above the 95 percent confidence level at the F-value of 3.75. There are quasi-triennial (QT) and biennial (QB) peaks of lesser significance (an F-test value of 0.73 represents the 50 percent confidence level), and some even smaller, but distinct lines at periods of less than 2 years. The tail of the annual cycle line can be seen at the beginning of the spectrum. The spectrum of the Arctic sea ice area (the ice extent less the amount of open water within the ice perimeter) time series in panel a of the first figure is very similar to that of the Arctic extent, but with generally smaller values of F, consistent with the idea that the marginal sea ice zone might be more sensitive to ENSO forcing than the interior pack. The situation is similar in the Antarctic (panel b, first figure), but the F-values are generally smaller than in the Arctic, and the QT component is much more prominent.

To permit a direct comparison between the microwave and LOD data, I have performed the above analysis on a subset of the LOD data corresponding in time to the microwave data. The LOD power spectrum has been presented by others elsewhere; here, I present the spectrum of the F-test parameter of the LOD in both panels of the first figure. There is a close match between the QB and QQ components of the LOD and those of the Arctic and the Antarctic. The QT component in the Arctic and Antarctic is missing in the LOD spectrum; it appears to be an alias frequency resulting from the beating of the satellite revisit frequency against the diurnal or semidiurnal oceanic/atmospheric tidal frequency.

Returning to the idea of possible greater ENSO forcing in the marginal sea ice zones than in the interior pack, I have selected for similar analysis some Arctic regions that include some of the perimeter seas. The strongest indication of the QQ component, about twice the strength of that in the Arctic ice extent (as seen in panel (a) of the first figure) occurs in the time series of the Greenland Sea ice areas (panel (a) of the second figure) where also the

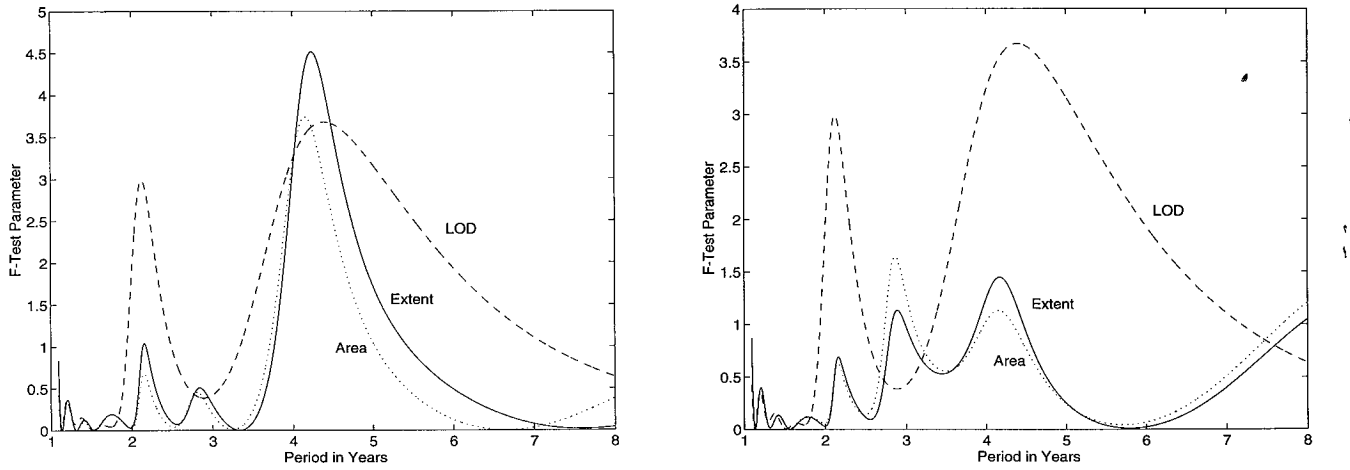

Spectral distribution of the F-test periodicity in the 9-year time series of sea ice area and extent in (a) the Arctic and (b) the Antarctic. The LOD spectrum is superimposed for comparison. In the Arctic, the QQ peak, at about 4.2 years, for the ice extent has a confidence level of 97 percent; those of the ice area and LOD, 94.5 percent. The strong QB peak in the LOD shows up in the sea ice area and extent with lower confidence levels, 60 percent or less.

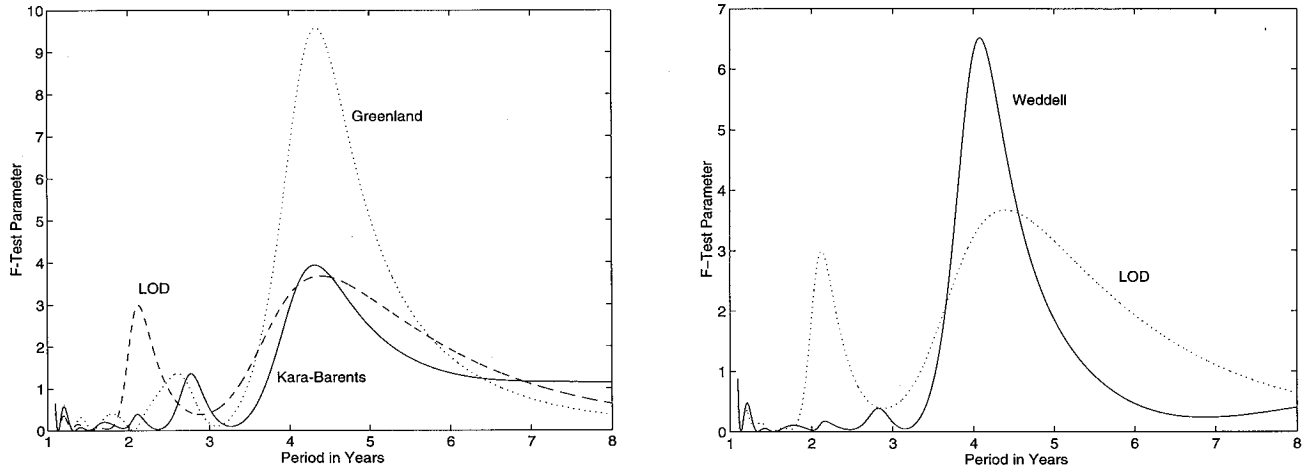

Same as the first figure, except for the sea ice area only in (a) the Greenland and Kara-Barents regions and (b) the Weddell Sea sector The confidence level of the QQ component in the Kara-Barents region is about 95 percent; in the Greenland Sea, well above 99 percent. In the Weddell Sea sector, the QQ component also predominates.

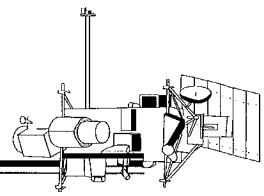

QB and QT components are not as distinct. The QQ component in the Kara-Barents region is comparable to that of the Arctic extent, while the QT component is more distinct. In the Bering region (not shown), the QQ and QT components appear to have shorter periods than the Arctic sum by about one-half year. In the Okhotsk-Japan region (not shown), the QQ, QT, and QB components run together and are all below the 70 percent confidence level.

Turning to the Antarctic, the Weddell Sea sector shows the QQ component as the only significant peak (panel b, second figure). In analyzing the data elsewhere in the Antarctic, it is found that the QB component is the strongest in the Bellingshausen-Amundsen Seas sector. Facing the central part of the South Pacific, the Ross Sea sector shows a strong QT peak and a weaker QB peak. In the Western Pacific and Indian Ocean sectors, only power beyond 5 years appears to be significant.

In conclusion, it is clear that variations in the areal coverage of sea ice on global, hemispheric, and regional bases contain periodicities of quasi-biennial and quadrennial components, very similar to the variations in the LOD parameter. These periodicities have also been observed by others in the ENSO Index and Atmospheric Angular Momentum parameters.

Contact: Per Gloersen (Code 971)
301-286-6362

Sponsor: Office of Mission to Planet Earth

Dr. Per Gloersen is a senior scientist in the Laboratory for Hydrospherics, Oceans and Ice Branch. He received his PhD in Physics from the Johns Hopkins University. He joined GSFC in 1970, after 14 years with the General Electric Company.

NUMERICAL SIMULATIONS OF EL NIÑO

EL NIÑO IS THE NAME given to the occasional warming of surface waters in the central and eastern tropical Pacific Ocean. El Niño events occur irregularly, typically every 3 to 5 years, and vary in both amplitude and in the details of their life cycles. Generally, however, we can say that the pool of warm waters normally confined to the western Pacific spreads eastward almost to the South American coast during an El Niño event. At the peak of the event, sea-surface temperature (SST) anomalies of 1 to 3°C extend along the equator westward from the South America coast to the central Pacific. The top two panels in the first figure show the distribution of SSTs for a normal December and for December of 1982, which was the peak stage of the largest El Niño event on record. The third panel shows the difference of SSTs between the mean December and December 1982.

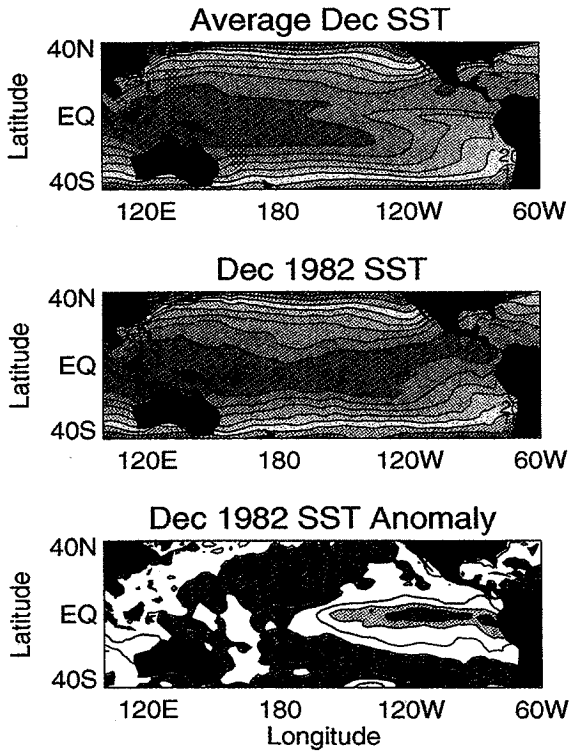

The distribution of SSTs for a normal December and for December of 1982, which was the peak stage of the largest El Niño event on record. In the upper panels, the contour interval is 2°C. In the lower panels, the contour interval is 1°C; red areas are waters over 3°C warmer than normal.

El Niño events are separated by periods of cold anomalies that have been whimsically named La Niña. Although much of the early attention to the phenomenon was devoted to the warm events with the intervening periods being regarded as normal times, the view now is that the situation is more symmetric, with El Niño and La Niña being regarded as warm and cold phases of an irregular oscillation of the ocean's circulation.

As one might expect, such large changes at the ocean's surface have a profound impact on events in the overlying atmosphere. Although most atmospheric variability occurs at much higher frequencies—the day-to-day variations of extratropical weather systems for example—it has been recognized since early in this century that large interannual variations also occur. One variation that seemed to be particularly regular was studied by Sir Gilbert Walker in the 1920s. It consists of a see-saw in atmospheric surface pressure across the tropical Pacific. Associated with these surface pressure changes, Walker also noted changes in temperature and precipitation. We now know that important changes also occur in the trade winds that flow from east to west over the surface of the equatorial Pacific. This interannual atmospheric variation was named the Southern Oscillation.

In the 1960s the two phenomena, El Niño and the Southern Oscillation, were linked. Warm temperatures in the eastern Pacific were associated with high precipitation and anomalously low atmospheric pressures in the eastern Pacific and anomalously high pressures in the western Pacific. These in turn resulted in weakened easterly trade winds. Opposite conditions occurred during cold events. This link between El Niño and the Southern Oscillation is illustrated in the three panels of the second figure, which show the history of observed SST anomalies in the eastern Pacific, of the east-west component of the surface wind over the equator and of rainfall anomalies in the central Pacific. When SSTs are anomalously warm, rainfall is anomalously high and surface wind anomalies tend to be positive (i.e., winds are less easterly). Because of the link between oceanic and atmospheric events, El Niño and the Southern Oscillation came to be regarded as a single phenomenon, which is often referred to as ENSO. Since the 1960s, research on ENSO has shown that not only are the ocean and atmospheric behaviors highly correlated, but that they seem to cause each other. The atmospheric behavior can be understood if the ocean behavior is given

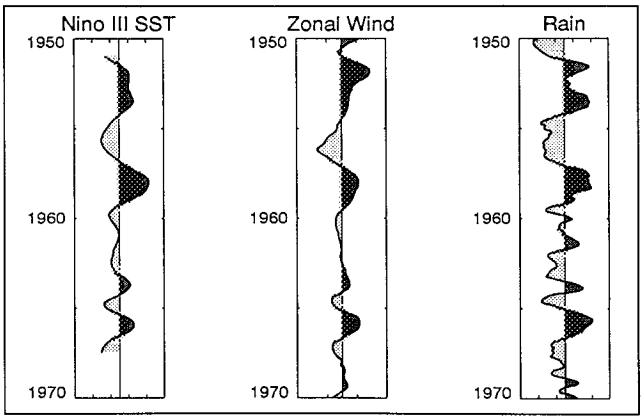

The link between El Niño SST anomalies, the strength of equatorial tradewinds, and rainfall anomalies over the central Pacific. Positive wind anomalies indicate weakened trades.

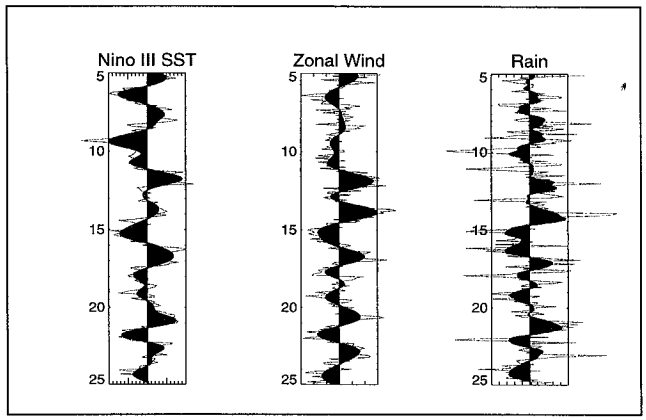

Results analogous to those in the second figure, but from the model simulation.

and vice-versa. This chicken-and-egg situation suggests that ENSO is fundamentally a coupled phenomenon. Modern theories, in fact, regard ENSO as a spontaneously occurring oscillation of the coupled system.

Current research on ENSO at GSFC focuses on simulating the phenomenon by using coupled ocean and atmosphere general circulation models, which are numerical models that solve the equations of motion for the two systems and produce simulations of the Earth's climate and its variability. Since ENSO should occur spontaneously if the ocean and atmosphere are properly modeled and their coupling is correctly represented, the ability of the models to produce ENSO-like variability without prescribing any ENSO-like forcing becomes a strong test of the quality of the models. The three panels in the third figure show results from the models. These are analogous to the panels in the second figure, but data are taken from a 20-year period of a long coupled run of the models. We see that the models produce qualitatively the same behavior as the ENSO observations, with a very similar synchronization of SST, wind, and rainfall anomalies.

Coupled simulations such as these allow us to study the ENSO phenomenon in ways we could not by using observations alone. Since we cannot experiment with the real system, observational studies are limited to diagnosing the evolution of the last few ENSO events. With the models, we can ask how sensitive ENSO is to existing conditions. For example, how does ENSO depend on the size of the Pacific basin? Does the dependence agree with that predicted by theory? Another important application of models will be to predict ENSO. In the near future, we may see 1- to 2-year forecasts of ENSO, just as we now have 5- to 10-day forecasts of midlatitude weather.

Contact: Max Suarez (Code 913)
301-286-7373

Sponsor: Office of Mission to Planet Earth

Dr. Max Suarez is a meteorologist at GSFC's Laboratory for Atmospheres. He earned his PhD in Geophysical Fluid Dynamics from Princeton University in 1976. Dr. Suarez has been at GSFC for 11 years and is now at the Climate and Radiation Branch. His main interests are climate modeling, interannual climate variability, ocean-atmosphere coupling, and the impact of hydrological processes on climate.

SCANNING RADAR ALTIMETER MEASUREMENTS OF SEA SURFACE MEAN SQUARE SLOPE DURING TOGA/COARE AND ITS RELATIONSHIP TO SEA SURFACE TEMPERATURE AND INTERNAL WAVES

THE LAST MAJOR undertaking of the 10-year Tropical Ocean Global Atmosphere (TOGA) program was the Coupled Ocean-Atmosphere Response Experiment (COARE), designed to clarify the role of the equatorial western Pacific warm pool in the mean and transient state of the tropical ocean-atmosphere system. The Intensive Observing Period (IOP) occurred from November 1, 1992 through February 28, 1993. During those 4 months, nearly 1,200 people from more than 20 nations conducted more than 700 days of ship operations, launched nearly 12,000 rawinsondes, completed 125 aircraft flights, and maintained continuous operation of 30 moored instrument systems. During November and December 1992, the Scanning Radar Altimeter (SRA) flew on one of the National Oceanographic and Atmospheric Administration (NOAA) P-3 aircraft for the TOGA/COARE, staging out of Guadalcanal in the Solomon Islands. The surprising results of a recent analysis, discussed here, were obtained in collaboration with Dr. Denise Hagan of the NASA Jet Propulsion Laboratory (JPL) and Dr. David Rogers of the Scripps Institution of Oceanography.

The SRA mode of the NASA Multimode Airborne Radar Altimeter (MARA) scans a pencil beam (1°, two-way) cross-track to produce raster lines at the rate of 10 Hz. It simultaneously measures the backscattered power at its 36 GHz (8 mm) operating frequency, and the sea surface topography at 64 points evenly spaced across a swath equal to 0.8 times the aircraft altitude. For a nadir-directed radar signal, the power backscattered from the sea surface falls off with increasing incidence angle at a rate determined by the mean-square-slope (mss) of the surface. For high wind speeds, the sea surface is generally very rough (high mss) and the falloff of power with incidence angle is gradual. For low wind speeds, the surface is smooth (low mss) and the falloff of power with incidence angle is rapid. The surface roughness is predominantly determined by short capillary waves (which are the steepest), rather than the large gravity waves that determine the wave height. Using a rigorous theoretical relationship quantitatively linking the falloff of backscattered power to mss, the SRA can characterize the short waves (which are most sensitive to the local wind), while its range measurements of the large wave topography determine the energetic portion of the directional wave spectrum.

On November 28, 1992, SRA topographic measurements indicated that the wave height was 1.5 m and that the sea surface gravity wave field was comprised of three swell components. A 430-m wavelength system propagated toward 195°, a second 430-m wavelength system propagated toward 115°, and a 150-m wavelength system propagated toward 25°. This day had the lightest wind of the experiment, with an average speed of about 2 m/s, based on measurements taken by the National Center for Atmospheric Research (NCAR) Electra aircraft at a height of 30 m. During the data collection interval, the mean wind direction was toward 70°. The mean surface current showed little variation for several days surrounding the flight and was about 0.45 m/s toward 60°, nearly in the downwind direction. This reduced the wind speed relative to the sea surface. With these very light winds there were times when the SRA backscattered power decreased by a factor of 20 by 3° off-nadir. This was an extremely specular region, despite the presence of the trimodal swell.

During a portion of the flight, the NOAA P-3 carrying the SRA flew wingtip to wingtip with the NCAR Electra carrying the JPL sea-surface temperature (SST) radiometer, which made thermal IR measurements of SST and total integrated water vapor. Shown in the figure are nonoverlapping 9-second averages of wind speed and SST data from the NCAR Electra and mss from the NOAA P-3. The data were gathered on a north-south-oriented flight line at 156°W. The top panel data were acquired between 03:53:34 and 04:05:35 Universal Time, Coordinated (UTC) with the two aircraft flying north at 60-m altitude. The bottom panel data were acquired between 04:11:53 and 04:22:56 while the aircraft flew south over the same flight line with the NOAA P-3 at 90 m altitude and the NCAR Electra at 30 m. The atmosphere was so unstable during this period that extrapolating the wind speed from the 30- and 60-m aircraft altitudes to 10-m height would only reduce its magnitude by 3 or 4 percent.

In the top panel the SST variation resembles the letter W while the mss variation resembles a letter M; the two variables are inversely correlated. The distance between the SST minima and the mss maxima is about 35 km. The 60-m height wind speed in the top panel shows a general arc over the ground track and does not reflect the oscillation seen in the middle of the leg in both the SST and mss.

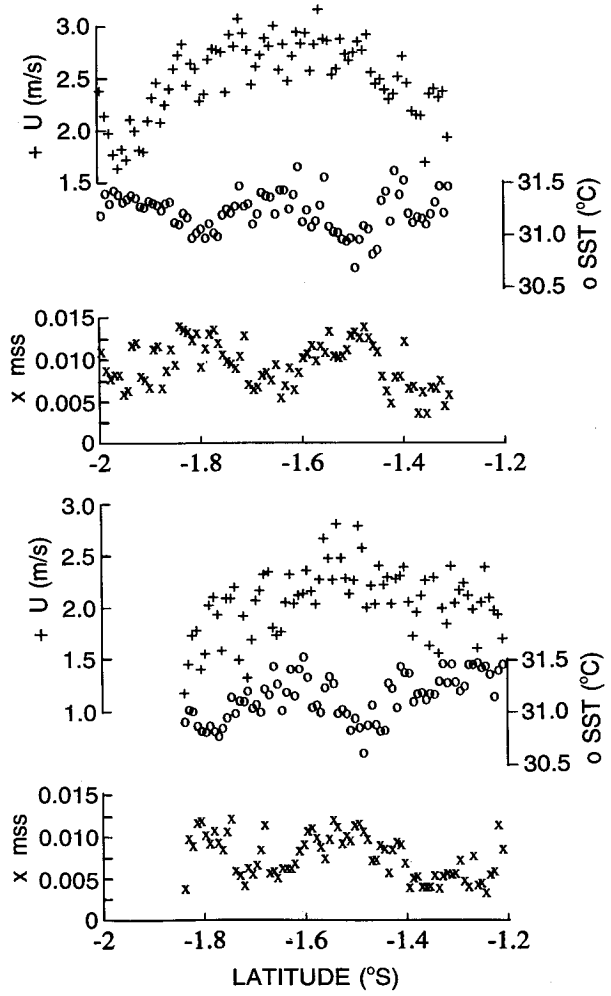

The spatial variation of wind speed (U), SST and sea surface mss during north (top panel) and south (bottom panel) passes over the same flight line at 156°W.

In contrast, variations in mss on spatial scales of a few km do seem to correlate with wind speed, but not with SST. For example, there are positive excursions in mss at 1.93°S and 1.89°S that correlate with positive excursions in wind speed (within the overall increasing mean value), while SST changed little. Negative jumps occur in both mss and wind speed at 1.8°S, with no change in SST. It is the lack of correlation of mss with wind speed on a 30-km scale, and its inverse correlation with SST that is surprising.

The southbound leg in the bottom panel stopped before mapping the entire variation, but the maxima in SST and minima in mss occur in approximately the same positions as they do in the top panel. Once again, the wind speed variation over the flight line does not reflect the variations seen in the SST and mss. At about 1.5°S the minima in SST and maxima in mss correspond to a maximum in wind speed, whereas at 1.8°S the same situation corresponds to a minimum value of wind speed.

The inverse correlation of SST and mss appears to be caused by internal waves. These waves form along the subsurface boundary of water layers of different densities and are frequently found along the main thermocline, the layer of large vertical temperature gradient below the surface mixed layer. Subsurface current and temperature measurements made during TOGA/COARE indicate that tidally forced internal waves with wavelengths on the order of 30 km are common features in this region, apparently generated by topography to the southwest. The vertical displacement associated with internal waves can be tens of meters at the thermocline, but diminishes above that level; there is almost no displacement signature at the surface. However, there are divergent surface currents wherever the internal wave causes the thermocline to rise and convergent surface currents wherever it causes the thermocline to descend.

Under light wind conditions, the convergent surface currents can thicken natural films that exist on the sea surface to the point where they will generate slicks which reduce surface tension and damp capillary waves. These glassy regions are visible both to the eye and the radar, although something on the scale of 30 km would not be observable visually from an aircraft flying at 30- or 60-m altitude. In the nonslick regions, the divergent surface currents have thinned the natural film. In the absence of clouds, most of the Sun's radiation is absorbed in the top meter of the sea surface and the surface water can be more than 2°C warmer than water a meter below the surface. Slick areas would be expected to be warmer during the day because the convergent surface currents would accumulate the warm surface water along with the slick material. The dispersive surface currents in the nonslick areas would expose the cooler water below. Since slicks reduce surface tension and damp the short waves which account for most of the mss, this simple model would predict an inverse correlation between mss and SST.

There is another mechanism associated with internal waves that could enhance the observed effect in this instance. The wind was blowing approximately in the direction that the internal waves were propagating. The oscillating surface current component due to the internal waves had about a 0.2 m/s amplitude. The maximum of the surface current generated by the internal wave in its direction of propagation would occur over the trough, collocated with the warm water and the slick. In this instance it would also be in the downwind direction, further reducing the relative wind over the surface (and the mss). Conversely, the internal wave current in the nonslick region would oppose the wind in this instance and increase its relative speed over the surface (and the mss). A modulation of 0.4 m/s in wind speeds on the order of 2 m/s would be significant. These data suggest that considering the effects of internal waves could be important in modeling air-sea interaction processes in light-wind regions.

Contact: Edward Walsh (Code 972)
303-497-6357

Sponsor: Office of Mission to Planet Earth

Dr. Edward Walsh has been with NASA since receiving the PhD in Electrical Engineering from Northeastern University in 1967. He received the NASA Outstanding Scientific Achievement Award in 1975. He has served at GSFC since 1981, where he works in the Observational Science Branch using radars to study both ocean and land.

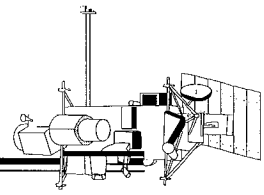

GEODETIC MEASUREMENTS ACROSS THE PACIFIC-NORTH AMERICAN PLATE BOUNDARY IN ALASKA

AMONG THE CRITICAL clues to understanding the dynamics of the subduction zone process is a knowledge of the rate and orientation of ongoing deformation in the overriding tectonic plate. It can be inferred from geological structures, topography, and stress release in earthquakes. Additionally, we can measure it directly using precise, space-based geodetic methods. The Alaska-Aleutian subduction zone has a significant portion of the overriding plate accessible for geodetic measurements in southern Alaska. Since subduction of the Pacific plate beneath the North American plate occurs by variable styles in different regions of Alaska, it provides a natural laboratory to study the subduction zone process.

For 3 weeks in June 1993, geodetic measurements were made in Alaska using the GPS. This study builds upon the earlier geodetic very long baseline interferometry (VLBI) measurements made between 1984 and 1990 at five sites as part of NASA's Crustal Dynamics Project. Repeated GPS measurements will be made in the next 2 to 6 years at approximately 25 sites across the oblique subduction plate boundary zone in southern Alaska and across Kodiak Island, as shown in the figure. Two of the sites show the average rate of deformation of the sites relative to Gilcreek (GILC) between 1984 and 1993. The rate of deformation at Cape Yakataga (YAKA) is 37 mm/yr at N34°W, and at Kodiak it is 9 mm/yr at N56°W.

The southern Alaska region has not had a large earthquake since 1899, and is thought to have the potential for a large earthquake sometime in the next 20 years. The Kodiak Island segment of the plate boundary ruptured in the great 1964 Prince William Sound earthquake. Relatively little is known about the cyclic pattern of crustal deformation associated with these earthquakes. Geodetic measurements are useful in determining the spatial and temporal variations in rates of deformation across the plate boundary zone and in measuring coseismic strain release in large earthquakes. For example, the offset of the VLBI Cape Yakataga site has been used to estimate the average slip during the 1987 to 1988 Gulf of Alaska earthquakes. Also, in the last year we used earlier geodetic and geologic measurements to invert for a detailed slip model for the 1964 earthquake. Rates of deformation (1984 to 1993) have been estimated from a combination of VLBI and GPS data at two sites in southern Alaska, as shown in the figure. Like the earlier VLBI-only estimates, these results have been used to test alternative tectonic models. With the denser distribution of stations in the GPS network, we will be able to better constrain tectonic models in the future. Additionally, the results of this study will provide important input to evaluate seismic hazard in Alaska.

It is hard to make measurements anywhere in Alaska without being close to a glacier. Ten of the sites shown in the figure are adjacent to coastal glaciers. During this century there has been a regional pattern of glacier retreat in southern Alaska that may be related to climatic warming. While deploying the GPS instruments, we made measurements that can be used to constrain rates of glacier thinning and recession. During the same time period that the overall ice volume of southern Alaska glaciers has decreased, one of the glaciers near our sites, the Bering glacier, has undergone at least six surges. This surging is a periodic, very rapid movement of large quantities of ice within the glacier, alternating with a much longer period of near stagnation or retreat. The most recent surge began in the late spring of 1993 and is still ongoing as of September 1994. The rapid transfer of ice mass from the accumulation region to the terminus region would result in elastic rebound of the solid Earth in the source area and loading (subsidence) in the terminus region. Geodetic measurements made in June 1993, combined with measurements planned for 1995, will yield discrete sampling of the unloading/loading displacement field. Our calculations suggest that these results will provide independent constraints on the magnitude of ice transfer during the Bering Glacier surge.

Oceanic tide gauge measurements in Alaska could provide an additional source of documentation of sea level change. The primary reason the Alaskan tide gauge data have not been used in past sea-level change studies is because the tectonic motion contaminates the secular sea-level change signal. As part of the Alaska study, we are developing methods to isolate eustatic sea-level from the tectonic motion and the annual Gulf of Alaska ocean signal. An ocean correction is being estimated using satellite altimetric measurements of sea level from the TOPEX/Poseidon mission. The tectonic motion can be directly obtained from geodetic measurements near the tide gauge station.

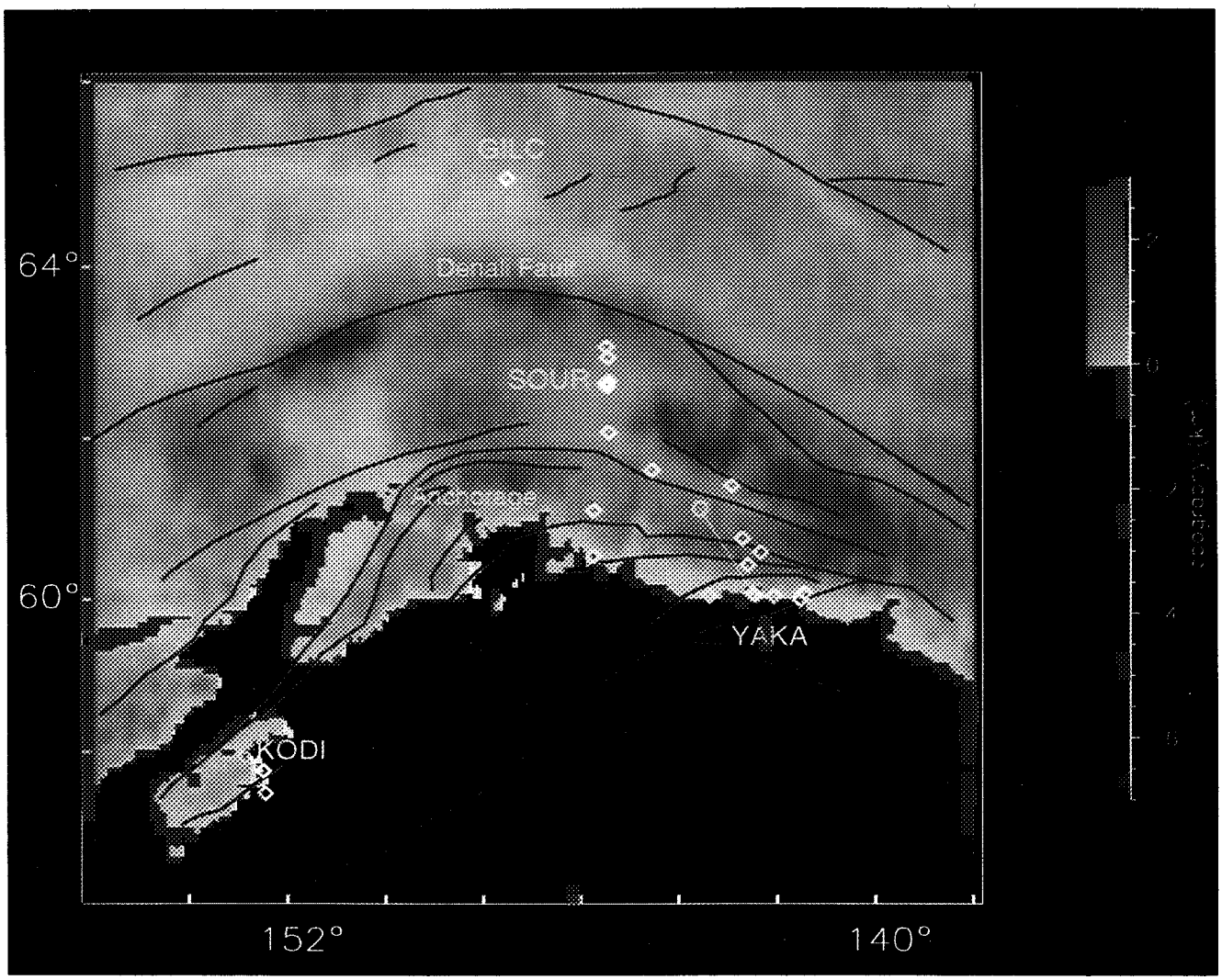

Southern Alaska topography and sites surveyed with GPS in June 1993. The GPS sites are given by white diamonds. The faults of southern Alaska are given by solid red lines. The topographic data are from the ETOPO5 data source. The sites that were previously occupied with VLBI are labeled in yellow and are YAKA=Cape Yakataga, KODI=Kodiak Island, SOUR=Sourdough, GILC=Gilcreek.

The author would like to acknowledge the substantial contributions of Mark Bryant (MDA), Lynda Bell (NVI, Inc.), Douglas Caprette (Hughes STX), Troy Carpenter (ATSC), Garth Franklin (JPL), and Steve Fisher (Sterling Scientific) in the planning and implementation of the field study.

Contact: Jeanne Sauber (Code 921)
301-286-8586

Thomas Clark (Code 926)
301-286-5957

R. Steven Nerem (Code 926)
301-286-3220

Sponsor: Office of Mission to Planet Earth

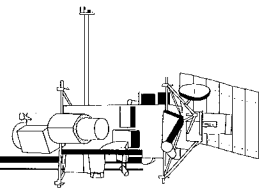

Dr. Jeanne Sauber is the principal investigator of the Dynamics of Solid Earth program to study the subduction zone process in Alaska by making precise geodetic measurements. Her research expertise includes geodesy and neotectonics, numerical modeling of lithosphere deformation, and the mechanics of the earthquake source. She joined the Geodynamics Branch in the Laboratory for Terrestrial Physics after receiving her PhD in Geophysics from the Massachusetts Institute of Technology in 1988.

Dr. Thomas Clark is the VLBI systems manager in the Space Geodesy Branch of the Laboratory for Terrestrial Physics. His special technical interests focus on the development of instrumentation and techniques for astronomical and geophysical measurements. Dr. Clark earned his PhD from the University of Colorado and has 26 years of experience at GSFC.

Dr. R. Steven Nerem, a specialist in space geodesy and satellite orbit determination, studies methods for determining the gravity field of the Earth and the planets using satellite tracking data and satellite altimeter data. He also uses satellite altimetry to study the circulation of the ocean and its variability. He has a PhD in Aerospace Engineering from the University of Texas at Austin.

TILTING AND FLEXING OF THE EARTH'S CRUST IN THE CENTRAL ANDES: GPS SURVEY OF SHORELINES OF PALEOLAKE MINCHIN

PALEOLIMNOLOGY IS the study of ancient lakes. A burgeoning subdiscipline of this field might be entitled limneotectonics, or the study of deformations of the solid Earth as recorded in the shorelines and sediments of lakes. The shorelines of paleolakes provide the unusual combination of unambiguous records of both climatic change and tectonic motions. Changes in the surface area of a closed-basin lake provide direct evidence of climatic change, and departures from horizontality of the shorelines of a lake provide evidence of vertical crustal motions. Together, these disparate types of evidence can be used to establish constraints on the rates and processes responsible for changes above and below the surface of the Earth. Lakes which occupy hydrologically closed drainage basins respond very sensitively to climatic change. An increase in precipitation or a decrease in evaporation will cause the surface area of the lake to increase until hydrologic balance is re-established.

An excellent opportunity for examination of these phenomena is found in the Altiplano of Bolivia, which is presently a cold high desert; but at elevations below 3,800 m, the landscape is dominated by coastal geomorphic features. During colder and/or wetter episodes in the past, the hydrologically closed basins of the Altiplano have contained substantial lakes. The largest of these was Lake Minchin, which extended 200 km east-to-west and 400 km north-to-south, and attained a depth of 140 m. It was thus roughly comparable in size to the present Lake Michigan. The sediments and shoreline deposits of Lake Minchin preserve a valuable but largely untapped record of tropical climatic change. The present climate of the Altiplano represents a region of extremely high precipitation gradients. The western flank of the basin is part of the hyper-arid Peruvian coast desert, with precipitation rates <100 mm/year, and the eastern flank of the basin abuts the Amazon rain forest, with precipitation rates >1,500 mm/year. The potential evaporation rates are less variable, averaging 1,400 mm/year. It is clear that even minor lateral shifts in the precipitation zones would produce major shifts in the hydrologic balance. To attain the highest level of Lake Minchin would require an increase in the basin-average precipitation of roughly 300 mm/year. Recent work on this problem has established that the highest shoreline was formed roughly 17,000 years ago.

As the lake fluctuates in depth, it forms erosional and depositional shorelines which record the positions of the lake surface at various epochs. Each of these shorelines are formed on a horizontal (geoidal) surface. Present departures from horizontality are thus a measure of accumulated net vertical motion since the shoreline formed. For sufficiently large lakes, the crustal load of the water itself is adequate to produce tens of meters of vertical deflection of the crust. The actual amount and spatial pattern of deflection depends on the geometry of the imposed load (which is well-known) and on the long-term strength of the substrate (which is almost completely unknown). Thus, examination of the spatio-temporal pattern of shoreline deformation provides an opportunity to determine the viscosity of the crust and upper mantle. This approach has been applied for over a century in a few selected locations, but has never before been attempted in the Central Andes.

In a recent application of space geodetic techniques to this problem, we have measured the amount and spatial pattern of net vertical crustal deformation which has accumulated in the Central Andes during the 17,000 years since formation of the shorelines of Paleolake Minchin. The measurement technique relied an a relatively new application of the GPS, which allows real-time positioning with ~1 m accuracy. The space component of the GPS is comprised of a constellation of 24 satellites in 6 different orbital planes. Each satellite broadcasts information from which an appropriate ground-based radio receiver can determine its range to the satellite. With a minimum of four satellites in view, a GPS receiver can determine the three components of its spatial position and a clock correction term. Typical real-time positional accuracy is 100 m, which is not good enough for our shoreline study. However, many of the error sources are shared between nearby receivers (separations up to several hundred km), so real-time differential positions better than 1 m can be obtained at 1 Hz sampling rates.

The strategy used for the Bolivian shoreline measurements included three receivers. One was left at a fixed location for the entire campaign. This served as a "fiducial" location for all of the shoreline traverses. The other two receivers were transported by vehicle to the shoreline sites. At each

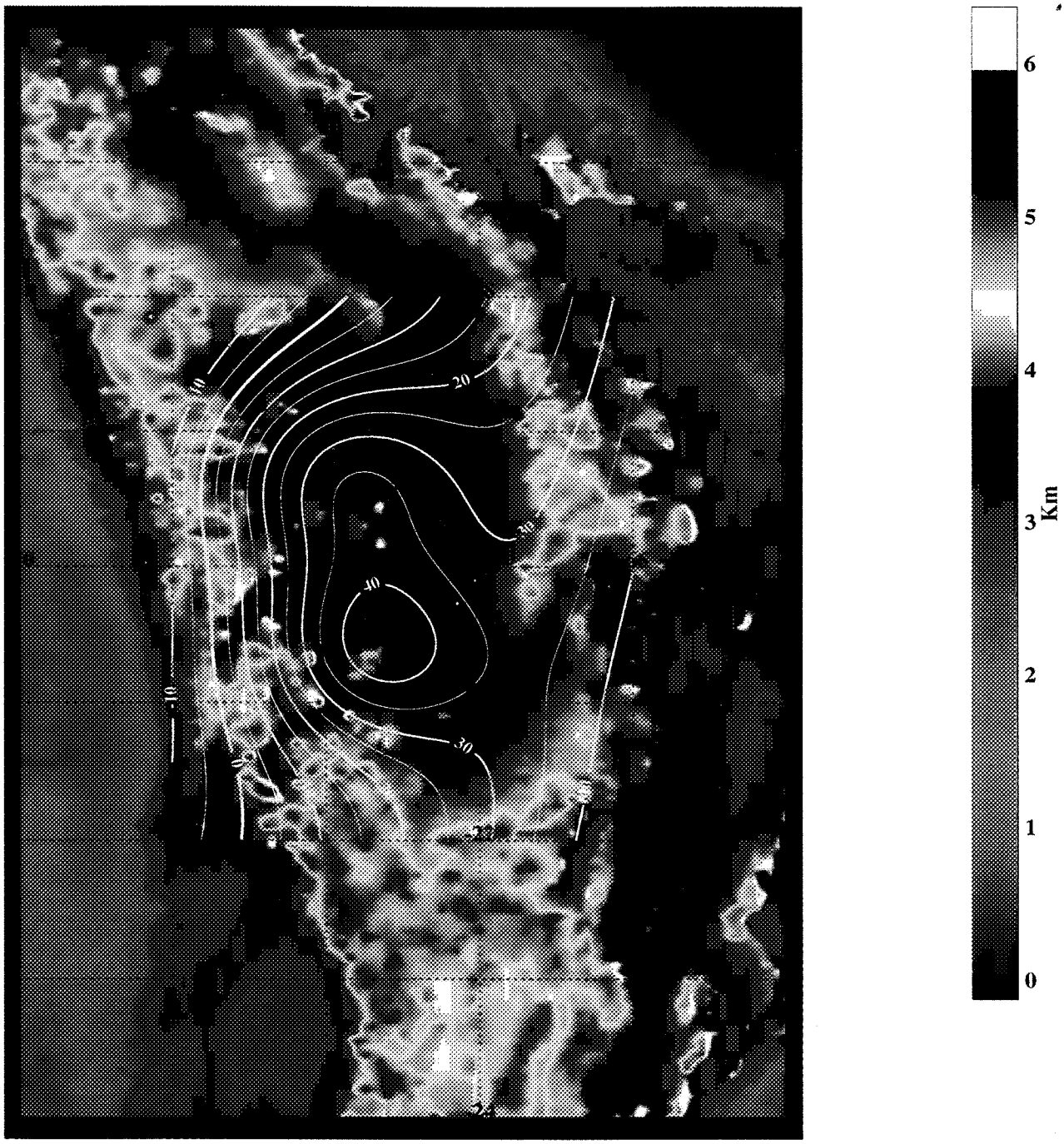

The spatial variation of wind speed (U), SST and sea surface mss during north (top panel) and south (bottom panel) passes over the same flight line at 156°W.

site, one receiver (the "base" station) would stay fixed, with its antenna mounted on a standard surveying tripod. The other receiver (the "rover") was placed in a backpack, and carried along as the team hiked over the sequence of shorelines. Real-time differential positions of the shoreline features were noted, with 1-m precision. The position of the "base" receiver, relative to the "fiducial" was determined later by simultaneously analyzing data from both receivers. The final analysis, which was intended to locate our local array within a global geodetic framework, also included GPS data from true fiducial sites in Santiago (Chile), Bogota (Columbia), and Fortaleza (Brazil).

We determined that the weight of the lake was sufficient to depress the crust of the Earth by 27±1 m. Radiocarbon dates from gastropod (snail) shells obtained at the highest shoreline establish that the lake reached its greatest extent roughly 17,000 years ago. This is somewhat later than the maximum of glacial loading in North America. The pattern and timing of the crustal response to the load implies that the effective lithospheric thickness is less than 40 km, and the effective viscosity of the upper mantle is less than 5×10^{20} Pa-s. The lithospheric thickness number is somewhat of a surprise, since seismic observations have established that the crustal thickness in the Central Andes is roughly 70 km. Further observations of the rebound pattern on the lower shorelines, and an improved chronology for the loading, will eventually provide better resolution of the strength versus depth profile.

Another surprise was that the pattern of shoreline elevations records a regional-scale tilting down to the northwest (see the figure). When the rebound signal is removed, the residual heights are roughly 40 m greater in the extreme southeast corner of the lake basin than they are in the northwest extremity. The cause of this tilting is still unknown, but it is presumably related to the ongoing subduction of the Nazca tectonic plate beneath the Andes. The rate of horizontal crustal convergence in that the subduction zone is ~100 mm/year, and the rate seems to have been reasonably steady for the last several million years. The observed tilting on the Lake Minchin shorelines corresponds to an average rate of differential vertical motion of 2 mm/year over approximately the last 20,000 years.

Contact: Bruce Bills (Code 921)
301-286-8555

Sponsor: Office of Mission to Planet Earth

Dr. Bruce Bills is in the Geodynamics Branch. Prior to coming to GSFC he worked at the Lunar and Planetary Institute in Houston, TX and at the Jet Propulsion Laboratory in Pasadena, CA. His main research interests include geodetic paleolimnology and the interactions between orbital, rotational and climatic dynamics on the Earth and Mars.

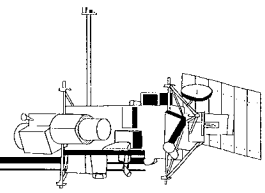

POTENTIAL IMPACTS OF CLIMATE CHANGE ON WORLD FOOD SUPPLY

IN THE COMING DECADES, global agriculture faces the challenge of feeding the world's population as it grows from 5 to 10 billion people under circumstances complicated by the prospect of a changing climate. Global warming is predicted to bring changes in the thermal and hydrologic regimes of many regions. The nature of such changes and their biophysical and socioeconomic consequences is the subject of the research field known as climate change impacts.

The goals of climate change impact research are to define the ranges of possible consequences, to identify the critical thresholds of our essential systems, and to engender flexibility in society's preparatory and responsive actions. There is a growing emphasis on the need for integrated assessment that considers both biophysical and socioeconomic consequences of climate change over time. For example, research on agricultural impacts aims to analyze the predictable changes and to evaluate what practical adaptations might be undertaken to prevent or overcome any possible adverse impacts on our ability to feed the world. Several complementary disciplines are needed to implement the complex task of assessing potential climate change impacts on global agriculture. These include the relevant aspects of atmospheric science, hydrology, soil science, crop physiology, and resource economics. Interactions of the agricultural system with other sectors energy, water resources, and natural ecosystems and their potential feedbacks on trace gas emissions are also beginning to be studied. There is also the potential for multiple environmental stresses on crop growth and production, among them increases in tropospheric ozone and increased UV-B radiation. Modeling capability is needed to assess the combined effects of these multiple stresses on crop growth and yield.

We are building research capacity for such global impact assessments and have recently completed an integrated study on climate change and world food supply. We derive climate change scenarios from global climate models (GCMs) and utilize them to test the sensitivity of crop yields to a range of predicted monthly changes in temperature and precipitation, as shown in the table. We use dynamic process crop growth models for wheat, rice, maize, and soybean that respond to carbon dioxide level, climate variables, soil conditions, and management practices. From site results we estimate changes in national yield due to the GCM-based climate change scenarios and then utilize these projected national changes in an economic model of world food trade.

GCM doubled CO_2 climate change scenarios.

				Change in Average Global	
GCM[1]	Year	Resolution (lat/lon)	CO_2 (ppm)	Temperature (°C)	Precipitation (%)
GISS[3]	1982	7.83° x 10°	630	4.2	11
GSDL[2]	1988	4.4° x 7.5°	600	4	8
UKMO[4]	1986	5.0° x 7.5°	640	5.2	15

1 When calculated.
2 Goddard Institute for Space Studies.
3 Geophysical Fluid Dynamics Laboratory.
4 United Kingdom Meteorological Office.

Our study found that crop yields are indeed projected to change with atmospheric carbon dioxide level and global warming, as shown in the first figure. Changes in crop yields are related to the level of warming: the greater the warming, the greater potential for decreases in crop yields. When climate change is considered without direct CO_2 effects on crop growth and water use, average national crop yields decline everywhere. When full direct CO_2 effects are included in the simulations, there is a marked latitudinal stratification in yield response. At high latitudes, increased temperatures may benefit crops now limited by cold temperatures and short growing seasons. In mid- and high latitudes, increased temperatures exert a negative effect on yields through shortening of crop development stages, but do not significantly increase heat or water stress levels. The climate change-induced warming at low latitudes may bring not only accelerated growing periods for crops, but greater heat and water stress as well, resulting in greater yield decreases than at higher latitudes.

Our studies are designed to determine how climate variables may affect the quantity, quality, and regional (and global) patterns of agricultural production. These impacts may be significant, because heat, light, and water are major biophysical drivers of crop growth. We know that suboptimal levels of these factors bring severe consequences.

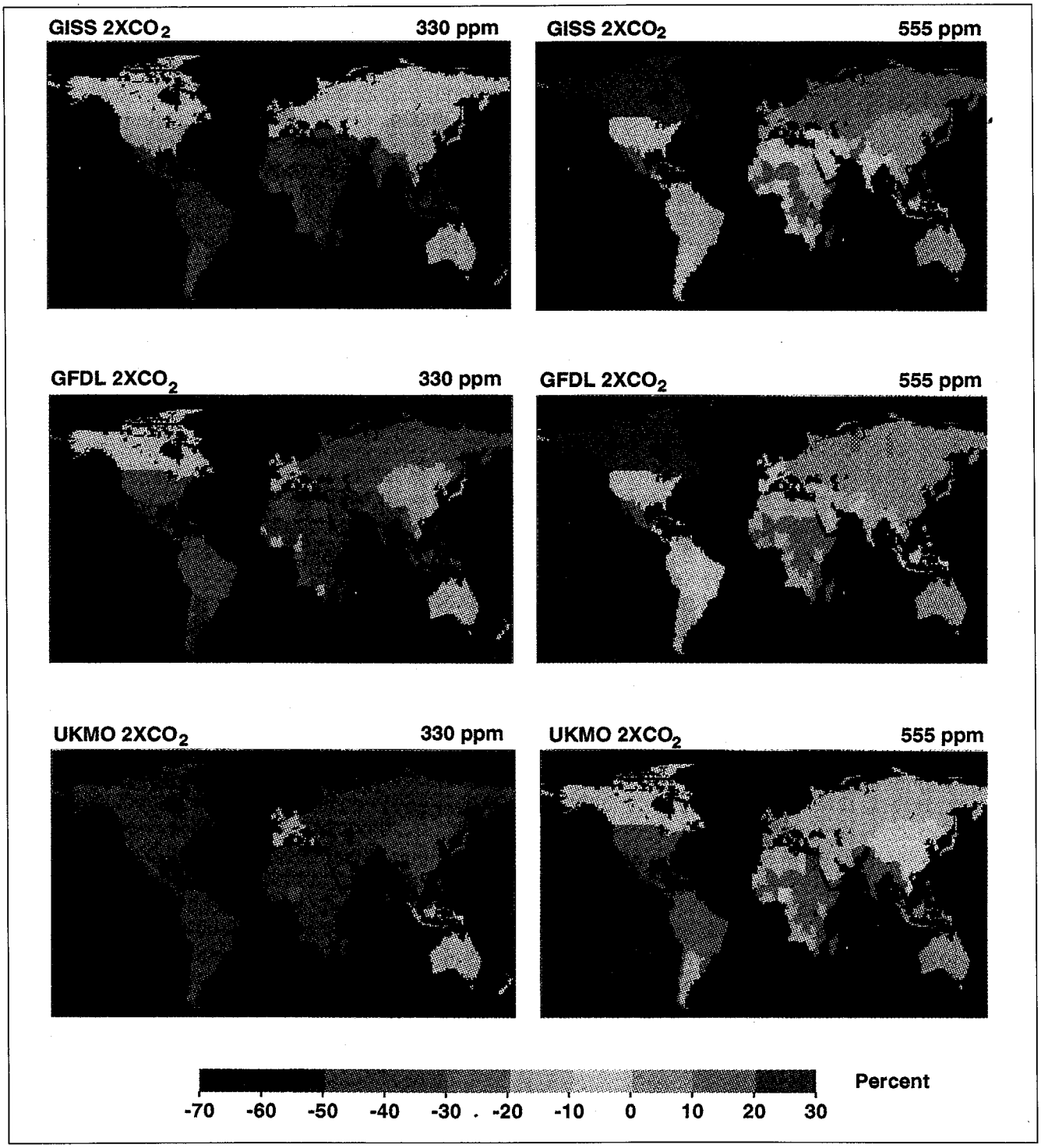

Estimated change in average national grain yield (wheat, rice, coarse grains, and protein feed) for the GISS, Geophysical Fluid Dynamics Laboratory (GFDL), and United Kingdom Meteorological Office (UKMO) climate change scenarios. The left-hand column shows the effect of the climate change scenarios on grain yields without enhanced CO_2. The right-hand column shows the effect of the climate change scenarios on grain yields with the direct effects of enriched atmospheric CO_2 level (555 ppm) on crop growth and yield. Regional variations within countries are not reflected.

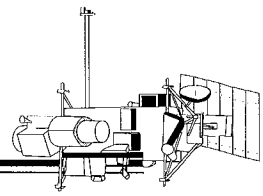

The Dust Bowl drought of the 1930s brought nearly 200,000 farm bankruptcies to the southern Great Plains, and the recent drought of 1988 in the midwest led to a 30 percent reduction in U.S. corn production. Above normal temperatures accompanied both of these droughts. In general, higher temperatures accelerate the phenology of annual cereal crops, resulting in hastened maturation and reduced yield potential. On the other hand, warmer and longer growing seasons in regions where crops are currently limited by cold but not by paucity of moisture may enjoy increased productivity in a warmer world.

If atmospheric carbon dioxide accumulations were occurring without concomitant changes in temperature and water regimes, it might indeed be a blessing for crop production. Atmospheric CO_2 is an essential ingredient of the basic process of photosynthesis by which that gas combines with soil-derived water with the infusion of sunlight to create carbohydrates and, ultimately, food for humans and other animals. Plants growing in air with higher CO_2 levels exhibit increased rates of photosynthesis because the absorption of CO_2 is facilitated by the increased concentration gradient between the external atmosphere and the air spaces inside the leaves.

Plants also exhibit partial closure of stomates in the presence of elevated CO_2 levels, thereby reducing transpiration on a per-unit leaf area basis. However, total crop evapotranspiration may not change significantly because the greater foliar growth due to the higher rates of photosynthesis partially compensates for the reduced transpiration per unit of leaf area. A net improvement may nevertheless result in crop water-use efficiency, defined as the ratio between crop biomass accumulation and the amount of water used in evapotranspiration. Considering these interactive processes in combination is a complex task, requiring a quantitative dynamic assessment of the relative magnitudes of both physiological and climatic changes. One area of our research involves the simulation of the direct physiological effects of increasing atmospheric carbon dioxide on crop growth and water use.

How climate change affects agriculture also depends on how the biophysical field-level effects (including those on soil fertility and pests) lead to changes in the socioeconomic sphere within which farmers operate. Decisions made by individual farmers in the face of changing climatic regimes will underlie society's collective response to climate change. These decisions involve cropping and irrigation systems, risk management, and ultimately the successes or failures of individual farms and—by extension—of entire regions and even of national economies. Some countries are highly dependent on agricultural products either for subsistence or for foreign exchange. Climate change effects may thus cascade into such areas as energy and machinery requirements, irrigation water use, storage and transportation facilities, and regional markets.

Beyond national boundaries, global patterns of supply and demand may change in far-reaching ways. Because of the interdependence of the world food system, the consequences of climate change for agriculture in the U.S. depends, to a large extent, on what happens elsewhere, and vice versa. Vulnerability of marginal or food-deficient regions to climate change may create markets for U.S. grain, but improved comparative advantage in more productive areas may limit those markets.

Although some countries in the temperate zones may reap some benefit from global warming, many countries in the tropical and subtropical zones appear to be more vulnerable. Particular hazards are increased flooding of low-lying areas from sea-level rise, the potential for increased frequency and severity of drought in semiarid areas due to increases in potential evapotranspiration, and potential decreases in crop production in developing countries, as shown in the second figure. International trade policy issues, such as the movement to lower agricultural trade barriers, and food security planning will be crucial in the development of climate change response strategies.

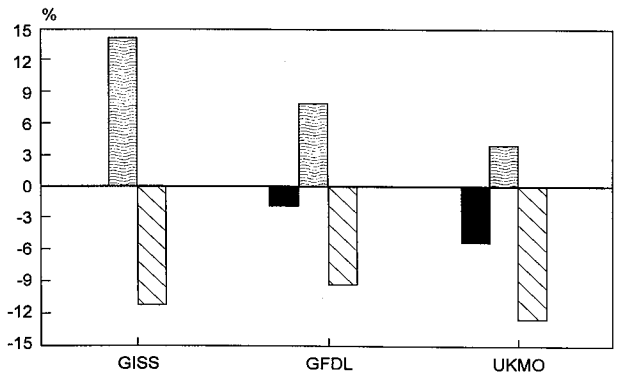

Change in global, developed country, and developing country cereal production (with direct CO_2 effects) in 2060 for three climate change scenarios. Adaptation level 1 assumes minor changes to existing agricultural systems.

Agriculture is no longer perceived as a benign or even neutral influence on the environment. Not only does agricultural development replace natural ecosystems with artificially managed ones wherever it takes place, but it also affects its surroundings by increasing rates of erosion and runoff and by the release of fertilizer and pesticide residues into surface waters and groundwaters. Moreover, as a result of potentially large climate changes, crop and livestock patterns may shift, invading regions now primarily covered by forest and other types of less intensively managed ecosystems. Such interactions among the changing climate, agriculture, and the environment will reverberate throughout the world food system, affecting rates of soil erosion, fates of agricultural chemicals, wildlife habitats, and greenhouse gas emissions. Of comparal significance, they may also intensify competition for water resources, another key impact sector.

Dr. Martin Parry of University College London is a coauthor of the integrated study of climate change impacts on world food supply described above.

Contact: Cynthia Rosenzweig (Code 940)
212-678-5591

David Rind (Code 940)
212-678-5593

Sponsor: Office of Mission to Planet Earth

Dr. Cynthia Rosenzweig is an agronomist who has been in the Climate Group at the Goddard Institute for Space Studies (GISS) for 10 years. She holds a PhD in Plant and Soil Science and her professional interests include the simulation of land-surface processes in global climate models and the integrated assessment of global climate change impacts.

Dr. David Rind holds a PhD in Atmospheric Science. His professional interests include theoretical modeling and numerical simulation of the atmosphere and ocean, and the use of global climate models for improved understanding of past, present and future climates.

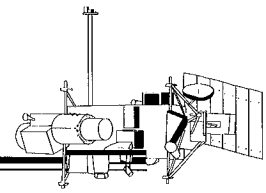

VEGETATION CANOPY STRUCTURE IN THE PACIFIC NORTHWEST: MEASUREMENT BY LASER ALTIMETER WAVEFORM PROFILES

THE SPATIAL ORGANIZATION of vegetation canopies is a fundamental boundary condition that influences many ecosystem processes—including energy and chemical exchanges—but data on the three-dimensional organization of canopies is difficult to obtain. Most remote sensing systems, although providing images of the horizontal organization of canopies, do not provide direct information on the vertical distribution of canopy elements. Ground observer or in situ measurements of canopy vertical structure are inherently laborious and time-consuming and are usually very limited in scope. Furthermore, measurement of ground topography in densely vegetated areas is not possible using traditional remote sensing methods. To address these limitations, we have developed an airborne laser altimetry technique that provides high-resolution, geolocated measurements of vegetation vertical structure, and ground elevations beneath dense canopies.

Traditional laser altimetry provides a direct method for obtaining surface elevation measurements of very high accuracy. The basis of the method is ranging to the surface obtained by precise timing of the round-trip travel time of short-duration pulses of backscattered laser radiation. We have extended the technique by digitizing the complete time-varying distribution of return pulse energy, or waveform, that results from the reflection of a single laser pulse from multiple targets occurring at varying heights within a large footprint. The waveform is a convolved measure of the vertical distribution of vegetation canopy components (e.g., foliage, twigs, branches) and the underlying ground's height distribution, introduced by surface slope and roughness. The time-varying amplitude of the return signal is weighted by the nadir-projected area of intercepted surfaces, their reflectivity at the monochromatic laser wavelength, and the spatial distribution of laser energy across the footprint. The height of the vegetation is readily extracted from the time delay between first and last returns, after conversion to distance based on the speed of light. By using large diameter footprints, on the order of one to two times the typical crown widths, each waveform includes returns from the highest elements of the canopy and from the ground. Ground returns occur where there are sufficient intra or intercrown gaps of any size extending at nadir to the canopy floor, which is usually the case in all but the densest canopies. In addition to vegetation height, the vertical distribution of vegetation surface area can be derived from the varying strength of the return signal down through the canopy.

The altimeter we use consists of a cavity-dumped, short pulse Nd:YAG laser operating at 1.06 μm with a pulse repetition rate up to 50 Hz. The backscattered laser energy is collected by a nadir-staring telescope and focused on a Si:APD detector. A time-interval-unit is used to determine the round-trip travel time of the laser pulse, and a digitizer records the time-varying amplitude of the return signal. The position and attitude of the aircraft platform is determined by means of kinematic GPS and a ring-laser gyro inertial navigation system (INS), respectively. By incorporating aircraft position and attitude knowledge, the laser range data are converted to surface elevations and footprint latitude and longitude, thus making it possible to relate the waveform data to specific canopy locations.

The altimeter system was deployed to the Gifford Pinchot National Forest in southeast Washington state in September of 1993 to evaluate instrument performance in an area of complex canopy structure. Old growth forest in this area has been extensively fragmented by clearcut timbering and subsequent introduction of fir plantations. Landsat Thematic Mapper (TM) images have been used in a study of Pacific Northwest forest fragmentation via NASA's Landsat Pathfinder Humid Tropical Forest Inventory Project, but the images are limited by a lack of direct information on the height distribution of vegetation.

Integration of laser altimeter waveform data with a geocoded TM image is illustrated in the figure. The upper panel shows the location of a laser altimeter profile across TM data displayed as a standard false-color three-band composite image in which old growth forest pixels appear dark red to purple, fir plantations appear light red and bare areas (clear cuts and a logging road) appear light blue. The image is highly enlarged, revealing the position of individual laser footprints (yellow pluses) within 30-m TM pixels. The lower panel shows a transect of vegetation structure derived from the laser waveform data; each waveform records canopy structure within footprints that are approximately 12 m in diameter

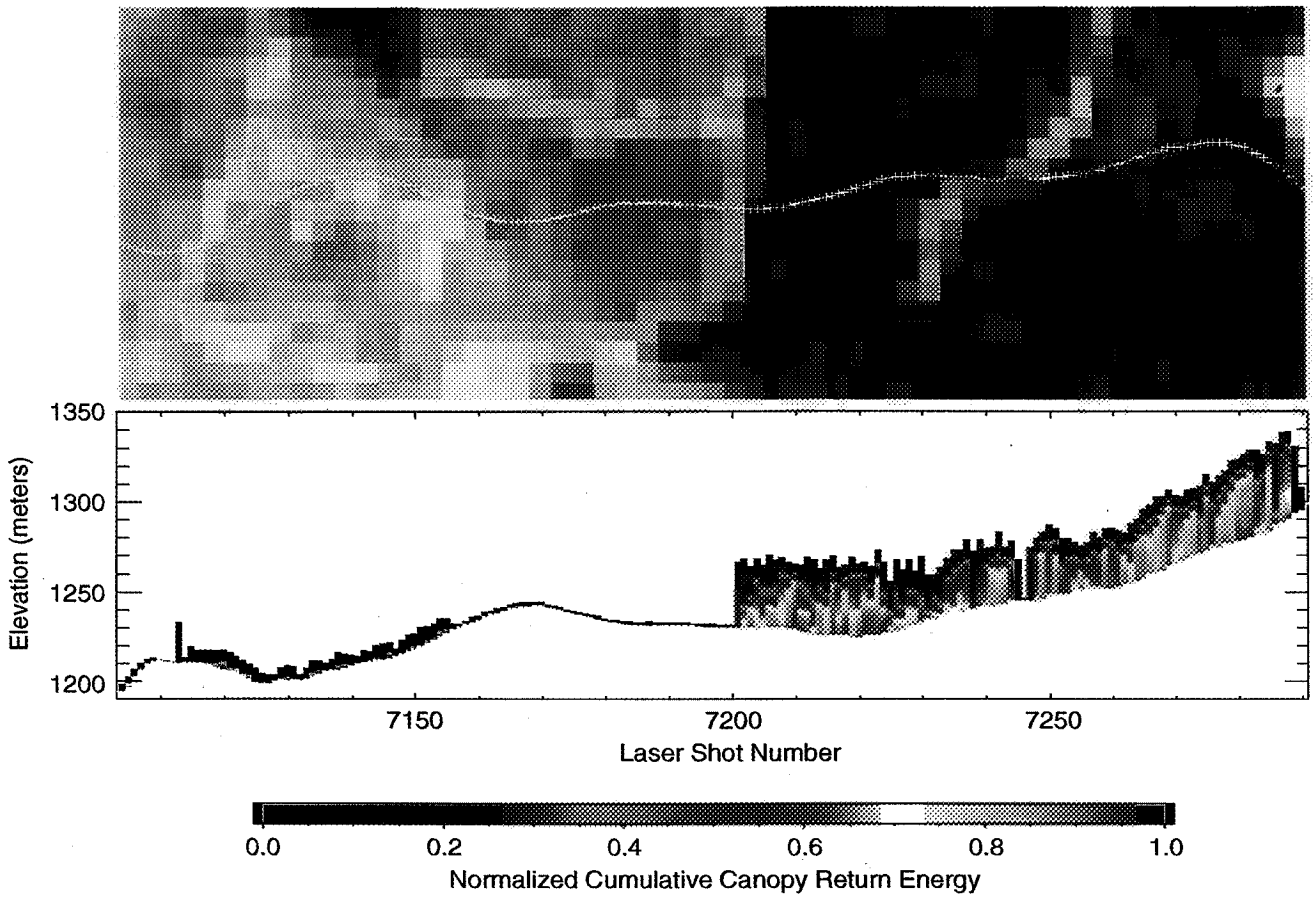

Enlarged Landsat TM image of an area of old-growth forest fragmented by clearcuts and plantations with location of laser altimeter profile (upper panel), and transect of vegetation canopy structure and ground elevations derived from waveform data (lower panel).

and that are nominally spaced 9 m apart. The elevations of first and last returns reveal a rough upper surface, inferred to be the canopy top, and a smooth lower surface, inferred to be the ground. Last returns consistent with a reflection from the ground were obtained for each of the laser shots, even in old-growth stands, where field observers reported canopy closure of 80 to 90 percent. Vegetation height derived from the distance between first and last returns delineates clearcut, fir plantation and old growth segments. The altimeter-derived heights are in close agreement with field measurements of tree heights in these stands. Several height anomalies of interest correspond to the road through the old-growth stand (shot 7245, highlighted in green on the TM image) and what is probably a "seed" tree left at the boundary between a clearcut and plantation (shot 7113).

The internal structure of the canopy is displayed as a normalized cumulative return energy for each laser shot; at each distance down through the canopy the color-coding depicts the fraction of total received energy returned from the canopy to that point. For the plantation stand, reflections from the canopy account for only 20 to 40 percent of the return energy with the remainder being reflected from the ground. For the taller old-growth stand, the canopy accounts for between 50 percent and nearly 100 percent of the return energy, documenting greater canopy closure. The old-growth stand is characterized by heterogeneous structure, with narrow gaps—where significant laser radiation penetrates to the canopy floor—interspersed among wider sections, where near-complete closure is reached higher in the canopy. The figure depicts only a small fraction of the approximately 4,000 km of

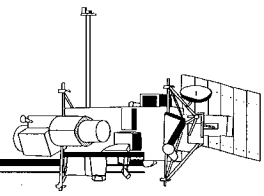

georeferenced waveform profiles which were collected in the Pacific Northwest. Studies are now underway using these unique data to model radiative transfer in the canopy, as verification of TM-derived measures of canopy characteristics and as input to models of forest gap formation. Assessment of ecosystem processes within forested landscapes that depend on canopy structure will now be possible on a scale heretofore not achievable with limited ground-based observations.

Contact: David Harding (Code 921)
301-286-4849

J. Bryan Blair (Code 924)
301-286-9809

Sponsor: Director's Discretionary Fund Office of Mission to Planet Earth

Dr. David Harding is a geoscientist in the Geodynamics Branch at NASA GSFC, where he works on the development and application of laser altimetry in geologic and ecologic applications. He earned a doctoral degree in Geological Sciences from Cornell University in 1988.

Mr. J. Bryan Blair is an instrument engineer in the Experimental Instrumentation Branch. He developed the flight software for the Mars Observer Laser Altimeter, and he implements advanced measurement and data systems for airborne lidars. He earned an MS in Computer Engineering from Loyola College in 1989.

COMPARISON OF TRUCK-MOUNTED RADAR MEASUREMENTS WITH SIR-C MICROWAVE DATA FOR SOIL MOISTURE ESTIMATION

DURING APRIL 1994, a three-frequency radar system flew on the Space Shuttle Endeavour during the STS-59 mission. Known as Shuttle Imaging Radar-C/X-Synthetic Aperture Radar (SIR-C/X-SAR), this radar system is the third in a series of imaging radars flown by NASA for basic and applied studies of the Earth's environment at microwave wavelengths. As part of the science activities of this mission, a major hydrology field experiment was conducted in the Little Washita River watershed near Chickasha, Oklahoma by the Hydrological Sciences Branch at GSFC in collaboration with the United States Department of Agriculture (USDA) and Princeton University. The main objectives of this experiment included determination of the spatial and temporal distribution of soil moisture in a humid-area watershed using SIR-C data, ground measurements, and hydrologic modeling, and the subsequent incorporation of the measured soil moisture patterns in models of larger scale water balance and partial area hydrology.

To complement the Shuttle radar data and provide an accurate means of comparison of microwave data acquired at different spatial scales from different platforms, GSFC's three-frequency truck-mounted radar was deployed to the hydrology experiment near Chickasha during the Shuttle mission. Designed and operated in conjunction with George Washington University, the truck radar consists of L-, C-, and X-band radars which closely approximate the L-, C-, and X-band radars on SIR-C and the L- and C-band radars on JPL's airborne AIRSAR system (refer to the table). The GSFC radars are mounted on a 1990 Navstar truck with a 19-m hydraulic boom; the truck also carries supporting equipment such as an inclinometer for boom platform angle, a helium-neon laser for pointing accuracy during external calibration runs, and a portable electrical generator for instrument power, as shown in the first figure.

The Little Washita River watershed covers an area of ~600 km^2 and is situated in southwestern Oklahoma in the southern part of the U.S. Great Plains. It has a moist and subhumid climate characterized by ~750 mm of annual precipitation, and has been the site of instrumented data collection for hydrologic research by USDA for decades. Surface cover in the watershed consists of approximately 63 percent rangeland/pasture, 20 percent winter wheat, 13 percent woodland, and 4 percent summer crops (corn, alfalfa, etc.). During the April field experiment (April 6 to 16, 1994), field conditions were initially dry, became wet as a result of a heavy rainstorm on the afternoon of April 10, 1994 and morning of April 11, 1994, and then gradually dried down throughout the remainder of the experimental period (see soil moisture curve in the fourth figure).

Radar System Parameters

	Truck Radar	AIRSAR	SIR-C
Frequency Band (GHz)	X - 10.0	C - 5.3	X - 9.7
	C - 4.75	L - 1.25	C - 5.3
	L - 1.6	P - 0.44	L - 1.25
Wavelength Band (cm)	X - 3.0	C - 5.7	X - 3.1
	C - 6.3	L - 24.0	C - 5.7
	L - 18.75	P - 68.1	L - 24.0
Operating Height	Up to 18 m	7,000 to 9,000 m	215 to 220 km
Look Angle Range (°)	10 to 80	20 to 70	17 to 63
Spatial Resolution* (m) Azimuth Direction Range Direction	 ~3 ~4	 3 6.67	 4.3 13.3
*For common operating parameters; single-look resolution			

SIR-C radar data of the watershed have been processed and received for two dates, April 12, 1994 (relatively wet) and April 15, 1994 (dry). The second figure shows a SIR-C L-band polarization image of a small portion of the watershed on April 12 taken on an ascending orbital pass at a radar look angle of 42°. Field #62 is a representative pasture test site where ground data and truck radar data were also acquired. In addition, NASA's airborne AIRSAR system flew over the Little Washita watershed on April 10 and 12, although AIRSAR radar data for this area have not yet been calibrated.

On each of 8 days of actual data collection, the truck radar took measurements at three frequencies (L, C, X), 4 polarizations (HH, HV, VH, VV), and 3 angles (30°, 40°, 50°) for four test fields, each of which represented a typical surface cover found in the watershed (pasture, winter wheat, corn/bare, alfalfa). Configured around an HP8719A network analyzer, the truck radar first identified the test field response in the time domain in order to

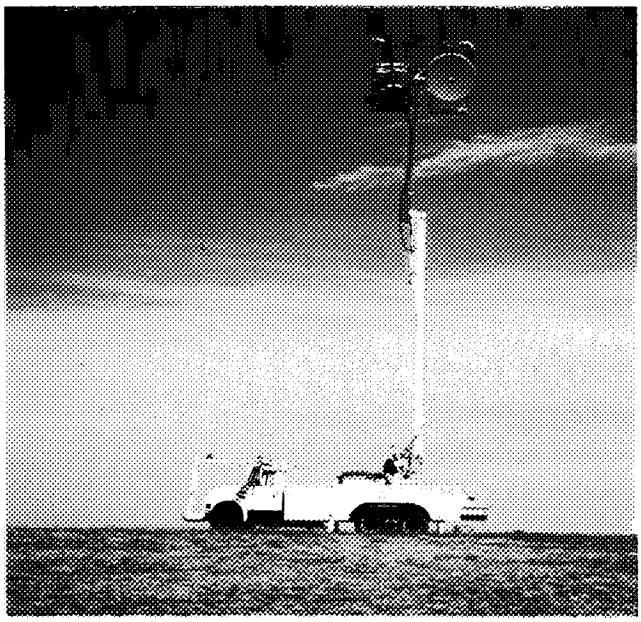

NASA/GSFC truck radar deployed at pasture field #62 in the Little Washita River watershed.

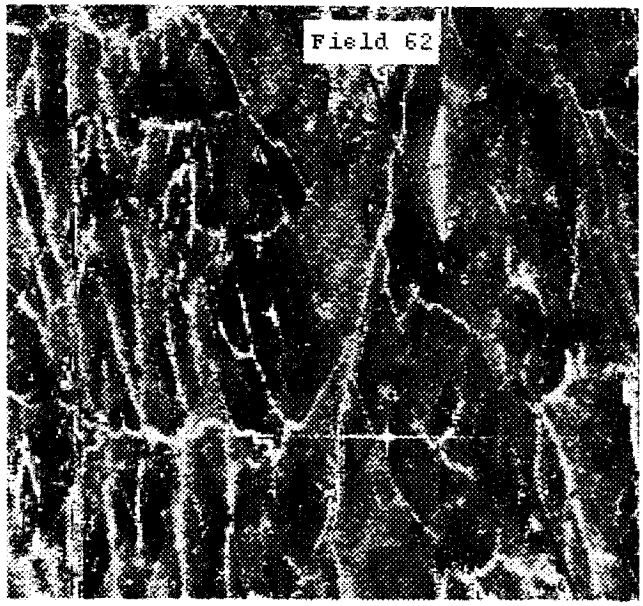

SIR-C L-band radar image from April 12, 1994 of part of the test watershed showing pasture field #62. LHH channel is in red, LVV in green, and LHV in blue.

determine the appropriate filter (see the third figure). This filter or gate was then applied to measurements in the frequency domain. Average radar backscatter values were obtained by sweeping the radar boom 120° in azimuth across the target fields. Calibration for both like- and cross-polarization was accomplished by recording the truck radar response to a target of known backscatter, in this case a large aluminum dihedral corner reflector mounted on a rotating wooden base. Despite variations in field setup conditions and sustained winds of 25 to 30 mph on most days during the April experiment, the radar system was very stable: the network analyzer always powered up to the same level as before in each channel (to within 0.05 dB) and calibration data from the dihedral target never varied by more than 0.1 dB. Cross-polarization data sensitivities of 30 dB above the noise floor at L-band and 15 dB above the noise floor at C-band were also achieved.

A preliminary comparison of truck radar and SIR-C backscatter values for pasture field #62 is presented in the fourth figure, along with the measured soil moisture data. Radar backscatter is referenced to the right axis with soil moisture to the left axis. The water content of the vegetation cover in the pasture was very low, on the order of 125 g/m^2. Results indicate that both the truck and Shuttle

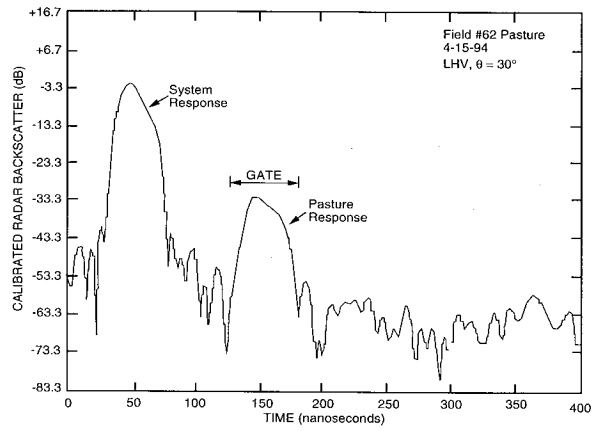

Time domain response of truck radar over the pasture site, used to determine gate setting for backscatter measurements in the frequency domain. The cross-polarization sensitivity of 30 dB above the noise floor is evident.

radars were able to track the changing soil moisture conditions quite well, responding almost identically to the soil moisture drydown in this pasture.

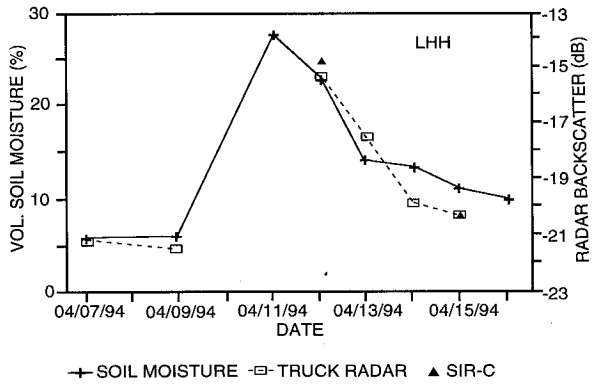

Soil moisture drydown and associated truck radar and SIR-C backscatter values for pasture field #62 during the April experiment.

As additional SIR-C and AIRSAR radar data from the Washita experiment become available, more detailed investigation of the usefulness of microwave measurements in scaling up hydrological models will be pursued. Soil moisture is an important component of the various physical, biological, and chemical processes of the terrestrial ecosystem, and also provides a link between the Earth's surface and the atmosphere through its effect on surface energy and moisture fluxes. Thus, the ability of radar systems to determine soil moisture patterns in space and time offers great potential for an integrated approach to the study of land surface hydrology.

Contact: Peggy O'Neill (Code 974)
301-286-8273

John Petrella (GWU)
202-994-9298

Sponsor: Office of Mission to Planet Earth
SIR-C Program

Ms. Peggy O'Neill, a GSFC employee for over 14 years, works in the Hydrological Sciences Branch of the Laboratory for Hydrospheric Processes as a physical scientist. Her studies focus on the dynamics of moisture storage and transfer at the soil-vegetation-atmosphere interface, primarily through microwave remote sensing techniques. She received a BS from Northern Illinois University, an MA from the University of California/Santa Barbara and is currently working on a PhD from Cornell University.

Mr. John Petrella has been at George Washington University for 12 years where, as Supervisor of Engineering Laboratories, he is responsible for the acquisition, requirements definition, and logistics support of all of the electrical engineering and computer science laboratories located in the School of Engineering and Applied Sciences. He has 10 years of USAF service in telecommunications and air navigation systems, and also works part-time as a consultant in the areas of microwave devices, computerized test equipment, and systems engineering.

NETWORKS, PLANNING, AND INFORMATION SYSTEMS

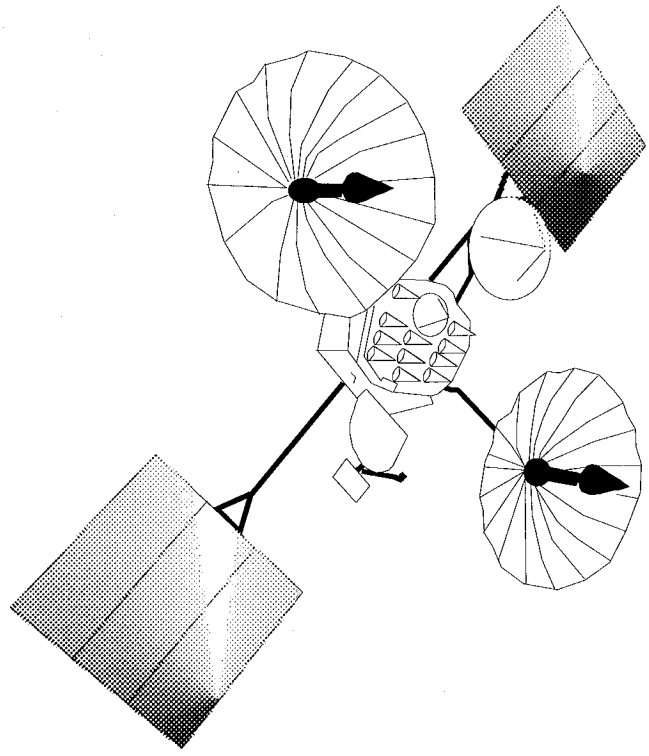

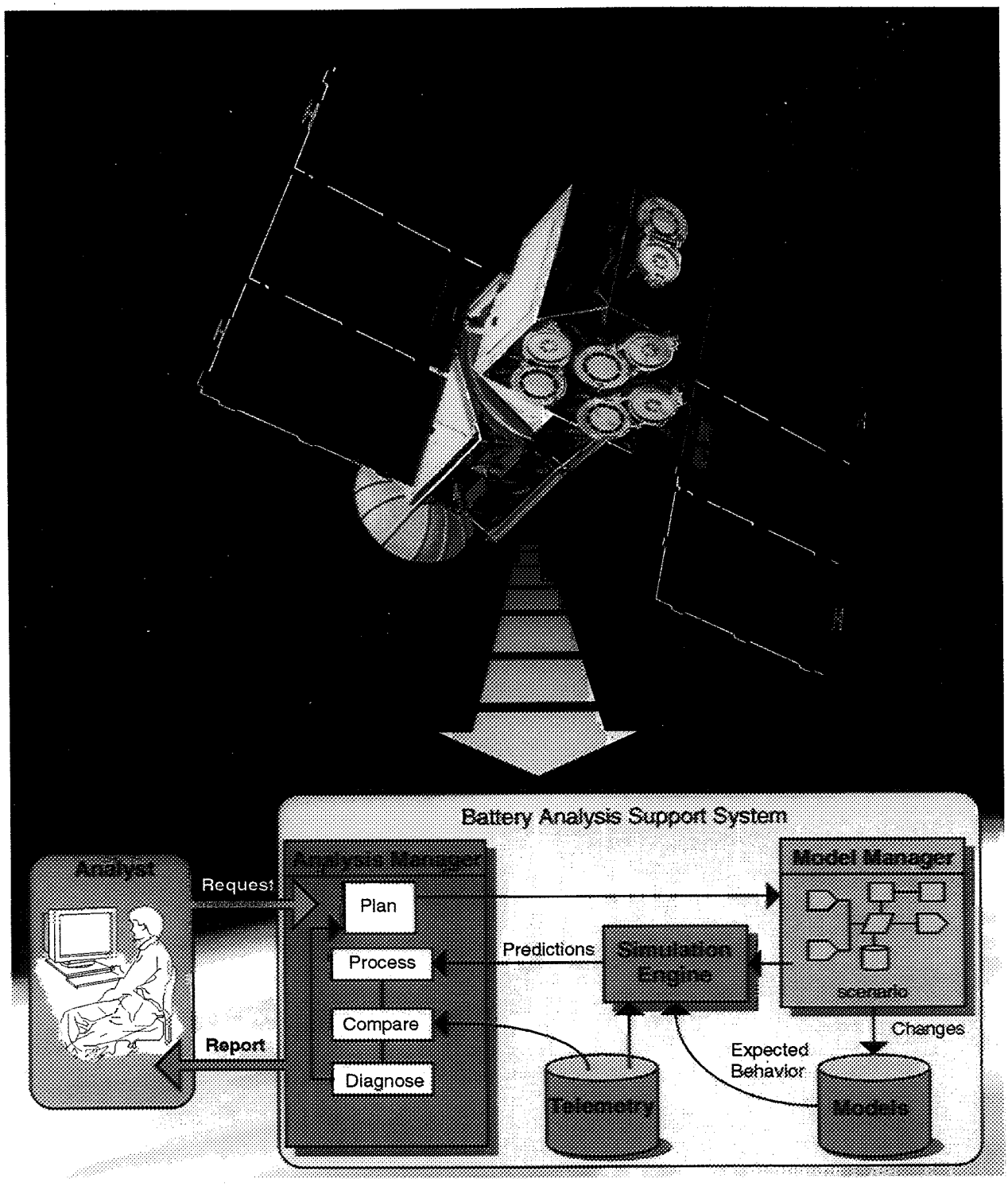

Flight operations analysts for future missions will have access to an array of software tools that provide higher levels of automated support for their tasks. One such tool is the Battery Analysis Support System (BASS) depicted above. This system utilizes model-based approaches for the identification of trends in battery behavior and the determination of any corrective or preventive measures required. BASS provides an example of the type of automated trending tools under current development.

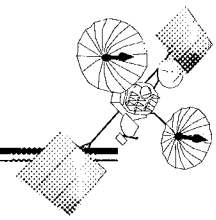

NETWORKS, PLANNING, AND INFORMATION SYSTEMS

THE MISSION OPERATIONS and Data Systems Directorate (MO&DSD) is responsible for developing and maintaining the advanced operational infrastructure required to support near-Earth unmanned scientific spacecraft missions from an end-to-end system's perspective. At one end of this operational megasystem is the spacecraft with its subsystems to be monitored and commanded along with the scientific equipment/experiments needed to support the science agenda for the mission. At the other end are the flight operations team who are responsible for the health and safety of the spacecraft and the scientists who are responsible for conducting scientific investigations and interpreting science data. Advanced information systems technology, knowledge-based systems technology, networking, and planning/scheduling are but some of the myriad of technologies that are required for operational success.

With its operational goals in sight, the MO&DSD has established an aggressive and innovative applied research and development program which allows it to keep current with state-of-the-practice and state-of-the-art technological developments required to sustain its leading role in mission operations. Its current program includes activities in such diverse areas as mission scheduling and operations which focus on applications of knowledge-based and advanced networking concepts; spacecraft operations and status monitoring which includes advanced systems reuse concepts, innovative approaches to attitude determination, and model-bases support for trending; software engineering with special emphases on access to reusable artifacts, advanced approaches for data distribution, and approaches for overall improvements in the software engineering process required for MO&DSD systems; and infrastructure support. The 16 articles in this section give an insight into some of the outstanding research and development work that is being carried on in these areas.

The Mission Scheduling and Operations subsection contains five articles. The "Autonomous Mission Scheduling" articles addresses a new concept in ground data systems a decentralized and distributed approach to mission planning and scheduling. In the "Agent-Based Approach to Automated Mission Operations" article the reader is briefly introduced to the current efforts in prototyping and evaluating agent technologies in operational applications. An agent-testbed has been developed for this purpose. The focus of the current testbed is to demonstrate time and cost savings that can be realized by agent-based information management. The "Distributed Intelligent Control and Status Networking" article indicates how state-of-the-art networking technologies are being applied at Goddard. In "An Intelligent Automated Command and Control System for Spacecraft mission Operations" some of the more important concepts associated with automating mission operations are presented. The idea of simplifying mission operations through the focussed application of knowledge-based techniques is of paramount importance. The "Test/Score/Report Simulation Techniques for Automating the Test Process" article addresses an extremely important aspect of operational systems development-acceptance testing. An approach for automating this life-cycle activity is discussed.

The seven articles in the Spacecraft Operation and Status subsection address innovations in such diverse areas as reusable software, expert system development, attitude determination, star tracker calibration, and trend analysis. In the article "Transportable Payload Operations Control Center Reusable Software A Satellite Control Center System Kernel that Fosters Reuse" the reader is provided an insight into how concepts of software and system reuse are being leveraged to support the development and operation of mission operations systems in a resource efficient manner. In "Generalization of the Generic Spacecraft Analyst Assistant" work on the generalization of the data interface to GenSAA, a software system that empowers spacecraft flight analysts to rapidly develop and use intelligent graphical monitoring systems, is discussed. Completion of this activity will allow GenSAA to be more widely utilized not only within NASA but in private and academic communities. The successful efforts of the Flight

Dynamics Division to enhance their systems with real-time monitoring and visualization techniques is discussed in the article "Advanced Distributed Attitude Determination System Concepts." In the article "Star Identification without A Priori Attitude Knowledge" the efforts of the Flight Dynamics Division to develop computation and memory saving approaches for attitude determination is discussed. The following article, "An Improved Transfer Function for the Fine Sun Sensor," discusses the determination of an augmented transfer function, a function which converts Fine Sun Sensor (FSS) counts into more useful Sun angle information, that dramatically improves the performance of the FSS. In the article, "Color/Magnitude Calibration for NASA Standard Fixed-Head Star Trackers," the author discusses analyses of calibration techniques required for accurate attitude determination. The missions focused on are the Extreme Ultraviolet Explorer (EUVE) and the Upper Atmosphere Research Satellite (UARS). The final paper in this subsection is "A Knowledge-Based Trend Analysis Tool for Satellite Battery Management." This article discusses a value-added capability to the Mission Operations Division's work on a Generalized Trending and Analysis System (GTAS). Using model-based and neural network technologies, the system under development will help automate the telemetry data analysis functions performed by members of the Flight Operations Team. The initial focus is on battery trend data.

The third subsection is Software Engineering and it contains three articles. The first article "Graphical Browsing Tool for Software Repositories," addresses the issues associated with providing the user of a software reuse library or repository the ability to quickly identify relevant components or assets of interest. The system developed to date is used as an interface to the Code 520 Data Systems Technology Division Reusable Software Library (DRSL). The "Mass Production of CD-ROMS In-House Information Processing Division Data Distribution Facility" article describes the current capability for using CD-ROM technology as the physical means of distributing spacecraft data to investigator facilities, science centers, and archives. The final paper in this subsection, "Software Process Improvement in the NASA Software Engineering Laboratory," describes the three-step paradigm for improving the software engineering process which has been developed by the lab over the past 17 years of experience.

The final subsection is Infrastructure Support. The sole paper in this subsection, "Business Process Redesign Rethinking the Logistics Process," addresses the new and efficient business processes and controls that are in place at the Logistics Support Depot.

Continued advancements in these and other areas of research, development, and application will significantly contribute to the MO&DSD's success in meeting the challenges of mission operations in this decade and into the 21st century. Enjoy the articles!

Walter F. Truszkowski

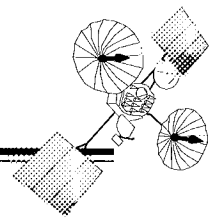

AUTONOMOUS MISSION SCHEDULING

AUTONOMOUS MISSION SCHEDULING, a new concept for ground data systems, is a decentralized and distributed approach to mission planning and scheduling. Systems and services are provided that enable users to plan and schedule activities for their own instruments. In autonomous mission scheduling, each instrument node is responsible for its own instrument operations, planning and scheduling, resolving its internal exceptions, and working with other instrument nodes to resolve inter-instrument exceptions. Similarly, one or more nodes are responsible for spacecraft operations, including planning and scheduling. One or more database servers, accessible to all nodes, enable users to share mission and science planning and scheduling information. Through the use of database triggers and stored procedures, updates are analyzed, exceptions are identified, and nodes are notified of relevant changes or a need to resolve inter-instrument or spacecraft-instrument exceptions. The architecture for autonomous mission scheduling is based upon a realistic mix of state-of-the-art and emerging technology and services (e.g., high-performance individual workstations, high-speed communications, client-server computing, and relational databases).

NASA's scientific spacecraft are unique and valuable resources. It has always been an important part of mission operations to assure that the time a scientific spacecraft spends in space is used as fully as possible in making observations and conducting experiments. To achieve this, most NASA missions plan their scientific activities well in advance, convert those plans into formal spacecraft and instrument schedules on a daily, weekly or monthly basis, and then generate and uplink the commands needed to carry out the scheduled activities.

There are two principal types of mission scheduling problems for NASA. The first type arises when a spacecraft must perform a large number of activities in serial fashion. An example is the Hubble Space Telescope (HST). There are always hundreds of proposed observations in the queue for HST, and typically only one observation can be made at a time. HST schedulers must select the observations to be supported and then lay them out into a single thread of activities. The problem is complicated further by the fact that an experiment may require several observations: if the HST is scheduled to look at a particular target today, then it may also be committed to viewing the target on future occasions as well. Serial scheduling problems are well known (they occur in many terrestrial applications), but they are inherently difficult and time-consuming to solve. Developers of automated schedulers for space missions that must handle this kind of problem tend to concentrate on devising algorithms that increase scheduled observing time while reducing the processing time needed to generate the schedule.

The second type of mission scheduling problem is where a spacecraft can perform a number of major activities in parallel. An example is the forthcoming Earth Observing System (EOS) AM satellite, which will carry instruments that can conduct their observing programs simultaneously and more-or-less independently of one another. It has long been recognized that this kind of parallel scheduling problem allows for a distributed solution. Investigators, responsible for each instrument on a spacecraft, generate the schedule for their own instrument. These detailed instrument plans can be collected and combined with a plan for spacecraft housekeeping activities to form a master schedule that can then be checked for conflicts or resource oversubscription.

Since 1986, the Data Systems Technology Division at the Goddard Space Flight Center (GSFC) has been investigating scheduling issues relevant to GSFC missions through analysis, prototyping tasks, and testbeds. In 1992 and 1993, work concentrated on EOS and on planning and scheduling in a distributed environment. A testbed was successful in demonstrating that distributed planning and scheduling is feasible for a project like EOS. Results are documented in the Earth Observing System Distributed Planning and Scheduling Prototype Lessons Learned Working Paper. One interesting result was that exceptions representing conflicts between instruments were usually best resolved by making the instrument investigators aware of the problem and letting them work it out for themselves. To aid in conflict resolution, it would have been useful for investigators to be able to see schedules for instruments other than their own (a feature that the testbed did not provide).

As the testbed progressed, it became clear that every scheduling node not just a central scheduler should have access to all information needed for scheduling, and every node should be able to view the spacecraft schedule and any instrument schedule. Central to this concept is one or more databases that make needed information available to all

nodes. A beneficial side effect is that specialized scheduling protocols are no longer necessary, as all scheduling system transactions become transfers of information to or from a database, using a standard query language (SQL). Also, while the ability to detect constraint violations and conflicts, and the potential to automatically resolve simple exceptions are important capabilities, these functions need not be implemented within a central scheduler, but can be implemented within a database framework.

Given a database approach, the client-server architecture seems ideal for a distributed scheduling system. Services that were previously provided by a central scheduler, like resource tracking, exception detection and exception resolution, are implemented as independent services that can be invoked by a scheduling node as needed. Distributed scheduling may be one of the first opportunities to actually apply the client-server architecture to space mission operations.

Autonomous mission scheduling functions are allocated to components or nodes, and nodes are integrated together to produce a ground system for a target mission. Possible functions include:

- Transfer frame processing and recording.
- Planning and scheduling.
- Network communications.
- Telemetry processing.
- State vector determination.
- Orbit determination.
- Tracking system calibration.
- Database setup and maintenance.
- Schedule generation and maintenance.
- Exception detection and notification.
- Exception handling and negotiation.
- Database management.
- Command data generation and maintenance.

In the simple architecture described by the figure, a Mission Operations Center (MOC), a single database server, the Flight Dynamics Facility (FDF), and the Network Communication Center (NCC) are all located at GSFC. Since the Science Operations Center (SOC) is remote, the MOC and SOC do not share telemetry processing and state vector determination functions. The FDF, located at GSFC, provides orbit and attitude planning and scheduling aides. The NCC, located at GSFC, provides network scheduling data to the MOC and remote SOC. A specialized node, a database server at the MOC/SOC, receives and stores these data. Nodes store planning and

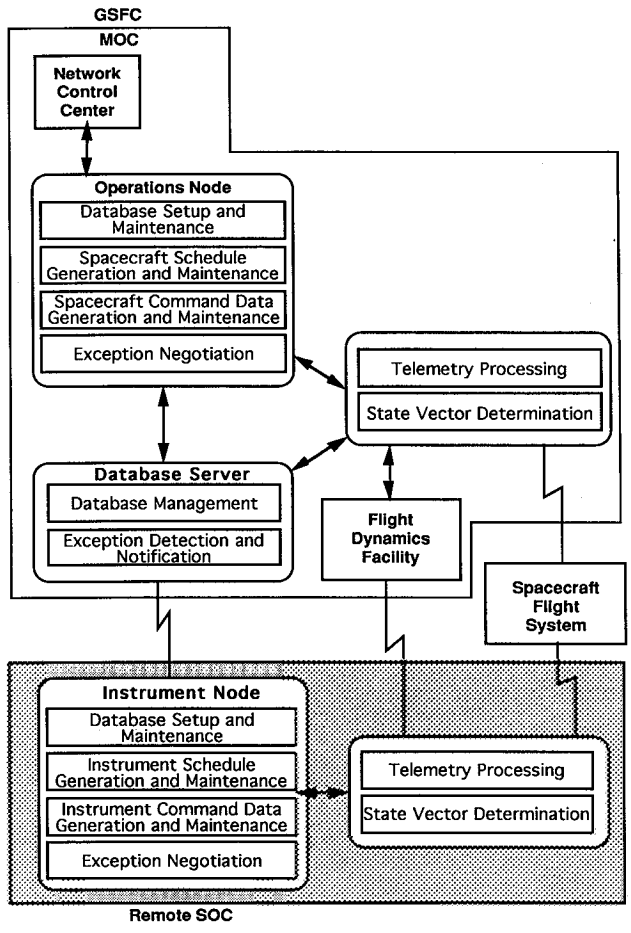

A distributed autonomous mission scheduling architecture, with application functionality and data partitioned between workstations (clients and servers) connected to local area networks.

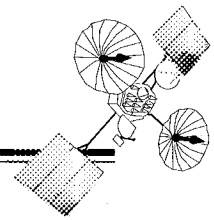

scheduling data on the database server and may access other nodes' planning and scheduling data of interest as well. Nodes can access a database server whether they are remote or not, the only difference being in the kind of network interface used; remote nodes access the database server through a wide area network (WAN) and local nodes through a LAN. The database server node also detects inter-instrument and instrument-spacecraft exceptions, and notifies affected nodes to begin negotiations in order to resolve the exception. GSFC nodes communicate with one another through a LAN, while the remote SOC communicates with GSFC nodes through a WAN.

In fiscal year 1994, the autonomous mission scheduling concept was developed and refined. A commercial database management system (Sybase) and existing scheduling tools and equipment (e.g., VAX workstations, SUN workstations) were used to rapidly prototype the fundamental capabilities needed for autonomous mission scheduling, to integrate a subset of the architecture shown here and to validate technical feasibility of the concept.

Contact: Larry Hull (Code 522)
301-286-3009

Sponsor: Office of Space Communications

Mr. Hull is a senior computer engineer in the Data Systems Technology Division at the GSFC. He has over 25 years of NASA experience in areas as diverse as real-time operational support for manned and unmanned spaceflight missions, computer performance and capacity management, discrete event simulation of computer and communications systems, expert systems, activity scheduling and project management. His current research interests include geographically distributed mission operations, prototyping and genetic programming.

AN AGENT-ORIENTED APPROACH TO AUTOMATED MISSION OPERATIONS

MAJOR ADVANCES have been made in the process of automating mission operations over the last several years. However, in keeping with changing operational requirements and the need to more effectively realize cost and manpower savings, the necessity for more advanced automation technologies is clear. Therefore, we are investigating an agent-based approach to automated mission operations.

In our context, an agent is a specialization of a process, characterized by five basic action-oriented capabilities:

- Migration, to promote load balancing among distributed nodes.
- Semi-autonomy, to promote low user intervention.
- Cloning, to promote dynamic parallelism and fault-tolerance.
- Persistence, for supporting time-extended activities.
- Communication, for supporting agent-to-agent and user-to-agent, interaction.

An agent testbed is under development. A major accomplishment this year has been the creation of the agent testbed infrastructure. This infrastructure allows us to begin developing prototype agent-based scenarios, and to begin accruing the set of benefits that can be realized by the proper application of agent-oriented technology in a mission operations environment. Our near-term focus is to investigate agent-based technologies applied to data/information management and spacecraft status data monitoring and analysis. The current testbed addresses some of the data management and report generation functions for the Explorer Platform (EP)/Extreme Ultraviolet Explorer (EUVE) Flight Operations Team (FOT).

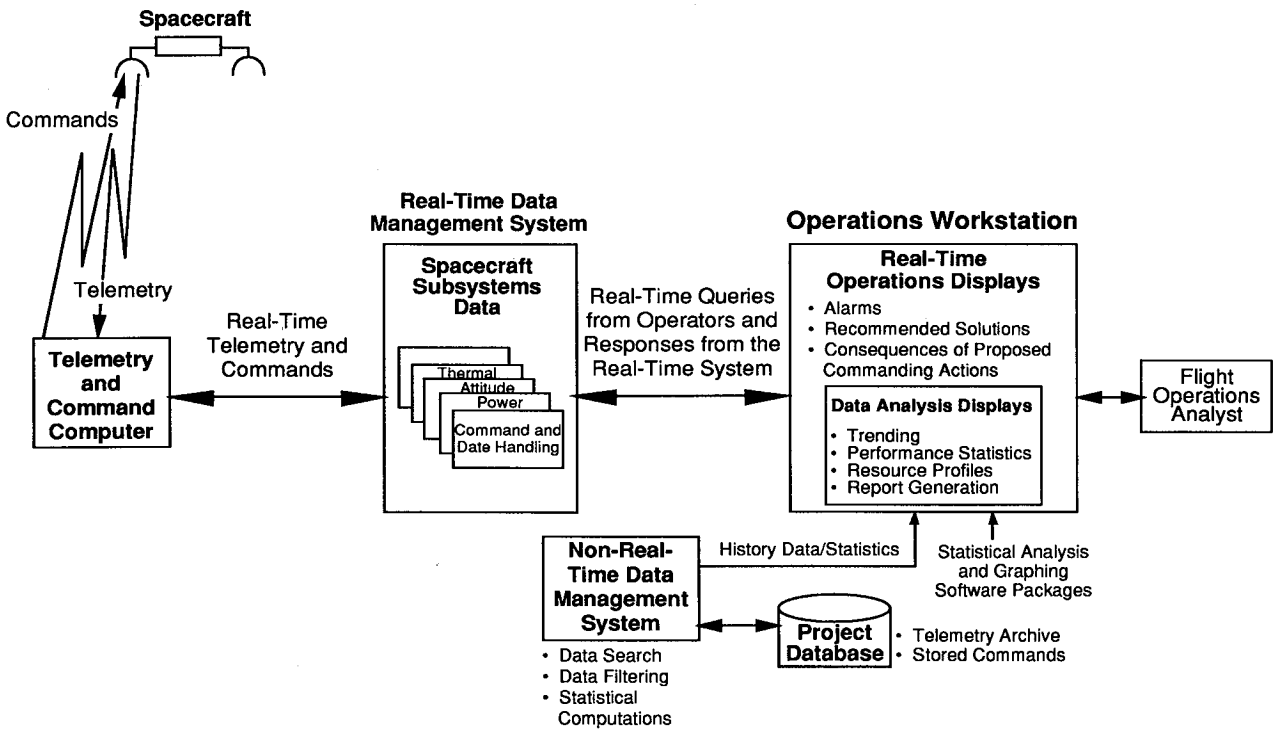

An overview of spacecraft mission operations from a data/information management perspective.

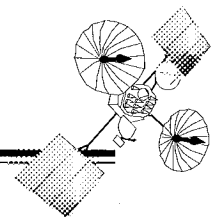

The figure gives a high-level schematic representation of the data-rich environment associated with current mission operations. Real-time and nonreal-time data/information management in the mission operations environment is an increasingly challenging task. Analysis of the EUVE gives some indication of the magnitude of this data/information management job. The EP/EUVE's operational environment is a heterogeneous network, consisting of two MicroVAXs, running VMS, a Sun workstation and an HP-9000 workstation, both running UNIX, and 386 personal computers, using X.25 and TCP/IP communications protocols. Subsystem engineers for EP/EUVE are responsible for: daily monitoring of the satellite's subsystem performance; detection of anomalous subsystem behavior; weekly reporting of subsystem performance; generation of commanding products for subsystem operations; and continuing preparation for subsystem anomaly detection, isolation, and resolution (DIR). Data for these activities reside on heterogeneous distributed computing nodes. Off-line analysis (Trend system) provides daily plots of over 600 mnemonics for visual checks of subsystem performance and trends. Each week, three of the EP's engineers spend approximately a total of 40 hours generating a weekly report on the performance of the system.

The current testbed demonstrates how application of agent-based technology to this report generation process can reduce workloads and increase reliability and completeness of reports.

Contact: Walt Truszkowski (Code 522.3)
310-286-8821

Jidé Odubiyi (Loral AeroSys)
301-805-0305

Sponsor: Office of Space Communications

Mr. Walt Truszkowski is Head of the Automation Technology Section. His major interests are in the areas of applied artificial intelligence, advanced software engineering environments, and human factors.

Dr. Jidé Odubiyi is a Principal Engineer and Senior AI Researcher in the Advanced Technology department of Loral AeroSys, Seabrook, MD. His principle areas of interest are multiagent-based systems, machine learning, and intelligent tutoring systems.

DISTRIBUTED INTELLIGENT CONTROL AND STATUS NETWORKING

OVER THE PAST 2 years, the Network Control Systems Branch has been investigating emerging networking technologies for control and status. Current uses of control and status networks include vehicle, home, and industrial automation. These networks consist of small, intelligent "nodes" that individually perform relatively simple tasks. Containing simple, inexpensive hardware and software, these nodes can be easily developed and maintained. Once networked, the nodes can perform a complex operation without a central host computer. Nodes on these networks monitor sensors and control devices. An example of a small network could be nodes connected to smoke alarms, with other nodes connected to lights near emergency exits. Should a smoke detector node sense smoke, it would send a signal to the light nodes, directing inhabitants to the safest exit. All of this would occur

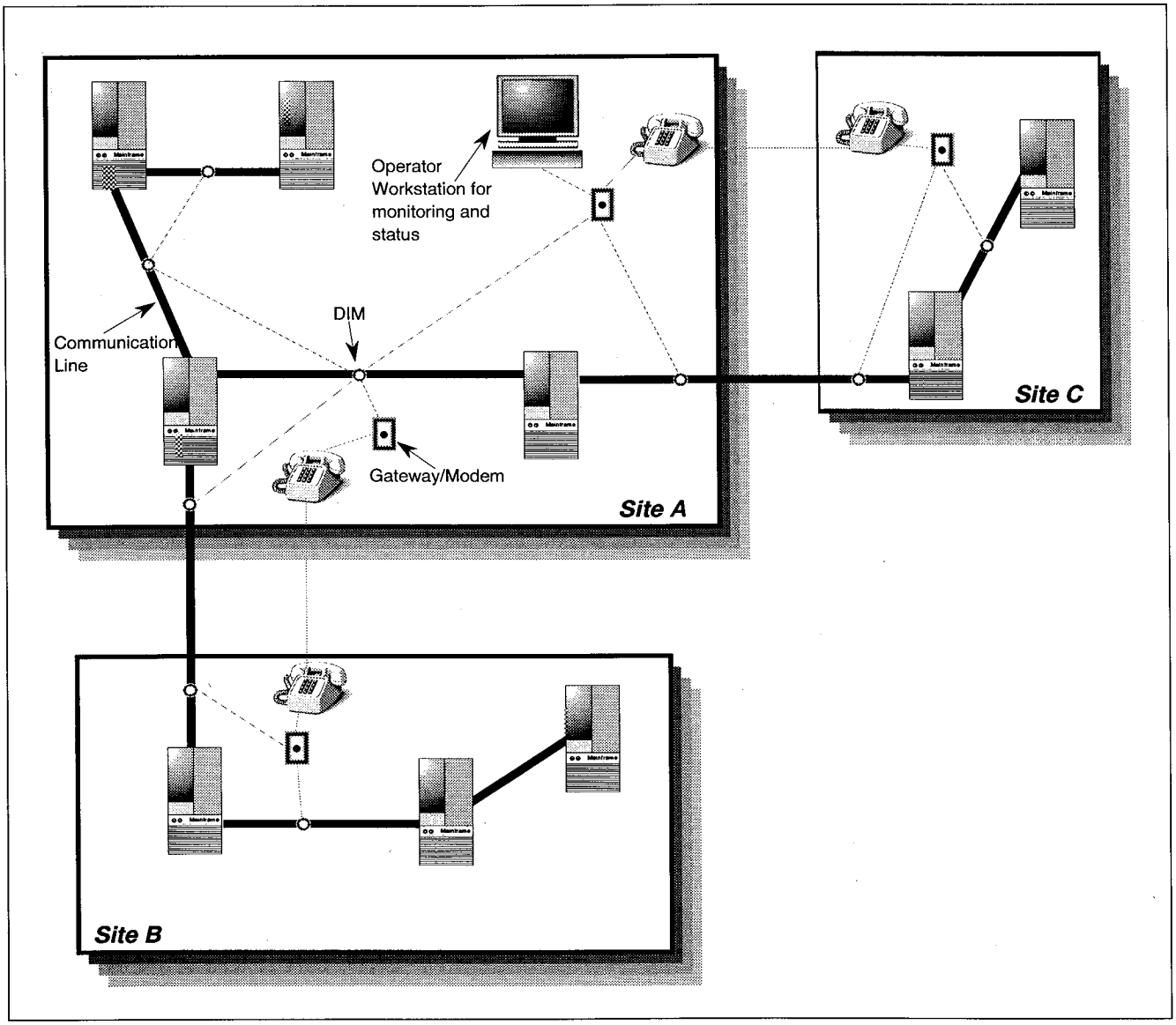

Possible scenario of a DIM system.

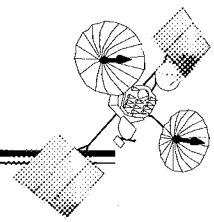

without affecting any other nodes on the network that have different functions, such as security, motor operation, other light nodes, etc.

One control and status network technology that the Branch is using is called Local Operating Networks (LON). This type of network permits a variety of methods for physically connecting nodes. They can be tapped off a serial bus or arranged in a star topology. They can even send signals between one another by radio frequencies or by signals piggy-backed on AC power lines. This type of network also allows nodes to be programmed with generic functionality ahead of time, but configurable at installation time to execute only the relevant subset of those system-level functions. This allows for easy production of one kind of node and access to spares. For example, in the previously mentioned scenario of smoke detectors and light nodes, other light nodes may be identical, but at installation time will not be logically connected to the smoke detector node because they may not be near emergency exits.

The Branch is prototyping a system that uses the LON technology for monitoring communication lines. The point-to-point communication networks at NASA Ground and Space Network facilities have become increasingly complex, and require monitoring for data activity and quality. By having a network of nodes that monitor various protocols (e.g., NASCOM, RS-232, GPIB) and a network status workstation to gather the status from the nodes, a system is created that determines line utilization, systems performance, and line connectivity.

Presently, nodes have been developed that monitor NASA Communication (NASCOM) lines. These nodes are called Data Integrity Monitors (DIM). Forty DIMs on NASCOM lines at the NCC will provide the time-tagged status of several parameters to the workstation, including NASCOM block count, bad block count, clock rate, and inverted data detect. Presently, these nodes are passive and do not record any data on the block itself, but future nodes may inspect user-specified data fields or inject data on the line to support system testing. The workstation logs the status from all the nodes. It provides the operator with physical diagrams of the NCC, annotated with DIM status to assist in fault isolation of improperly patched cables. Active lines can be detected by block counts appearing on the site connection diagrams. Graphical windows also provide the operator with histograms of past line activity and provide the operator with performance monitoring. By comparing the graphs of data entering and exiting a particular system, the time delay associated with system processing can be determined.

The figure shows a possible scenario of a DIM system that spans several NASA sites, with one workstation showing the communication line activities between each system and each site. With this scenario, the efficiency of troubleshooting a faulty path will be greatly enhanced.

Contact: Andre Fortin (Code 532.2)
301-286-7829

Sponsor: Office of Space Communications

Mr. Andre Fortin is a computer engineer who designs, develops, and implements hardware and software systems for the Space Network and the Ground Network. He received his BS in Electrical Engineering from the University of Dayton and has been at GSFC for 8 years.

AN INTELLIGENT AUTOMATED COMMAND AND CONTROL SYSTEM FOR SPACECRAFT MISSION OPERATIONS

THE INTELLIGENT COMMAND and Control (ICC) System research project was organized to provide the technology base necessary to develop an intelligent, automated command and control (C&C) system capable of performing the ground-control C&C functions currently performed by a MOC's project FOT.

Increasingly, mission operations personnel are being required to operate more complex ground systems with less FOT personnel and lower budgets than in the past. The ICC will address these requirements through automation and intelligent machine case-based reasoning and decision-making. The need for the ICC is due in some cases to the fact that FOTs will be asked to C&C complex missions—such as those of the EOS—and in others to the fact that FOTs will be required to operate several spacecraft concurrently from the same MOC—such as the Small Explorer (SMEX) and the International Solar and Terrestrial Physics (ISTP) missions. This requires that we develop an intelligent C&C that is capable of acting as a cooperative assistant to the FOT, in order to reduce the workload of existing FOTs and reduce the cost burden of creating ever-larger FOTs. Many valuable interim products are being produced in the course of this development work which can be implemented to improve, automate, and reduce the cost of MOC operations generally.

The stated ICC program objectives are to:

- Demonstrate that we can improve and simplify spacecraft MOC C&C by building and operating a real-time ICC utilizing artificial intelligence (AI), object-oriented programming techniques, and animated graphical user interfaces.
- Create a C&C system that can act as a cooperative member of an FOT.
- Demonstrate that MOC C&C functions can be fully automated and that such a system can perform intelligent machine-based decision-making.
- Demonstrate that such a system would show tremendous cost savings by:
  - Limiting or reducing the number of FOT personnel.
  - Intelligently automating spacecraft MOC functions to the point where management-by-exception can become a reality.
  - Reducing operator error through more-intuitive user interfaces, automation, the use of true machine decision-making, and the application of standardized commands.
  - Generating faster, more cost-effective and more robust spacecraft system status, and operations simulators and models.
  - Simplifying and reducing the cost of training through the use of a C&C system that is both more generic, or standardized, for all missions, and internally more flexible (i.e., easier to modify for specific missions).

When fully integrated into Mission Operations Division (MOD) operations, the completed operational ICC will reside in the Transportable Payload Operations Control Center (TPOCC) workstation, accepting data from the Front End Processor (FEP) Data Server Task (DST). It will provide an intelligent, object-oriented C&C system capable of accepting downlink telemetry in real time and passing the telemetry (or database) updates to the ICC Reasoning Machine (RM). The RM, or inference engine, using case-based (or a combination of AI machine reasoning) techniques, will match the input with robust spacecraft and ground control system models, and then decide what actions should be taken. The ICC will decide whether these actions are to be taken by the ICC directly, sent to the human operators (i.e., the FOT) for further action, sent to other ground control systems (e.g., small Generic Spacecraft Analyst Assistant (GenSAA)-built expert systems), or other users (e.g., Primary Investigators or subsystem engineers). What actions the ICC takes can be preset by the FOT, have default settings, or be based on previous cases or extrapolations from such cases.

The command side of the ICC will be capable of acting cooperatively as another member of the FOT. It will be capable of accepting and sending commands in real time

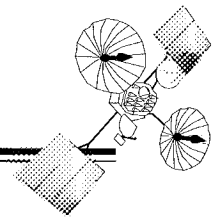

from a number of sources: default routine commands set by the FOT prior to the mission, commands set by the FOT for a given pass, or RM-ordered commands sent in response to electronic input. Whatever the source of the commands, they will be converted from either operator-generated graphical commands or from RM-generated commands into the Systems Test and Operations Language (STOL) commands that will be processed by the existing STOL Processor.

Most of the user interfaces will be animated graphical user interfaces. The guiding principle behind any user interfaces design and the first question to be asked in designing each user interface will be, "What type of user interface most enhances task (and thereby mission) performance?"

The Operator Function Model (OFM) is a hierarchical-heterarchical decomposition of the FOT functions required to carry out the real-time operations involved in satellite ground control. The OFM provides a detailed normative model, specifying how operations are to be carried out. At the highest level, the OFM specifies the components that comprise the overall, real-time, prepass, on-pass, and post-past operations. It decomposes each function into component activities that may be mapped to lower levels, including subfunctions and tasks. At the lowest level, the OFM specifies operator actions, both manual and cognitive, needed to carry out individual tasks. Its components depict the concurrent activities typical of satellite ground control. The dynamic component provides the context; triggers represent how new operator activities manifest themselves as a result of system events and previously executed operator actions.

Task analysis of anomaly detection and correction processes is designed to understand how often and what happens when unanticipated events occur. The study addresses events that occur in the period immediately after launch and early orbit (L&EO) (i.e., examination of those events that are considered to have occurred during the nominal operations phase). In particular, the study documents for each anomaly (other than those identified by one of the experts as a peculiarity of the L&EO) the process of (1) failure detection (i.e., when, how, and by whom the anomaly was first noticed); (2) failure management (i.e., how long it was and what happened between the time the anomaly was first detected and when corrective action is initiated); (3) fault compensation (i.e., what was done and who did it) with emphasis on the decision-maker's qualifications. The study will include identification of the time required to resolve the anomaly and distribute information to the FOT. This study will be coordinated with the OFM, particularly with respect to the issue of nonpreplanned activities. Recall that the OFM will include comments on what actions are preplanned or opportunistic. In the latter case, we will attempt to document the types of opportunistic activities undertaken, and the personnel who formulate and execute them.

The project will build a knowledge base of experience in real-time decision making. This component of the ICC project will investigate the use of case-based reasoning technology to accumulate a knowledge base of actual operations experience and, subsequently, to use that experience as aid or advice in an intelligent decision support system. Initially, such a system monitors real-time operations forming a knowledge base that reflects the range of nominal operations. As unplanned and/or anomalous events occur the case base grows: it automatically learns, broadening its knowledge base to include operations experience accrued in managing these unanticipated events. Such a system uses case-based reasoning technology to build an extensive repository of operations experience (i.e., cases, that over time, can function as the knowledge base for an autonomous system). This project represents one of the first applications of case-based reasoning to real-time decision making and system control. It provides an alternative, and potentially richer, knowledge base than such applications as rule-based systems. Given the extent of operational experience that comprises the foundation of FOT expertise, a case-based system that can learn from skilled operators is a promising way to encapsulate and capitalize on human experience, and subsequently make it available to human operators and other intelligent, machine-based systems.

For training, we plan to use a tutor-aid paradigm, based on the concept that an effective approach to operator aiding and training is the integration of aid and training into one comprehensive system that differentially responds, depending on the skill level of the operator. An integrated tutor-aid provides a great deal of assistance and guidance to unskilled operators (i.e., operators-in-training). As the operators skills increase, the tutor becomes less active and becomes a well-understood assistant. The knowledge bases that support an intelligent tutor-aid system (e.g., system and task models of what to do, how, and when to do it) are exactly those needed for more autonomous system operation and control.

In addition to research concepts exploring intelligent systems, the ICC project is concerned with proof-of-concept demonstrations and evaluations of these technologies. Long term, the intent is to provide a side-by-side demonstration comparing conventional operations with operations incorporating the proposed systems. In the interim, the individual research efforts can be demonstrated and empirically evaluated in the context of a research-based, experimental ICC-TPOCC testbed. The ICC-TPOCC testbed is a real-time simulation of the operator interface to the satellite ground control system. It is modeled after the TPOCC MOC operations. The testbed provides the ICC project with the ability to implement the proposed system, and, using NASA operations personnel as subjects, conduct experiments that compare current and proposed systems.

Two studies comprise the final component of the ICC: an in-depth analysis of the feasibility of a completely autonomous control center, and a statement of working assumptions that support the concept that an autonomous control center is possible. The feasibility study will examine the existing facilities and procedures integral to satellite ground control, specifically focusing on impediments to a completely autonomous control center. As impediments to intelligent automation are identified, the study will attempt to suggest technological alternatives to those impediments. These sets of impediments and technological alternatives define the basis of the second study, which will articulate a set of working assumptions that define the operating practices (current or future) essential to moving to fully autonomous ground control operations.

To date, we have accomplished the following:

- Completed a ready-for-development and implementation user interface that allows one person to perform the job currently being performed by two FOT members.
- Completed the first task analysis.
- Completed generation of a first OFM.
- Completed development of an initial ICC MOC simulator which accepts actual spacecraft telemetry data as input.
- Completed task analysis of anomaly detection and correction processes.
- Developed the first case-based reasoning tool capable of browsing operational mission data.
- Completed automation analysis for implementation of control center management-by-exception.
- Completed task analyses of the Gamma Ray Observatory (GRO), the Solar and Heliospheric Observatory (SOHO), EUVE, and ISTP mission activities.
- Completed development of an initial, basic research ICC prototype.

This work was performed in collaboration with Dr. Christine M. Mitchell, Center for Human-Machine Systems Research, School of Industrial and Systems Engineering, Georgia Institute of Technology, Atlanta, GA, and Dr. Patricia M. Jones, Department of Mechanical and Industrial Engineering, University of Illinois at Urbana-Champaign, IL.

Contact: A. William Stoffel (Code 513.1)
301-286-8853
bstoffel@stimpy.gsfc.nasa.gov

Sponsor: Office of Space Communications

Mr. A. William Stoffel has implemented VITA (see the 1992 GSFC Research and Technology Report). His training and past experience was in human factors and experimental psychology, particularly auditory and visual perception, cognition, and neuroscience. Mr. Stoffel's primary research interest is in the area of machine reasoning, functionally independent robotics, and human-computer integration as they apply to NASA.

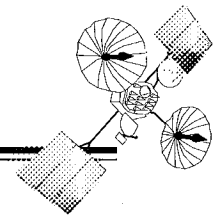

TEST/SCORE/REPORT: SIMULATION TECHNIQUES FOR AUTOMATING THE TEST PROCESS

THE TEST/SCORE/REPORT simulation technique used to perform acceptance testing of ground support system software deliveries allows automation of the test process. By making use of the design features of the system under test, testing ground support systems can be accomplished in a shorter period of time and at reduced cost. To achieve test process automation and to provide a test tool that can be used in the ground system environment, several features common to the test tool and the system under test must be present: (1) a script language for automating the operations and test process, (2) a hardware configuration with a minimum of special hardware, (3) a graphical user interface based on industry standards such as OSF/Motif, (4) a software reuse library where the designer can select appropriate building blocks, and (5) other industry standards, such as C, TCP/IP, sockets, and XDR. Test/Score/Report techniques for automating the test process are based on these features, and are described here.

The TPOCC Advanced Spacecraft Simulator (TASS) system has been designed to support development, test, and operational aspects of control center software deliverables. The figure shows the typical data flow for a test configuration. The TASS system simulates spacecraft telemetry and command functions. TASS takes advantage of the TPOCC architecture by using a backup control center system configuration hardware for the simulator. TASS can be separately hosted on a streamlined version of the control center system, thus eliminating the need to schedule and setup external communications circuits during various test configurations. In essence, the user has an on-call simulator.

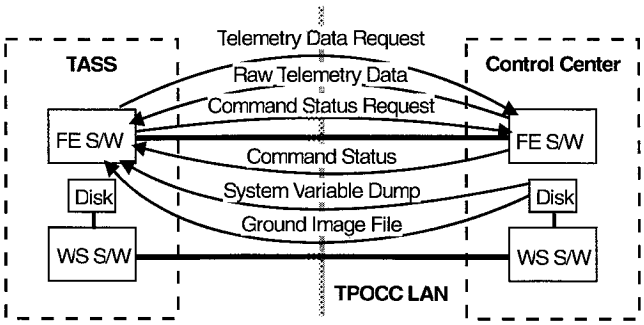

Data/control flow between TASS and the control center.

TASS can simulate the communications link protocols required to support satellites and generate simulated spacecraft telemetry streams using the control center's operational database. TASS validates spacecraft commands and alters the real-time telemetry stream in response to those commands. The user can alter the telemetry stream either by database mnemonic or by specifying individual bits in the telemetry frame or packet. Similar telemetry display pages at both the simulator workstation and the control center workstation help identify telemetry processing irregularities. As part of the system design software hooks are available so that more complexity can be added by providing various dynamic models for the telemetry generating function.

In the control center test environment, the TASS system provides a means for saving and restoring predefined test scenarios and results, telemetry stream contents, and data structures to allow the user to accurately repeat specific tests, retest with known data, or continue testing from a given point in the test scenario. These features allow the user to perform regression tests in the shortest possible time.

TASS records all received data in history files that can be viewed for detailed analysis with an offline utility program. All system events, errors, operator input, procedure input recorded in the event log, and spacecraft memory images that are saved can be viewed. After completing the test, the user generates test reports for analysis using the report generation subsystem.

Unique implementations of spacecraft memory-load and -dump capabilities are provided, as are communications protocols when TDRSS support is required.

Taking advantage of the ground support system features, a typical control center system processing string can be used to host the TASS software. A typical string consists of FEPs, workstations, and X-terminals all tied together by a LAN.

TASS makes extensive use of the same TPOCC reusable software that control center developers use, mainly the user interface (display and user script language) and the communications interface. The display system is based

on X-windows and fully adheres to industry-standard OSF/Motif principles. The user script language is used to control the TPOCC application system (either the control center system or the TASS system) and is also used to develop operational scenarios and test procedures. Presently, TPOCC reusable software comprises approximately 78 percent of the TASS system. Another 16 percent of TASS is reusable from mission to mission, such that only about 6 percent of TASS needs to be newly developed with each added mission.

The Test/Score/Report capability currently being developed will automate testing the control center software in three areas: telemetry decommutation, spacecraft command processing, and spacecraft memory-load and -dump processing. TASS takes advantage of the ground system attributes in designing the Test/Score/Report capabilities. Both TASS and control center systems are using some of the same reusable building blocks of TPOCC software and run on the same hardware. By using this approach, TASS can easily add features that enhance the automated test process.

The TASS system simply establishes a socket connection with the control center system to make requests for and to receive data, as shown in the figure. This connection is transparent to the control center system and requires no new software to be written on the control center side. The TASS system also reads the control center's system-variable dump and ground-image files, both of which reside on the workstation's disk. The system-variable dump file contains all the telemetry parameters located in the operational database, and counters and status information. This file is needed for initialization purposes before requests for data can be made. The ground-image file is used to validate spacecraft memory-load and -dump processing.

Telemetry decommutation is tested in two ways. The first is by comparing the values of telemetry parameters decommutated by the control center against the telemetry parameters commutated by TASS. Ideally, the decommutated values should match the commutated values. The second way is by comparing the limit specifications previously set with the status words of decommutated telemetry parameters. Every telemetry parameter located in the operational database is automatically checked. Each discrepancy is displayed as an event message which gives the value of the decommutated telemetry parameter and the value of the commutated telemetry parameter. Summary event messages for the two telemetry decommutation tests state the total number of telemetry parameters that decommutated correctly, the total number of telemetry parameters checked, and the percentage of telemetry parameters correctly decommutated.

For spacecraft commanding, the test process validates the various fields in the data block header for all spacecraft command blocks received by TASS and validates the individual spacecraft commands received in valid command blocks. TASS also checks whether the control center verified the commands after they were executed by TASS. This is accomplished by making data requests to the control center for values of command status parameters and counters. Summary event messages are displayed which give the number of valid command blocks, the number of valid commands, the number of commands verified by the control center, and the percentages for each of the above tests.

The spacecraft memory-load and -dump processing is tested by comparing the spacecraft image maintained by TASS against the ground-image file maintained by the control center. This test is performed after memory-load data are sent to TASS from the control center via a spacecraft command and after TASS transmits a memory dump to the control center via the telemetry stream. Ideally, the memory values maintained by TASS should match values in the control center ground-image file. A summary event message informs the user of the number of bytes that miscompared, the total number of bytes in the spacecraft image, and the percentage of bytes that had the same value.

At the present time, the initial scoring method is in terms of percentages and raw counts. Using experience in testing and evaluating data results, the user can develop several different types of scoring methods depending upon a specific environment.

The TASS system displays statistics on the success of the control center system in each of the three areas as well as event messages pertaining to the Test/Score/Report processing. A display page gives the summary counts and scores for the various tests. The page also includes a scrolling region which displays all event messages generated during Test/Score/Report processing. The TASS system also provides formatted reports documenting each step performed during the tests and the results of each step. The user can issue reports for each type of test (i.e.,

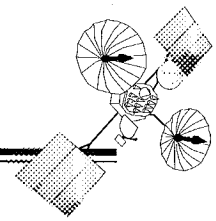

telemetry, limits, command, memory loads/dumps). Report options include showing all parameters tested or just those parameters that miscompared or were in error.

A prototype of the Test/Score/Report capability is now available and is being used to automate the testing of the Wind, Polar, SAMPEX, FAST, SWAS, SOHO, and XTE control center software deliveries. This prototype includes the "test" and "score" features described in this report. The "report" features (other then the Test/Score/Report display page) are currently being developed by the TASS development team and are planned for release early next year.

Contact: Jack Koslosky (Code 511)
301-286-8947

Clayton Sigman (Code 511)
301-286-4821

Barbara Hageman (Integral Systems, Inc.)
301-497-2415

Sponsor: Office of Space Communications

Mr. Jack Koslosky is a Section Head in the Control Center System Branch. He manages the development of real-time ground-support systems for Payload Operations Control Centers. Mr. Koslosky has worked on the TPOCC project since 1985 and has 20 years of experience in control center design and management at GSFC.

Mr. Clayton Sigman is a computer engineer performing systems engineering, integrating, and testing of TPOCC systems. He earned a BS in Electrical Engineering under the Cooperative Education Program from the University of Maryland at College Park. Mr. Sigman has been at GSFC for 8 years, where he works in the Control Center System Branch developing TPOCC ground systems.

Ms. Barbara Hageman is the technical lead in the development of GSFC Control Center System Branch simulators and test tools. She holds a BS in Aerospace Engineering under the Cooperative Education Program from the University of Maryland at College Park. Ms. Hageman has 12 years of experience in the development of various spacecraft simulators.

SPACECRAFT OPERATION AND STATUS

TRANSPORTABLE PAYLOAD OPERATIONS CONTROL CENTER REUSABLE SOFTWARE: A SATELLITE CONTROL CENTER SYSTEM KERNEL THAT FOSTERS HIGH REUSE

NASA'S GSFC MOD PROVIDES ground support systems for a variety of scientific satellites. The MOD designs, implements, tests, and delivers control centers—both traditional Payload Operations Control Centers (POCCs) and the newer, functionally expanded MOCs—that provide command management and mission planning functions. In recognition of the many similarities between mission requirements, the MOD has always made software reuse a priority.

The TPOCC is a control center architecture that takes advantage of workstation-based technology to improve mission operations and reduce development costs for POCCs and MOCs in GSFC's MOD. The TPOCC development team has established an extensive library of 14 software subsystems with over 100,000 delivered source instructions (DSI) of reusable, generic, software components. The reusable TPOCC software is integrated with mission applications software to provide health and safety monitoring and command capabilities for various NASA satellites, including the capability to process and display telemetry, build and send commands, and perform special processing. In addition, TPOCC provides a graphical user interface and a procedural command language that automates ground system test and operations activities.

To date, six TPOCC-based applications systems have been configured to support eight different spacecraft. The first three POCCs developed for the SMEX program, Solar, Anomalous, and Magnetic Particle Explorer (SAMPEX), Fast Auroral Snapshot Explorer (FAST), and Submillimeter Wave Astronomy Satellite (SWAS), also serve as a case study in determining the levels of reuse that can be attained with the TPOCC architecture within a series of missions. The SAMPEX POCC consists of commercial off-the-shelf (COTS) products, 67 percent TPOCC-generic software and 33 percent mission-specific software as shown in the table. By reusing both SAMPEX mission-specific software and the expanded TPOCC-generic software, the FAST POCC achieved an 81 percent reuse level. The SWAS POCC, expanding this reuse base to include FAST mission-specific software, achieved a reuse level of 92 percent.

Using the TPOCC software and architecture framework, mission development teams have also been able to support unique needs of individual spacecraft requirements. The Wind/Polar POCC, supporting two spacecraft scheduled to be launched within the next year, handles two physical channels of time division multiplexed (TDM) telemetry, while other TPOCC missions use the Consultative

NASA/GSFC Control Center TPOCC Reuse Data

Project Name	Mission-Specific DSI	Reused DSI	Total System DSI	Percent Reuse	Total Generic Change Requests (ICCRs)
ICE/IMP	25407	72552	97959	0.75	17
ISTP series:					
WIND	43,372	81,895	125,267	0.65	23
POLAR	7,414	124,934	132,348	94	0
SOHO	43,690	94,840	138,530	68	8
SMEX series:					
SAMPEX	38,308	77,125	115,433	67	16
FAST	22,707	96,534	119,241	81	11
SWAS	9,800	114,434	124,234	92	1
XTE	133340	128520	261860	0.49	14
TRMM	14450	235360	249810	0.94	2

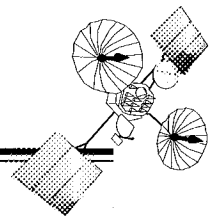

Committee on Space Data Systems (CCSDS) standard. The POCC for SOHO, scheduled to launch in mid-1995, must handle a unique, combined TDM and CCSDS telemetry format.

Two other missions, the X-ray Timing Explorer (XTE) and the Tropical Rainfall Measuring Mission (TRMM), have chosen a TPOCC-based MOC approach, integrating the traditional POCC, mission planning, and command management functions together into one system by sharing functionality and reusable software which had previously been implemented separately. Since the TRMM and XTE spacecraft have significant similarities, much of the mission-specific code in XTE will be reusable in TRMM.

To make this effort successful while controlling cost, temporary teams with members from the TPOCC group and mission development teams are formed to design and implement new generic software. In addition to providing additional staff to implement generic capabilities, TPOCC staff gets insight into what portions of a capability are generic and helps to identify likely differences among missions. For the missions, these teams provide insight into designing software for reusability and experience in differentiating the mission-unique elements of a problem from the generic.

Another indicator of TPOCC reuse across missions is the number of new generic capabilities asked for by mission development teams and users. Totals by mission of new generic capability requests, documented as Internal Configuration Changes Requests (ICCRs), are listed in the table.

The TPOCC approach to software support is similar to that of many operating system vendors. The development team makes each release of reusable software available to application development teams for incorporation into their deliverable. If an application group elects not to incorporate the new TPOCC release then software support from the TPOCC development team will not be guaranteed. Any reusable software changes made by the application teams without following the CRB standard procedures for configuration control will nullify TPOCC's support agreement with that application.

New capabilities are scheduled in TPOCC releases based on mission need dates, with an average of two software releases a year. An applications implementation of a generic capability is initially delivered as part of its mission-specific software and then folded into the TPOCC release at a later time. Larger subsystems such as the NASCOM interface, packet processing, or NCC interface have been implemented with TPOCC and mission support staff.

New technology advances are incorporated into the TPOCC architecture by integrating new and/or upgraded COTS products, integrating new ground system tools and/or components developed by NASA organizations external to the MOD, and enhancing TPOCC software. An institutional prototyping and technical evaluation group looks at various products from each area for its applicability to the TPOCC architecture, based on mission requirements and industry trends. As members of the TPOCC Working Group, users and mission development teams provide significant input into the prototyping and technical evaluation activities. New systems for trend analysis, spacecraft subsystem monitoring, and spacecraft visualization have been integrated in TPOCC's loosely coupled architecture.

TPOCC software averages 75 percent of a mission's control center deliverable, and thus has reduced cost and shortened the control center development life cycle. Established standards, both in industry and spacecraft development, have increased the reuse factor to well over 90 percent. A successful process for evolving the TPOCC software with new capabilities and new technology is in place.

Contact: Jack Koslosky (Code 511.1)
301-286-8947

Ron Mahmot (Code 511.1)
301-286-8523

Ed Beach (CSC)
301-497-2585

Barbara Schwarz (ISI)
301-497-2559

Sponsor: Office of Space Communications

Mr. Jack Koslosky is a Section Head in the MOD's Control Center Systems Branch at GSFC. He manages development of real-time ground support systems for POCCs. Mr. Koslosky has worked on the TPOCC project since 1985 and has 20 years of experience in control center system design and management at GSFC.

Mr. Ron Mahmot works in the MOD's Control Center Systems Branch. He holds a BS in Computer Science from the University of Maryland.

Mr. Edward Beach is a System Engineer for the TPOCC project. His professional interests include graphical user interfaces such as for TPOCC. He holds a BS in Computer Sciences and Russian language from Dartmouth College.

Ms. Barbara Schwarz is the lead developer for TPOCC Reusable Software. She has 12 years of experience in control center system development and holds a BS in Mathematics from Valparaiso University.

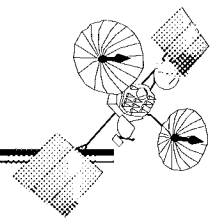

GENERALIZATION OF THE GENERIC SPACECRAFT ANALYST ASSISTANT

THE GENSAA IS A SOFTWARE SYSTEM that empowers spacecraft flight analysts to rapidly develop intelligent graphical monitoring systems. Using direct manipulation, GenSAA allows users to specify a graphical user interface, the telemetry data to be connected to the graphical objects, and expert systems rules that can infer higher levels of information than is available directly from the telemetry data stream. These steps allow users to create complete data monitoring applications without writing any source code. For more information on the capabilities of GenSAA, please see Advancing Satellite Operations with Graphical Expert Systems in the 1993 GSFC Research and Technology Report, pages 134-135.

Numerous groups have witnessed demonstrations of GenSSA and have expressed strong interest in using it. However, many of the data sources used by these groups are not in the telemetry data format currently used by GenSAA. For this reason, we have begun an effort to generalize the data interface to GenSAA. The goal of this generalization is to create an interfacer's package that will make interfacing external data streams to GenSAA as easy and quick as possible. This interfacer's package includes a tool to specify data types and variables, several code generators, and a section of code that must be filled in with details to enable GenSAA to connect to and receive data from the external data source.

New data sources are connected to GenSAA by creating a bridge program (as shown in the figure) that retrieves data from the source and sends it to GenSAA's data server. This bridge acts as a translator from the host's data format to GenSAA's. New bridges must be created for each new data source; however, reusable bridges that interface to standard database protocols (such as SQL) are planned.

To create a bridge, the interfacer first uses the software tool that generates a specification of the data types around which the external data source is built. These types must be based on a set of primitive types that GenSAA supports. Next, the same tool is used to specify the data elements that will be instances of the previously defined types. These data items will be available to the user within GenSAA once the integration is complete. The types and variables specification files are used to automatically generate code for the bridge.

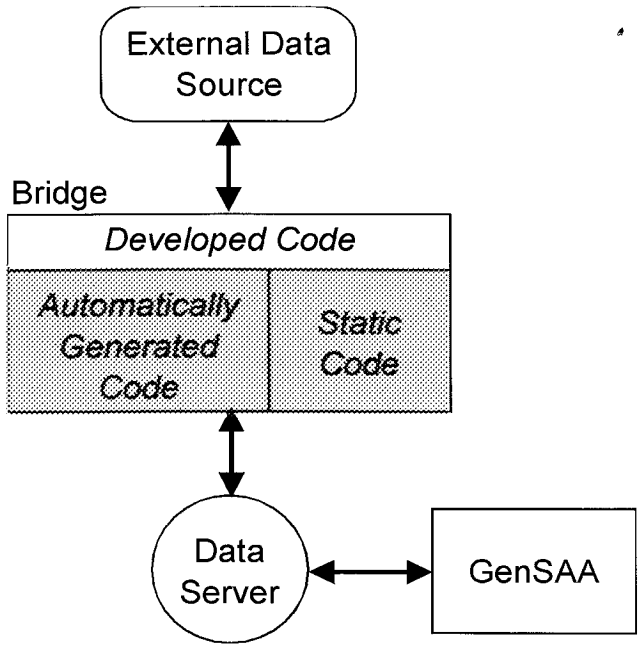

Bridge architecture for the Generalized GenSAA.

Finally, the interfacer must fill in code that requests the data from the external data source and hands that data off to the rest of the bridge software. The majority of the bridge consists of source code that either never changes or is generated automatically; only a small portion of the bridge code is filled in by the interfacer. Once this code has been completed, the bridge is linked and is ready to connect the external data source to GenSAA.

A beta release of the generalized GenSAA extension to GenSAA should be available in the first quarter of 1995. The GenSAA project is eager to expand its customer base by allowing other data sources to provide data to GenSAA; however, we are still firmly committed to supporting our primary customers who use the telemetry format that is native to GenSAA.

Contact: Gregory Shirah (Code 522.3)
301-286-7903

Peter Hughes (Code 522.3)
301-286-3120

Sponsor: Office of Space Communications

Mr. Gregory Shirah works in the Automation Technology Section. He received a BS in Computer Science from The University of Georgia and an MS in Computer Science from The George Washington University.

Mr. Peter Hughes works in the Automation Technology Section. He received a BS in Computer Science from The College of William and Mary and an MS in Computer Science from The Johns Hopkins University.

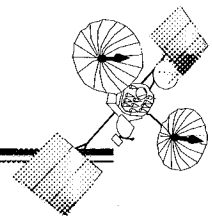

ADVANCED DISTRIBUTED ATTITUDE DETERMINATION SYSTEM CONCEPTS

THE FLIGHT DYNAMICS DIVISION (FDD) has been involved in continuing efforts to enhance operational systems used for spacecraft attitude determination support. Traditionally, FDD mission support has consisted primarily of mainframe-based Attitude Ground Support Systems (AGSS). Although an AGSS provides the necessary attitude determination support, it lacks sufficient real-time feedback and contains minimal graphics capabilities. The need for better real-time monitoring and enhanced visualization of spacecraft attitude data led to the recent development of heads-up display (HUD) architectures within the FDD environment. Modeled on aircraft instrument panels, these systems provide visual representations of attitude control system characteristics, sensor fields-of-view, and onboard spacecraft attitude solutions available through telemetry. The early HUD systems relied on mainframe software to retrieve, unpack, and convert telemetry data to engineering units, and used IBM PC/AT-compatible workstations to graphically display the information. A more recent HUD system used in support of the SAMPEX mission extended the concepts by eliminating the mainframe interface and allowing the PC platform to receive telemetry directly from the control center. The system, known as the SAMPEX Real-time Attitude Determination System (SRTADS), also incorporated real-time attitude solution processing, providing FDD personnel with immediate feedback of the spacecraft's ground computed attitude.

These systems focused on enhancing attitude systems through evolution of user interfaces, advanced graphic techniques, and distributed processing architectures. To further meet the FDD's goal and implementation strategy of transporting and integrating selected products and services to the MOC environment, FDD's support for the FAST mission included development of the FAST Real-time Attitude Determination (FASTRAD) system. Originally planned as a proof-of-concept system to demonstrate the capability of providing real-time attitude determination support within a transportable UNIX workstation environment, the FASTRAD system is now targeted for use in actual mission support. FASTRAD is the first flight dynamics system made available in the MOC for use by FDD and FOT personnel during mission support.

The FASTRAD system will be used to determine real-time spacecraft spin-axis attitudes and will provide graphical displays of current and previous attitude solution information. During each spacecraft pass, FASTRAD will access telemetry data from the TPOCC data server located in the MOC and compute the spacecraft spin rate and spin-axis attitude using single frame and Kalman filter algorithms. Attitude displays based on lambda/phi and right ascension/declination attitude representations will be updated with the most recent solutions. These displays contain several regions, including alphanumeric areas with current and previous attitude and sensor values, plots with graphical depictions of attitude solutions and reference objects, control regions for plot orientation and zooming, and a message box for user information (refer to the figure).

FASTRAD is designed to execute on a Hewlett-Packard Series 700 UNIX workstation, using an X-Windows and OSF Motif user interface. A shared memory approach is used to provide communication between the system's user interface and attitude determination processes. This allows the system operator to modify parameters through the user interface without interrupting execution of the attitude-determination algorithms.

The development of attitude determination systems on distributed workstation environments and their integration into the MOC environment, represent significant steps in providing enhanced FDD products. In addition to support for the FAST mission, FDD efforts are also underway to extend these concepts in support of several other near-term NASA missions. These systems remove the processing burden from mainframe computers, and provide a framework for creating high-quality, transportable mission support products that reduce operational interfaces and overall operational costs.

Contact: Scott Green (Code 552.1)
301-286-5076

Joseph Sparmo (Code 552.1)
301-286-6435

David Matusow (Code 552.1)
301-286-9231

Sponsor: Office of Space Communications

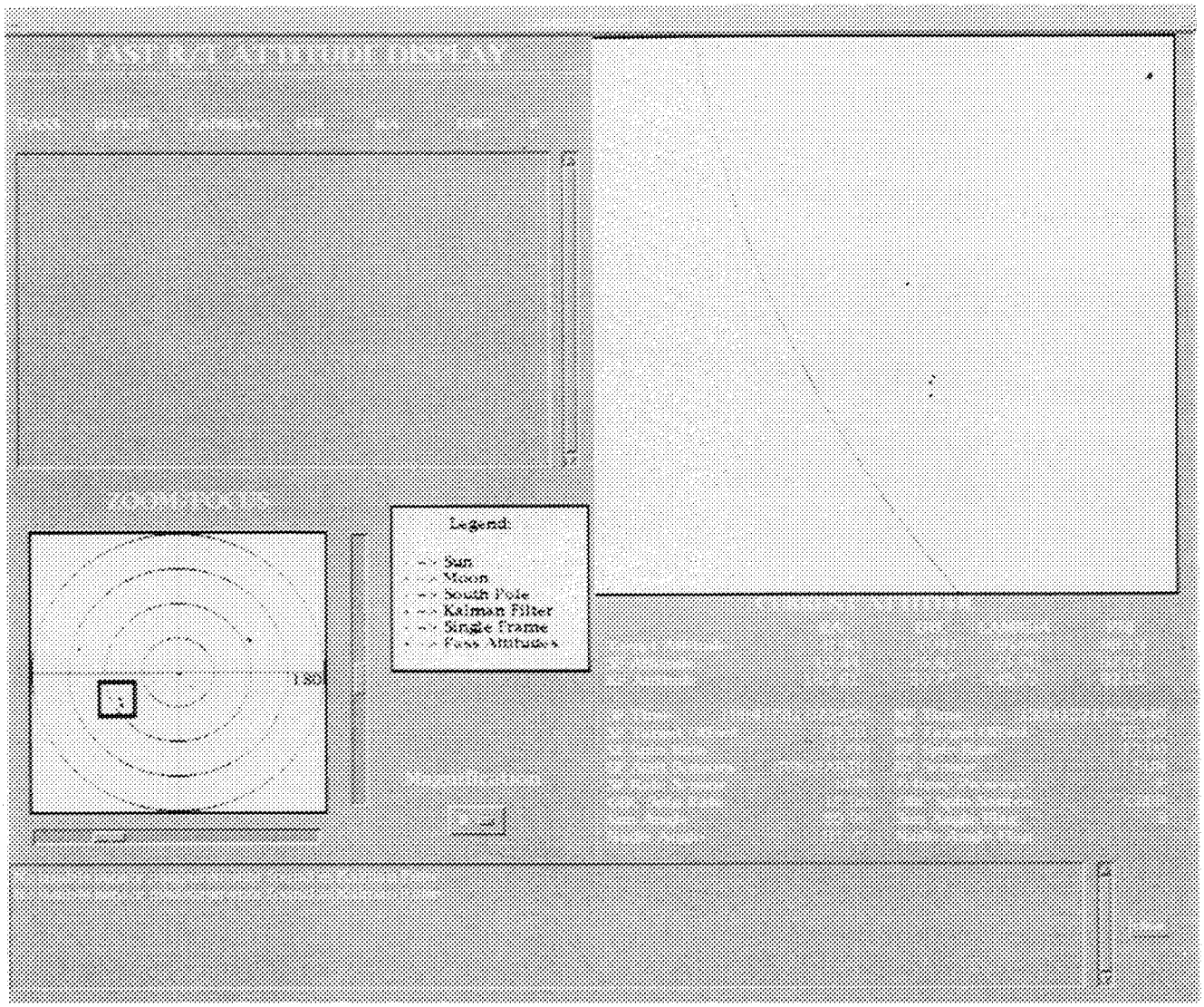

FAST FDD real-time attitude display showing a lambda/phi attitude plot, alphanumeric summary regions, and zooming capability.

Mr. Scott Green manages development of flight dynamics systems in the FDD Software Engineering Branch and was the FASTRAD system development project manager. He has worked at GSFC for 11 years and received his BS in Computer Science from Loyola College.

Mr. Joseph Sparmo is a Software Systems Engineer in the Software Engineering Branch and led the development effort for the FASTRAD real-time application process. He received his BS and MS degrees in Electrical Engineering from the Catholic University of America and has worked at GSFC for 7 years.

Mr. David Matusow is a Software Systems Engineer in the Software Engineering Branch and led the development effort for the FASTRAD user interface process. He holds a BS from Drexel University and has worked at GSFC for 4 years.

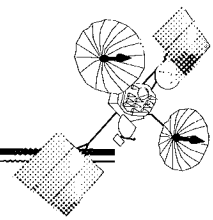

STAR IDENTIFICATION WITHOUT *A PRIORI* ATTITUDE KNOWLEDGE

LOW-EARTH-ORBIT SATELLITES supported by the FDD have traditionally used star observations for fine-tuning the spacecraft attitude. Gimbaled and fixed-head image-dissector star cameras have given way recently to more accurate charge-coupled device (CCD) star trackers. These trackers can determine the instrumental magnitude and angular position of a number of stars in the field of view (FOV). With an a priori attitude estimate, well-documented methods can identify observed stars and, hence, spacecraft attitude. However, without some coarse estimate of the spacecraft attitude the task becomes more difficult. Some methods to address this problem include extending normal methods to perform a full-sky scan, which can be computationally expensive and consequently time consuming. Other methods that run in real-time require either extensive memory, which is impractical for onboard or even some LAN considerations, or a large FOV tracker, which may not be appropriate for some high-accuracy missions. In response, the FDD has developed a method appropriate for FOVs as small as 8° x 8°, which requires almost 90 percent less storage than current methods that need no a priori estimate and significantly reduces the time to identify the stars from full-sky scans.

While flexible enough to be used for any star tracker (i.e., based on FOV size, etc.), specifications for the Ball CT-601 solid-state star tracker, scheduled to be used on several upcoming FDD missions including the XTE and the SWAS, were used for this study. The tracker has an 8° by 8° square FOV; however, a 4° radius FOV was assumed, since the star observations in the corners of the FOV are often not considered. The tracker is capable of tracking up to five stars at a time and can search the entire FOV for the five brightest. This study also assumes an inertially fixed spacecraft. For the purposes of this study, the standard GSFC FDD Multimission System star catalog—containing 8,949 stars ranging in visual magnitude from -1.65 to 6.5—was used. However, any star catalog fitting the needs of a particular mission can be used.

The general method is as follows: The celestial sphere is essentially divided into nearly evenly spaced subcatalogs, which form a minimally overlapping complete covering. Only the positions of the centers of these subcatalogs need be stored, along with the magnitude of the brightest star within the FOV radius (called a Primary Bright Star). Unfortunately, there is nonzero probability that no Primary Bright Star appears in any given observed FOV. The observed brightest star is then called a Secondary Bright Star; these are identified preflight by attempting to solve the following constrained equation for each star in the catalog:

$$x^2 + y^2 = r^2$$

Subject to: $$(x - x_i)^2 + (y - y_i)^2 > r^2$$

where (x_i,y_i) are the coordinates of the planar projection of all the brighter neighbor stars within 8° of the star being checked, and r is the radius of the FOV of the tracker.

If the solution exists, then x and y correspond to the center of the FOV that contains the star, a Secondary Bright Star, and no brighter neighbor. There are 2,001 stars in the reference catalog used for this study that have at least one solution to the above constrained equation. The size of the continuum of solutions determines the weight associated with each Secondary Bright Star. The algorithm itself involves noting the magnitude (visual or instrumental) of the brightest observed star, determining which parts of the sky—which subcatalogs—are not being observed, then performing a weighted search of the remaining subcatalogs.

Of the more than 100 random tests run on a 486/66MHz PC, the algorithm identified the correct star each time. The average time to find a star was 5 seconds, a significant savings over full-sky scans that have taken as long as 20 minutes. A thorough analytical study showed that, depending on the ability of the tracker to measure magnitude (the study varied the measurement uncertainty from 0.1 to 0.6 visual magnitude, while the random tests assumed an uncertainty of 0.2 visual magnitude), the true mean time to identify a star ranged from 3 to 11 seconds. Finally, the total storage needed to perform the identification is roughly 100 Kbytes, a savings of more than 90 percent over another popular no *a priori* attitude, star identification method.

Contact: Eleanor Ketchum (Code 553.1)
301-286-3082

Sponsor: Office of Space Communications

Ms. Eleanor Ketchum has been working in the Attitude Section of the Flight Dynamics Analysis Branch for the last 8 years. She received her BA in Mathematics from The College of William and Mary, her MS in Applied Mathematics from The Johns Hopkins University, and is a Doctoral Candidate in Mechanical Engineering at The George Washington University.

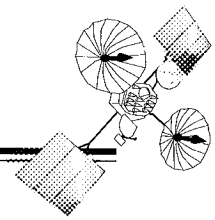

AN IMPROVED TRANSFER FUNCTION FOR THE FINE SUN SENSOR

FINE SUN SENSORS (FSSs) provide spacecraft attitude information by reporting the direction of the Sun in the sensor FOV, whose orientation is well-known with respect to the spacecraft. The FSS actually provides raw instrument counts in two directions; the FSS manufacturers supply the coefficients necessary to convert these raw FSS counts, via a transfer function, into the more useful Sun angles. Since the manufacturers cannot calibrate for all environmental effects preflight, the FDD has determined an augmented transfer function, with coefficients to be solved for in-flight, that dramatically improves the performance of the FSS.

The new transfer function adds two terms for each axis. These terms correspond physically to contributions from the component of Sun direction along one axis to the apparent position of the Sun on the other axis. The manufacturers cannot consider these cross terms ahead of time, as they do not have a suitable single light source; in-flight observations of the Sun itself are used to solve for these extra coefficients.

This new transfer function form reduces the errors observed in the FSS from 73.1 to 13.4 arcseconds in one direction, and from 52.4 to 16.9 arcsec in the other. These results were obtained using a sample set of more than 16,000 observations over the entire 64° by 64° FOV for the Upper Atmospheric Research Satellite (UARS) FSS. Similar results were found for the EUVE Sun sensors.

The importance of these results lies in the way that the FSS is used operationally. FSSs are normally used as backup sensors to Fixed-Head Star Trackers (FHSTs) which are traditionally more accurate. If an FHST fails, missions have had to attempt to achieve their science objectives with a significantly lower level of attitude accuracy. The use of an FSS, calibrated with the new transfer function, will allow the attitude to be computed with only a small decrease in accuracy. Because of sensor geometry or observability constraints, in some missions use of the FSS might actually increase attitude accuracy over accuracies found with two FHSTs. It is also possible that some future missions might be designed without expensive FHSTs because the FSS could be used as an adequate replacement at a hardware cost savings of greater than $1 million. In addition, because they operate on the same principles as the FSS, more accurate Sun sensors such as the one flown on the Solar Maximum Mission (SMM) or the one to be flown on SOHO might be improved considerably beyond specifications through use of this new transfer function.

Contact: Eleanor Ketchum (Code 553.1)
301-286-3082

Joseph Hashmall (CSC)
301-794-1279

Sponsor: Office of Space Communications

Ms. Eleanor Ketchum has been working in the Attitude Section of the Flight Dynamics Analysis Branch for the last 8 years. She received her BA in Mathematics from The College of William and Mary, her MS in Applied Mathematics from The Johns Hopkins University, and is a Doctoral Candidate in Mechanical Engineering at The George Washington University.

Dr. Joseph Hashmall supports the Flight Dynamics Analysis Branch for Computer Sciences Corporation. He received his BS in Chemistry from the University of Chicago and PhD from the University of Texas at Austin. He has been at CSC for over 10 years.

COLOR/MAGNITUDE CALIBRATION FOR NASA STANDARD FIXED-HEAD STAR TRACKERS

SATELLITE-BASED MISSIONS require calibration for accurate attitude determination. Examples of such missions, used in the analysis reported here, are the EUVE, the UARS and, as part of our data set, the Compton Gamma Ray Observatory (CGRO). The EUVE satellite was launched in June 1992. It began its mission operations during the survey mode phase, where EUVE scanned the entire sky in the extreme ultraviolet wavelength to make a complete extreme ultraviolet sky map. After the mapping phase was completed, EUVE went into the spectroscopy, or inertial phase of the mission, to observe specific ultraviolet sources. Since attitude determination instruments are calibrated in survey mode, EUVE re-enters the survey mode periodically for calibration. UARS, which was launched in September 1991, is an Earth-pointing satellite with a constant pitch rate of 1 revolution per orbit (RPO).

The primary instruments used for attitude determination on EUVE and UARS are NASA standard FHSTs. When an FHST scans for stars, it returns two pieces of data: an observed intensity count value and a position in the FOV. EUVE experienced occasional problems in inertial mode when only one guide star was in the tracker FOV and the on-board computer (OBC) would not identify the star because of an error in the observed intensity of the star. As a result, it would break track on the star. This led to the FHST continuously scanning the FOV but never having the OBC identify anything. Many times when this problem occurred, the star in the FOV was a dim star with a high blue minus visual (B-V) value. A star's B-V value is defined as its color index. Because stars have different temperatures, their spectral energy curves peak at different wavelengths. Therefore, hotter stars are bluish and cooler stars are reddish. Based on the B-V color index, a bluish star has a negative B-V value (because it is brighter in blue (smaller B magnitude) than at longer wavelengths (larger V magnitude)). Conversely, a reddish star has a positive color index because it is brighter in V than in B. This color index value takes into account the interstellar medium by measuring the star temperature and the scattering of blue wavelengths due to interstellar gas and dust.

Because the FHSTs of EUVE and the CGRO have both experienced these types of problems, it was decided to evaluate the UARS FHSTs to determine if they were experiencing similar problems. As UARS is nominally in the 1 RPO mode, the FHSTs are constantly acquiring new stars in their FOV. Therefore, a problem with observed magnitudes could go unnoticed unless specifically tracked. It should be noted that since each FHST has its own spectral response, analysis must be performed on each FHST independently.

On board EUVE and UARS are two pairs of FHSTs, NASA standard star trackers built by Ball Electro-Optics/ Cryogenics Division. These sensors search for, detect, and track stars by focusing light from the object being tracked on the photocathode of an image dissector tube, thereby determining the intensity and position of the star. The FHSTs can track stars in the instrumental magnitude range of 2.0 to 5.7. The instrumental magnitude is the magnitude that is expected of a star based on its intensity and color, along with an averaged standard spectral response of an FHST. As a star passes through the FOV of the FHST, a 0.2 magnitude fluctuation is expected. Each FHST has an 8° by 8° square FOV, with a digital resolution of 7.78 arcsec. The intensity information is converted from counts to volts, and eventually to star instrumental magnitude. The conversion equations are given below as:

$$I_{obs} = 0.02 * (\text{intensity counts})$$

$$M_I = A * \text{Log}_{10} (I_{obs} - I_{ref}) + M_{bias}$$

where I_{obs} is the observed intensity in volts, I_{ref} is the reference intensity, M_{bias} is the magnitude bias, M_I is the calculated observed magnitude, and A is a constant. Since each FHST needs to be calibrated independently, each FHST can have its own values.

Data were chosen for EUVE from the survey phase of the mission. More stars are acquired during survey mode, so trends and patterns become more evident than with inertial mode data. Approximately one orbit's worth of data for seven different time spans were chosen for analysis. For processing of UARS data, five one-orbit spans of data were chosen, spanning approximately 15 months. The difference between the instrumental magnitude and the observed magnitude is referred to here as the delta magnitude (Instrumental Magnitude - Observed Magnitude), or magnitude error. A positive error implies that the star being viewed by the FHST is brighter than the expected value.

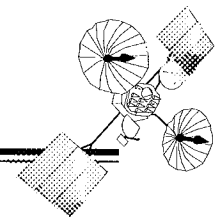

The analysis showed that EUVE's FHST1 is experiencing the most problems with magnitude errors, and EUVE's FHST2 is having the least. EUVE's FHST1 was the FHST that prompted this study. Using the EUVE data to illustrate the problem, the figure shows that the EUVE FHST1 has an almost linear dependence of the delta magnitude versus B-V. Conversely, FHST2 for EUVE can be seen to have no evident color dependence.

Regression analysis of the delta magnitude versus B-V for both EUVE and UARS shows that EUVE's FHST1 has a high slope value and a high dependence on the B-V value, with the R^2 value indicating more than 50 percent of the correlation coming from the B-V value. EUVE's FHST2 has almost zero slope in comparison, with a much lower dependence on the B-V value. Analysis of UARS statistics gave results similar to those for EUVE. For UARS' FHST1, there is a higher dependence upon B-V value, with 30 percent of the correlation due to the B-V value. The slope is also higher for FHST1 by about a factor of seven. UARS' FHST2 indicates no color dependence. These numbers demonstrate that the UARS FHST1 experiences a problem similar to EUVE's.

Color index has an effect on two of the FHSTs: EUVE FHST1 and UARS FHST1. Both show a significant correlation between magnitude error and B-V value. It should be noted that these two FHSTs have serial numbers of SN005 (UARS FHST1) and SN006 (EUVE FHST1). EUVE and UARS swapped star trackers before launch, due to a problem with the SN006 FHST. UARS was launched with EUVE's original FHST1 in place of its original FHST2. Once the problem with SN006 was repaired, it was put on board EUVE as its FHST1. It is assumed that since these two FHSTs were originally built for UARS, they were built at the same time. These color-caused magnitude errors could have some dependence upon the manufacturing process of the FHSTs. Values derived from our analysis support the need for new coefficients in Equation (2). This has already been done for EUVE. These calibrations should allow for more stars to be identified properly and, therefore, more accurate attitude determination by the onboard processor.

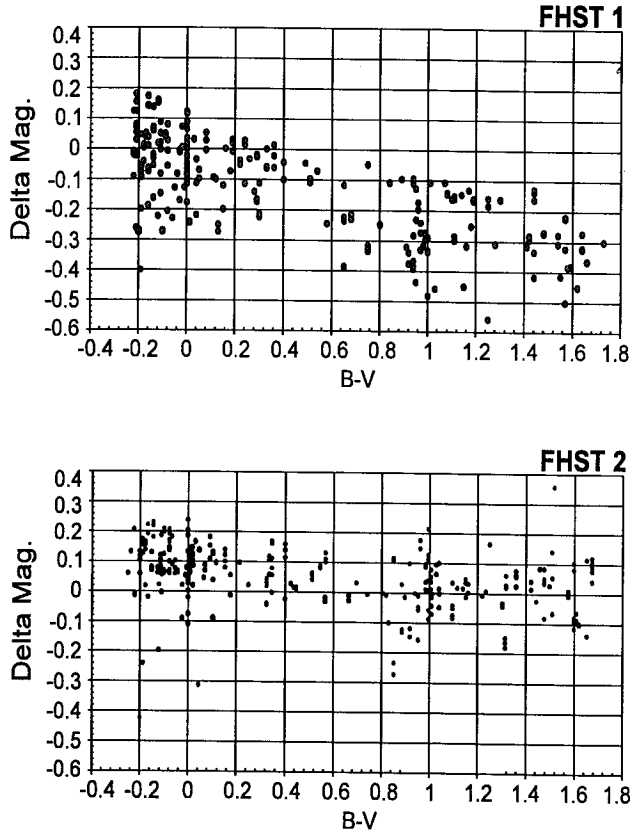

Delta magnitude versus B-V.

Contact: Michael Lee (Code 553)
301-286-5685

Jon Landis (CSC)
301-286-1224

Sponsor: Office of Space Communications

Dr. Michael Lee has been an aerospace engineer at the GSFC for the past 3 years. He earned a PhD in Physics from the University of Maryland.

Mr. Jon Landis has been with Computer Sciences Corporation for 2.5 years. He earned a BS in Physics from Drexel University.

A KNOWLEDGE-BASED TREND ANALYSIS SUPPORT TOOL FOR SATELLITE BATTERY MANAGEMENT

IN OUR USAGE, trend analysis is the process of examining incoming spacecraft status telemetry data, developing mathematical representations of the data (usually statistical curves), and analyzing the derived information. The analysis is used to evaluate the functional status of spacecraft components and to determine if a dangerous trend can be detected in the information. If such a trend is detected, then corrective or preventive measures may be pursued. Currently, analysis and interpretation of trend information is a manual process. The MOD is building a Generic Trend Analysis System (GTAS) for several current and upcoming missions, targeting the data collection, statistical analysis, and data visualization aspects of telemetry monitoring. GTAS, as currently planned, does not attempt to automate the analysis functions performed by FOT. However, in an attempt to increase functionality, we look forward to a new level of automation for the GTAS work by providing knowledge-based approaches to the identification of trends and the determination of possible corrective and/or preventive measures.

The initial focus of our trend analysis work will be on the battery subsystem for the SMEX family of missions. Battery subsystem analysis presents several challenges that require sophisticated automation techniques. Among them are:

- Simultaneous consideration of multiple pieces of information, including day/night transitions, solar array output, and subsystem temperature; Considerations for the behavior of a given battery system, taking into account sub-components that are known to have failed or degraded.
- Consideration of historical data, as multiple failures can mask each other.
- Use of actual, usually unique, battery signatures, since there are differences between batteries regardless of their age.

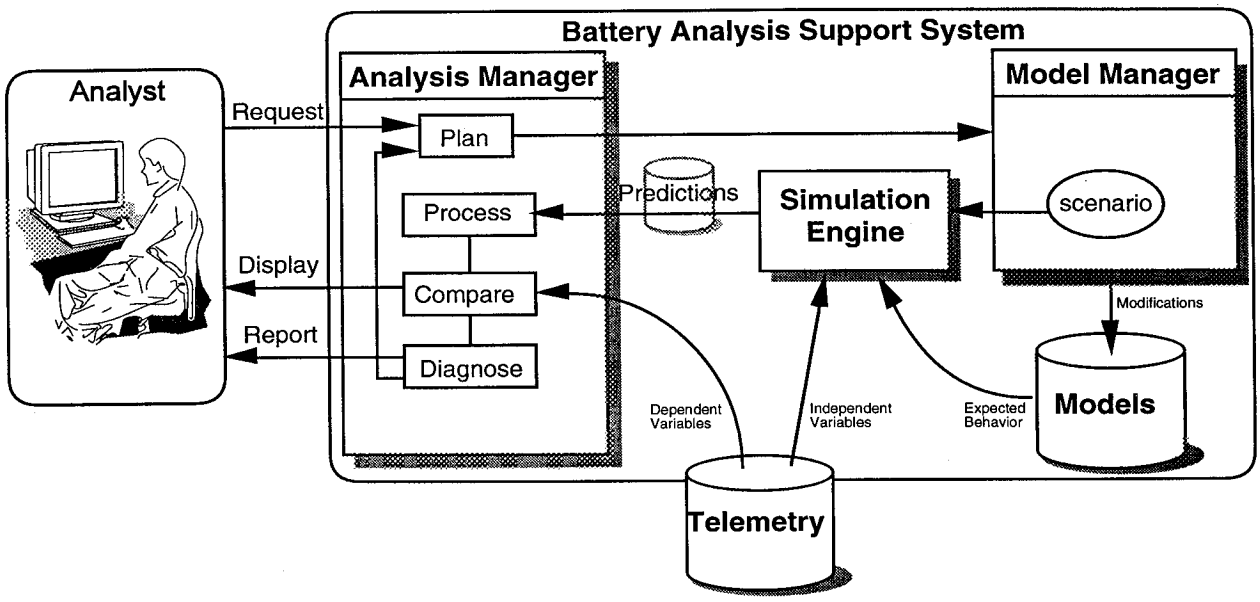

Functional battery analysis support system architecture.

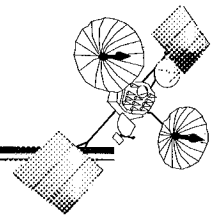

- Assessment of battery failure characterized not only by abrupt changes in functionality but also by subtle drifts in the telemetry signature.

- Use of abstract knowledge about battery life cycle stages and how they manifest themselves in cell voltage differential plots, since working backward from a plot to battery life stage is subjective.

These characteristics have lead us to investigate qualitative modeling techniques and machine learning as probable solution techniques. Qualitative modeling languages and techniques have been designed specifically to support reasoning about changes over time such as the changes in slopes found in battery voltage differential plots. These techniques fit the abstract expertise we have available. Machine learning has been used to empirically identify normal and anomalous modes of operation from historical information. This technique accommodates the peculiarities of individual battery signatures as well as subtle drifts in those signatures.

The current approach to realizing a knowledge-based trending capability involves incorporating a battery model and simulator into a Battery Analysis Support System as a basis for preliminary identification and interpretation of battery trends, as depicted in the figure. Our recent work has allowed us to develop a design for a battery trending subsystem, and to provide a proof-of-concept demonstration of knowledge-based trend analysis.

Contact: Troy Ames (Code 522.3)
301-286-5673

Sponsor: Office of Space Communications

Mr. Troy Ames currently works in the Automation Technology Section. He received a BS in Computer Science and an additional BS in Mathematics from the University of Idaho. He received an MS in Computer Science from The Johns Hopkins University and has been at GSFC for 10 years.

SOFTWARE ENGINEERING

GRAPHICAL BROWSING TOOL FOR SOFTWARE REPOSITORIES

IN THE DECLINE AND FALL of the American Programmer, Edward Yourdon wrote that "Software reusability will go down in history as one of the major technical contributors to software productivity and quality in the 1990s." The Data Systems Technology Division (DSTD) at GSFC recognizes the paramount importance that software reuse will play in the development of large, complex systems which support satellite missions. Not only will reuse facilitate ground systems development in shorter time and at lower cost but, more importantly, reuse will enable the development of higher-quality systems with increased reliability, properties that are essential in our mission-critical applications. DSTD is actively looking at technologies which can be used to dramatically increase software reuse.

One way to increase reuse is to provide systems that facilitate code-level object reuse. DSTD has created a tool that allows developers to easily and intuitively browse the contents of a software repository. The DSTD's Reusable Library Interface (ReLI) graphical browser is a tool that gives a software developer the ability to quickly identify relevant reusable code components or assets of interest in a particular software repository. ReLI is currently being used by DSTD software developers to browse the C++ code-level components, or assets, located in the DSTD Reusable Software Library (DRSL). ReLI allows a user to navigate a hierarchical description of a software repository, search for assets based on a key-word search mechanism, view selected assets, and deliver desired assets to a specified location.

ReLI draws much of its usefulness from an extensible characterization and organization system which is called the Experiment in Libraries via Incremental Schemata and Cobweb (ElvisC). ElvisC is comprised of an extensible characterization language, a case base of assets, and a nonsupervised inductive classification system known as Cobweb. ElvisC classifies and organizes a domain, such as telemetry processing, through a characterization language—a vocabulary which defines the domain. This vocabulary is based on input from human domain experts who are very knowledgeable about a given domain and how objects, such as code elements, should be organized within it. ElvisC's characterization language—referred to as its feature space—is hierarchically arranged and is extremely flexible, capable of handling dynamic and poorly understood domains. Its feature space is a classification tree composed of descriptive terms, that can be modified and extended to completely characterize a domain. The domain expert develops the feature space through the addition of new features. Features can be added to the hierarchy in one of four ways:

- The new feature is added as one of a mutually inclusive set of features which describes some characteristic of the asset. This defines the Or relationship. For example, the "Hardware Platform" feature of an asset can be characterized by one or more of the following sub-features: "Sun", "Macintosh", or "Hewlett-Packard."

- The new feature is added as one of a mutually exclusive set of features which describes some characteristic of the asset. This is the Exclusive Or relationship. For example, "Language" can be "C" or "C++" but not both.

- The new feature joins a set of mandatory features which describes some characteristic of the asset. This is the And relationship. For example, an asset characterized by the feature "Storage" must be further refined by the type that is stored ("What") and the characteristics of the storage structure ("Where").

- A feature requires no further refinement. This indicates no relationship. For example, the feature "Ada" may be deemed to require no further refinement. This is a terminal or leaf node in the feature space hierarchy. If the repository evolves to contain Ada9X as well as Ada83 assets, then the feature "Ada" could be modified to an Exclusive Or Relationship type, with the features "Ada9X" and "Ada83" as possible values.

ElvisC stores information associated with each asset in the software repository; this stored information is referred to as the asset space. The asset space is the set of nodes located under the leaf nodes in the feature space. An asset may be located under one or more feature space leaf nodes. For example, an asset may be classified as certified, be

written in C++, be targeted for the Hewlett-Packard and Sun hardware platforms, and do character string processing.

The ElvisC asset space is organized in two ways: as an inverted index containing the list of assets that contains a given feature and as a concept hierarchy that organizes assets into kinds-of-things. ElvisC has a nonsupervised inductive classification system, Cobweb, which is based on the concept hierarchy. Cobweb automatically sorts contributed assets into a hierarchy of concepts based on differences found in the features that characterize the assets. With this automated sorting, Cobweb is able to identify the closest match to a query that failed (i.e., did not find exact matches in the inverted index). Cobweb utilizes the notion of concepts and does not need to resort to any domain-specific heuristics for classification, nor does it require any human intervention in this process. Thus, Cobweb is well-suited for any domain.

ReLI allows the user to browse the feature and asset spaces discussed above. For example, from the sample ReLI screen shown in the figure, we see a developer has navigated down one of the branches in the feature space: Function->Collection->Organization->FIFO. At the leaf level feature node, FIFO, there are a number of assets, one of which is "NIH Set". An important point to note is that a particular asset can occur at more than one leaf level feature node. Thus, NIH Set could be located under the following feature node as well: Environment->Hardware Platform->Hewlett-Packard. NIH Set has a number of associated attributes (i.e., NIH Set has a description,

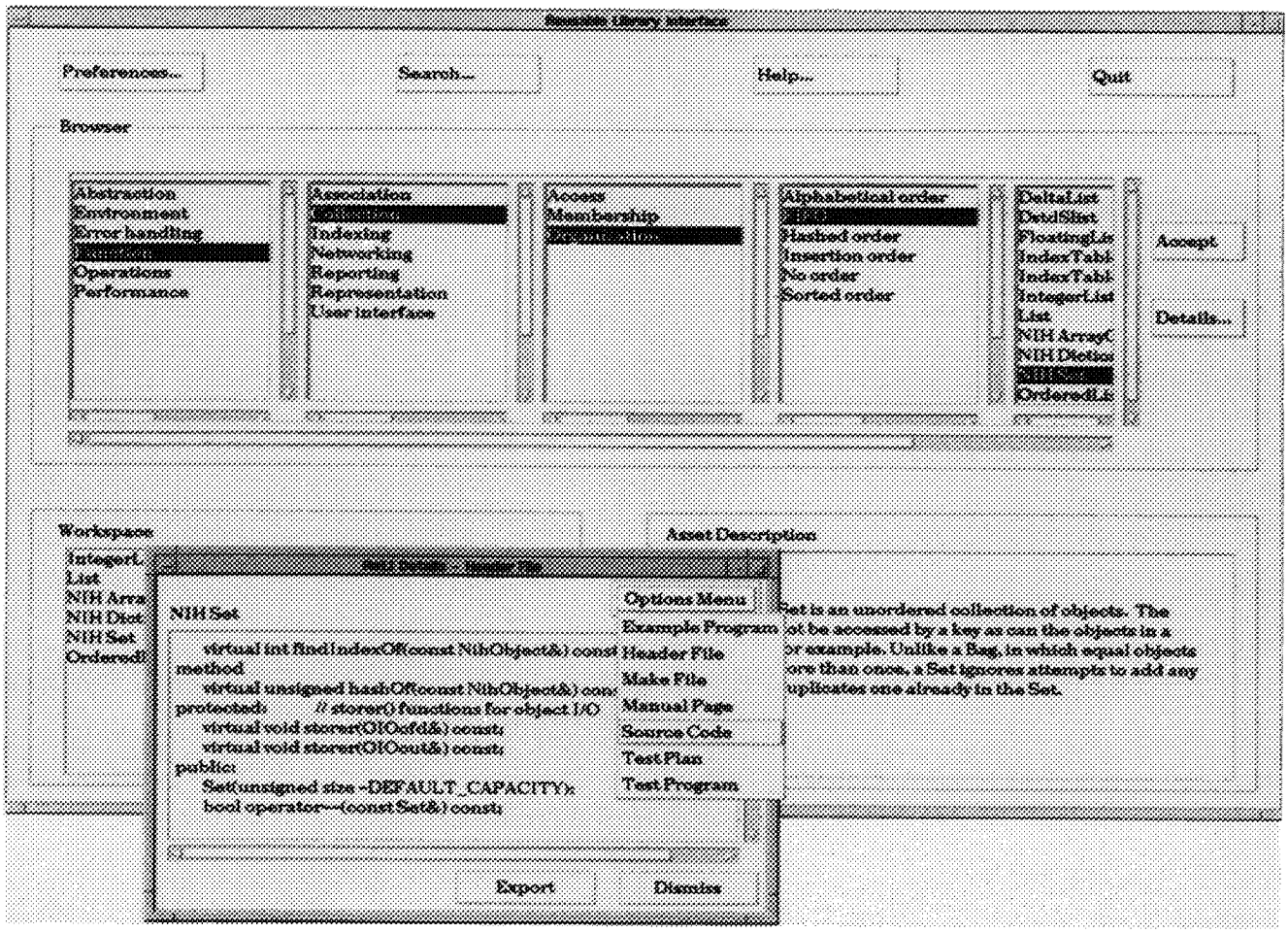

ReLI browsing a sample repository.

example program, header file, make file, manual page, source code, test plan, and test program associated with it). From the diagram we can see that the developer is currently looking at the NIH Set's header file and is about to view its source code.

Using ReLI, a software engineer can browse any software repository, each containing thousands of code-level objects, for suitable candidates. A particular repository can have any number of different classification schemes or feature spaces layered on top of it. This allows developers from different domains to have their own tailored view of a single repository. ReLI provides a short synopsis of each asset in the library that the developer can use to quickly determine if an asset might be of use. If an asset appears suitable, the developer can view any of the information associated with that asset. Currently, this may be any type of textual information such as source code, header file, test plans, example programs, or help documentation. When the developer has found suitable candidate assets, ReLI can deliver these assets to an electronic mailing address or to a specified directory.

ReLI provides an organization with the ability to manage its software repository in an effective and intuitive fashion. Further, ReLI is not constrained to manage a particular type of information: it intrinsically has the potential to manage any type of information, from a software repository to a library of multimedia images, sounds, and movie clips. For example, ReLI could easily manage a library that contained both graphical and textual files, such as the images and associated text obtained from observations of the Comet Shoemaker-Levy 9 impact with Jupiter.

Contact: Karl Mueller (Code 522.3)
301-286-7524

Sponsor: Office of Space Communications

Mr. Karl Mueller performs research and development in advanced technologies concerning artificial intelligence and software reuse. He has been at GSFC for 4 years and currently works in the Automation Technology Section. He holds a BS in Zoology as well as an MS in Computer Science from the University of Florida.

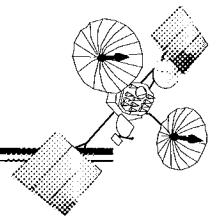

MASS PRODUCTION OF CD-ROMS IN-HOUSE: INFORMATION PROCESSING DIVISION'S DATA DISTRIBUTION FACILITY

THE INFORMATION PROCESSING Division's (IPD) Data Distribution Facility (DDF) is responsible for distributing spacecraft data to investigator facilities, science centers, and archives. The DDF can distribute data electronically or on physical media. The DDF became operational in 1992, supporting magnetic tape distributions for the ISTP Geomagnetic Tail Laboratory (GEOTAIL) mission. In mid-1993, the DDF added Compact Disk-Read Only Memory (CD-ROM) and 8-mm tape cartridges as media options for physical distribution. Starting in 1995, the DDF will begin the transition to a client-server type of architecture that will support multiple missions with a variety of physical and electronic distribution capabilities. In addition to the ISTP GEOTAIL mission, the DDF currently supports the Calibrated ancillary data Output Processing System (COPS) and Spacelab data from the Shuttle missions. Some of the future missions that the DDF will support include ISTP's Interplanetary Physics Laboratory (WIND), Polar Plasma Laboratory (POLAR), and SOHO missions, as well as some of the SMEX missions. Details of our CD-ROM conformance with established standards and the structure of the data on each disk may be found in the 1993 GSFC Research and Technology Report, page 138.

The portion of the DDF that produces CD-ROMs is called the Data Recording Subsystem (DRS). The first figure displays the current DRS configuration. The DRS consists

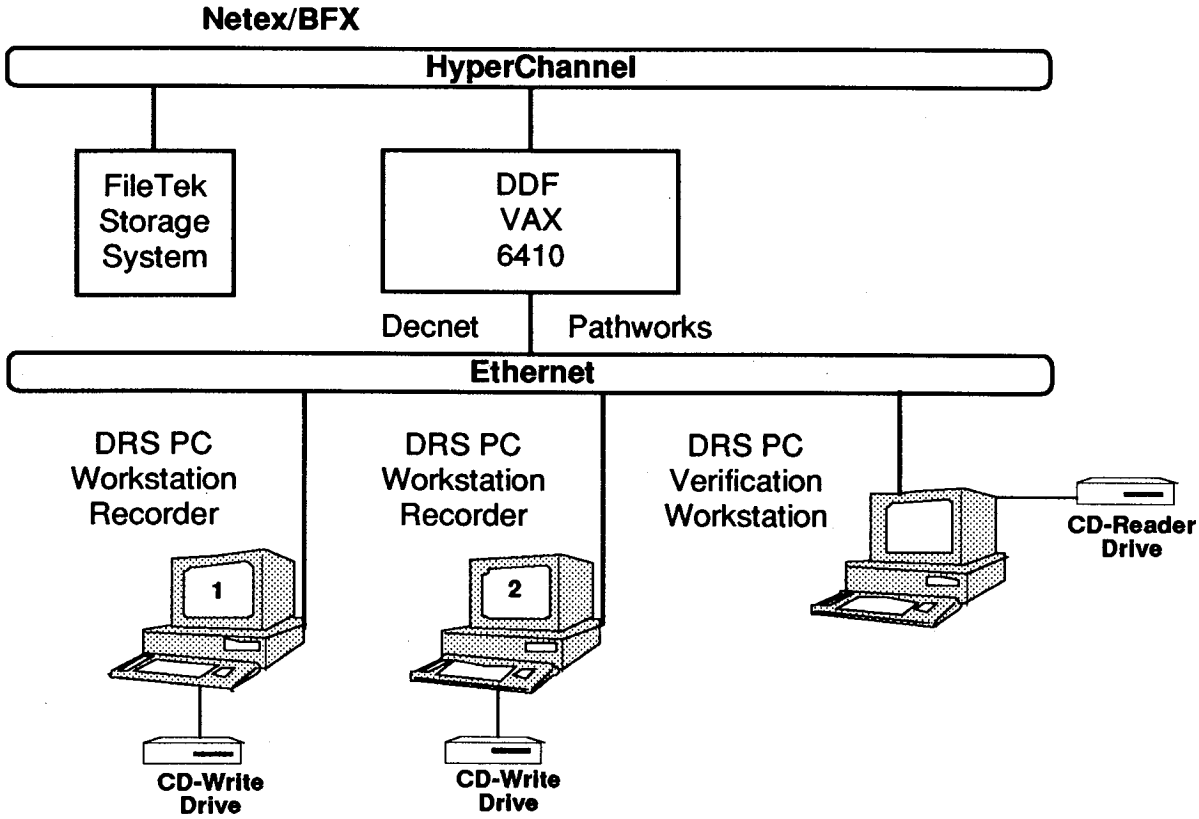

Current DRS configuration.

of two PC workstations, each with a Philips 2X CD-write drive and a 1 gigabyte hard drive. Each workstation utilizes COTS software to create virtual images and to record the media. The third PC acts as the verification workstation by utilizing IPD-developed software with an external CD-ROM reader. The DRS communicates with the DDF VAX system via a DECnet interface; each workstation operates independently from the others. The DRS can produce up to 50 CD-ROM products per week. Some recent accomplishments of the DRS include:

- Being one of the first facilities in the U.S. to operationally utilize CD-Recordable technology as an in-house CD-ROM production system.

- Redistributing 100 gigabytes of GEOTAIL data previously released on 9-track magnetic tape. The redistribution effort took 15 weeks to complete, with 181 unique products and a total of 859 CD-recordable units. The entire effort was completed 6 weeks ahead of schedule.

- Successfully producing, as of September 1994, over 2,800 CD-recordable products with less than one-half of 1 percent return rate.

In late 1994, IPD will upgrade the DRS to a configuration that will increase production and automate much of the CD-ROM production process. The second figure shows the upgrades to the DRS, which will result in the DRS+ configuration. DRS+ will increase the number of PC workstations from two to five. Two new systems in the configuration are a control PC and a PC file server. The control PC will centralize operational use of the DRS+, while the PC file server will store up to eleven products that are ready for distribution on CD-ROM. The file server will act as the primary interface between the DDF VAX and the DRS+ via Novell Network File Server (NFS). All DRS+ systems are connected through Novell Netware. Some of the improvements that the DRS+ configuration offer include:

- Increased production and performance. With three additional workstations in use, the production capabilities are increased. Preliminary tests show that workstation performance is improved under this new configuration.

- Automation of the CD-ROM production process. The control PC can operate in an auto-allocation mode that allows it to automatically assign write and verification jobs to the workstations. No keyboard or mouse interaction is required during this mode. The only role the operator plays is the loading and unloading of media from the CD-write drives. Manual allocation is also an option.

- Centralization of operations. The control PC is a menu-driven system that runs the entire DRS+ configuration. The operator need not interact with any software on the workstations. The control PC maintains logs and statistics for all workstations on a daily, weekly, and monthly basis. These statistics can be used to graphically display DRS production and status.

- Enhanced verification capabilities. The current DRS system has one workstation dedicated to the verification of all CD-ROMs. The DRS+ allows all workstations to perform both write and verification functions. One rule of thumb that the DRS (current and new) follows is that verification of a product must be done by a drive other than the one that created it. This rule is coded into the control PC software so that verification jobs can only be assigned to workstations other than the creation workstation.

To further enhance in-house CD-ROM production capabilities, DDF personnel have examined CD-ROM duplication systems that can simultaneously record multiple copies of a product. Presently, the DDF utilizes a deposit account with the National Technical Information Service (NTIS) for mass replication. CD-ROM products replicated by NTIS typically require 100 or more copies for this option to be economical. However, there will be some products that require as few as 10 to 35 copies on a daily basis. These products fall into a grey area, since sending these products to NTIS would not be economical, yet producing these products in-house would tie up workstation usage. For this reason, CD-ROM duplication systems were evaluated. IPD decided to acquire a duplication system called CD-MAKER by Alea Systems, Inc. The CD-MAKER can utilize up to four Yamaha 4X CD-write drives. A 4X CD-write drive records a full 74-minute CD-recordable product in just 18 minutes,

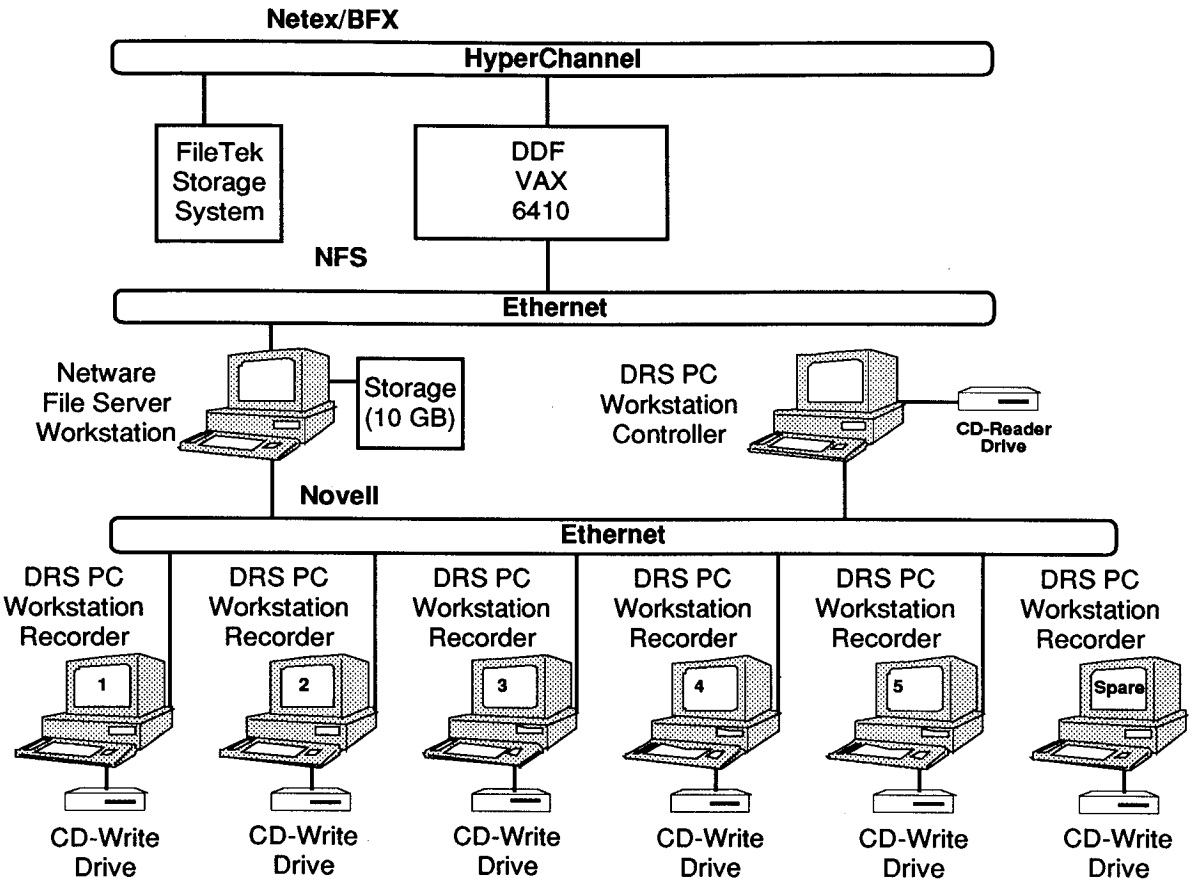

DRS+ configuration.

twice as fast as the 2X CD-write drive. With all four of the Yamaha CD-write drives burning simultaneously, the CD-MAKER can produce up to 12 copies in 1 hour. Together, the DRS+ and the CD-MAKER systems will enable IPD to produce all CD-ROM products (of less than 100 copies) in-house.

Contact: Pat Carreon (Code 563)
301-286-3668

Sponsor: Office of Space Communications

Ms. Patricia Carreon serves as IPD's expert on CD-ROM technology. She is responsible for the design and procurement of the DRS. She earned a BS in Electrical Engineering at Southern Methodist University and an MS in Electrical Engineering at George Mason University. She joined GSFC in 1989.

SOFTWARE PROCESS IMPROVEMENT IN THE NASA SOFTWARE ENGINEERING LABORATORY

FOR OVER 17 YEARS, the Software Engineering Laboratory (SEL) at GSFC has been dedicated to understanding and improving the process of developing, managing, and maintaining software supporting all elements of flight dynamics for flight projects. The experiences from this effort have been synthesized into an approach for software process improvement.

The SEL is composed of over 300 staff members from three organizations: GSFC, the University of Maryland, and the Computer Sciences Corporation (CSC). Approximately 275 people responsible for developing and maintaining flight dynamics systems make up the largest component of the SEL, while the others directly support the SEL's software process improvement program. The SEL's approach to process improvement treats each software project as an experiment through which existing baseline models and practices are verified and updated, and evolving mature processes are assessed and infused into the organization. All facets of the process and the products are continually measured in detail so that understanding the software and the impacts of process change can be quantified. Since its inception, the SEL has applied the concept to over 100 development projects, each providing new insight into the software development process and the impact on resulting products.

SEL process improvement follows a three-step paradigm, each of which is characterized by extensive measurement. First is the Understanding step, where both the process and products are baselined. This includes all product characteristics (e.g., cost, reliability, software size, reuse levels, and error classes) as well as the processes used. Second is the Assessing step, where potential improvements to the process are incorporated into development projects and evaluated. Quantified SEL experiences (e.g., most significant causes of errors) and clearly defined goals for the software (e.g., decreased error rates) drive the selection of candidate process changes. After these changes are selected, training is provided and experiment plans are produced. Then the processes are applied to one or more production projects from which detailed measurements are taken. These data are used to quantify process changes and product impacts; the new process is assessed by comparing these measures with the continually evolving baseline. As a result of the analysis, processes are adopted, discarded, or tailored for ensuing efforts depending on the observed impacts. The third step of the paradigm is Packaging, where all identified improvements are infused into the standard SEL process. This includes updating and tailoring standards, handbooks, training materials, and development support tools.

During 1994, the SEL evaluated the impacts of this 17-year effort. This evaluation was undertaken to determine whether this particular process improvement approach resulted in sustained improvement in all areas of the software process and product. The results of this evaluation are impressive. The SEL has quantitative evidence of the gradually maturing process within the SEL environment as a whole. Over the past 17 years, the data indicate a modest decrease of 10 percent in the cost of producing a new line of code. The more significant impact of this approach has been the improvement of error rates in developed software. The figure shows an overall decrease of 75 percent in development error rate over the last 17 years. Each point on this figure shows the error rate for a specific mission support software project; the projects are also differentiated by programming language used. Not only has the overall error rate for the projects decreased over this time period, but the amount of variation of error rate has also decreased. This decrease in variation leads to an increase in the predictability of future software projects.

As the improvement approach has evolved and matured, the SEL's product baselines of reliability and cost have also been measured and periodically reassessed. By grouping sets of projects with similar operational functionality into representative time periods, SEL baselines are evaluated and compared to measure overall process impacts. Two 4-year periods were assessed and demonstrate the following significant impacts:

- Reuse increased by 300 percent; typical mission cost (to deliver several systems) decreased by 55 percent; and amount of time required to develop software to support a mission decreased by 38 percent.

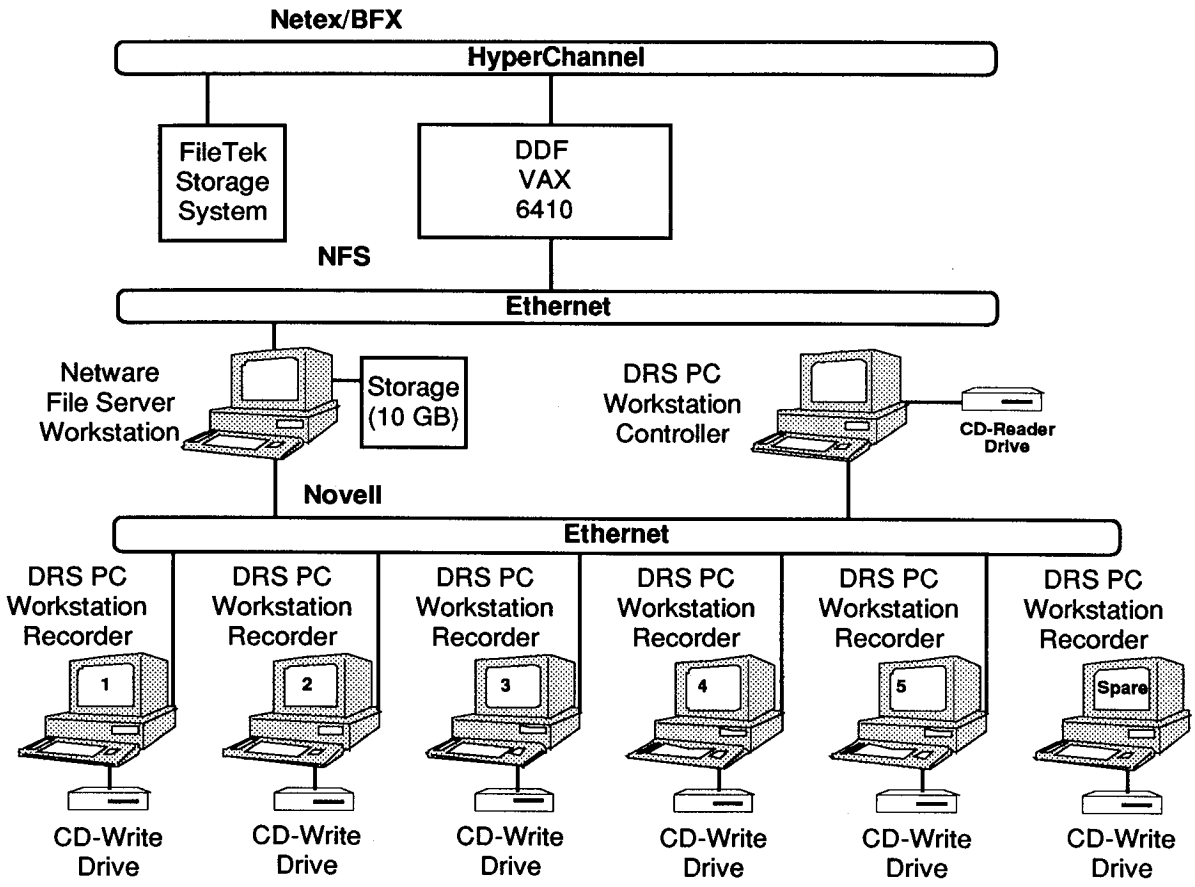

DRS+ configuration.

twice as fast as the 2X CD-write drive. With all four of the Yamaha CD-write drives burning simultaneously, the CD-MAKER can produce up to 12 copies in 1 hour. Together, the DRS+ and the CD-MAKER systems will enable IPD to produce all CD-ROM products (of less than 100 copies) in-house.

Contact: Pat Carreon (Code 563)
301-286-3668

Sponsor: Office of Space Communications

Ms. Patricia Carreon serves as IPD's expert on CD-ROM technology. She is responsible for the design and procurement of the DRS. She earned a BS in Electrical Engineering at Southern Methodist University and an MS in Electrical Engineering at George Mason University. She joined GSFC in 1989.

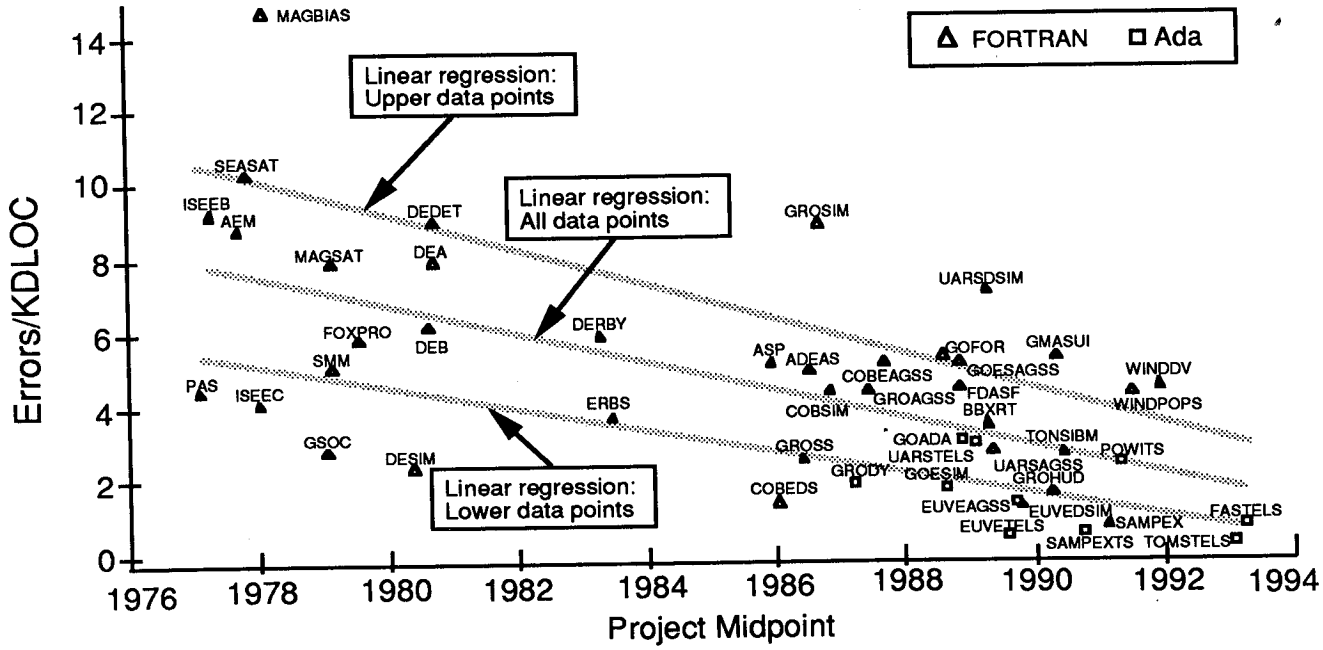

Software project development error rates.

- The results of this first evaluation of the process improvement approach were used to nominate the SEL for the First IEEE Computer Society Award for Software Process Achievement. After multiple rounds of elimination, the SEL was selected as the winner of this prestigious international award. The SEL was recognized for its sustained and measured "outstanding achievement in improving the software process."

Contact: Jon Valett (Code 552)
301-286-6564

Kellyann Jeletic (Code 552)
301-286-7698

Sponsor: Office of Space Communications

Mr. Jon Valett is a software engineer in the Software Engineering Branch at GSFC. As a director of the Software Engineering Laboratory, he leads research efforts into improving software development and maintenance within the branch. Mr. Valett received his MS in Computer Science from the University of Maryland, College Park, and his BS in Computer Science from the University of Iowa. He has been at GSFC for 11 years.

Ms. Kellyann Jeletic has been a software engineer in GSFC's Flight Dynamics Division for the past 10 years. She received a BA in Computer Science from LaSalle College.

INFRASTRUCTURE SUPPORT

BUSINESS PROCESS REDESIGN: RETHINKING THE LOGISTICS PROCESS

BUSINESS PROCESS REDESIGN (BPR) or re-engineering has been successfully applied to create new, efficient business processes and controls at a major NASA logistics facility, the Logistics Support Depot (LSD). The BPR methodology used has allowed NASA to make a rapid transition into a new information and business control technology. The new technology had to meet rigorous specifications for exact accounting controls on all logistics purchases. This included logistics purchases made at all levels, down to and including the project level, throughout the world at key network sites. These include Ground, Space, Deep Space Network, and NOAA-reimbursable sites.

This technology will substantially increase depot performance and warehouse process modernization, and facilitate customer operations. Current implementation continues to indicate that significant potential cost savings can be realized. Specifically, application of BPR has led to a move away from a centralized mainframe information processing concept to a client-server model, with more processing power in the hands of the purchasing and customer-servicing personnel. Concurrent redesign and streamlining of work-flow processes are also a direct result of the BPR methodology used. Most importantly, NASA customers will experience direct improvements in speed of service. This transition promises to deliver a significant payoff both in operational performance and customer satisfaction. By refocusing the centralized mainframe approach, NASA is also getting rid of traditional barriers to re-engineering which plague many medium to large corporations and logistics facilities today. By eliminating barriers to logistics modernization, NASA can focus on providing faster service to the hundreds of station managers, engineers, and scientists depending upon the depot for daily provisioning, as well as for critical and one-of-a-kind items. A central process change theme was user involvement, which gives the development an essential human touch. The essence of our BPR development philosophy focused human performance as a development paradigm.

One avenue of modernization opened up by the BPR was efficient employment of a modern IBM Reduced Instruction Set Code (RISC) computer and a smooth transition to a Pentium file server-based Novell network for an integrated, super-fast procurement and material management system. The IBM RISC machine, with its open system-oriented database (Sybase), gigabyte-level hard drive capacity, and 268 megabytes of RAM, make this machine the ideal transition engine for this change. Once fully operational, it will provide the power necessary for a modern logistics information system. System capabilities will include retrieval of the engineering and provisioning historical data necessary to perform a full-flown automated logistics support analysis, as well as to provide additional purchasing and supply status support to NASA customers.

The heart of all this change, BPR, required a detailed and rigorous analysis, defining each sequence of actions necessary to acquire, receive, store, and distribute material. In this analysis, there was an exhaustive enumeration of each action step based upon application of modern process algebra and a graphical portrayal of process requirements for development, using a modern power programming tool, PowerBuilder. Use of process algebra, the same algebra used in the theory of communicating processes, allowed an exhaustive enumeration which classified actions in terms of their inherent delay and impact upon overall customer requisition cycle time—the time it takes to fill and deliver any order. The process algebra identified 282 action steps required to process customer requisitions and place purchase orders. In this process, a requisition could fall into one of 56 possible process states. This BPR methodology allowed rapid sorting through these details in order to identify for wholesale elimination three major sources of system delays. These were (1) process delays in the purchasing and warehouse processes, (2) external logistics delays in the upstream logistics coming from the manufacturer or vendor, and (3) system delays in the old mainframe processing system. One interesting result was that small internal delays of hours often triggered larger, vendor-caused delays of days.

Essentially, the BPR methodology was a change from a traditional systems analysis to a user-oriented process analysis. The tool, PowerBuilder, was itself process-oriented. With PowerBuilder we were able to use a quick build-test-evaluate development cycle inherent in PowerBuilder. This rapid development and iterated evaluation cycle forced early and continuous involvement by depot system users (i.e., buyers, expediters, and others), ensuring the

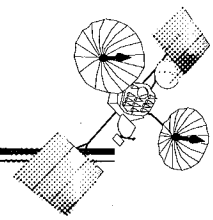

usability and practicality of the development. Because of the intense analysis forced by the BPR and the tools developed using power programming development methods, transition to a new Windows-based business central processor is an acceptable upgrade path. In effect, the rigorous BPR and the modern tools used in both process analysis and development have provided a broad spectrum of upgrade opportunities, and have provided an acceptable migratory pathway away from a relatively dated, centralized mainframe with an inherently narrow scope of upgrade, process, and integration opportunities. What this development has shown is the unique logistical possibilities that have come to the fore in the last few years, with a quantum leap in system-analytical, -processing and -development technologies. Logistic system modeling is now possible using tools that allow exhaustive evaluation of business and engineering processes themselves.

Modern power-programming technology provides the rapid build-test-evaluate cycle necessary for migration from large, older mainframe systems with their associated dependency-creating technologies and self-limiting development philosophies. Power-programming tools, especially using one of the available COTS, such as PowerBuilder or Visual Basic, capture the essence of this liberating development style. Even extremely detailed development problems, requiring extra design considerations at the front end, can be expedited while retaining the required system integrity.

Contact: Dan Kashporenko (Code 530)
301-286-5220

Sponsor: Office of Space Communications

Mr. Kashporenko is a systems engineer at the NASA LSD and is responsible for business process redesign at the depot. He has specialized in introduction of modern software and logistics systems in both the public and private sectors.

ENGINEERING AND MATERIALS

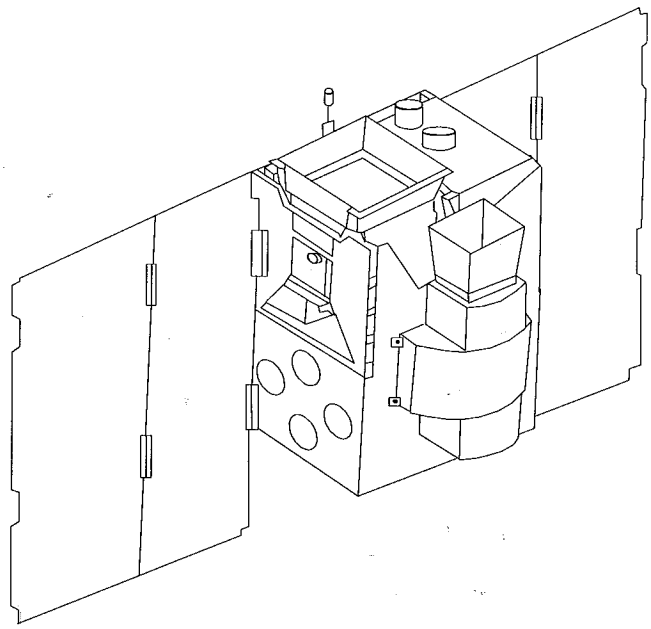

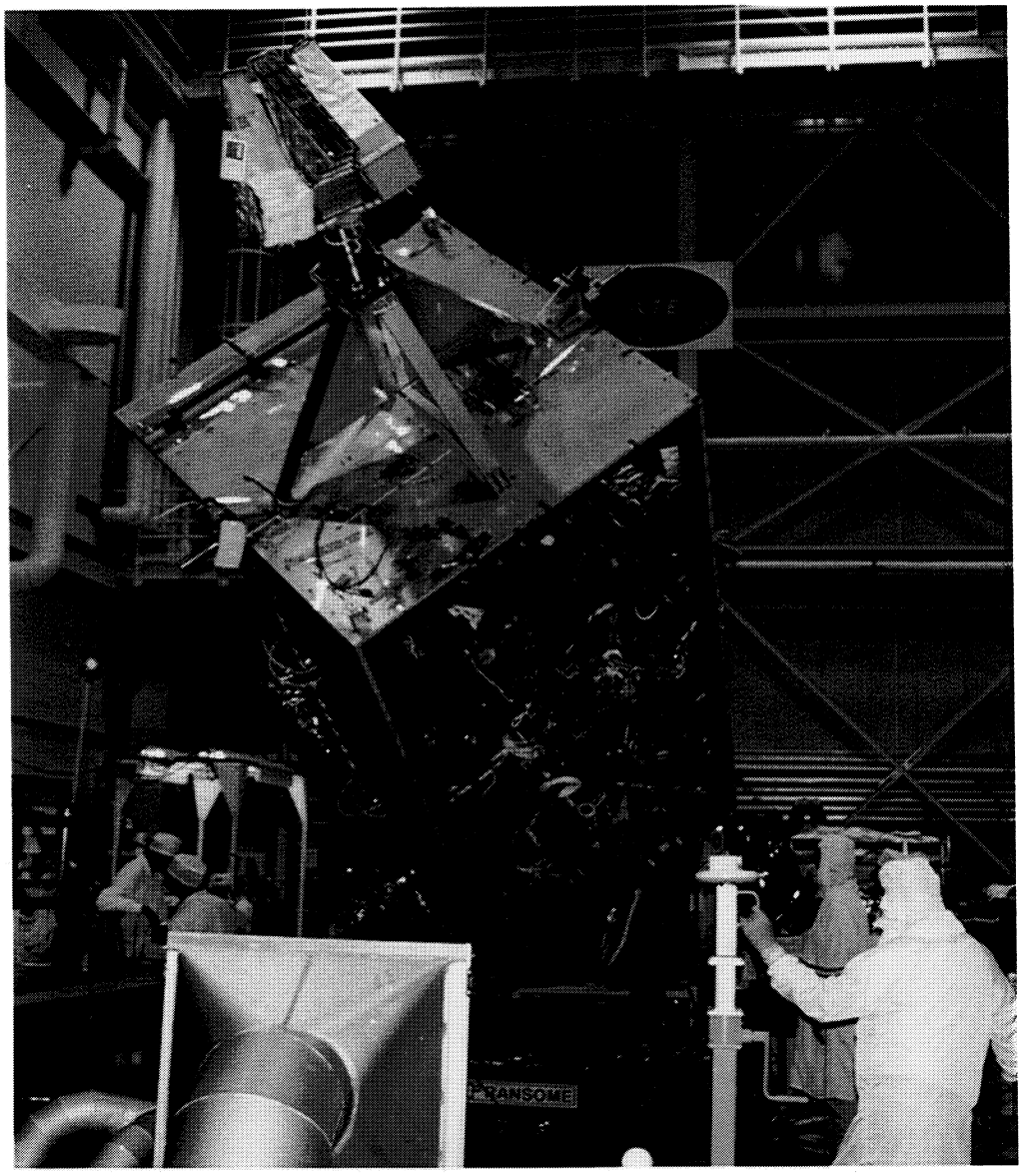

The X-ray Timing Explorer (XTE) spacecraft, designed and built in the Engineering Directorate at the Goddard Space Flight Center, is shown during integration and testing in the photograph above. The XTE mission is one of two X-ray astronomy missions planned by the Office of Space Science for this decade. The primary objective of the XTE observatory, which is to be launched in 1995, is the study of temporal and broadband spectral phenomena associated with stellar and galactic systems containing compact objects such as white dwarfs, neutron stars, and possibly black holes. Major questions remain unanswered about the internal structure of neutron stars, the existence of black holes, and the origin of the cosmic X-ray background. The scientific instruments span the energy range 2 to 200 keV, and time scales from microseconds to years can be investigated. The rotating monitor detectors were built by the Massachusetts Institute of Technology and two clusters of phoswich detectors were provided by the University of California San Diego. An array of five large proportional counters was designed and built at Goddard .

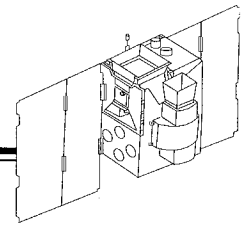

ENGINEERING AND MATERIALS

FOR MORE THAN 35 years GSFC has been at the forefront of space research and exploration, achieving many milestones and leading the world to new knowledge about the Earth and the universe. GSFC is a unique facility whose personnel have expertise encompassing all phases of space missions, enabling them to design, build, and test spacecraft; communicate with, track, and operate satellites in orbit, and analyze data from them.

During its first three and a half decades, GSFC has developed more than 40 satellites in-house, managed some 160 satellites for NASA, launched more than 170 payloads on Delta rockets, flown scientific payloads on more than 2500 sounding rockets and over 550 balloons, and provided tracking, communications, and data handling for all low-Earth-orbiting satellites operated by NASA, including the space shuttles. This scientific expertise is supported by a superlative engineering staff that has generated many technological advancements in instruments, spacecraft and ground data systems, cryogenic sensors, lasers, and spacecraft thermal systems; mission and quality assurance, materials and parts control, and environmental testing; suborbital flight planning and mission safety, payload and payload carrier design, development, fabrication, and testing; and, launch operations, recovery, and data acquisition.

This section of the R&T Report is comprised of seventeen articles which typify the gamut of activities conducted in GSFC's Flight Assurance, Engineering, and Suborbital Projects and Operations Directorates to support the objectives of the scientists in GSFC's Space and Earth Sciences Directorates. The first four articles deal with spacecraft subsystems, from cryogenic coolers and batteries to command, control, and data encoding systems. The next four deal with various aspects of balloon, sounding rocket, and Pegasus launch vehicle systems. Two articles follow which describe developments in spacecraft thermal control using Rankine cycle vapor compression and heat pipe systems, followed by two articles devoted to new mechanisms for actuators and control systems. Finally, the last five articles describe developments in disciplines from ultrasonic and radiographic imaging to parachute test systems.

While we work to support the primary objectives of the Space and Earth Science programs, we also attempt to find other worthwhile uses of these technologies, particularly for application to problems in the world of industry and commerce, apart from space. Thus, we fully expect that the work in lossless data compression, described by Miller and Yeh, will lead to benefits in data storage, transmission, and manipulation which will affect not only the handling and archiving of Earth observation and other space science data, but also the storage, transmission, and manipulation of X-ray, magnetic resonance, and computed tomographic images in medicine, and will find wide application to data in other disciplines far too numerous to mention here. Similarly, the magnetic bearing research and development for cryogenic coolers and attitude control systems, described by Sparr and Vranish, respectively, will serve not only to advance our understanding of the Earth and space by permitting us to design and develop detectors of heretofore unattainable sensitivity, but also will spin off advanced technologies that will permit the building of super-stable telescopes, and magnetic levitation vehicles for high-speed mass transportation of the future.

Walter B. Sullivan, Jr

SPACECRAFT SUBSYSTEMS

A NEW SYSTEM FOR COMMAND AND CONTROL OF SPACECRAFT SUBSYSTEMS AND INSTRUMENTS

TO HELP REDUCE COSTS and increase utility, the Electrical Systems Integration Branch has developed a new Spacecraft Ground Support Equipment (SGSE) system, the Advanced System for Integration and Spacecraft Test (ASIST). The ASIST system is based on Open System Interconnect (OSI) concepts, and is comprised of a real-time data synchronization and decoding subsystem, a near-real-time data distribution subsystem, a command generation and routing subsystem, and a distributed user interface and analysis system. The system can synchronize, decode, and route multiple physical telemetry channels at up to 10 megabits per second. The system is now supporting the development of flight software, attitude control system software, independent validation and verification, instrument development, and the integration and test of spacecraft for three missions: X-ray Timing Explorer (XTE), the Tropical Rainfall Measuring Mission (TRMM), and Cassini. The system is comprised of approximately 740,000 lines of code and has been under development since December 1991. The cost of the system was kept under $5.00 per line of code through heavy reliance on free and reused software.

The system interfaces to a generalized spacecraft utilizing international standards for telemetry and command, provided by the Consultative Committee on Space Data Systems (CCSDS). The CCSDS standards are based on the commercial CCITT layered network model. Current spacecraft have implemented connectionless data transport services which are optimized for fast telemetry transport to the ground at speeds of several megabits per second. Telemetry data are transported by variable length data packets carried asynchronously by fixed-length transfer frames. The transfer frames are optionally encoded with any combination of Viterbi, Reed-Solomon, convolutional or pseudo-random noise encoding schemes. A high-reliability command protocol is also provided to guarantee the transport of spacecraft commands through the use of spacecraft acknowledgments and ground system command buffers.

ASIST is designed to reduce integration and test costs and to optimize schedules by providing a distributed telemetry display capability, distributed commanding, a highly maintainable telemetry and command definition database system, and a graphical page display development system. The distributed command and display capability allows multiple integration activities to be conducted in parallel, allowing integration personnel to perform independent integration, diagnostic, and calibration duties simultaneously; integration time is reduced by eliminating the need for performing these activities serially. Further, team efficiency is increased by providing a system which can concurrently support the activities of engineers and scientists from many disciplines.

Test activities are controlled from the ASIST user interface workstations using the Spacecraft Test and Operations Language (STOL). STOL provides a simple, FORTRAN-like language for test and operations personnel to send spacecraft and ground system commands, change displays, and define sequences of operations in procedures. The STOL language provides looping and branch statements, arithmetic operators, mathematical functions, and macro substitution. STOL also provides the capability to start external programs and define new language statements while the system is running. STOL commands are converted to a binary form as described in the command definition database. The binary commands are routed through a single user workstation, designated the primary workstation. The primary workstation monitors and controls all spacecraft command traffic, and functions as a general user workstation as well. Since the command interfaces are binary, foreign machines can route commands through the primary workstation even if they do not use STOL.

ASIST uses OSI interfaces for all ground system components. Telemetry and command distribution is implemented through the use of Internet protocols. A client-server architecture is maintained throughout. Ground system interfaces were developed in conjunction with a set of spacecraft simulators. The simulators are furnished to instrument development teams at universities and at instrument contractors. The simulators provide data transport and electrical interfaces to the instruments while duplicating the ground system interfaces for the associated Instrument Ground Support Equipment (IGSE). Each instrument and IGSE is developed with external interfaces which closely match the interfaces which will be encountered during the actual integration of the spacecraft. Since ASIST provides a distributed, client-server architecture,

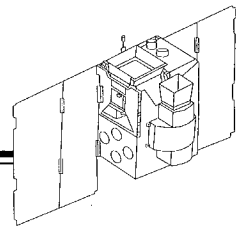

the IGSEs can be used during the integration of the spacecraft in the same manner as during instrument development. No restrictions are placed on the IGSE hardware or functionality, allowing instrument teams to build appropriate instrument analysis functions into their IGSEs as well as capitalize on institutional capabilities to a high degree. IGSEs have been integrated to ASIST with an average time of less than one-half of a working day. Prior to delivery of an IGSE, early integration and test data can be provided to instrument teams via Internet for analysis and interface verification. Investigators can also remotely monitor telemetry at their home institutions during integration. The open system interfaces have also been used to provide command capability and "telemetry" displays to the vehicle environment dynamic simulations and detector simulators used by the attitude control system development team.

Telemetry and command definitions change during the development of spacecraft components and are modified throughout the integration and test of the spacecraft. Telemetry and command definitions are verified during the integration and checkout of each spacecraft subsystem component. The telemetry and command formats often change as the result of flight software updates, re-engineering of spacecraft components, and the addition of new thermal and electrical measurement points. ASIST provides a telemetry and command definition database subsystem that allows interactive changes to conversion coefficients and limit definitions. Permanent changes to the database can be edited into the database definitions and reloaded for operational use in less than 10 minutes. The database is defined using a simple keyword = value language. A language-sensitive editor is provided with many database constructs available as menu items. Command and telemetry definitions are localized to single constructs to provide a single point of entry when changing the definition of a particular data point or command definition. The database provides the capability to define data type, array definitions, offset, bit subfields, a variety of limit classes, units, polynomial conversions, discrete range to text conversions, and a text description. Packet and transfer frame data can also be displayed in raw form as arrays of integer data.

The data definition database can also be used to define derived equations of telemetry data. All functions, operators, and branching statements are available from the STOL language for calculation of derived telemetry information. Common statistical functions are optionally calculated for telemetry and are available for display and analysis.

The user interface workstations provide data analysis capability. The workstation can display flight or ASIST telemetry data, flight events, ASIST events, or derived equations of telemetry data. The information is displayed in text or graphics form. The display pages are developed using a simple, graphics editor. Complicated pages can be created in a short time and modifications can be made in under 1 minute. Data are periodically sampled for real-time display. All packet data samples are used for offline display, analysis and trend plotting. All telemetry data and derived equation data are available for use as predefined variables in STOL. Data are decommutated by each workstation independently. The data analysis is distributed and can be independently configured for each user workstation. Each workstation may be sent all or any subset of the telemetry data packets. Only data that are displayed, used in STOL, used in derived equations, or limit-checked by a given workstation are decommutated. The system can be used to support a range of data rates and sizes simply by reconfiguring the system.

All integration and test data are stored for post-test analysis. The data are stored in datasets corresponding to each physical channel. The data are stored using on-line magnetic disks and then migrated to bulk storage on optical disks using a commercial hierarchical file management system. Data storage is sized to provide regression test capability through all integration and test activities and early orbit checkout. Data of any age is available in minutes and the physical location of the data is transparent to application programmers as well as users. The data are available through an interface which is identical to the real-time telemetry system.

ASIST provides greater transparency and easier access to spacecraft data than previous STOL systems for both integration and test personnel and experimenters. Through the use of open system concepts and distributed system technology, the system provides an integrated environment for experiment payloads from development to launch. ASIST will support the development, integration, and test of in-house GSFC spacecraft for the next decade and beyond.

The system was developed using a civil service and contractor team involving Digital Equipment Corporation, Jackson and Tull, Design America, Aydin Monitor, and Hughes/STX. Special thanks should be given to the National Center for Supercomputing Applications, the San Diego Supercomputer Center, and MIT's Open Software Foundation for the high quality, free software they have made available.

Contact: Richard Hollenhorst (Code 733.3)
301-286-7525

Sponsor: Office of Space Science
Office of Mission to Planet Earth

Mr. Richard Hollenhorst is a physicist and computer scientist in the Electrical Integration Branch at GSFC. He is the Ground Software Systems Section Head. Mr. Hollenhorst earned an MS in High Energy Physics and an MS in Computer Science from the University of Wisconsin. He has been developing scientific and engineering data analysis systems for 15 years.

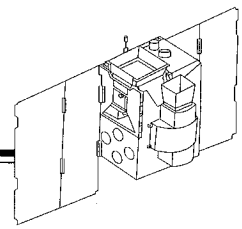

UNIVERSAL SOURCE ENCODING FOR SPACE

LOSSLESS DATA compression has been suggested for many NASA applications to either increase the science return of missions, or to reduce the requirement on onboard memory, station contact time, and data archival volume. This compression technique guarantees a full reconstruction of the original data without incurring any distortion in the process (see the figure).

In most studies on scientific data, the Rice algorithm performs better than the other available lossless data compression algorithms. The algorithm has been implemented in a number of NASA's science exploration missions. The earlier applications implemented the algorithm in software form, executed by an onboard microprocessor. In 1991, a proof-of-concept hardware engineering model was built in an application-specific integrated circuit (ASIC), the Universal Source Encoder/Universal Source Decoder (USE/USD). The USE/USD chipset has been integrated into a printed circuit board interfaced with computers in an Advanced Orbiting Systems (AOS) testbed. A successful end-to-end system test was conducted in 1993. The test started with sending compressed data in a packetized format to the Tracking and Data Relay Satellite System (TDRSS) and ended with receiving the signal at a ground station, followed by decompression processing.

The data compression chip was later redesigned for Landsat-7 with several additional capabilities. These include extending the range of information rate measured in bits/sample; four different types of prediction schemes; a data bypass/packetizing option; and the ability to process bipolar data. The new circuit is implemented in very large-scale integration (VLSI) circuits, using gate arrays suitable for space missions. It can process up to 20 million samples per second, with sample quantization levels selectable from 4 to 15 bits. The flight circuit is referred to as Universal Source Encoder for Space (USES), and is now being integrated into flight programs.

The extended Rice algorithm has been proved mathematically to be equivalent to a set of Huffman codes without lookup code tables. In simulation studies performed on both imaging and nonimaging data, its data rate reduction performance is better than most other available

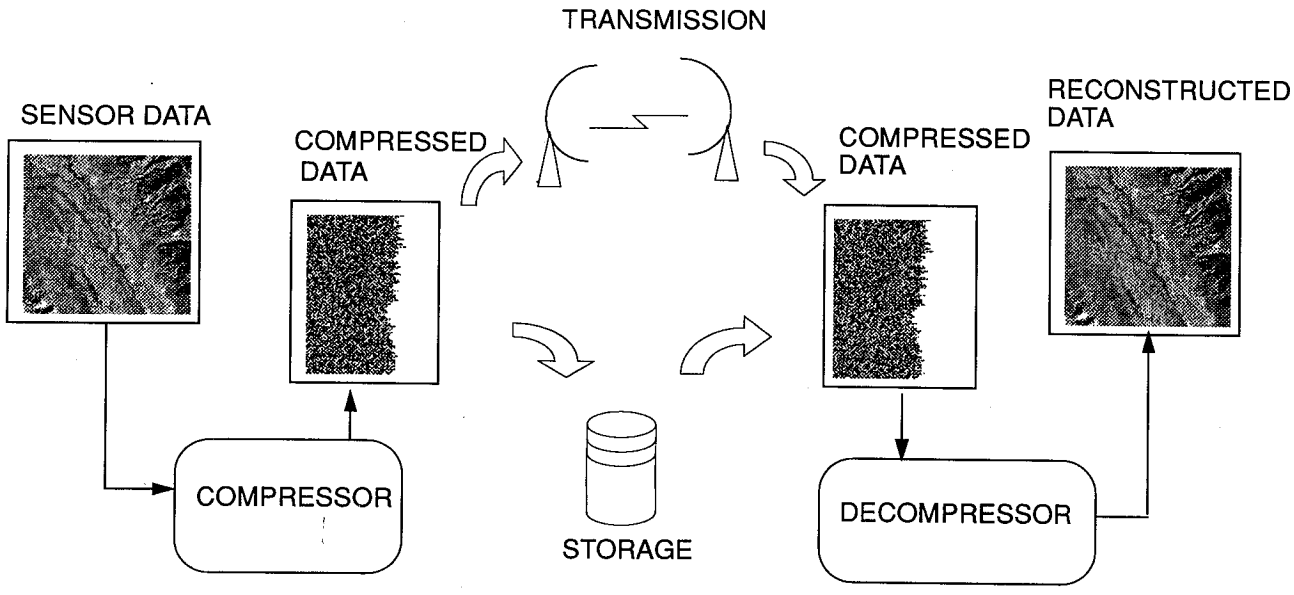

Lossless data compression optimizes science data collection requirements with no loss of information—the original and reconstructed images are identical.

lossless compression techniques. The algorithm adapts to data statistics by selecting a code option within a block of input sample data; this simple property makes it suitable for implementation in a packetized data system for error containment in the case of bit-error during data transmission.

Currently, the extended Rice algorithm is under consideration at GSFC as a space data systems standard for lossless data compression. The algorithm demonstrated applicability to a wide range of data from instruments for remote sensing and space exploration, and has found its way into more terrestrial applications, such as medical imaging and speech signal processing.

Contact: Warner Miller (Code 738.3)
301-286-8183

Pen-Shu Yeh (Code 738.3)
301-286-4477

Sponsor: Office of Advanced Concepts and Technology

Office of Space Communications

Mr. Warner Miller has been at GSFC for over 30 years. He has an MS in Applied Engineering from George Washington University. Mr. Miller has supported many flight programs, and also conducts research and development in the area of communications and onboard processors.

Dr. Pen-Shu Yeh earned a PhD in Electrical Engineering from Stanford University. She has been at GSFC for 6 years, where she conducts research and technology development in the area of source coding in the Electronics Systems Branch.

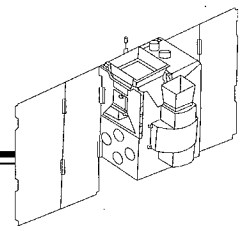

ADVANCED AEROSPACE BATTERIES

OF THE VARIOUS available battery technologies, nickel-cadmium (NiCd) batteries and, to a lesser extent, nickel-hydrogen (Ni-H_2) batteries, have been used in NASA and non-NASA spacecraft over the last 40 years. These batteries have low specific energies, or energy densities. Studies are underway to examine for future NASA use aerospace cells utilizing new electrochemical couples (e.g., nickel-metal hydride (NiMH) and lithium ion) that have the potential to increase the specific energy of a battery, and single pressure vessel (SPV) Ni-H_2 batteries, that have the potential to increase the volumetric energy of a battery. A summary of the development of three advanced battery technologies is presented here.

The Ni-H_2 battery used in the Hubble Space Telescope (HST) consists of a number of serially connected individual pressure vessel cells; its specific energy is < 40 Wh/Kg. One approach to increase the specific and volumetric energy is to use a single pressure vessel. The SPV Ni-H_2 battery consists of multiple serially connected individual Ni-H_2 cells within a single pressure vessel sharing a common hydrogen atmosphere. The SPV Ni-H_2 battery has been the subject of intense study since 1984. Lightweight aerospace SPV Ni-H_2 batteries are under development by Comsat Laboratories (COMSAT), and Eagle-Picher Industries (EPI) in Joplin, MO and in Butler, WI. The SPV Ni-H_2 battery technology is considered to be mature because there exists a substantial database documenting its performance, possible failure modes, and limitations. Previous SPV Ni-H_2 batteries were not qualified for low-Earth-orbit applications. A program was initiated to procure specially designed SPV batteries from EPI in Joplin, MO and Butler, WI. The vendors designs differ in the cell encapsulation technique, hydrogen diffusion membrane, and weld configuration. Both vendors have successfully fabricated the batteries, and vendor acceptance testing is now in progress. The batteries will be characterized for their electrical performance and subjected to electrical, thermal, and mechanical testing using procedures previously documented by GSFC to qualify SPV batteries for aerospace applications.

The NASA-standard rechargeable nickel-cadmium (NiCd) battery, when operated under stringent charge control requirements, has demonstrated a charge/discharge cycle life of over 3 years aboard low-Earth-orbit and geosynchronous-Earth-orbit satellites. These NASA-standard NiCd cells utilize cadmium negative plates that contribute to operational difficulties. Cadmium dendrites and/or cadmium migration has been proposed as the one of the root causes of NiCd battery failures. Moreover, dealing with the new Occupational Safety and Health Administration (OSHA), safe-manufacturing cadmium level of 1 to 5 $\mu g/m^3$ is likely to increase the production cost of NiCd cells in the U.S.During the last several years, some progress has been made in replacing NiCd cells with nickel-metal hydride (NiMH) cells in aerospace batteries. The NiMH battery uses a hydride-forming-alloy negative plate. Two Small Business Innovative Research (SBIR) awards were granted to develop and manufacture metal hydride plate materials to replace cadmium negative plates in aerospace battery cells. In the Phase I study, both the Ovonic Battery Company and Materials and Electrochemical Research Corporation have demonstrated the feasibility of using Ovonic metal hydride alloy (AB_x) and fullerenes, respectively, as a negative plate in NiMH battery cells. Phase II awards were recently granted to scale up and manufacture negative plates, to build aerospace cells, to characterize the cells, and to deliver cell samples for GSFC qualification testing.

The lithium ion rechargeable battery has potential application in electronics, telecommunications, and aerospace industries. The battery uses an intercalated anode, such as lithiated carbon (LiC), and an intercalated cathode, such as lithiated nickel oxide ($LiNiO_2$), lithiated cobalt oxide ($LiCoO_2$), lithiated spinel ($LiMN_2O_4$), etc., in an organic electrolyte. The battery is safe and does not contain metallic lithium. The advantages of the lithium ion battery for aerospace use are its high specific and volumetric energy densities. It is an attractive replacement for the currently used nickel-cadmium and nickel-hydrogen batteries. There are numerous technical issues which need to be resolved before the battery is ready for aerospace application. Among them, charging and charge control schemes should be specifically developed and optimized. Because the battery uses an organic liquid electrolyte that is unstable beyond a specific cell voltage, the charging voltage needs to be controlled to achieve maximum cycle and wet life. It is not yet clear how this charge cut-off voltage responds to temperature, rate of charge, and repeated charging from a partially charged state. Discharge control is also important because structural deformation occurs in the electrodes when the battery is discharged to

very low voltage. The battery is prone to erratic behavior if high rate of charge and discharge is used—unlike the aqueous batteries—because of the higher resistivity of the electrolyte and the slow mass transport property of the electroactive species in the electrolyte. A program has been initiated to evaluate the performance of commercially available lithium ion cells. SAFT, Cockeysville, MD, provided two lithium ion D cells for NASA evaluation. COMSAT Laboratories has performed preliminary characterization of the cells. The initial evaluation is very encouraging; we intend to continue the work.

Contact: Gopalakrishna Rao (Code 734.5)
301-286-6654

Sponsor: Office of Advanced Concepts and Technology

Dr. Gopalakrishna Rao is Head of the Energy Storage Section in the Space Power Application Branch, which provides battery engineering support to GSFC flight projects. He has over 15 years of research and development work experience in government, industrial, and academic laboratories. He has published two books and about 50 publications in technical journals.

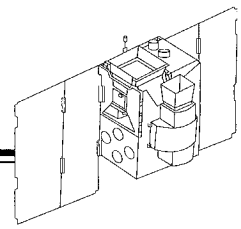

LONG LIFE, TWO-STAGE CRYOGENIC COOLER

OVER THE LAST 2 YEARS, Ball Aerospace has developed an engineering model cryocooler under contract to GSFC. It was completed during the winter of 1994 and delivered to GSFC; since then it has undergone extensive testing.

The cryocooler mechanical assembly weighs 8 kg. Its operational frequency is nominally 35 Hz. It produces over 400 mW of cooling at 30 Kelvin, with a heat sink temperature of 20°C. The cryocooler is a linear, split-Stirling-cycle machine. It has twin opposed compressors connected by a 12-inch transfer tube to a single two-stage expander with an opposed, active counterbalancer. The linear motors are high-efficiency, moving-coil motors. A photograph of the cooler is shown in the first figure.

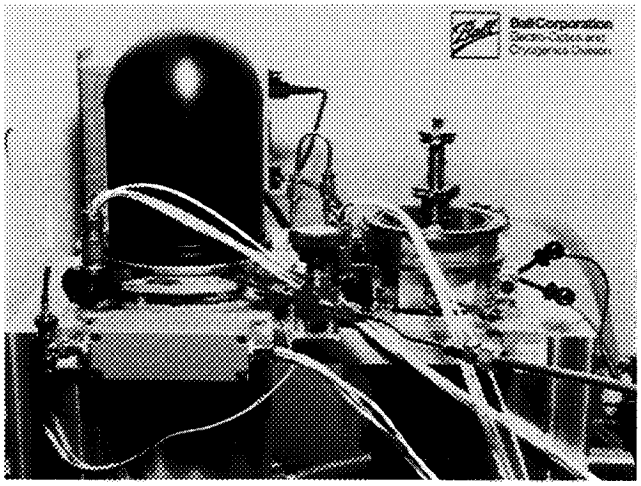

Photograph of Ball long life, two-stage cryogenic cooler.

Data for the Ball cooler performance as a function of heat load on both the cold-stage and the mid-stage are shown in the second figure. These mid-stage heat loads span the heat loads expected on a thermal shield surrounding detectors in a typical space-based instrument. Some degradation is seen in the cold-stage performance as this mid-stage heat load is applied. The upper three curves show the mid-stage equilibrium temperatures. There is a significant upward shift in the mid-stage temperatures with larger heater loads. The power input corresponding to these curves slowly decreases with increasing heat load on the cold-stage and is almost independent of the applied mid-

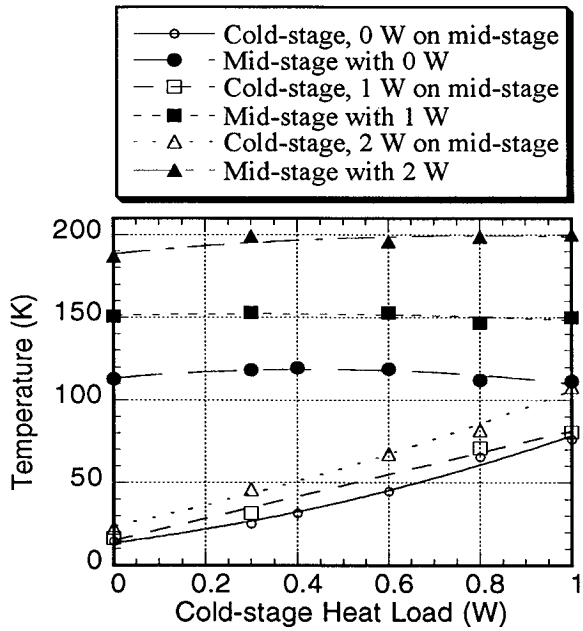

Ball two-stage cooler cooling power vs. temperature.

stage heat load. The input power, measured at the input to the electronics, decreases from about 95 W (with no load on the cold-stage) to about 85 W (with 1 W on the cold-stage). Total input power for the Ball cooler is expected to be reduced by 15 to 20 percent when the cooler is operated with flight electronics instead of laboratory electronics.

The cooler incorporates an innovative alignment system. With the cryocooler running under normal operating conditions in any orientation, the system can be used to measure the radial displacement of the moving components as a function of compressor piston axial displacement. This technique is of tremendous value in assuring no touch contact within the compressor assembly in any orientation over the full operating range of heat sink temperatures. This alignment system could be used during instrument and system integration, ground testing, and, if desired, launch, to verify that the no touch contact feature of this cryocooler remains intact. The compressor assembly has undergone launch vibration testing with no change in the alignment of the compressor pistons.

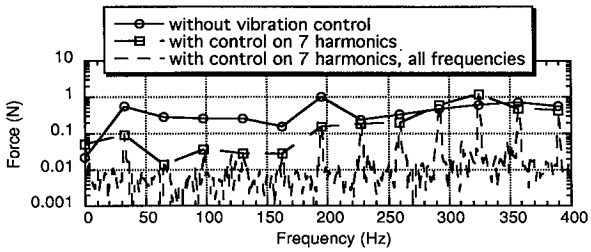

Ball compressor axial vibration comparison launch vehicles.

The original intent was to build a cooler with no touch contact at the seals to ensure an operational lifetime of 5 years. However, due to funding restrictions, only the compressor design is entirely new, and incorporates noncontacting bearings. A prototype cooler is now being fabricated that will incorporate noncontacting bearings into both the compressor and the expander.

The Ball cooler electronics also provide a vibration cancellation feature to null axial vibrations through the first seven harmonics. The resulting vibration spectrum is compared to the uncompensated residual vibration in the third figure. Only the peaks in the vibration spectrum are plotted for the uncompensated vibration In general, these peak values occur at harmonics of the cooler operating frequency.

Contact: Leroy Sparr (Code 713)
301-286-6024

Sponsor: Office of Advanced Concepts and Technology

Mr. Sparr is in the Cryogenics Systems Development Section. He is the Technical Officer on the GSFC contract with Ball for the development of flight coolers and operates the GSFC cryogenic cooler test facility.

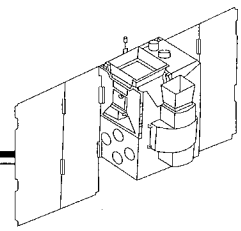

ANALYSIS AND VISUALIZATION OF THE PEGASUS XL RELEASE MECHANISM

COMMON TO THE VARIOUS analyses routinely performed on spacecraft hardware is the need to obtain information about the behavior of structures. This information is then used to expand any existing body of knowledge and understanding. When GSFC s Total Ozone Mapping Spectrometer (TOMS) Project chose the Pegasus XL launch vehicle, review of that vehicle revealed a need to establish such a body of knowledge for the XL's Release Mechanism.

The Orbital Sciences Corporation (OSC) Pegasus XL launch vehicle is designed to attach to a modified L-1011 aircraft during flight. At altitude, the captive launch vehicle is dropped and orbit insertion maneuvers are initiated. The drop event was investigated by the Engineering Directorate Systems Analysis Branch at the request of GSFC s Orbital Launch Services Branch. Four major objectives were outlined: (1) the generation of a computer 3D model of the release mechanism and spacecraft, (2) a kinematics study, (3) a dynamics study, and (4) the delivery of a visualization tool that would integrate the results of the studies with the display capabilities of a high-resolution graphics workstation. A priority issue for the Orbital Launch Service (OLS) was a full description of the release mechanism mechanics, since prior design reviews and documentation did not adequately describe how the mechanisms worked. Therefore, to make sense of any of the analyses, the mechanism itself had to be clearly understood. The Engineering Directorate Systems Analysis Branch was asked to provide a visualization tool to remedy this immediate problem.

Using the 3D robotics CAD package IGRIP, a detailed computer model consisting of 65 parts was created from the drawings provided by the manufacturer of the release mechanism, Marshall Aerospace, and other visual media documentation provided by OSC (see the first figure). Fifty-nine of the model parts were assigned kinematic motion parameters based on the information provided. In many cases, the motion had to be solved and then defined using mathematical equations. The kinematics study probed into the connectivity of each of the parts, and predicted the exact motion of each part for several deployment scenarios. The results of the kinematics study—the motion of the release mechanism during deployment—were then recorded and delivered along with the 3D model to the dynamics analysts for detailed investigation of the dynamics of the drop event. The dynamics study sought to perform an independent review of various launch scenarios and their effects on the critical components of the mechanism. This study utilized the dynamics analysis program, the Data Archive and Dissemination Service (DADS). A memo summarizing the findings of these studies was released July 13, 1994.

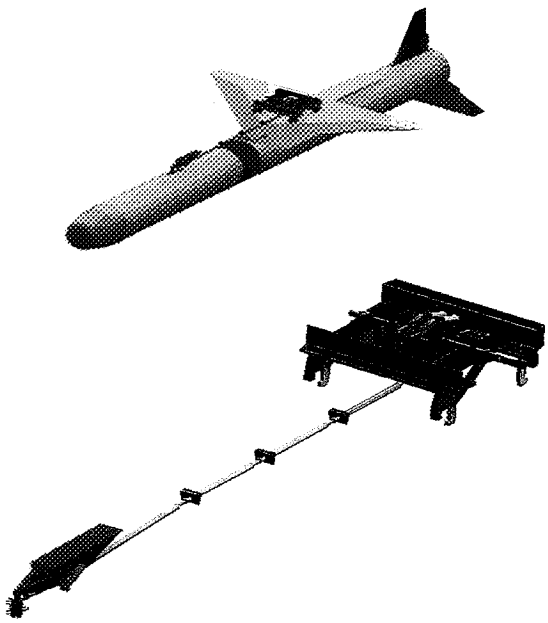

The Pegasus XL release mechanism and spacecraft.

We also developed visualization software that uses the results of the kinematics and dynamics studies for interactive viewing (see the second figure). Running on a state-of-the-art Silicon Graphics workstation, that will be delivered as part of the response to the visualization tool task, this software has made post-processing of the results as simple as mouse-clicking a button on the screen. The viewer was designed to be versatile enough for an engineer seeking useful information about the mechanism, and as a presentation tool for a curious layperson. Playback controls, similar to a videotape player, are provided to examine the various deployment scenarios. The software also allows the user to interactively rotate, translate, and

C-3

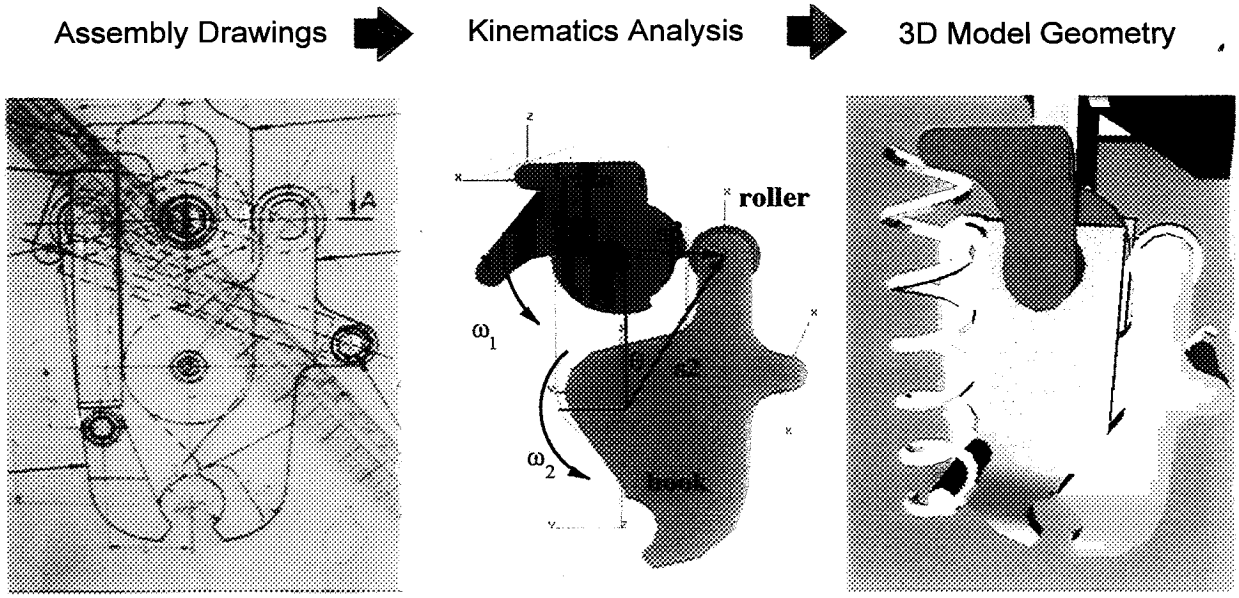

Model development process.

zoom views while the results are playing. This visualization tool is powerful in demonstrating in seconds what was almost impossible to relate after hours of research using conventional media.

Mr. Timothy Carnahan supervised the analysis effort and coordinated the visualization project. Mr. Marco Concha, Systems Analysis Branch, performed the modeling effort and conducted the kinematics study. Dr. Wen-Hu Tsai and Mr. Robert Cutlip, both of ATR, performed the dynamics analysis and authored the analysis viewing software, respectively.

Contact: Marco Concha (Code 721.1)
301-286-7499

Sponsor: Office of Space Science

Mr. Marco Concha is an aerospace engineer in the Mechanical Systems Division of the Engineering Directorate. He has provided analysis support for several projects utilizing three-dimensional modeling and visualization techniques. Mr. Concha earned his BS in Aerospace Engineering from the University of Maryland, College Park. He has been a civil servant at GSFC for 3 years.

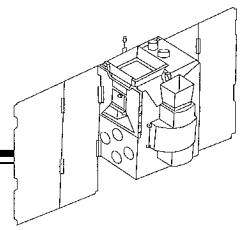

A NEW SOUNDING ROCKET PROGRAM VEHICLE

A TERRIER-IMPROVED ORION 12.046 WT was successfully flown from Wallops Flight Facility in April 1994. The primary purpose of this launch was to test a new sounding rocket vehicle configuration, utilizing a Mark 12 MOD1 Terrier and the Improved Hawk rocket motor, which would allow a different family of scientific payloads to be flown at a reduced cost. In an effort to gain as much benefit from this launch as possible, attempts were made to achieve several secondary objectives, including use of spin motors to reduce dispersion, flight qualification of Global Positioning System (GPS) for a sounding rocket application, flight qualification of position and rate gyroscopes, measurement of fin loads, measurement of bending moments on payload, measurement of re-entry dynamics, qualification of a recovery aid deployment system.

This payload configuration evolved as a result of a combination of requirements to simulate future operational payloads to be flown on this vehicle, and to meet needs of the various secondary objectives listed above. The 17.25" diameter body was felt to be the most likely to be flown on this vehicle; in addition, the GPS wraparound antenna was already being built to this diameter. The 750-pound Ogive Recovery System Assembly (ORSA) was readily available from sounding rocket stock because there are very few current requirements for this smaller system. Antenna sections were available from previously flown hardware, and the 60 in. skin was a test section that already had strain gauges installed on the outside. Accommodations for bulkheads on both ends allowed this section to be made watertight. The only portions requiring fabrication were the transition ignition housing section and the shelves and longerons for the instrumentation inside the 60 in. skin. There were three inertial-referenced attitude gyros, one three-axis rate gyroscope, and two single-axis rate gyroscopes mounted on one shelf in this section. Two guidance dynamics gyroscopes were being flown for flight qualification, with a Midas platform flown as a reference. The single-axis gyroscopes were being flight-qualified, while only the circuitry for the three-axis gyroscope was being qualified. The GPS receiver and support electronics to be qualified were housed in this sealed section, as were power, timing, and telemetry to allow recovery. The re-entry configuration with a recovery weight of 321.5 lbs was successfully recovered by the Coast Guard the same day as the launch.

The flight mission profile is based on trajectory for a launch of a 510-pound payload from Wallops, using an 80° launch elevation with a ballistic impact predicted at 133.5 km. The flight sequence of events is outlined below in the table.

The flight of Terrier-Improved Orion 12.046 WT accomplished the following:

- It was the first flight of the Improved-Orion rocket motor (surplus Improved Hawk) in the NASA Sounding Rocket Program.
- The first flight of this vehicle combined the Terrier (MK 12 MOD 1) for the first time with the Orion motor in either of its configurations.
- A Spin Motor Module was flown on this vehicle to reduce dispersion.
- The logic for the Spin Motor Module was used to initiate clamp release for first to second stage separation.
- The vehicle was flown with bulbous payload (17.26 in vs. 14.00 in), which was considered more representative of payloads to be flown when this vehicle is operational. This is not the normal procedure for the first flight of a new vehicle configuration.
- The first known successful application of the GPS to a spinning rocket.
- Thermistors were flown on the aft dome of the Orion motor to monitor potential hotspots. This qualified motors with cracked aft insulators as being flightworthy for sounding rocket applications and eliminated a costly refurbishment.
- Strain gages and thermistors were flown on one of the Orion fins to measure fin loads and temperatures to be used in performance study.
- Strain gauges were flown on the payload to measure flight bending loads for comparison to predicted loads.

Nominal Flight Sequence of Events

Event	Time (sec)	Altitude (km)	Range (km)
Terrier Ignition	0	0	0
Rail Exit	0.4	72.3 ft	0
Spin Ignition	0.7	138.3 ft	11.94
Terrier Burnout	5.2	1.96	0.38
Terrier Separation	5.5	2.16	0.42
Improved Orion Ignition	16	7.85	1.67
Improved Orion Burnout	40.5	34.5	9.2
Nose Tip Deploy	101.6	100	33.8
Apogee/Despin	185	132.5	66.5
Payload Separation	268.4	100	99.2
Ballistic Impact	355.7	0	133.5
Drogue Deploy	438.5	20.0 Kft.	137.3
Mai Chute Deploy	458.5	16 kft	137.4
Chute/Payload Impact	902	0	137.4

- Vibrometers were flown in the payload to measure flight vibrations for comparison to the levels presently being used for environmental testing. Additionally, a self-contained programmable shock and vibration recorder was flown for comparison, as well as providing a direct measurement of water impact loads.

- Three inertial-referenced attitude gyroscopes were flown on this payload. Two were from a new vendor and were flown for flight certification. The third was a flight-qualified unit, from a different vendor, flown for comparison.

- A three-axis Rate Gyro was flown to flight qualify newly designed Driver and Decommutation circuits.

- First flight of the 25-foot Cross Parachute, which successfully recovered the payload.

- First flight of the Deployable Recovery Instrumentation Package (DRIP), designed to float alongside a buoyant payload while tethered to the payload. Onboard the DRIP is a transmitter and strobe light to aid in the location/recovery of the payload.

- The first sounding rocket application of Sea Water Activated Release Switch (SEAWARS) parachute release, to disconnect two of the four confluence points of the parachute to prevent it from becoming a sea anchor, thereby reducing the possibility of sinking the floating payload.

- Payload fabrication was held to a bare minimum by utilizing previously flown and recovered payload skins, antennae, and recovery system. Fabrication was held to instrument decks, longerons, and the transition section between the second stage and the payload which housed the logic for second stage ignition, despin, and payload separation.

Contact: Carl Ballance, Jr. (Code 841.2)
804-824-1422

Sponsor: Office of Space Science

Mr. Carl Ballance, Jr. is Project Manager on the 12.046 WT mission. Mr. Ballance earned a BS in Mechanical Engineering from the Virginia Polytechnic Institute. Mr. Ballance has been at GSFC/WFF for 31 years, where he is Head of the Flight Vehicles and Systems Section, supporting the NASA Sounding Rocket Program.

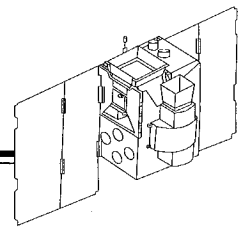

THE FIRST FLIGHT OF A GPS RECEIVER ON A NASA SOUNDING ROCKET

IN SUPPORT OF PAYLOAD science on sounding rocket flights, we undertook a test to determine the suitability of a commercial off-the-shelf (COTS) Standard Positioning Service (SPS) GPS receiver for flight in a sounding rocket environment, and to quantify the accuracy of the position fixes computed by the receiver during the ballistic portion of the flight.

The sounding rocket on which this test was conducted was a Terrier-Improved Orion development round launched from Wallops Island on April 5, 1994. This two-stage rocket lifted the nominal 1,120 kg (509 lb) payload to a 125 km maximum altitude and achieved a maximum velocity of about 1,400 meters per second.

The receiver chosen for this test was the Trimble Advanced Navigation Sensor (TANS) II because it is a COTS design. It can be purchased conveniently from the GSA schedule for less than $10,000, and the TANS technology has been flown previously on the Pegasus launch vehicle. The TANS II is a six channel, C/A code receiver, with dimensions of 12.7 by 24.1 by 5.1 cm (5 by 9.5 by 2 in), weighs 6.6 kg (3 lb), and consumes 3 watts of primary power. The receiver was configured to compute its own navigation solution on an as-soon-as-possible basis. The serial data output from the receiver was combined with the payload pulse-code-modulated telemetry for real-time transmission to the ground.

The Physical Sciences Laboratory of the New Mexico State University developed a microstrip, wraparound antenna to receive the L-band GPS satellite signals during this flight. This antenna, which conformed to the 43.84 cm (17.26 in) payload diameter, had an axial length of 13.97 cm (5.5 in), and a thickness of 0.32 cm (1/8 in), including the integral Teflon radome. The antenna consists of two subarrays which are fed in-phase through a power combiner. Axial nulls exist on the nose and tail. The polarization is right-hand circular, with peak gain of 2 dBi, and -4.6 dBi gain for 90 percent coverage. The bandwidth (VSWR=2) is greater than 70 MHz, nominally centered on 1575.4 MHz.

Vibration was the only parameter that created problems during environmental qualification of the receiver. Payload structures typically exhibit mechanical resonance at specific frequencies; in this case, such a resonance caused the random vibration power spectral density (PSD) to be amplified from 0.051 to 6.8 g^2/Hz at 200 Hz. The receiver ceased operating under these conditions and exhibited current surges on the primary power leads. The receiver had been tested satisfactorily to 8.3 g (rms) by the manufacturer and to 20.6 g (rms) at the component level after receipt by the government. However, neither of these tests reached PSD levels anywhere near those created by the payload resonance. The payload random vibration response was modeled, and component-level tests were conducted to diagnose the problem. A quick fix was developed by placing a rubber material between the two stacked printed circuit cards and between the circuit card assembly and the top and bottom of the case. The receiver then passed the payload level random vibration test. During flight, the receiver reported position fixes continually; however, it did experience one momentary current surge at the time of the second stage ignition transient.

On the day of the launch, an unexpected problem occurred. With the launcher elevated, the GPS receiver could only acquire three GPS satellites, even though there were seven satellites visible at the time. This problem was attributed to blockage by the launcher and the position of the antenna null on the nose of the launch vehicle. The problem disappeared at lift-off, when the receiver acquired a fourth satellite; it remained locked on four satellites throughout the flight.

The flight of the Terrier-Improved Orion lasted about 15 minutes. The powered portion of flight ended with second stage burnout at about +41 seconds; the flight remained ballistic until about +300 seconds, when the payload began to re-enter the Earth's atmosphere. The parachute was deployed at +421 seconds, the GPS receiver was turned off at +500 seconds, and the payload went into the water at about +915 seconds.

Within its 500 seconds of operating time during flight, the GPS receiver reported navigation solutions continuously with a mean time between samples of 0.982 seconds. All of the data were valid except from 0 to +5 seconds and from +16 to +21 seconds. During these two time intervals, the thrust axis acceleration exceeded 10 g, a not unexpected result. The receiver computed 236 navigation

solutions during the ballistic portion of the flight. These data were compared to a reference trajectory generated from radar data acquired at the same time. The polar coordinate radar data were transformed to the GPS reference system which is an Earth-centered, Earth-fixed Cartesian coordinate system. The three-dimensional, 1σ error between the GPS data and the radar trajectory was 126 m. Most of the error is a slowly varying bias component caused by the effects of selective availability in the GPS system.

Contact: Alan Selser (Code 822)
804-824-1472

Sponsor: Office of Space Communications

Mr. Selser is an electronics engineer in the Instrumentation Engineering Branch at the Wallops Flight Facility. He earned a BS in Electrical Engineering from Drexel University and has worked at GSFC for 31 years as a radar systems engineer.

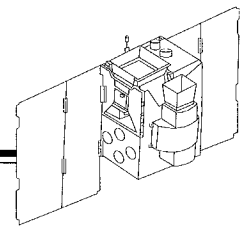

REINFORCEMENT OF THIN BALLOON FILMS USING IN-SITU FIBRILS

FUTURE LONG-DURATION BALLOON (LDB) flights, with durations exceeding 100 days (global capability) and with altitude excursions of less than 2,000 feet, require a different film material than that currently utilized for short-term, zero pressure (ZP) balloon systems. Altitude stability of LDBs depends on the material stiffness. Altitude variations, such as occur when the internal pressure and temperature change between day and night values, depend on the elastic modulus of the material. Long-term, viscoelastic growth of the balloon depends on the creep compliance of the material, which is related to the ratio of the average load applied to the total strain at the end of the service life at a given average temperature. Furthermore, deployment stresses during launch, and the harsh environment encountered during ascent and float, require certain strengths. Structural analysis, balloon design, and flight-test efforts have indicated the need for a film material with higher stiffness and yield-stress, and lower creep compliance than that currently used for conventional, or ZP-type, balloon flights.

To meet these requirements, the Balloon Projects Branch has invested in research efforts to produce a film that meets the above requirements while retaining the toughness, low temperature characteristics, and balloon fabrication advantages of current polyethylene (PE) films. The technical challenge is quite rigorous, since it is axiomatic that high toughness, that is usually associated with high elongation, and high modulus/yield strength are mutually exclusive.

Since such rigorous requirements cannot be achieved through adjustments in the extrusion processing parameters for existing polyethylene film, other alternatives were explored to develop an appropriate material. One feasible approach is the addition of a second, rigid phase—such as fibers or other additives—to the base matrix to combine the desired properties from each phase to form a composite with enhanced mechanical properties. However, although rigid fibers are quite effective in raising the modulus and yield-stress in bulk polymers, their effectiveness in thin films is highly sensitive to their actual thickness. Almost all possible fiber additives are available only in diameters that are comparable to the desired final film thickness. As a result, the fiber acts not so much as a reinforcing element but rather as a defect, resulting in undesirable effects on the strength and fracture characteristics of the resulting composite thin film.

In situ film formation is another unique approach to achieve the reinforcing effect of additives in the thin film environment. Ideal candidates for such fibril formation are liquid crystal polymers (LCP). This class of polymeric materials is mostly known for its high stiffness and exceptional moldability despite its high heat and chemical resistance. Liquid crystal is a term that is now commonly used to describe materials that exhibit partially ordered fluid phases that are intermediate between the three-dimensionally ordered crystalline state and the disordered (or isotropic) fluid state. When an LCP blend is processed under elongational flow conditions, the partially ordered meso-phase intermediate between the crystalline and isotropic states of the LCP allows the development of an oriented fibrillar morphology, which may be retained upon solidification. The fibrillar structure of the LCP contributes significantly to the tensile modulus of the blend. We made extrusions of integrally stiffened high-density polyethylene (HDPE)/linear low-density polyethylene (LLDPE) film, using LCP as the reinforcing element. A mechanical blend of PE and LCP was melted and subjected to high shear to produce LCP fibers. With proper temperature control, the higher-melting fibers could be solidified while the PE matrix remained molten. The melt could then be pelletized with the fibers dispersed or extruded directly. A typical set of results obtained under various extrusion conditions for a blend of 1 HDPE/2 LLDPE mixed with 10 percent LCP is shown in the table.

Composite Film Modules of LCP/PE Blends

Extruder Temperature Profile (°F)	Screw Speed (rpm)	Film Thickness (mm)	Modulus (MPa)
[370, 400, 420, 420]	10	0.08	487
[370, 400, 420, 420]	15	0.10	745
[370, 400, 420, 420]	20	0.15	674
[370, 400, 420, 420]	25	0.15	911
[370, 400, 420, 440]	20	0.14	726

The reinforcing effect of the fiber is quite obvious when these results are compared to a typical modulus value of approximately 100 MPa for a homogeneous PE film.

Films made with in situ LCP fibrils are anisotropic (i.e., their properties are a function of direction). As a result, the reinforcement effect of these fibrils on the mechanical properties is achieved only in the direction of fibril orientation. Properties normal to the fibril axis tend to be an order of magnitude or more lower than the longitudinal values, resulting in low stiffness or strength. To fully exploit the microfibrillar reinforcement properties of LCP blended with a thermoplastic matrix, the inherent anisotropic characteristics of these films need to be overcome.

More random fibrillar orientation in flown films is successfully achieved using a counter-rotating die as shown in the figure. The counter-rotating die is made up of concentric inner and outer cylinders. They rotate in opposite directions at the same speed. Melt is fed from the extruder entering the side of the die through an adapter pipe.

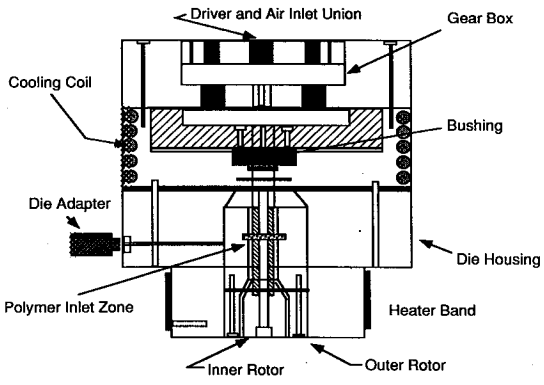

Schematic of the counter rotating die.

Polymer is then pumped through slots or holes cut on the outer rotor and forced into the channel along the outer rotating mandrel. Biaxial orientation of flow is induced by the counter rotation of the two rotors. Upon exiting the die, the film is inflated with air from a valved opening in the inner rotor, further oriented by stretching, and then wound on rolls. The technique gives rise to biaxial orientation and correspondingly balanced film properties.

LCP in situ fibrils, although quite effective in raising the modulus, is found to have little effect on increasing the yield-stress of the resulting composite film; this is likely due to poor adhesion between the LCP fibrils and the polyethylene matrix. Improvements in the technique are being made by selecting more compatible systems, such as nylon/PE or polyethylene terphthalate (PET)/PE. Recent data obtained from these systems show noticeable improvements in both the modulus and yield stress of the resulting film.

This work was done in collaboration with Dr. Ian Harrison, Professor of Polymer Science and Engineering, at The Pennsylvania State University.

Contact: Magdi Said (Code 842.0)
804-824-1386

Sponsor: Office of Space Science

Dr. Magdi Said is a materials engineer at the Balloon Projects Branch, Wallops Flight Facility, Wallops Island, VA. He has a multidiscipline background in chemistry, chemical and materials engineering. He earned his MS and PhD from North Carolina State University, Raleigh, NC. In his current position, he is responsible for developing various techniques to characterize thin polymeric films as well as to technically monitor all aspects related to materials R&D efforts at various research institutions. He has been at GSFC since 1989.

SPACECRAFT THERMAL CONTROL USING RANKINE CYCLE VAPOR COMPRESSION SYSTEMS

FUTURE GENERATIONS of spacecraft will continue to shrink in size with miniaturization of spacecraft electronics and scientific instrumentation and reduced budgets, pursuant to NASA policy. Current thermal control systems will, therefore, become increasingly large on a relative basis, and cannot provide the necessary architectural flexibility required in compact spacecraft. Rankine cycle vapor compression machines appear to be one promising thermal control technology permitting the development of effective, efficient, and smaller thermal control systems. Rankine devices are known to be the most efficient and reliable thermal transport/control devices in the relevant temperature range (250°K to 360°K). The inherent temperature lift associated with the operation of the Rankine cycle will allow smaller radiators. Employment of compact heat exchangers will allow greater architectural flexibility to the spacecraft designers, and will require significantly less volume dedicated to the thermal system. These heat exchangers also improve the thermodynamic efficiency of any thermal transport loop.

The Thermal Engineering Branch at GSFC has begun an analytical and experimental assessment of Rankine-based vapor compression applications for spacecraft thermal control. The program will include determination of environmentally safe (nonchlorofluorocarbon) refrigerant performance, evaluation of compact heat exchangers, and optimization of system equipment. This program will provide a fundamental data base to evaluate specific application designs for suitability.

In the past year, a thermodynamic evaluation of non-CFC refrigerant performance has been conducted using Cycle_D (NIST Standard Reference Database 49). This analysis provides a relative measure of specific refrigerant performance at varying operational conditions. This work will allow the user to identify the most promising refrigerant candidates for a given application. Determination of actual refrigerant, component, and system performance requires experimental evaluation; therefore, the Breadboard Vapor Compression System (BVCS) has been fabricated and prepared for operation in the GSFC Thermal Laboratories.

The BVCS is a robust experimental tool designed to evaluate vapor compression system components such as working fluids, heat exchangers, and expansion valves. The figure shows a schematic representation of the loop. The electric motor, torquemeter, and compressor assembly permits accurate measurement of the work input to the system. Refrigerant flow rate is determined by the mass flow meter. For initial testing, the system heat exchangers are smooth tubes bonded to relatively thick plates, with sufficient instrumentation for determination of overall and local heat transfer and pressure drop through the heat exchanger. The expansion valve is simply a needle valve with a vernier handle for calibrated adjustment. Any of the components can be replaced for comparison with alternative candidates.

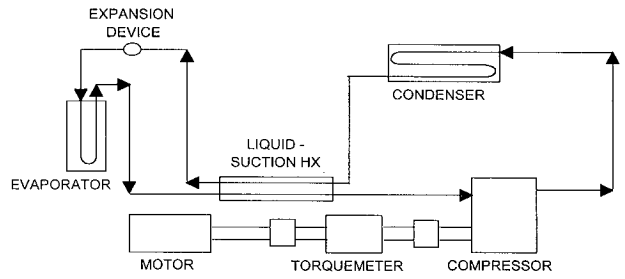

Schematic of GSFC breadboard vapor compression system.

Experimental efforts validating the performance of refrigerant HFC-134a are to begin during the fall of 1994. Performance assessment of the refrigerant will be based upon system efficiency at a given condition. System efficiency is measured in terms of Coefficient of Performance (COP), which is simply the amount of heat transferred by the evaporator divided by the amount of work input to the system. Additionally, the heat exchanger performance will be characterized in terms of the relevant figure of merit, j/f. The term j/f is a dimensionless number comparing the amount of heat transferred to the pressure drop experienced in the heat exchanger. Local and overall heat transfer coefficients will be established. Similar experiments with other refrigerants will follow in 1995.

Plans for future years include experimental evaluation of compact heat exchangers, capillary heat exchangers, and design and development of optimized thermal control systems for small spacecraft.

Mr. Theodore Swanson, Head of the Advanced Development and Flight Experiments Section, provided technical and programmatic direction for this work. Messrs. Mario Martins and Pat Gonzales of Code 724.2/Jackson and Tull have provided technical and design support in the fabrication of the breadboard loop.

Contact: Jeffrey Didion (Code 724.6)
301-286-4363

Sponsor: Office of Advanced Concepts and Technology

Mr. Jeffrey Didion is a mechanical engineer in the Thermal Engineering Branch at GSFC. He has been at GSFC for 5 years involved with analytical and experimental evaluation of advanced thermal control systems. Mr. Didion is a member of the ASME K-12 Aerospace Heat Transfer Committee and a PhD student in Mechanical Engineering at the University of Maryland through the GSFC Part-Time Graduate Study Program.

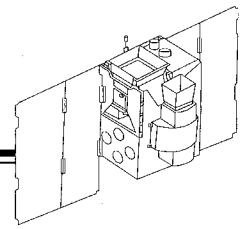

HEAT PIPE PERFORMANCE (HPP-2) FLIGHT EXPERIMENT

THE HEAT PIPE IS a very efficient heat transfer device commonly used for cooling electronic components and sensors in spacecraft. A heat pipe is essentially a closed, evacuated tube that is lined with a porous structure called a wick. The wick is saturated with a small quantity of liquid called the working fluid. Heat is absorbed at one end of the heat pipe, evaporating the working fluid contained in the wick structure. This vapor is transported to the heat rejection end of the heat pipe, where the heat is released as the vapor condenses. The condensate is transported back to the heated end of the heat pipe by capillary forces formed in the wick, and the cycle is repeated. It is important to note the evaporative phase change stores heat energy in the vapor at a constant temperature. The vapor will remain at this temperature until it meets a colder surface and condenses. This results in near-isothermal operation, making the heat pipe a very-high-thermal-conductance heat transfer device.

The design of effective spacecraft thermal control systems requires an understanding of heat pipe fluid dynamics in a microgravity environment. This behavior cannot be adequately evaluated on Earth because gravity tends to dominate the capillary forces developed in the wick. In the microgravity environment, however, surface tension forces within the wick become the dominating factor. Additionally, in the absence of gravity, excess fluid in the heat pipe can partially block the condenser, which decreases the thermal transport capability. For these reasons flight experiments are critical for collecting the data necessary for computer model validation (see the figure).

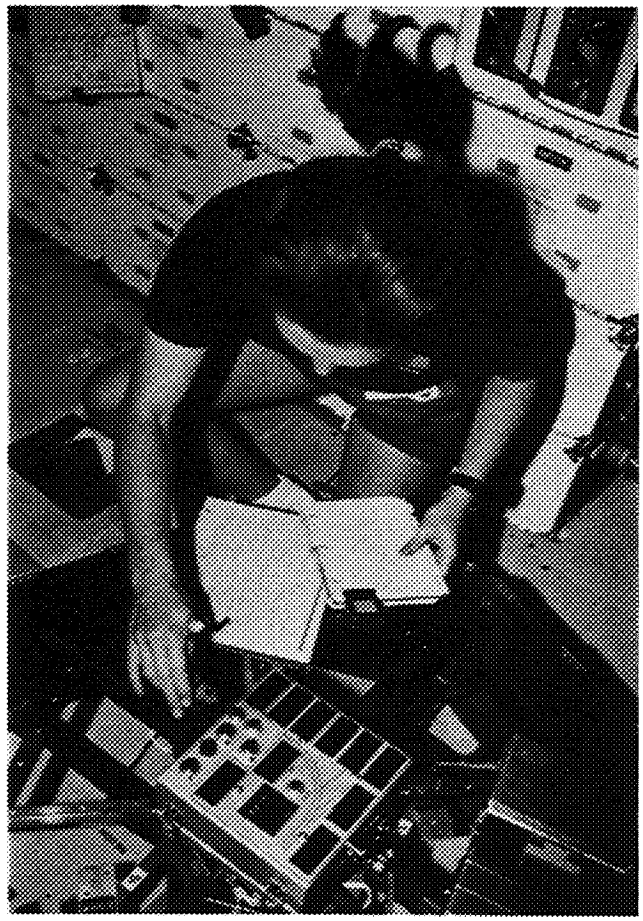

Heat pipe performance flight tests permit design refinement and model validation.

The original Heat Pipe Performance Flight Experiment (HPP-1) was flown on STS-52 in October 1992, to investigate and document the microgravity behavior and performance of several different types of heat pipes. Data from HPP-1 was used to modify and validate a NASA heat pipe computer model known as the Groove Analysis Program (GAP). The current version of the GAP model heat pipes with single and uniform heating and cooling zones; it is available from the Computer Software Management and Information Center (COSMIC).

The Heat Pipe Performance (HPP-2) Experiment will further investigate the thermal performance and fluid dynamics of heat pipes operating under microgravity conditions. It is a reflight of the highly successful HPP-1 experiment. The Thermal Performance Apparatus (TPA) from HPP-1 will be reused with minor modifications to accommodate the testing of new aluminum/freon heat pipes. The HPP-2 experiment will test heat pipes with asymmetric and multiple heating zones, providing data for correlation with new modifications to the GAP model. The basic difference between the two experiments is that HPP-1 tested ideal case, or simple heat pipes, while HPP-2 will test more realistic heat pipe designs that mirror the complexity of actual spacecraft applications. The experiment is manifested as a secondary middeck payload on STS-66, with launch scheduled for October 27, 1994. A TPA is mounted to middeck seat studs and allows the Orbiter crew members to test individual heat pipes in the crew compartment during the flight. Thirty-five tests will be performed with ten different, axially grooved aluminum/freon heat pipes.

The experiment hardware is modular and is stowed in three middeck lockers when not in use.

The end product of the HPP-1 and HPP-2 Flight Experiments will be a GAP model capable of accurately predicting the performance of any type of axially grooved heat pipe design prior to manufacture, so large costs incurred by building and testing prototype heat pipes can be avoided. Data and knowledge gained in HPP-1 significantly contributed to a 40 percent reduction in cost for heat pipes manufactured by Hughes Aircraft for communication satellites. The final version of GAP will allow thermal system engineers to be less conservative in their designs, leading to fewer heat pipes per spacecraft, thereby achieving significant weight and cost savings.

Contact: Matthew Buchko (Code 724.2)
301-286-8537

Sponsor: Office of Advanced Concepts and Technology

Mr. Matthew Buchko is a thermal engineer in the Advanced Development and Flight Experiment Section. He received his BS in Physics from Millersville University and an MS in Mechanical Engineering from Wright State University.

A SIMPLIFIED P4R MECHANISM WITH BASE-MOUNTED ACTUATORS

COMPARED TO ORDINARY closed-loop, two-degree-of-freedom (DOF) mechanisms with five links, coordination between the actuators of a simplified, P4R mechanism is much simpler. The name P4R is used for the mechanism, because it contains one prismatic (P) joint and four revolute (R) joints, as discussed below. A patent application has been filed for the simplified P4R mechanism.

Many researchers have studied regular five-bar linkages as two-DOF manipulators. The first figure shows such a manipulator. Base-mounted actuators at points D and E drive the DA and EB links, respectively. Passive revolute joints are placed at points A, B, and P. Point C can be considered the output point.

If the distance between points D and E is reduced to zero, we obtain a simplified five-bar linkage. As shown in the second figure, in such a configuration two base-mounted actuators exist at point D (one above the planar mechanism and one below it). The actuators drive the input links DA and DB.

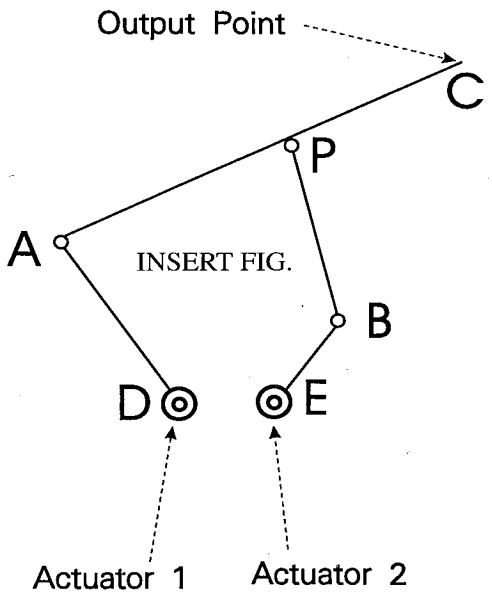

A regular five-bar linkage.

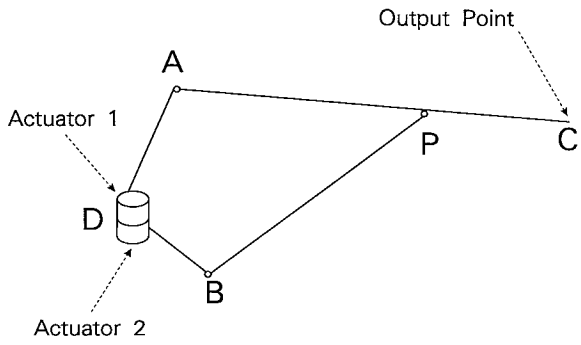

A simplified five-bar linkage.

As shown in the first and second figures, in a regular or simplified five-bar linkage, any point along the AC or BP links can be considered the output point. For a given displacement of the output point, the inverse kinematic problem of the mechanism has to be solved to obtain the required actuator displacements. This computationally demanding process can be slow and expensive.

The third figure shows a simplified and symmetrical five-bar linkage. Again, the two base-mounted actuators (one above and one below of the planar mechanism) drive the input links DA and DB. Also note that

$$|\overline{DA}| = |\overline{DB}| = a$$

$$|\overline{AC}| = |\overline{BC}| = b$$

If point C is used as the output point, its displacement can be resolved into a radial component and a tangential one (with respect to a circle centered at point D and passing through point C). The radial component can be obtained if the actuators make equal and opposite displacements. The tangential component can be obtained if the actuators make equal displacements. Therefore, the required actuator inputs can be determined very quickly. It has been shown that the simplified and symmetrical five-bar linkage can provide a very high resolution at point C, if the ratio a/b is made much smaller than one. However, due to the existence of the revolute joint, mounting a device such as an end-effector at point C may not be desirable.

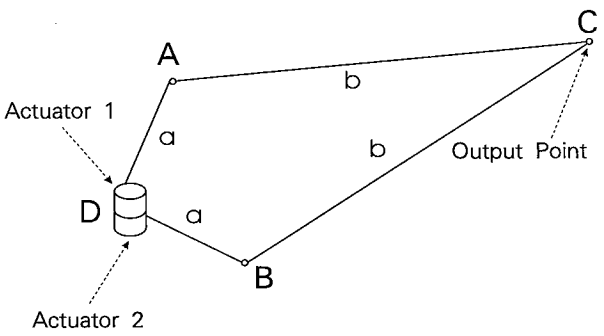

A simplified and symmetrical five-bar linkage.

The simplified P4R mechanism eliminates the restriction on the output point location which exists in the simplified and symmetrical five-bar linkage. The mechanism consists of four revolute joints (two actuated joints at point D, and two others at points B and P), a prismatic joint, and five links (including the ground link). Therefore, mobility analysis can be used to show that it has two DOF. The fourth figure shows a simplified P4R mechanism. Two actuators exist at point D (one above the planar mechanism and one below it). Actuators 1 and 2 drive the input links DA and DB, respectively. Revolute joints are placed at points B and P. The output link is connected to link DA by a prismatic joint.

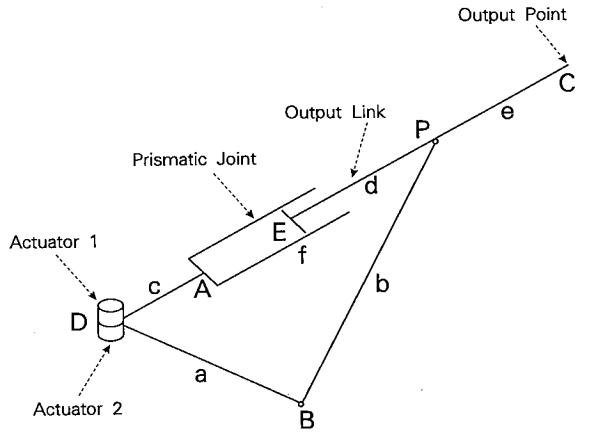

A simplified P4R mechanism.

The output point C can be connected to an input link of another mechanism. For example, a simplified P4R mechanism can be used as a driver for a six-DOF parallel minimanipulator. Also, the simplified P4R mechanism can serve as a stand-alone manipulator, if an end-effector is mounted at point C. Note that the simplified P4R mechanism is different from a crank-and-slider mechanism mounted on a turning base. In such a crank-and-slider mechanism, the crank actuator is not base-mounted and moves with the mechanism. The link lengths of the simplified P4R mechanism (parameters a, b, c, d, e, and f in the fourth figure) can be optimized to obtain desirable objectives, such as high mechanical advantage, large and uniform workspace, and force isotropy.

While the simplified and symmetrical five-bar linkage in the third figure offers a similar simplification in coordination between its actuators, this is true if and only if its output point is at the intersection of the DAC and DBC branches. Again, due to existence of a joint, connecting a device (e.g., an end-effector or an input link of another mechanism) to point C may not be practical. However, in the simplified P4R mechanism, the output point can be anywhere along the output link. If it is desirable to have the output point at the tip of the output link and outside of the EP segment, then the length of the output link can be varied to obtain an infinite number of output point possibilities.

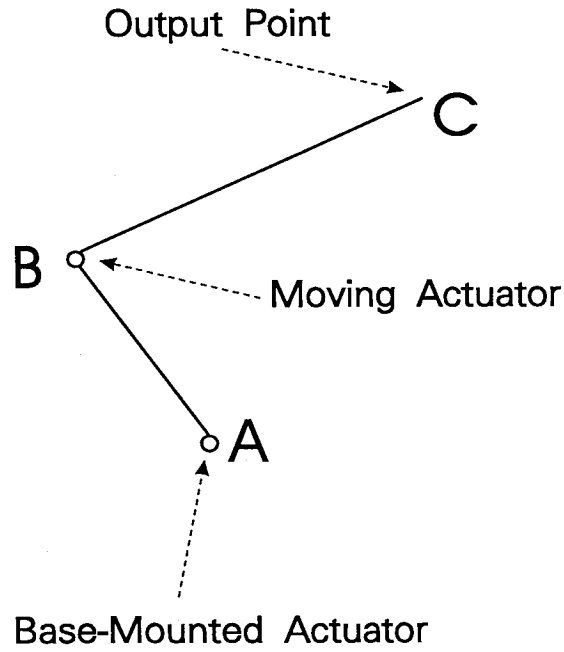

An open-loop two-DOF manipulator.

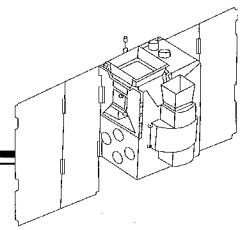

Open-loop, two-DOF mechanisms with a moving actuator have been discussed in the literature, as shown in the fifth figure. A base-mounted actuator, such as the ones used in driving the simplified P4R mechanism, has several advantages over a moving one: its weight is not a load for the other actuators, it does not create any structural deformations and positioning errors, and it is much easier to route its power and data lines.

Contact: Farhad Tahmasebi (Code 721)
301-286-5203

Sponsor: GSFC Research and Study Fellowship Program

Dr. Tahmasebi is an aerospace engineer in the Systems Analysis Branch. He graduated Summa Cum Laude with a BS and a PhD in Mechanical Engineering from the University of Maryland, College Park. He has been working on various computer-aided-design and robotics projects at GSFC since 1983. He holds two U.S. patents, and has taught graduate and undergraduate-level courses in Mechanical Engineering at the University of Maryland.

MAGNETIC BEARING ATTITUDE CONTROL WHEEL DEVELOPMENT

THE ELECTROMECHANICAL BRANCH at GSFC is in the process of developing an attitude control wheel based on magnetic bearing technology to replace the standard ball-bearing wheels currently in service with superior technology. Magnetic bearings have been in existence for more than a decade and their superior performance characteristics have long been recognized. However, these devices have yet to be used on a regular basis on NASA spacecraft and satellites because of practical considerations, and because ball-bearing momentum wheels are simple, safe, rugged, and reliable, and have extensive space heritage. Still, ball-bearing momentum wheels are no match for magnetic bearings in smoothness of operation, speed, predictability (as there are no lubrication uncertainties), wear, precision control, and operational flexibility. Clearly, this technology should be applied to attitude control wheels on satellites developed at GSFC as standard hardware. It is a technology whose time will have come as soon as several nagging practical problems can be eliminated.

While the state-of-the-art magnetic bearing (such as shown in the figure) will be thoroughly characterized and tested on Earth prior to launch, inevitably there will be differences between expected performance and actual performance in space. Understanding these variations in data will be invaluable in upgrading models and revising and improving test procedures, and will also help determine where improvements need to be made in the wheel design. The experience of developing and testing a flight electronics controller will also be valuable. Accordingly, the Electromechanical Branch is undertaking a two-pronged development thrust: (1) to fly an existing, state-of-the-art, GSFC-sponsored magnetic bearing in space as a Get Away Special (GAS) can experiment to see how it performs as an attitude control wheel; and (2) to establish a near-term R&D effort aimed towards making magnetic bearings as simple, rugged, reliable, and safe as ball-bearing wheels.

It is already clear that much can and must be done to simplify the construction, operation, and safety of magnetic bearings. From the standpoint of safety alone, it is mandatory that a magnetic bearing attitude control wheel undergo graceful degradation in the event of a power failure in its motor or bearing control electronics, such that the satellite can reconfigure its attitude control system and keep the satellite on mission. For example, if the auxiliary touch-down bearings are at a 3-in. radius from the wheel center, and if the wheel is turning at 6,000 rpm, touch-down will involve contact at a speed of 100 mph. On the other hand, if the touch-down bearings are located at the center line of the wheel, initial calculations indicate

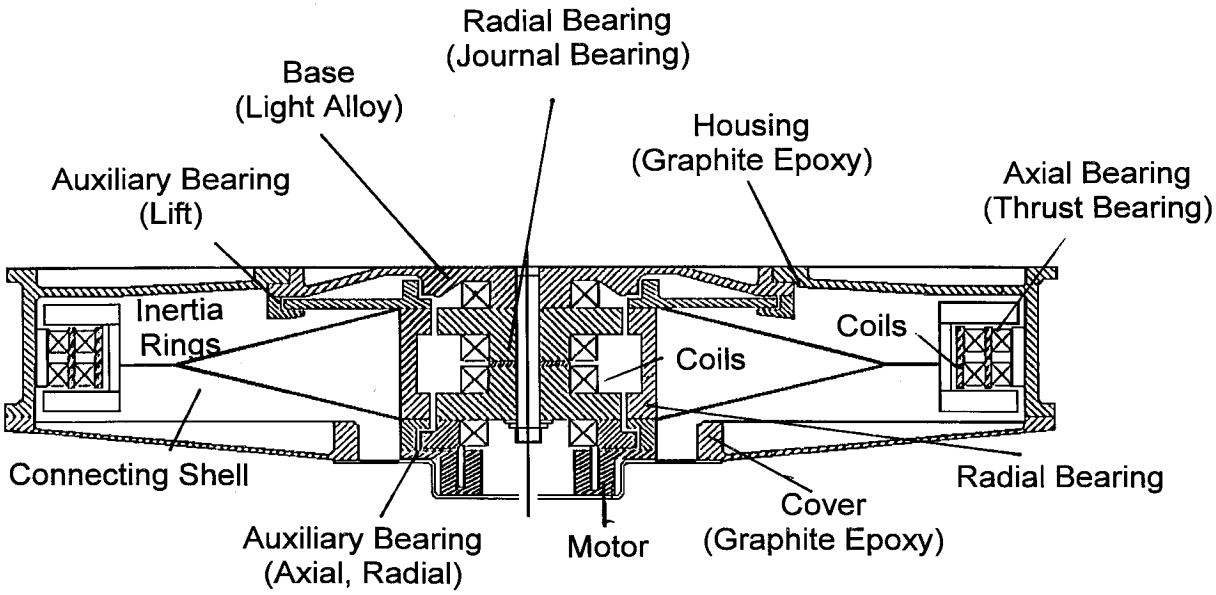

Magnetically suspended momentum wheel component layout. (Courtesy of SATCOM Technology.)

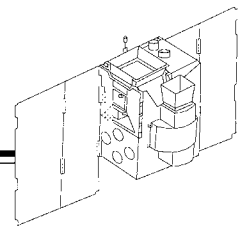

that touch-down will involve contact speeds on the order of 0.1 mph, an improvement of three orders of magnitude. As a result, GSFC researchers are examining ways of reconfiguring the magnetic bearing to relocate the contact auxiliary bearings. Also, launch survival of magnetic bearings requires special locking and caging techniques, also being examined by GSFC researchers. A solution to both problems appears possible. Still another problem with present technology involves permanent magnet biases in the magnetic bearing control circuits, which make the bearing inherently unstable during operation. Normally, active control can easily compensate for this, but a power outage would eventually force contact with the auxiliary bearings at speed. GSFC researchers are exploring techniques to eliminate or drastically reduce this bias so that the bearing is essentially gyroscopically stable with the power off.

The GAS experiment is being sponsored, in part, by the GOES project. The state-of-the art magnetic bearing is the product of an SBIR effort undertaken by SatCon Technology Corporation, of Cambridge, MA.

Contact: John Vranish (Code 723)
301-286-4031

Sponsor: Office of Advanced Concepts
and Technology

Mr. John M. Vranish, an aerospace engineer, holds several patents on robotic electromechanical systems, mechanisms and tactile/proximity/force sensors. His first invention, the Robotic Deriviter, was the top-rated Department of Defense robot innovation in fiscal year 1979. He received his BS from the U.S. Military Academy at West Point, and an MS in Electrical Engineering from The George Washington University.

TESTING AND EVALUATION

AN INNOVATIVE DATA INTEGRATION METHOD FOR ULTRASONIC IMAGING

NONDESTRUCTIVE EVALUATION (NDE) technology, which encompasses a broad field of applications such as material selection, properties characterization, defect detection, damage assessment, process monitoring, in-service sensing, etc., is an integral part of modern hardware life cycles. Although typical quality assurance procedures do not specify detailed inspection requirements, imaging techniques that directly correlate measured parameters with specimen coordinates are preferred methods for inspection reporting, and data archiving and referencing.

In recent years, advancements in computer hardware, software, and peripheral electronics technology have facilitated the development and improvement of NDE systems. Consequently, many ultrasonic imaging systems with varying degrees of sophistication have been devised. The basic ultrasonic imaging system plots proportional-gated RF amplitude with respect to each sampling coordinate. More elaborate ultrasonic imaging systems digitize and acquire entire A-scan waveforms at all sampling positions for versatile post-scan signal processing and data manipulations.

There are three basic schemes of ultrasonic image acquisition and presentation, namely B-scan, C-scan, and Time-of-Flight (TOF). The acquired ultrasonic signals are typically processed and presented in one of the following forms of visualization: grayscale, false-color, 3-D mesh, or the combination of mesh and grayscale or false-color images. Since there are no natural colors associated with the ultrasonic signals, false-color pallets are assigned to represent different bands of signal amplitude to enhance the image. In any of the above listed forms of image presentation, a single image can only display one measured parameter. We have developed a unique data acquisition and image processing system that enables the presentation of two ultrasonic parameters in an image.

First generation C-scan systems were based totally on analog technology. The images were generated by a current-driven pen across a special carbon paper. State-of-the-art systems are based on digital technology with data storage and retrieval capabilities. After the signals have been acquired by the computer, they can be manipulated in many different ways. Typically, there are three methods to present ultrasonic C-scan data: grayscale, false-color and 3-D mesh images. In all cases, the principle of image presentation is to transfer ultrasonic C-scan data to a display, where it can be expressed as: C-scan (x, y, Amplitude (x, y)) > Display (x', y', Indicator), where (x, y) are the specimen coordinates and (x', y') are the display coordinates. It is relatively easy to convert the range of ultrasonic data to a corresponding range of display indicators such as grayscale.

In our approach, in addition to acquiring amplitude information, we also simultaneously acquire TOF for each (x, y) sampling point. In this case, the transformation can be written as: C-scan (x, y, Amplitude(x, y), TOF(x, y)) > Display (x', y', Indicator1, Indicator2). The idea of using a line drawing to display specimen geometry and using color or grayscale to display associate information is not new; many finite element analysis software packages have used color to display different stress intensities on a 3-D mesh component model. Other graphic software packages also use color or grayscale to enhance 3-D mesh data drawings. Since TOF is a form of specimen depth information, we can use a 3-D mesh to display (x, y, TOF) and use color or grayscale to display amplitude. However, it is necessary to define and implement appropriate hardware and software for an ultrasonic C-scan system to provide combined amplitude and TOF image data in order to utilize the concept described here.

We have configured and integrated an advanced ultrasonic C-scan imaging system with enhanced signal acquisition, data archive/retrieval and image generation software routines. The hardware for the improved system is similar to an upgraded off-the-shelf ultrasonic C-scan imaging system that consists of a system controller, an X-Y mechanical scanner, an ultrasonic pulser/receiver, a gate-peak detector, two stepless timing gates, and a timer/counter. The X-Y scanner is programmed to move in a raster fashion using a motion controller. The scanner enables the transducer, which is mounted on the Z-axis and perpendicular to the specimen surface, to scan the specimen over the area of interest. Gate-peak-detected amplitude signals and TOF measurements at each (x, y) sampling position are acquired and stored for post-scan image generation.

Specifically, in our ultrasonic C-scan system configuration, an IBM compatible PC with an 80386 CPU, is used

as the system controller. Software routines have been developed for scan control, signal acquisition, data archiving, and image generation. An ultrasonic pulser/receiver is used to transmit and receive signals from a one-quarter-inch, 10 MHz transducer. The stepless timing gate is set to follow the front surface pulse and the gate width is set to cover the area between the front surface and back surface, including the back surface. An X-Y scanning table and a Plexiglas water tank form the mechanical subsystem.

The gate-peak-detected amplitude is acquired from a digital multimeter; the TOF between the front surface and defect pulses is acquired from a digital timer/counter through an IEEE-488 bus interface. The measured TOF of the defect indication is referenced to the front surface and can be easily converted to represent the depth of the defect from the surface. The amplitude and TOF data of each scanning coordinate are stored in a computer data file with sequential data stream architecture. A unique image processing algorithm was developed to retrieve the data from the file, process the acquired data, and produce a combined amplitude/TOF C-scan image.

To demonstrate the concept of combining two measured ultrasonic parameters, a unique test specimen was conceived and fabricated. The test piece is an 8.89-cm (3.5-in) long by 5.08-cm (2.0 in) wide by 0.64 cm (1/4 in) high aluminum plate with six 0.80 cm (5/16 in) diameter pegs as shown in the figure. The pegs are of various lengths to simulate defects of various depths in the material. The surfaces of the pegs were crafted to produce nonuniform reflections. For the experiments, the water path was set to 5 cm above the top surface of the base to give the height of the specimen. The mechanical scan speed was set to 0.25 cm/sec. The stepless timing gate was set to include the area between the main pulse and the base, including the base. The reflected pulse within the timing gate amplitude is digitized and transmitted to the computer as the amplitude measurement. The sampling increments were set to 0.025 cm for both the X-and Y-axis. The main pulse was used as the start trigger and the gated RF pulse was used as the stop trigger for the timer/counter in order to obtain the TOF measurement.

After a scan is completed, an image generating routine is executed to produce a graphic display of the acquired data set; a 3-D mesh drawing of detected flaws is displayed. For each (x, y) point, the pixel is assigned with a grayscale

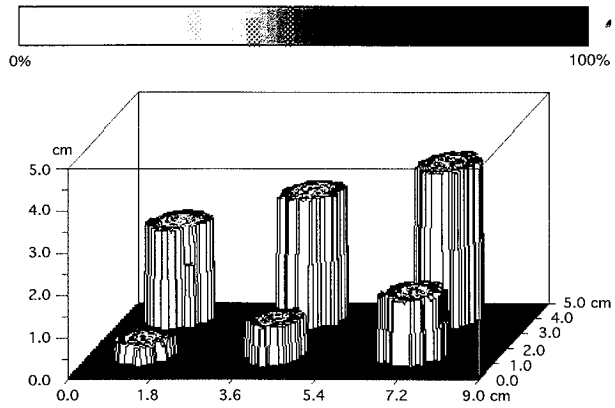

An example of the combined ultrasonic amplitude and time-of-flight C-scan image.

or false-color value based on the proportional amplitude at this position. The figure is the resulting combined ultrasonic amplitude and TOF C-scan image of the test specimen. It can be seen that the improved C-scan image directly correlates both ultrasonic amplitude and TOF data with the specimen geometry. The apparent defect parameters such as depth, size and shape can be estimated. Engineers can easily interpret the inspection result and identify anomalies associated with the specimen to determine the integrity of the structure. The inspection can be incorporated as part of a concurrent engineering process.

In modern applications, multiple NDE methods and techniques are often required to obtain various aspects of materials and defect properties of a hardware component. This new system promotes an emerging area of NDE research interest in data fusion and integration. The objective is to consolidate all pertinent NDE information and convey the results to other engineering disciplines in a comprehensive manner. Also, advanced concurrent engineering requires active integration of various manufacturing procedures into one harmonious process. It is thus necessary to convey all engineering information among each other in a common platform, namely specimen coordinates. The method that combines two distinct ultrasonic parameters in one image represents a practical example of data fusion.

Contact: E. James Chern (Code 313)
301-286-5836

Sponsor: Director's Discretionary Fund

Dr. E. James Chern is a materials engineer in the Materials Branch, Assurance Technologies Division. He earned his PhD in Physics from the College of William and Mary in 1981. Dr. Chern has been at GSFC for 5 years. His prime responsibility is research, development, engineering, and application of NDE technology for space flight project support.

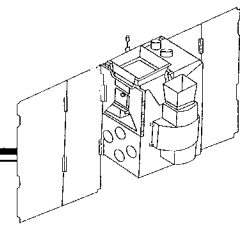

DIGITAL RADIOGRAPHY SYSTEM

THE MATERIALS BRANCH has developed a digital x-ray system that combines a real-time capability with an image quality approaching that of film-based systems. The system, assembled using off-the-shelf components, uses electronic detection; there is no consumption of film, as a result of which operational costs and the system's environmental impact are reduced. The microfocus x-ray source permits magnifications in excess of 40x. Its four-axis, motion control system yields all of the benefits of typical real-time radiographic systems. When a particular radiographic view has been set up using the real-time system, a slow-scan, charge-coupled device (CCD) camera can acquire a radiograph with near-film-quality.

The system consists of a microfocus x-ray source, a four-axis motion control system, an image intensifier with dual-port distributor, a slow-scan CCD camera, a video camera, and a Macintosh computer to control the camera system. The microfocus x-ray source has a 20- to 125-kV range (suitable for many spaceflight materials), 60 watt maximum power, and 10 μm minimum focal spot size. The system can be remotely controlled by computer. Software has been written that automatically selects and performs the tube warm-up procedure. The motion control system can manipulate a part or component in four axes (x-y-z-θ). Movements can be entered using jog keys or via joystick.

The image intensifier has a 4-inch screen. It is directly connected to a dual-port distributor that can remotely switch the intensifier output between a video camera (for real-time use) and the high-resolution, slow-scan, CCD camera (for higher-quality, digital radiographs). This latter system has 1 k by 1 k by 12-bit, slow-scan CCD. With its electromechanical shutter permitting variable exposure times, the camera system can be thought of as "electronic film."

The controlling computer has 20 Mb of random access memory (RAM) and a 19-inch color display. The computer controls the slow-scan camera system and displays images it acquires. We have written a program that automatically warms up the x-ray tube each time it is powered up. The computer also provides storage of files and access to printers (a 600-dpi laser printer using half-tones, and a continuous-tone, dye-sublimation color printer for high-quality output).

The system has been used to support a number of GSFC flight projects such as HST, XTE, FUSE, TIROS, CIRS and GCMS (the latter two are Cassini instruments). Two inspections in particular have demonstrated the system's utility. A honeycomb panel, with embedded copper antenna traces, had failed after a series of thermal cycles. The panel was positioned in the x-ray beam path, and the operator scanned the panel for breaks in the embedded conductor. A crack was readily located in one of the traces, its location precisely determined, and hardcopy of the radiograph printed out, as shown in the first figure.

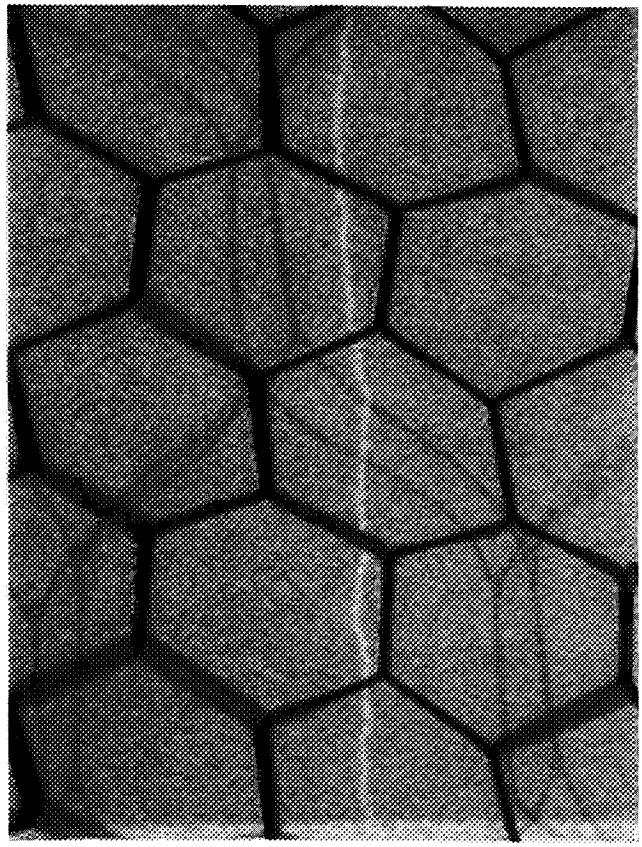

Digital radiograph of a honeycomb panel with embedded copper antenna traces. The aluminum honeycomb structure appears as dark hexagons; a composite honeycomb is visible as larger but less distinct hexagons. Most of this image includes a copper trace (note boundary between light and dark grays at top). The crack can be seen running from top to bottom through the copper trace.

The system is well-suited for inspection of printed circuit boards (PCBs). The real-time system permits high magnification inspection of relatively large PCBs, and the slow-scan system permits high-quality documentation of any flaws that are found. The second figure shows a radiograph of four plated-through holes on a coupon board. Misaligned internal annular rings can be seen as varying shades of gray circles loosely centered around each hole in the PCB.

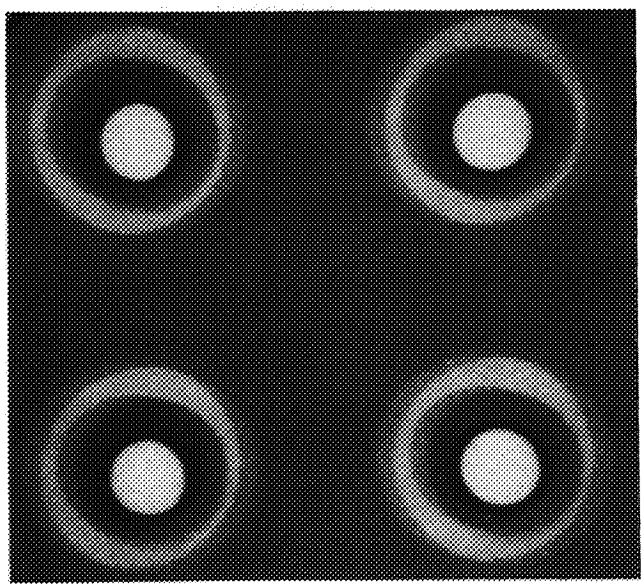

Digital radiograph of four plated-through holes on a multilayer, PCB. Misaligned, internal annular rings can be seen as varying shades of gray circles loosely centered around each hole in the PCB. The hole diameter is 0.76 mm.

Ms. Kennita Johnson, Meyerhoff Scholar from University of Maryland Baltimore County, wrote software to perform the x-ray tube warm-up.

Contact: Timothy Van Sant (Code 313.3)
301-286-6024

Bruno Munoz (UNISYS)
301-286-8425

Sponsor: Office of Safety and Mission Assurance

Mr. Timothy Van Sant is an electrical engineer in the Materials Branch. He has been at GSFC for 9 years, working on the measurement of the electrical properties of materials and the automation of materials testing.

Mr. Bruno Munoz is a senior electronics engineering technician with Unisys Corp. He has worked in GSFC's Parts Analysis Lab and Materials Branch in the course of his 10 years with Unisys.

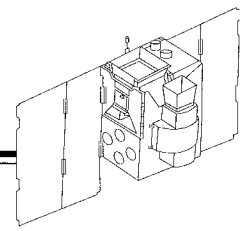

QUALIFICATION OF MULTICHIP MODULES AND ADVANCED INTERCONNECT TECHNOLOGIES FOR HIGH-RELIABILITY SPACE APPLICATIONS

THE REQUIREMENT THAT A NEW technology perform within a range of proven reliability and functionality is an impediment to transferring that new technology into space flight projects, as it is easier to use mature technologies through standard-part programs. Yet, new technologies are finding their way into space flight applications because there are increasing demands for systems with greater functionality and higher density requirements than can be provided by existing technologies. The Electronic Packaging and Processes Branch at GSFC uses several powerful techniques to understand the reliability risks associated with each new technology. By combining the use of theoretical and empirical data we are able to identify potential concerns in making new technology available for critical space flight applications.

Qualifying new electronic packaging technologies is essential to validate the design, manufacturing, and overall integrity of these technologies to reduce or avoid the risk of failure. Traditional screening and qualification methods developed for monolithic devices may not adequately address failure mechanisms associated with new advanced interconnect technologies (AIT). These AITs, such as multichip modules (MCMs) and sealed-chip-on-board (SCOB), provide space-related projects with improvements in performance, size, volume, and weight. The advanced interconnect structure undergoes technical assessment, product evaluation, and reliability modeling to determine screening and qualification guidelines, and to identify and understand the failure mechanisms. The technical assessment of the advanced interconnect structure involves a design review and a process survey, which entails an assessment of the design process to ensure that the advanced interconnect structure is designed for reliability, manufacturability, and testability.

Potential quality problems and issues are further examined in the product evaluation phase through thermal characterization and materials testing. Thermal evaluation involves characterizing the thermal performance of the AIT under full-power conditions. Materials testing is performed as necessary to determine effects of such nonlinear behavior as creep and stress relaxation. Additionally, construction analysis is performed to "reverse engineer" the AIT to obtain data and information about materials, assembly processes, and the overall integrity of the AIT structure. The first figure shows a 10 Megabyte memory stack module in the preliminary stages of the construction analysis.

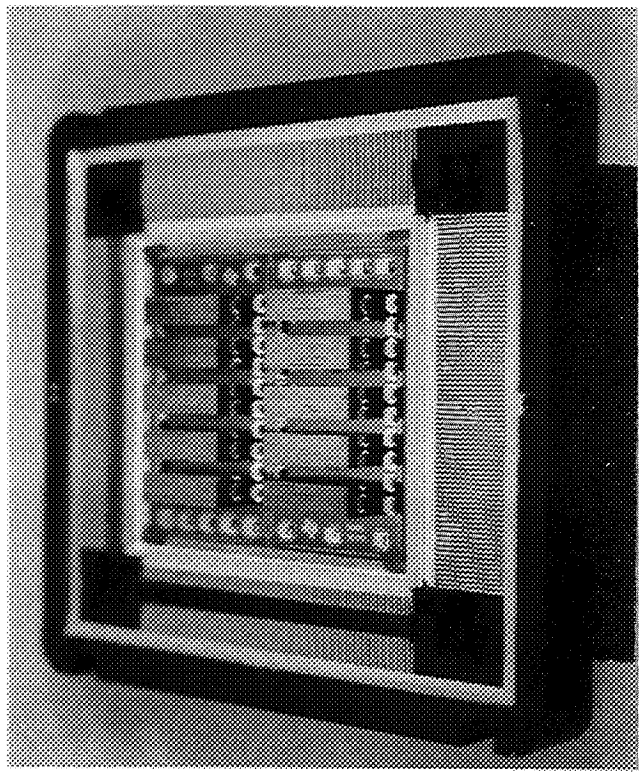

Memory stack module under construction.

The reliability modeling task involves closed-form modeling and finite element analysis (FEA) to predict the limits of temperature, temperature range, thermal gradients, and vibration environments necessary to induce overstress in the advanced interconnect structure leading to failure of structural elements. The second and third figures depict stresses caused by vibration at the natural frequency and thermally induced stresses for a memory stack module, respectively.

Closed-form modeling is performed to assess potential wear-out mechanisms and provide the boundary conditions necessary to determine performance in space environments. In addition, minimum test requirements for accelerated testing are evaluated and projected to various

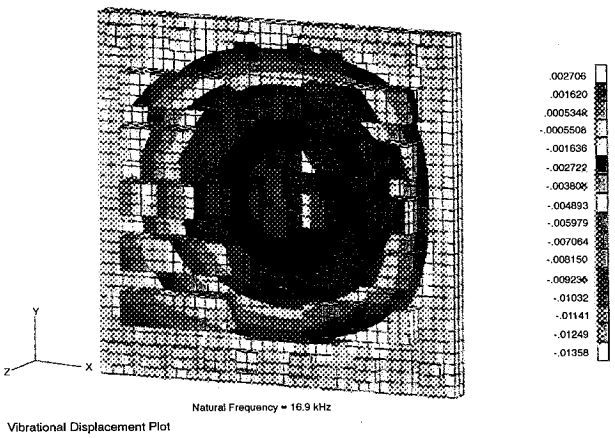

Vibration-induced stresses on the memory stack module.

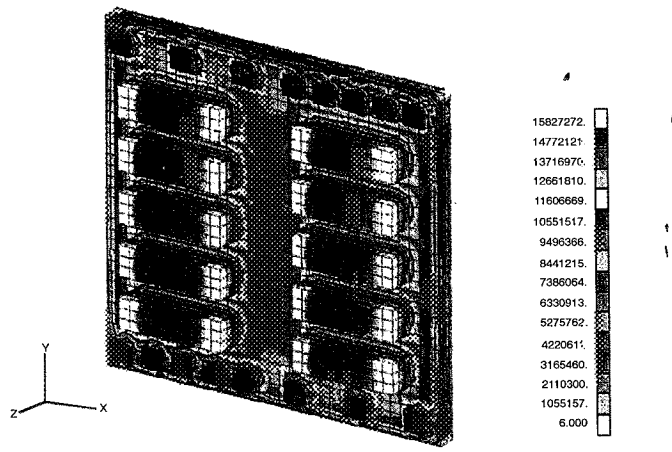

Thermal-induced stresses on the memory stack module.

environments. Closed-form predictions are refined with FEA techniques to calculate thermal and structural responses of the overall structure to various environments. Parametric studies for various environments and material characteristics are also performed to put bounds on stresses and temperatures and to determine conditions necessary for overstress. After testing and evaluating the advanced interconnect structure, failures will be analyzed to determine the cause of failure. This information is provided to the designers to enable them to modify their designs.

This approach to determining screening and qualification guidelines for using AIT in space flight hardware has been successfully completed for various GSFC projects including the Global Geospace Science Project (GGS) (using SCOB on the SEPS instrument), the Explorer Project (SMEX SWAS) (using a stacked-chip approach for a high-density memory), and the TRMM (using high-density interconnect with 56 microcircuit chips of mixed technology buried in a substrate).

This methodology is vital in closing the knowledge gap between what is known about traditional mature packaging technologies—such as the long-established military ceramic parts found on Qualified Products Lists—and the newer AIT's.

Contact: Ann Garrison (Code 312)
301-286-7123

Sponsor: Office of Safety and Mission Assurance

Ms. Ann Garrison is the Branch Head for the Electronic Packaging and Processes Branch. She holds a BA from Penn State University and an MS from the University of Maryland. She has extensive background in private industry manufacturing electronic components for high reliability applications.

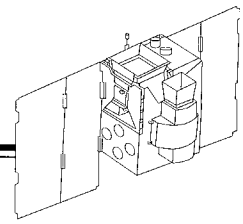

DEVELOPMENT OF A REUSABLE PARACHUTE TEST SYSTEM

A UNIQUE, REUSABLE instrumented drop body has been designed for flight qualification testing of new, larger capacity parachute recovery systems for the Black Brant family of sounding rockets. Project duration and costs have been greatly reduced by designing a deployable ballast section. This ballast section, which is jettisoned after completion of the main parachute test phase, allows the remaining instrumented drop body to become buoyant in water and to be recovered by a surface vessel, allowing economical testing using existing local NASA tracking facilities and personnel. The drop body, which is deployed from a NASA aircraft, contains an on-board video camera, self-contained and programmable triaxial acceleration sensors, and an on-board telemetry system for transmitting acceleration and housekeeping data to a ground station.

Design requirements for the 43.8 cm- (17.25 in-) diameter test body include a variable length parabay whose diameter is 33.0 cm (13.0 in), designed to be reusable and deployable from existing NASA aircraft; on-board instrumentation to measure flight parameters; a minimum and maximum weight capability of 147.6 and 681.0 kilograms (325 and 1500 lbs), respectively; and able to use local NASA facilities to track payload impact in the Atlantic Ocean near Wallops Island. The test vehicle consists of a Standard Black Brant Ogive Recovery System Assembly (ORSA), retrofitted to a parabay length of 66.0 cm (26.0 in); a sealed, watertight section with a self-contained and programmable triaxial acceleration sensor, accelerometers, and other housekeeping components that transmit data to a ground station through an on-board telemetry system, and system logic; an externally mounted, watertight video camera housing; and a deployable ballast section. The recoverable portion of this Modified ORSA Recovery Test Instrument (MORTI) is 2.439 m (96 inches) long, and includes a 1.296 m (51 in) long floatation compartment. Ground-based optical and radar tracking devices provide additional data.

The system is armed as it exits the aircraft. When passing through an altitude of 3,353 m (11,000 feet), the drogue plate (which extracts the reefed drogue parachute) is pyrotechnically deployed by a pressure-sensing switch. The drogue unreefs 6 s later. The reefed main is extracted 14 s after initial drogue deployment. The ballast section is dropped when a timer activated pyrotechnic fires at approximately 610 meters (2,000 feet) above the water. The remaining portion of the drop body descends on the parachute until it impacts and floats in the ocean.

The MORTI test body, as described, has been successfully flown, recovered, refurbished, and reused three times.

Contact: Mendel Silbert (Code 841.2)
804-824-1527

Christopher Shreves (Code 823.1)
804-824-2184

Sponsor: Office of Space Science

Mr. Mendel Silbert received a BS in Mechanical Engineering from the University of South Carolina. He has worked with NASA Sounding Rockets and Balloons projects for over 30 years.

Mr. Christopher Shreves received a BS in Mechanical Engineering from the Virginia Polytechnic Institute and State University. He has worked on various NASA engineering projects for over 7 years.

A TENSION FIELD MODEL FOR USE WITH COMMERCIAL NON LINEAR FINITE ELEMENT CODES

SCIENTIFIC BALLOONS are low-cost platforms for space and upper-atmosphere exploration. Lacking good predictive methods, the design of scientific balloons in the past has been an expensive trial-and-error process. Successful designs arrived at by this method became a confining mold; departure from this mold was fraught with danger.

Weight-efficient and sound design of balloons requires reliable prediction of their structural response for the full flight regime, from launch to float at altitude. This remains a goal that has not yet been achieved. However, during recent years, good analytical predictions of the at-float shape have been obtained. These predictions are the basis for the current development of a long-duration balloon vehicle concept that departs sharply from limitations imposed by simplifying assumptions.

During ascent, the gas volume contained in the pneumatic envelope expands to approximately 250 times the volume at launch and the balloon undergoes large configuration changes. So far, structural analysis predictions are limited to the at-float shape in which the pneumatic envelope is fully deployed. A trial-and-error analysis sequence, during which the analyst uses information from the previous analysis step to modify the model for the subsequent step, extends the predictive capability to configurations with mild deviations from the fully deployed shape.

To automate the analyses of such configurations and to allow analysis of more general balloon configurations that exhibit partial wrinkling of the skin, a tension field (TF) formulation has been developed for use with a commercial nonlinear finite element code. This is a first step towards developing tools for the analysis of ascent shapes.

Stiffened thin skins and membranes have no or only minimal capability to sustain compressive forces, while their capability to sustain tensile forces is limited only by the material properties. In a statically indeterminate configuration, these 2-D structural elements may respond to a loading by a large, out-of-plane oscillatory deformation (i.e., wrinkling) to effect a rearrangement of the load path, leaving the 2-D structural element in a uni-axial stress state. Standard 2-D continuum strength-of-material models—such as the membrane, or the thin shell—are not suitable to represent this nonlinear structural response. In structural elements that possess some bending stiffness, the onset of this condition represents an elastic instability, and the stable, load-sustaining configuration is a post-buckling state.

An appropriate 2-D continuum model for this structural response mode is the tension field. The TF may be viewed as a degenerate state of the standard 2-D strength-of-material continuum model (plate, shell, or membrane). It avoids the details of the out-of-plane displacement altogether and responds to in-plane displacements that shorten distances perpendicular to the tension direction by yielding without resistance. The TF concept was introduced in the 1920s in a statically determinate application. More recently, a TF theory based on a relaxed-strain-energy-density (RSED) concept was developed, and an RSED concept in a finite element (FE) application broadened that approach by including a visco-elastic material model. This last TF model falls short of computing true tension field response by accepting the strain transverse to the nonzero principal stress as computed from Poisson's effect in the nondegenerate case.

The TF/FE formulation, that was developed for the Balloon Projects Branch, models the in-plane deformation of the TF correctly, if approximately. It uses a penalty parameter formulation for developing the tangent stiffness matrix. It is suitable for use with a commercial non linear FE code that has provisions for interfacing with a user-furnished material model subroutine. This TF model was developed for FE analyses of balloons that exhibit moderate degenerate membrane response (wrinkling) in some regions of the pneumatic envelope.

Several validation tests have been conducted with: (1) the suspended flat panel uniformly loaded at the free bottom edge; (2) the clamped initially plane square membrane pressurized into a bubble; (3) the pressurized right cylindrical cantilever tube with a transverse tip load; and (4) the pressurized infinite cylinder subjected to twisting deformation. The TF behavior and the extent of the degenerate regions are well approximated by this formulation for test cases 1 through 3. The twisted cylinder problem is also solved. In this problem, only kinematic conditions are imposed. The entire model is in a tension field state.

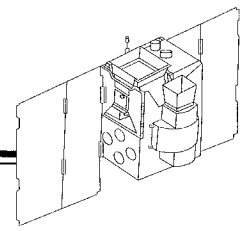

Test case 1 is somewhat similar to the tension testing of a thin film test coupon; the top and bottom edges of which are clamped and the mid-section wrinkles when the sample is subjected to tension. The tension field formulation predicts the extent of the degenerate region for test case 1 (first and second figures). Other comparisons between the predictive model and observed phenomena are underway.

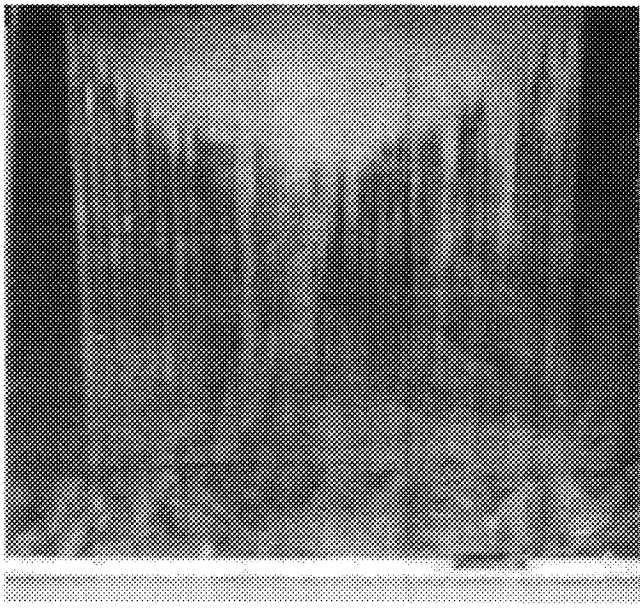

Flat sheet with weights suspended from bottom edge to demonstrate wrinkling of the material.

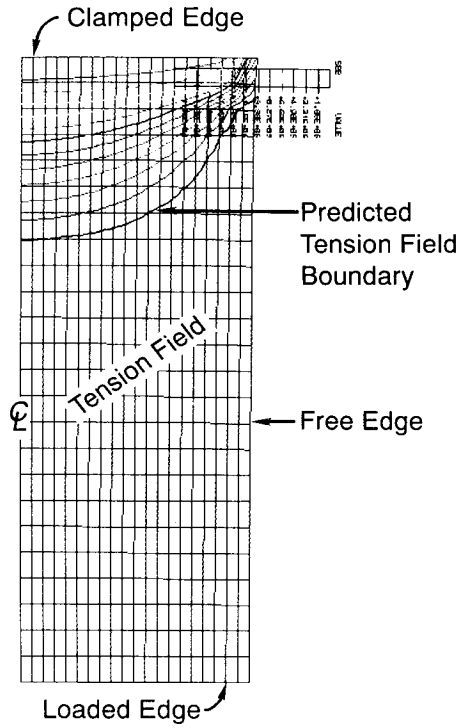

Half model of the flat sheet. The nonlinear finite element analysis with the tension field formulation predicts the extent of the wrinkled region.

This work is being done under contract by Dr. Willi W. Schur of New Mexico State University/Physical Science Laboratory.

Contact: Joel Simpson (Code 842)
804-824-1070

Sponsor: Office of Space Science

Mr. Joel Simpson is an aerospace engineer in the Balloon Projects Branch at Wallops Flight Facility. He is currently involved in performing balloon structural and performance analysis and in the development of new balloon systems. He received his BS in Aerospace Engineering from the University of Maryland, and has been working in the Balloon Branch for 8 years.

FLIGHT PROJECTS

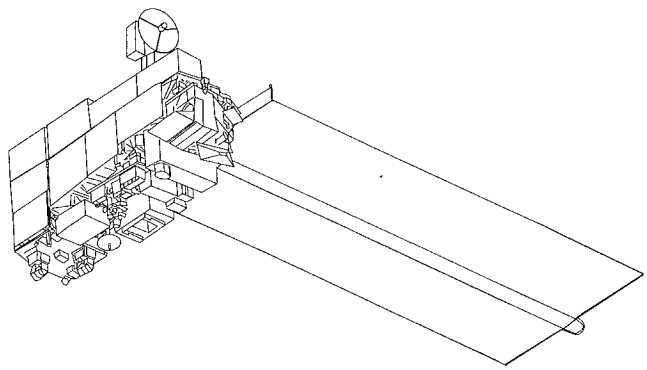

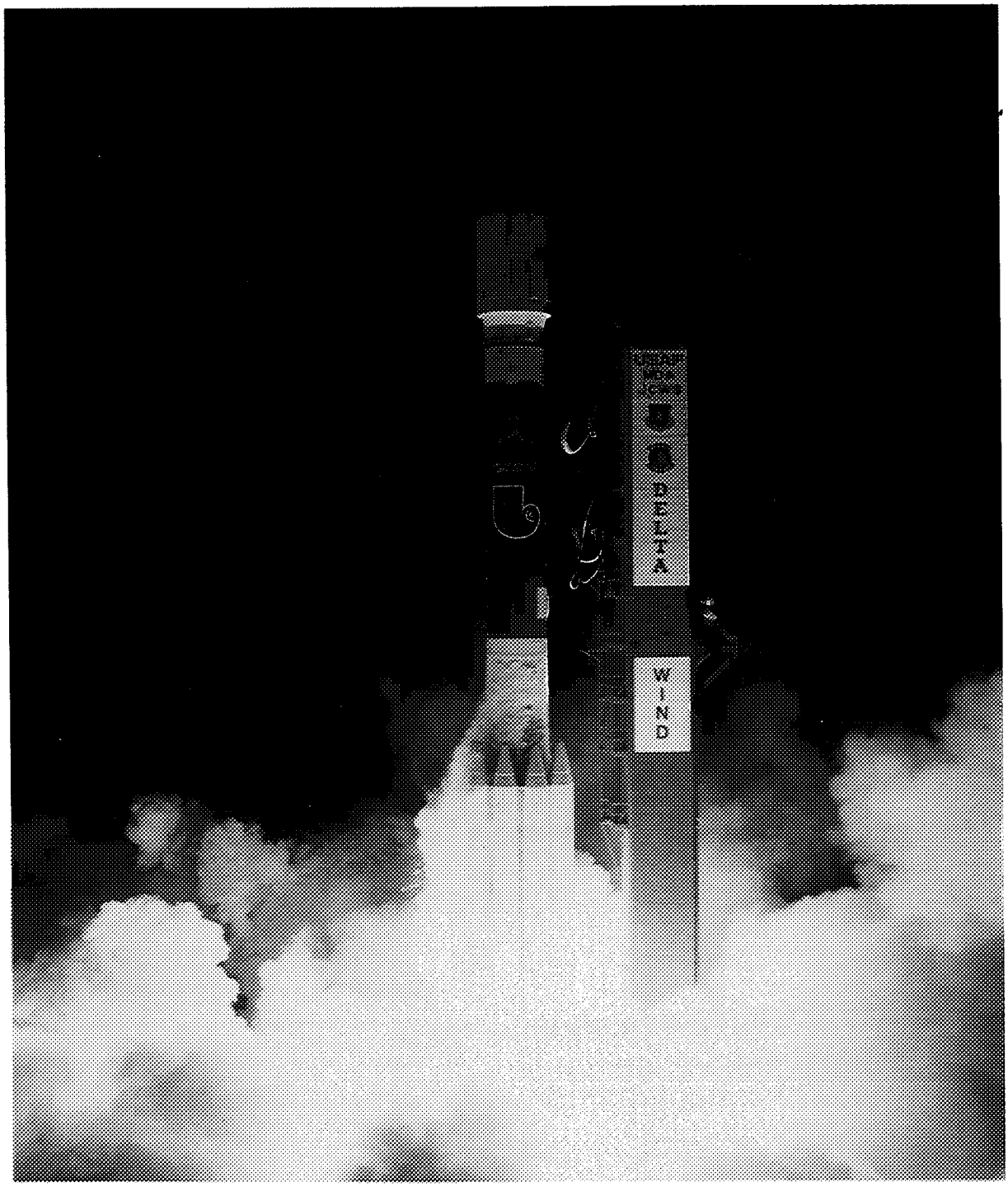

A Delta II was successfully launched from Complex 17B at Cape Canaveral Air Station on November 1, 1994 at 4:31 a.m. EST. The Delta II was carrying the NASA Wind Satellite into orbit.

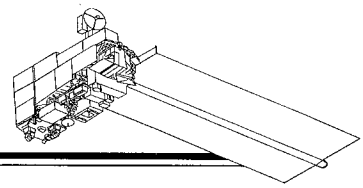

FLIGHT PROJECTS

THIS PAST YEAR was a banner one for the Flight Projects Directorate. The spectacular and flawless Hubble Space Telescope (HST) First Servicing Mission (FSM) in December 1993 culminated years of intensive effort and detailed preparations and set the stage for a remarkable number of accomplishments in 1994 as the telescope was restored to a condition which exceeded its initial design specifications. Most visible to the public were images of the Comet Shoemaker-Levy impact on Jupiter. These near-real-time views of an unprecedented observable cosmic event caught the attention and sparked the imagination of people throughout the world. The first "proof" of the existence of a black hole and the first measurements of the elusive Hubble constant were also provided by the HST. Seeing this important national facility operating as well as (and better than) initially designed is a source of great satisfaction for the entire extensive Goddard and contractor team.

In April 1994, another major milestone was passed with the successful launch of the long-delayed GOES-I geostationary weather satellite. Following an intensive checkout phase, the satellite (renamed GOES-8 at launch) was turned over to the National Oceanographic and Atmospheric Administration (NOAA) for use by the National Weather Service. From its first test image to its most recent operational products, the quality and usefulness of this very capable new satellite has been obvious. Our customer is delighted with the results. The ultimate reward will come when lives are saved during severe storms because of the precise information provided by the GOES system.

In early November, the Wind spacecraft was launched into its unique orbit by a workhorse Delta launch vehicle. As of this writing, the spacecraft is checking out perfectly, and all instruments have been turned on successfully.

The year was not without its disappointments. Failure of an Air Force launch on a Pegasus rocket in June delayed subsequent launches, including the environmentally important Total Ozone Mapping Spectrometer (TOMS), as well as FAST, the second small Explorer spacecraft.

The next polar orbiting weather satellite (NOAA-J) is in final preparation for launch at Vandenberg Air Force Base in December 1994. All of this activity is a forerunner of the coming year with 11 Goddard launches currently planned during 1995. These include the last of the current series of Tracking and Data Relay Satellites, another GOES, the next polar orbiting weather satellite (NOAA-K), TOMS, small Explorers FAST and SWAS, Delta-class Explorer XTE, three satellites in the International Solar-Terrestrial Physics program (Polar, SOHO, and Cluster), and the Argentinian spacecraft (SAC-B).

Vernon J. Weyers

HUBBLE SPACE TELESCOPE PARTICIPATES IN WORLDWIDE CAMPAIGN TO OBSERVE COMET SHOEMAKER-LEVY 9'S PLUNGE INTO JUPITER

DURING ONE INCREDIBLE week—July 16 to 22, 1994—members of the Hubble Space Telescope (HST) Project at the Goddard Space Flight Center (GSFC), the Space Telescope Science Institute (STScI) in Baltimore, and a competitively selected team of Hubble scientists joined astronomers worldwide in a campaign unique in the annals of astronomy and astrophysics: observations of the destruction of more than 21 cometary nuclei plunging into the atmosphere of Jupiter, and measurements of an extremely diverse array of effects and changes to the giant planet's atmosphere and surroundings following the impacts. The "collision" of comet Shoemaker-Levy 9 (S-L9) with Jupiter is the first time in history that the impact of one solar system body with another was known more than a few seconds in advance. In this case, astronomers had over a year to plan, and the scientific results are so wonderful that they strain our vocabularies.

Comet S-L9 is (or was) a comet that became tidally disrupted during an extremely close passage by Jupiter in July 1992. Discovered as an extraordinary "train" of material and emission in March of 1993 by Eugene and Carolyn Shoemaker and David Levy using a wide-field Schmidt telescope at Mt. Palomar, the comet was soon discovered to be multiple, and in orbit around Jupiter. Because nearly all known comets orbit the Sun, this association with Jupiter was highly significant. A detail of its orbit sent pulses racing: the location of the next so-called "peri-Jove"—or closest approach to Jupiter—in July 1994 was calculated to be inside Jupiter's atmosphere! In contrast, the previous peri-Jove, in July 1992, which was unobserved and responsible for the tidal breakup, was above the cloud tops—evidence that the comet's orbit had been perturbed by the Sun's gravitational field between 1992 and 1994.

In the fall of 1993, the STScI Director issued a special Call for Proposals for HST observations of the comet fragments, their impacts, and their effects on Jupiter and environs. This resulted in the selection of six teams addressing: comet S-L9 (Hal Weaver, Principal Investigator), spectroscopy (Keith Noll), atmospheric dynamics (Heidi Hammel), cometary particles and aerosols in Jupiter's atmosphere (Robert West), Jupiter's upper atmosphere (John Clarke), and comet S-L9's impact on the Io Torus (Melissa McGrath). This science team was granted more than 100 orbits of HST time to conduct observations before, during, and after the impact week of July 16 to 22. A great deal of attention was given to planning a strategic timeline and to maximize the scientific output of HST observations. The team had to grapple with a great many operational concerns and restrictions in developing its "final" plan, not the least of which was the constant change in the orbital solutions and associated impact times for each of the 21 fragments.

In the final weeks before the first impact (that of fragment "A"), there had been much speculation that the 1- to 3-kilometer (km) diameter (estimated) cometary nuclei would not hold together. Some analyses indicated that they would become tidally dispersed into much smaller chunks that individually (and collectively) would not be capable of producing the spectacular subcloudtop explosions and fireballs that had been predicted on the basis of very sophisticated computer modeling of intact impactors. In some scientific circles there was a sense that the whole campaign was going to fizzle (that at best an observer on Jupiter would witness a supercloudtop meteor storm (21 of them, actually) but no huge fireballs and rising plumes).

The plunge of fragment "A"—supposedly one of the smaller ones of which little was expected—proved the optimists right. HST's Wide-Field and Planetary Camera 2 (WFPC2) obtained a multiorbit block of exposures commencing shortly after the predicted time of impact of "A". When the images were inspected by the Science Team, there was cause to break out champagne: a prominent "plume" of heated gases rose to >1,000 km above the limb of Jupiter, and then fell back down to the planet in a manner nearly identical to computer models of kilometer-size impactors exploding below the cloudtops. On subsequent orbits, as the impact site of "A" rotated into the field of view (all 21 impacts took place on the backside of Jupiter, close to the rim of the planet), HST provided extremely detailed views of startling new and long-lived features associated with the impact—a small dark spot and wedge surrounded by a thin circular ring, outside of which, in the southwest direction, was a diffuse and dark "smudge" in the shape of an unclosed oval. This morphology would be seen by HST again and again in the days ahead as a result of subsequent impacts. The interpretation is that the small central spot and wedge mark the fragment's entry into the atmosphere, and the extended smudge is the light-absorbing plume "blanket" (i.e., the plume material after

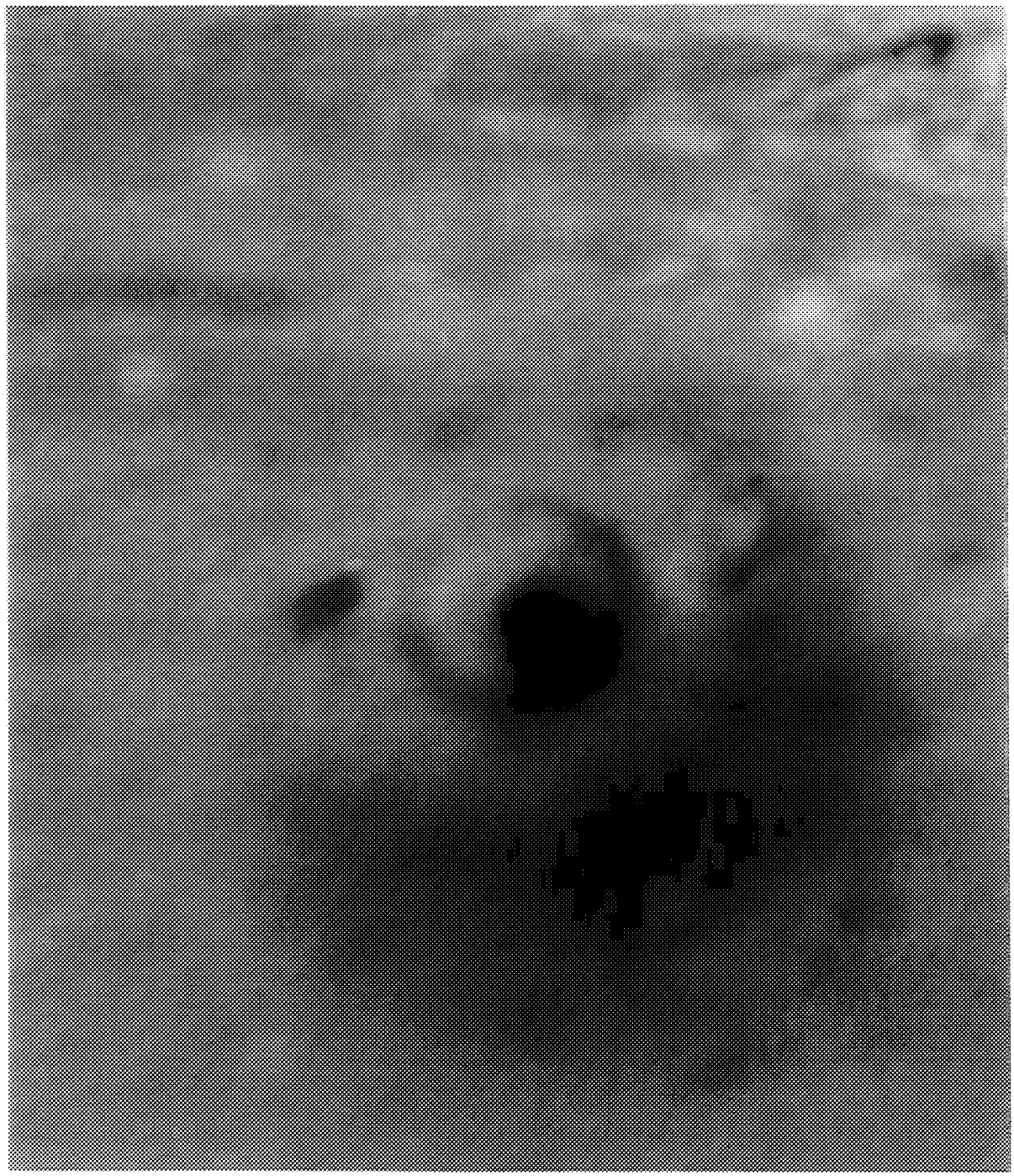

HST image of the impact site of fragment "G" from comet S-L9. The image has been processed to correct for the curvature of the disk of Jupiter, so that the spot appears as it would to an observer looking overhead. The dark crescent was produced by material thrown high into Jupiter's stratosphere by the G explosion. The inner ring is probably a sound wave expanding from the site of the explosion. The dark spot just outside of this ring is the impact site of (smaller) fragment "D." (Credit: Hubble Space Telescope Comet Team and NASA.)

collapse back onto the planet), its directionality and lack of closure produced by all fragments' 45 degree angle of entry into the atmosphere. The nature of the thin ring(s) became apparent following the impact of large fragment "G" on July 18.

Much was expected of "G"—it was among the 6 or so "major" fragments and was thought to be about 3 times the size of "A" (3 vs. 1 km); the ratio of energies to be delivered by impact was therefore predicted to be about 25:1. If "A" was so spectacular, what would "G" bring? The HST Team didn't have long to wait. A tremendous fireball and plume rising 2,200 km above the limb were seen in association with "G", and images of the impact site (see the first figure) arranged in a time lapse or movie format showed that the thin ring expanded with time. The measured expansion speed, 800 meters per second, is essentially identical to the predicted sound speed in Jupiter's stratosphere. Close examination of the images showed a faint ring inside the principal one; its expansion speed matched that expected of tropospheric sound waves. What we have, then, is the excitation of acoustic shocks and waves as a result of the impacts. One can even see evidence for the variation of sonic speed with atmospheric height.

Because previous impact sites were still very obvious and dramatic as the newer fragments entered the atmosphere and exploded, Jupiter began to take on a very scarred look as the "Impact Week" wore on. The HST image in the second figure is evidence for the large-scale longevity of the spots. Essentially, all of the impacts produced visible spots of greater or lesser size and contrast. With time, these features began to spread out due to diffusive (e.g., wind-driven) processes, but it is clear that the visible effects of the impacts will be with us (and Jupiter) for a long time.

HST spectroscopy with the Faint Object Spectrograph (FOS) and Goddard High Resolution Spectrograph (GHRS) produced some of the most spectacular results. The principal goal of this effort was the detection of new chemical species not previously seen on Jupiter, brought up from the lower levels of the atmosphere as a result of the buoyant plumes produced by the fragments' final explosions below the cloudtops. The spectroscopists also wanted to look for evidence of the molecular and atomic remains of the exploded comet fragments. In fact, it was critical to try to decide what was cometary and what was Jovian in any new detections. "Before" and "after" comparisons of impact site "G" showed that, in addition to the startling changes seen in the images, there were profound alterations in chemistry. The surface brightness was substantially depressed in the ultraviolet (UV, around 2,000 Angstroms) after the impact, a sure signature of absorption by newly created ammonia in the gas phase (ammonia normally exists on Jupiter in the form of solid ice crystals in ammonia clouds). There are many other "new" spectroscopic detections; indeed, too many to describe here. Of note is the detection of diatomic sulfur (S_2), the likely presence of hydrogen sulfide (H_2S), and comet-associated metals, such as magnesium (Mg II). Disentangling the chemistry of the various regions before and after the impacts will be a real challenge for the modellers, and it is especially fascinating that the different species have their own characteristic behavior with time following the impacts.

Far ultraviolet imaging by HST using both WFPC2 and the European Space Agency (ESA) Faint Object Camera (FOC) showed profound auroral and magnetic field effects as a result of the cometary impacts. Because scattering of sunlight is more pronounced in the UV than at visible or infrared wavelengths, UV images probe the upper atmosphere and can show the effects of Jupiter's "northern and southern lights", produced when energetic electrons travelling along the planet's magnetic field come streaming down into the upper atmosphere near the north and south poles, causing the gases there to glow. What we saw with HST during "impact week" was the production, in the northern hemisphere, of aurorae at lower latitudes, where they are not normally seen. The evidence that these are probably comet related is magnetic: field lines connecting the southern impact sites to the northern hemisphere are predicted to lie on top of the anomalous aurorae seen in the HST images. These were very exciting results.

This is but a snapshot of the total science output of the Hubble Space Telescope for July 16-22, and it does not address the invaluable contributions made by other orbiting spacecraft, such as the International Ultraviolet Explorer (IUE) and Galileo, by high-flying aircraft, like the Kuiper Airborne Observatory (KAO), or by the ground-based (especially infrared) observatories, such as the Infrared Telescope Facility (IRTF), Cerro Tololo InterAmerican Observatory (CTIO), and Keck facilities. The weeks and months ahead will be exciting ones as scientists pore over their data and begin to understand the many and complicated phenomena produced by these extraordinary cometary impacts into Jupiter. Based on what we've learned so far, it would seem that this campaign

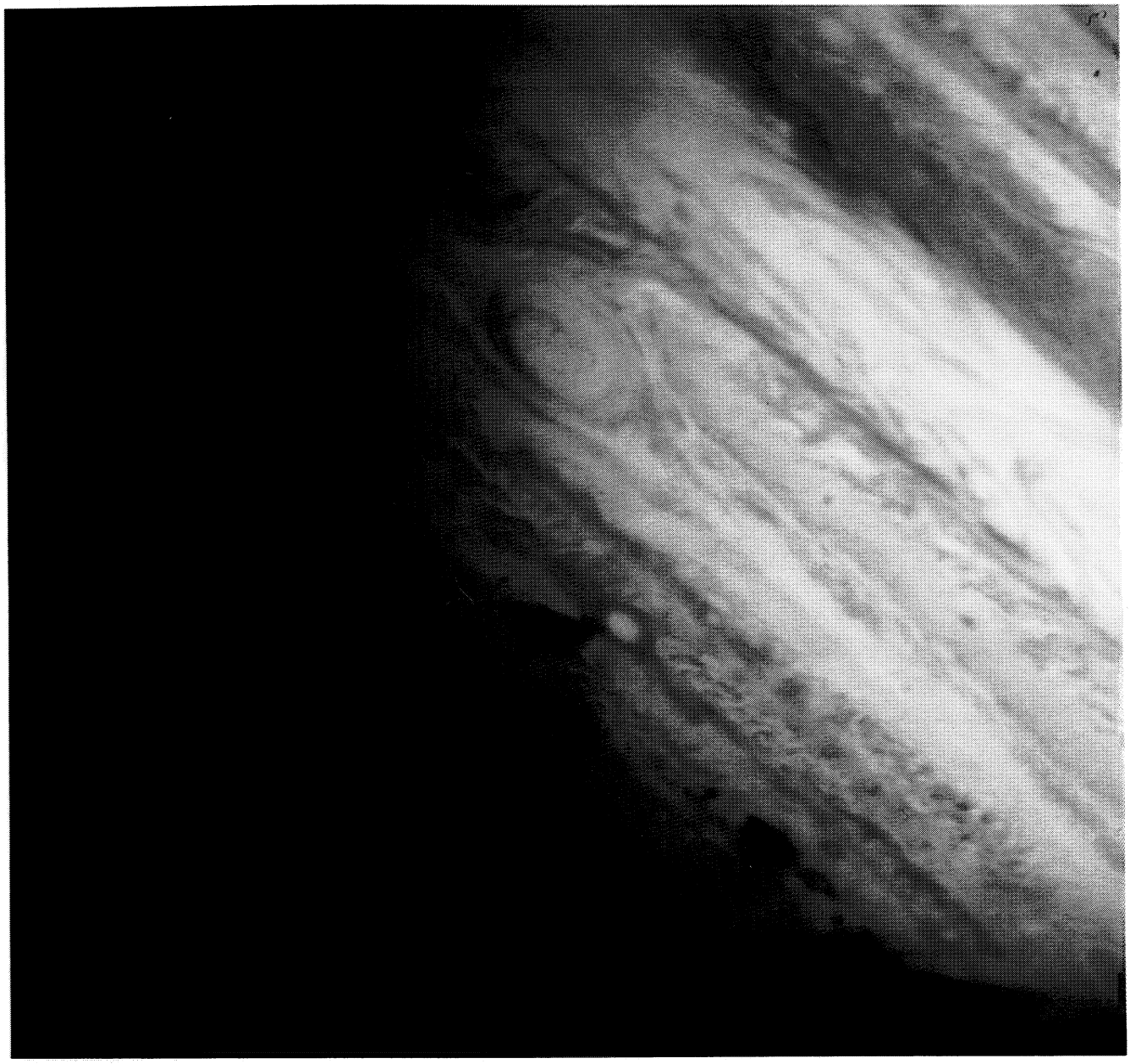

HST image of Jupiter showing eight impact sites. From left to right are the E/F complex (barely visible on the edge of the planet), the star-shaped H site, the impact sites for tiny N, Q1, small Q2, and R, and on the far right limb the D/G complex. (Credit: Hubble Space Telescope Comet Team and NASA.)

has far exceeded even the most optimistic of preimpact predictions.

From the Hubble Space Telescope point of view, I do not cease to marvel that a scant 7.5 months separated two incredible weeks in our lives: the First Servicing Mission, which restored our dreams for the HST, and comet S-L9/Jupiter, which reawakened in all our minds the knowledge of how incredible the universe and our solar system really are.

It is a pleasure to acknowledge the scientific heroes of this tale for the Hubble Space Telescope Project. They are Drs. Hal Weaver, Keith Noll, Heidi Hammel, Robert West, John Clarke, Melissa McGrath, Alex Storrs, and their colleagues. It was these individuals who, working with members of the STScI and the National Aeronautics and Space Administration (NASA)/GSFC, assembled the productive "timeline" of observations that resulted in the enormous treasure of data briefly summarized here.

Contact: Malcolm Niedner (Code 684.1)
301-286-5821

Sponsor: Office of Space Science

Dr. Malcolm Niedner, Jr. is an astronomer and Deputy Senior Scientist for the Hubble Space Telescope. He has been a civil servant for 14 years at GSFC. He received an MS and a PhD in Astronomy from Indiana University, and a BS in Physics from Brown University. His primary research interests are in the areas of comets, their interactions with the solar wind, and the structure of the solar wind in three dimensions.

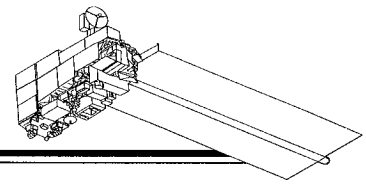

DEVELOPMENT OF AN OPTICAL DATA STORAGE AND RETRIEVAL SYSTEM FOR THE HUBBLE SPACE TELESCOPE

MAJOR ADVANCES in astronomy are expected from the HST Program during its 15-year lifetime. We have already seen some amazing results, particularly the photographs of the impact of Comet Shoemaker-Levy on Jupiter. More data will be collected by Hubble than by any previous unmanned spacecraft. Indeed, approximately one terabyte of new data will be received annually. Collected data must be managed, and a system put in place to provide an efficient means for astronomers to access those data. In response to this challenge, NASA, the STScI, and Loral AeroSys are putting the finishing touches on the HST Data Archive (HDA).

The HDA provides rapid and easy access to the immense quantities of data in the archive. Researchers will consult the catalog, that describes the archived data, to identify datasets of interest, which can then be requested from the archive. To manage reprocessed data and extended mission life, the archive is designed to accommodate up to 65 terabytes of data over the life of the mission. Up to 12 gigabytes of data can be received, cataloged, and stored on optical disk daily. All data received is copied and sent to the European Coordinating Facility (ECF) in Munich, Germany, as well as at the Canadian Astronomy Data Center (CADC) in Victoria, BC. Up to 146 users may be logged on to the system simultaneously; these users will request the electronic transmission of up to 22 gigabytes of data per day, with a peak of 2 gigabytes per hour. Approximately 2.5 gigabytes of data will be distributed daily on magnetic and optical media.

HDA functions can be logically divided into three groups, as shown in the first figure. The archive is responsible for receiving, maintaining, and distributing data from the HST.

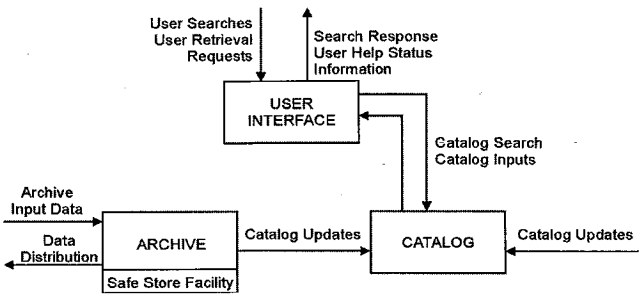

HDA functional overview.

Data received from the ground system are written to optical disk for insertion into the archive. A second copy of the optical disk is written and placed into a safe-store facility to ensure that data are not lost in the event of a problem at the primary archive site. The archive function will also retrieve data and distribute them to authorized users. The catalog assists users in identifying specific datasets to support their scientific research. Users can rapidly search through descriptive information about the data contained in the archive. This descriptive information is extracted from the data as part of the archival process. The user interface function provides the facilities to communicate with users on a variety of networks and systems. It also provides menus and forms to simplify the user's task of locating information.

A key challenge to system designers was to develop a cost-effective system design that supports scientific research and provides a growth path as requirements change. Through the use of modular architecture, growth paths are simplified, as modules can be both added and expanded. A modular design allows future changes to be localized to the affected module without having an impact on the entire system.

The HDA system design (shown in the second figure) uses a modular approach to implement the required functionality. The archive, catalog, and host subsystems implement the three functional groups described above. A backup subsystem provides redundancy to increase system availability. The subsystems are configured in a clustered architecture. This cluster environment allows for sharing of data and distribution of workloads to provide higher system and data availability than what is currently afforded by a single processor. A cluster configuration provides flexible growth as processors can be added or processes within the cluster can be upgraded for increased processing capability.

The Archive Subsystem is based on a VAX processor connected to redundant input/output (I/O) computers. These I/O computers reduce the processing load on the main processor, thereby allowing more devices to be connected. They also add flexibility by localizing device dependencies at the I/O computer, making technological changes in storage and distribution devices transparent to the VAX architecture. In addition, overall performance is

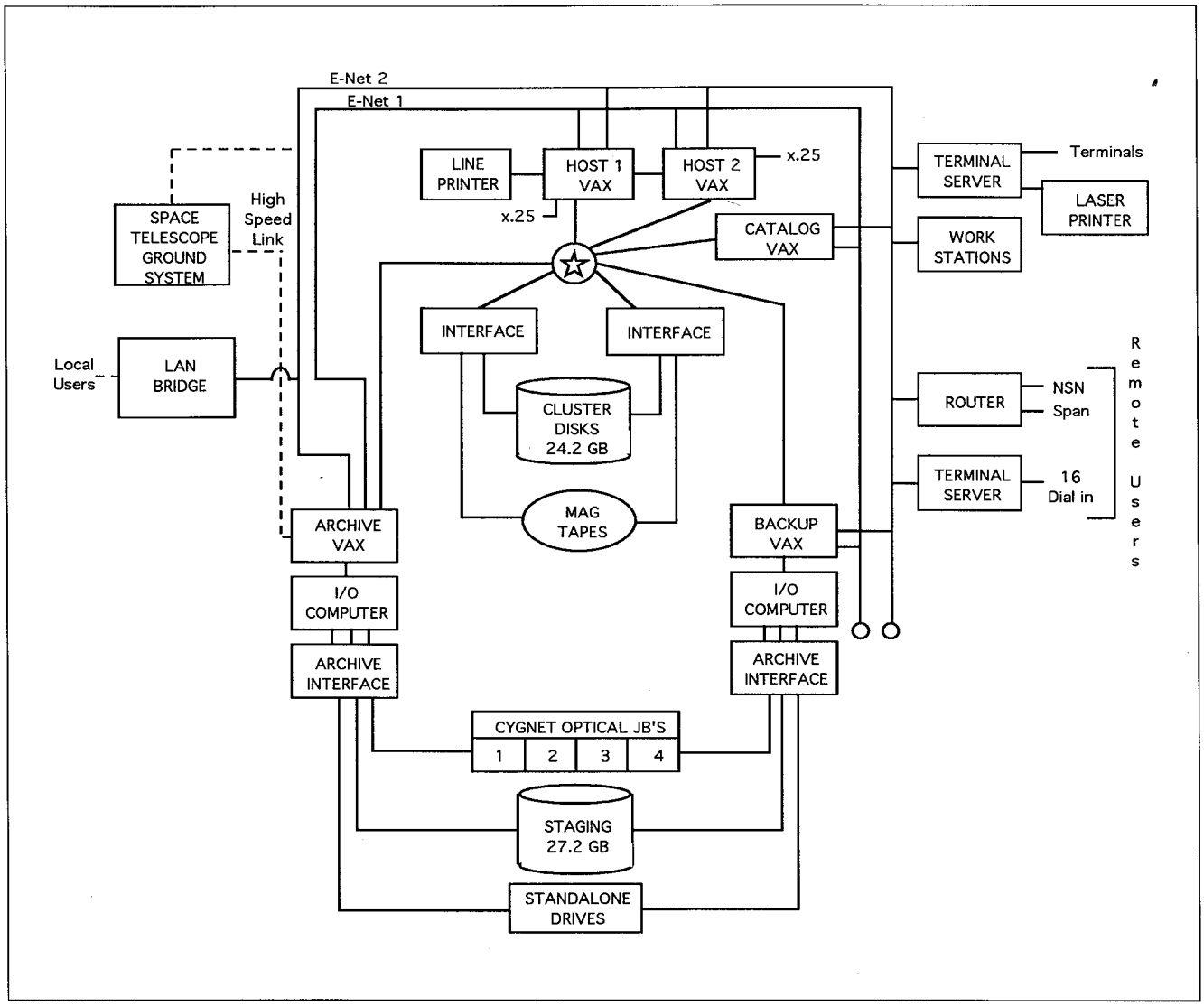

HDA system design.

improved by moving I/O processing to the I/O computer, thereby making the VAX available for central processing unit (CPU)-bound computations.

The storage system is based on Write Once, Read Many (WORM) optical disk technology. This technology helps to ensure that valuable data will not be overwritten or lost. Four Cygnet optical disk jukeboxes are connected to the I/O computer. Each jukebox contains 131 optical disk platters and two Sony optical disk drives. At 6.55 gigabytes per optical platter, there are 3.4 terabytes of storage available in the on-line archive. The two optical drives per jukebox allow one platter to be fetched while another is being read. Higher performance can be gained by implementing small computer systems interfaces to the I/O computer and additional drives to the jukebox (each jukebox can handle up to four drives). Stand-alone optical drives are also connected to the I/O computer. These drives are used to produce the optical platters distributed to the international archives. Using stand-alone drives allows these platters to be produced without interfering with ongoing archive and retrieval functions.

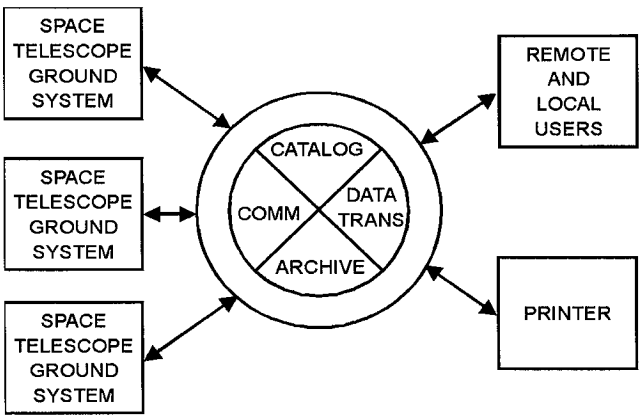

HDA transaction processing system.

Viewing the HDA as a transaction processing system leads to a software architecture based on a client-server model, as shown in the third figure. This model provides isolation of system functions and loose coupling among the system elements by allocating services (e.g., archive management, catalog access, and communications) to individual servers. Client elements make requests from the servers to provide a specific service.

Software in the Archive Subsystem controls the jukebox robotics and manages data. The system must know the specific platter on which all files are located and where within the archive each platter is located. If the platter is on-line, the system must know in which slot of which jukebox the platter is situated. For a platter which is off-line, the system must send a message to operators to load the platter. The HDA also implements a migration policy so that the most-often-used platters are maintained on-line, and less-frequently used platters are migrated to the off-line archive.

Database functions, including the catalog, are implemented through a commercial Relational Database Management System (RDBMS) provided by Sybase. The data server portion of the RDBMS executes on the Catalog Subsystem, while the client portion executes on the Host Subsystem. Catalog data is volume-shadowed for data integrity and fault tolerance. Records written to one disk of the shadow set, for example, are duplicated on a second disk. In the event of a disk failure, processing continues uninterrupted on the remaining disk.

The HDA is currently being loaded with data in preparation for opening this facility to the astronomical community. Full operations are expected by the end of 1994.

Contact: P. Christopher Schwartz (Code 441)
301-286-7345

Mark Kaufman (Loral AeroSys)
301-805-0534

Sponsor: Office of Space Science

Mr. Christopher Schwartz is the HST Deputy Systems Development Manager on the HST operations and Ground Systems Project. He earned his BS in Physics and Computer Science from the University of Maryland and his MS in Biomedical Engineering from George Washington University. He has been at GSFC for 6 years.

Mr. Mark Kaufman is currently the manager of systems, hardware, and test engineering at Loral AeroSys, Seabrook, MD. He earned a Bachelor of Engineering from Stevens Institute of Technology and an MSEE from University of Maryland.

THE SERVICING AID TOOL: A HIGH PERFORMANCE TELEROBOTIC SYSTEM

IN DECEMBER 1993, the world watched as NASA restored the HST to full health. This mission proved beyond doubt the value of manned servicing, but because of the unprecedented amount of extravehicular activity (EVA) it also strained the resources of the Shuttle systems and warranted the assignment of the most experienced crew in history. In a March 1994 study (Applications of a Robotic Serving Tool to the HST Second Servicing Mission: An Internal Study of Benefits and Constraints, HST Flight Systems and Servicing Project, Flight Projects Directorate, Goddard Space Flight Center, March 1994), the HST Flight Systems and Servicing Project concluded that, by assisting the astronauts in servicing tasks, a robotic tool could provide reduced EVA timelines, increased probability of mission success, increased mission flexibility, increased science capability, and reduced mission risk. The Servicing Aid Tool (SAT) is a GSFC-built system that provides these benefits.

The SAT is a flight qualifiable, teleoperated robotic tool designed to meet servicing mission and manned flight safety requirements (see the figure). It was conceived in 1987, when the GSFC Satellite Servicing Project identified a need for a low-cost, robotic manipulator to accomplish Orbital Replacement Unit (ORU) servicing of the Extreme Ultraviolet Explorer (EUVE) satellite. Flight hardware development began in 1991, with an eye towards a planned 1995 EUVE mission. When this mission was later dropped, the SAT was picked up by the HST Flight Systems and Servicing Project as an advanced servicing system for potential HST servicing missions. In the past year, these efforts culminated in delivery of the flight hardware, and successful testing to flight-predicted levels in vibration, thermal/vacuum, and electromagnetic environments. In so doing, the SAT program constitutes an achievement for GSFC in providing the viability of adapting inexpensive commercial robotic hardware for space flight application.

The SAT achieved a remarkable cost effective $5 million from concept to tested hardware by modifying a sound, commercially available manipulator system to survive spaceflight. Modularity in its design has further magnified its cost-effectiveness by allowing for inexpensive reconfiguration from EUVE to HST use and, most recently, Space Station applications. Expensive avionics and computer systems were avoided by basing the systems on a suite of flight-standard hardware and MIL-grade hardware tested vigorously at full-system testing.

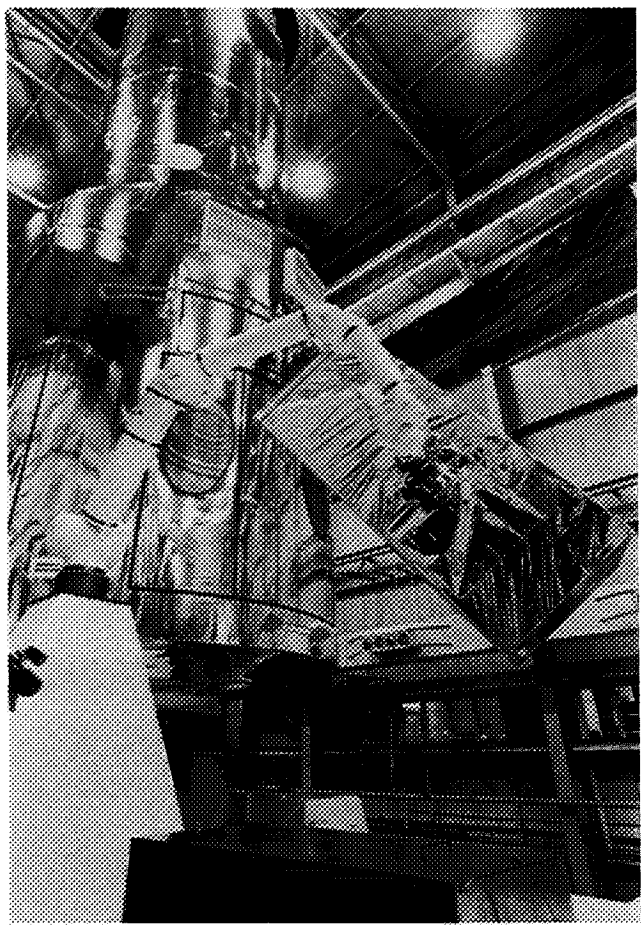

The SAT holds the axial instrument mockup, with a full-scale model of the HST in the background.

In its present configuration, the flight-qualifiable SAT system consists of a six degree-of-freedom (DOF) slave arm, kinematically similar to the Shuttle Remote Manipulator System (RMS), mounted on a one-DOF positioning link. The arm is smaller, stiffer, more precise, and more dexterous than the RMS. The positioning link, which is controlled separately from the arm, is used to position the arm and end-effector properly into the required work space.

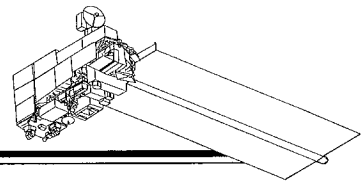

The arm will be controlled by the astronauts from a workstation located in the Shuttle's aft flight deck. Two, 3-DOF rate controllers of the same design and function as the units currently used to control the Shuttle's RMS are used to operate the manipulator. The astronauts monitor the arm's operation through the starboard aft window, as well as on the Orbiter's closed circuit television system, control panels, and multifunction cathode-ray tube (CRT) display system. Additionally, the arm's operations will be monitored on the ground at the Johnson Space Center Payload Operations Control Center.

Extensive end-to-end testing of proposed HST Second Servicing Mission task simulations have recently been completed; astronaut evaluations are to be received by the end of 1994. Results have been promising, and indicate the SAT could speed EVA changeout operations, improve lighting and camera operations, and potentially assist in HST reboost. Associated computer model studies indicated an increase of 66 percent in reach (from 12 ft to 20 ft); an additional joint would enable access to all primary servicing bays of HST with minimal cost impact.

The SAT is uniquely well-situated to benefit from innovations in NASA's robotic research centers and, in turn, to facilitate the commercialization of these technologies for industry. Both are direct results of deriving the flight SAT's hardware and architecture from the existing commercial line of Robotics Research Corporation (RRC) manipulators. In the first case, RRC's manipulators have become the de facto standard in NASA's research centers and sponsored academic institutions; thus most of the products of the various research efforts are "plug-compatible" with the flight SAT. Hence, the process of transferring these technologies to the SAT for flight applications is simple, straightforward, and virtually prewired. We call this the "spin-on" process. The "spin-off" process is also facilitated via the RRC connection for the same reasons. In fact, RRC has already commercialized joint technologies developed in the SAT program, and has proposals pending for the transfer of the highly advanced controls technologies to industry in partnership with some of the nation's largest manufacturers. The GSFC-developed SAT is the right solution at the right time.

Contact: Mark Jaster (Code 442)
301-286-9232 (GSFC)
202-358-4527 (NASA Headquarters)

Sponsor: Office of Space Systems Development

Mr. Jaster is the EVA Servicing Manager with the HST Flight Systems and Servicing Project. He earned a BS in Biomedical Engineering from Duke University in 1984, and an MS in Manufacturing Systems Engineering from Stanford University in 1990. Mr. Jaster has been employed at GSFC for 4 years, where he has managed the SAT Program and led the EVA efforts supporting the HST First Serving Mission. He is presently on detail to NASA Headquarters in the Space Station Program Support Office with responsibilities for robotic systems and technologies in the International Space Station Program. In 1994, Mr. Jaster was awarded GSFC's Exceptional Achievement Award and the Astronauts' Silver Snoopy for his contributions to the HST First Servicing Mission.

GLOBAL GEOSPACE SCIENCE EQUIPOTENTIAL SURFACE CONTROL

TWO SOPHISTICATED spacecraft, the Wind and Polar Laboratories, have been developed by the Global Geospace Science (GGS) Project. These cylindrically shaped (2.4-m diameter by 1.8-m high), spin-stabilized spacecraft contain numerous scientific instruments that measure the properties of particles and fields in the upstream region between the Earth and Sun, as well as the effects of the solar wind on the Earth's magnetosphere. The accuracy of many of these experiments is strongly affected by the presence of ambient plasma-spacecraft electric potentials. Thus, a spacecraft design is required that is immune to the effects of electrostatic charging in orbit, and that eliminates differential charging of outer surfaces caused by particle bombardment and geomagnetic substorms. Electromagnetic cleanliness has been achieved for the Wind and Polar Laboratories by meticulous attention to the elimination of stray electric and magnetic fields through state-of-the-art material screening and selection processes and by incorporation of careful grounding schemes. Equipotential surface control considerations have had a particularly profound influence on the designs of solar array panels and long lanyard deployed booms as well as in the choice of all insulation blanket materials and external coatings. This article highlights some of the unique methods employed to maintain electrostatic cleanliness and to limit the potential difference between any two points on the outer surfaces of these two spacecraft to an exceptionally low value (not to exceed 1 volt).

Power is provided to the Wind and Polar spacecraft by curved, body-mounted solar array panels. The substrate of each panel is aluminum honeycomb, populated with 2- by 2-centimeter (cm) solar cells. Each solar cell is protected from radiation damage by a 40 mil quartz coverglass, overcoated with 700 Angstroms of indium tin oxide (ITO), a conductive layer that allows even charge distribution and electrical connection to adjacent coverglasses. As with all such arrays, the complete assembly has a mosaic appearance with small gaps or seams between cells. For most spacecraft, these gaps are of little consequence, but for the GGS missions exposure of nonconducting materials used in the construction of a solar array panel would result in unwanted local charging and potential differences. A development program was undertaken early in the design phase to evaluate methods of eliminating this concern. Three test- (or Q-) boards were fabricated, each with a different coverglass interconnect scheme, and were cycled over wide temperature extremes (-150° to +130°C) to determine what manufacturing technique would ensure that flight arrays could survive worst-case environmental conditions experienced during launch and in orbit. After extensive testing, it was shown that filling these gaps with 2 mil-thick silver mesh strips was the best technical approach, even though this method is labor-intensive. Integral tabs were fashioned at right angles to these strips, which allowed bonding of the mesh to the ITO coating on the coverglasses, as shown in the first figure. A conductive silicone adhesive (CV 1500) was chosen for this purpose. In addition, an oval spot of epoxy was used to electrically link the adjacent corners of every four-cell combination. Finally, to prevent differential charging of coverglasses with respect to neighboring spacecraft materials, the coverglasses along the edges and cut-outs in each solar array panel were grounded to the substrate.

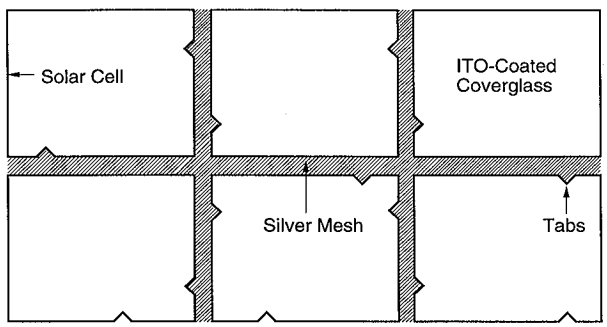

Solar array surface features.

Long, lanyard-deployed booms, built by Able Engineering, are employed on both the Wind and Polar Laboratories to position sensitive electric and magnetic field instruments far from the main body. The two Wind booms are each 12 m in length and are normal to the spin axis, whereas the two for Polar are 6 m each, and are canted downward about 3.5° to minimize field-of-view impacts on imaging instruments. All booms are curled up and stowed in canisters for launch. By necessity, many of the materials used in construction of such flexible structures are nonconducting. The three longest members, or longerons, are single-filament fiberglass rods. Battens of like material, and diagonals made of phosphor-bronze braid maintain the triangular shape and stiffness of the booms after deployment, as shown in the second figure. Titanium plates, chosen to reduce eddy currents induced by

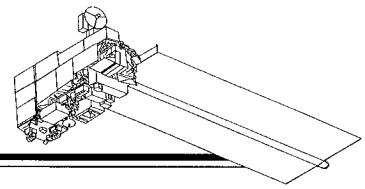

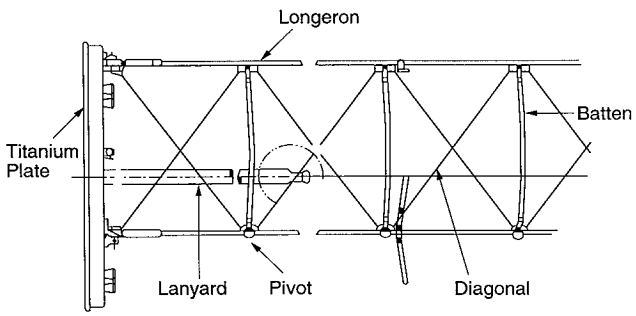

Lanyard boom configuration.

temperature gradients, support the instruments at the appropriate location. To meet electrostatic cleanliness requirements, each fiberglass member and all associated electrical cabling are covered with an aluminum wire braid. The nature of the assembly is such that there are hundreds of joints and pivots that must be conductively tied together. To maintain end-to-end electrical integrity, the three longeron braids and six diagonal elements at the base of each boom are connected to spacecraft ground.

An extensive test program was conducted to verify that all requirements were met. Because of difficulties with braid abrasion that occurred during initial vibration testing, stack compression was increased, an anti-clocking device added to two of four booms, and chafe guards incorporated near every pivot point. Subsequent tests, including numerous deployments, have demonstrated that corrective measures have provided the desired performance. Despite the large number of joints and piece-parts in these complex structures, a conductive area in excess of 99.95 percent of the total surface area has been achieved.

A comprehensive evaluation of insulation blanket materials and external coatings was also conducted to define an acceptable treatment for exposed spacecraft and instrument surfaces. Thin-film (2 mil), aluminized Kapton with a sputtered ITO coating on the outboard Kapton face was chosen as the outer layer for all GGS blanketing. To maintain electrostatic cleanliness in flight, the ITO coating and all blanket layers are electrically coupled to the spacecraft structure by ground wires and conductive Velcro strips. Because of concerns over potential damage to the integrity of the ITO coating from handling during blanket fabrication, installation, and removal during certain ground operations, crumple tests were performed. Results indicated that, with reasonable care, cracking and flaking could be avoided. In addition to insulating films, various paints and optically selective coatings were tested to determine their suitability for use on GGS thermal radiators, instrument outer surfaces, collimators, and aperture covers. White, yellow, green, and black conductive paints as well as bare metal samples and selective films were exposed to an electron beam with a current density and energy levels representative of those in orbit. The tests were performed over a temperature range from +25° to -150°C. It was found that bare metal surfaces generally met requirements. Some selective coatings fared well after exposure to the simulated Wind environment, but were adversely affected by Polar radiation levels. Evaluation of paints yielded mixed results. Some yellow, green, and black paint formulations were judged satisfactory for Wind and Polar application, but were nevertheless used sparingly. A careful review of each coating was performed prior to use to determine its range of acceptability for the intended application.

All of the electrostatic cleanliness and equipotential surface control provisions described here have been verified to comply with previously stated requirements. Resistivity of external spacecraft surfaces and electrical resistances between outer surfaces and spacecraft ground have been measured with sensitive ohm-meters. These measurements, an adjunct to a comprehensive component and spacecraft qualification program, are further assurance that methods employed to meet the challenging set of GGS science objectives will be successful in orbit.

Contact: Paul Caruso (Code 406)
301-286-8019

Sponsor: Office of Space Science

Mr. Paul Caruso is the GGS Observatory Manager and Technical Representative for the spacecraft prime contract with Martin Marietta. He earned a BS in Engineering Physics from Loyola College in Baltimore, Maryland and an MS in Aeronautical Engineering from the Pennsylvania State University. He has been employed by GSFC for 27 years.

THE POLAR DESPUN PLATFORM MECHANISM

THE POLAR LABORATORY is one of two space craft being developed under the auspices of the GGS Project. In compliance with primary science objectives, it will monitor interactions between the solar wind and the Earth's magnetosphere, and will also provide dynamic pictures of the aurora at different wavelengths, with far higher resolution than that afforded by any previous mission. The spacecraft, illustrated in the first figure, is spin-stabilized in a highly eccentric polar orbit. A despun platform provides an inertially stable mounting surface for several imaging instruments. The orientation and control of this platform is performed by the Despun Platform Mechanism (DPM), a high-precision electromechanical device that maintains a fixed platform position while the main body of the spacecraft rotates at 10 rpm. This mechanism has some unique features and capabilities, and, as a result, presented some technical difficulties during the development cycle.

Designed and built by Honeywell Satellite Systems Operations in Glendale, Arizona for a specified 3-year life, the DPM has presented numerous technical challenges. Its principal components (shown in the second figure) include brushless motors, bearings, an optical encoder, control electronics, and a 69-ring slip ring assembly that provides uninterrupted electrical contact between the platform and spacecraft. A retention/release clamp band assembly and metal diaphragms unload the bearings and lock the platform for launch. Control of the unit is maintained by dedicated software resident in the spacecraft command and attitude processor. The DPM is about 43 cm in diameter by 41 cm high. Its mass is 37 kilograms (kg); it consumes an average power of 8 watts. By comparison with similar devices, the bearing assembly has a relatively large diameter of about 22 cm. The unit can operate on the ground while supporting a load of 113 kg.

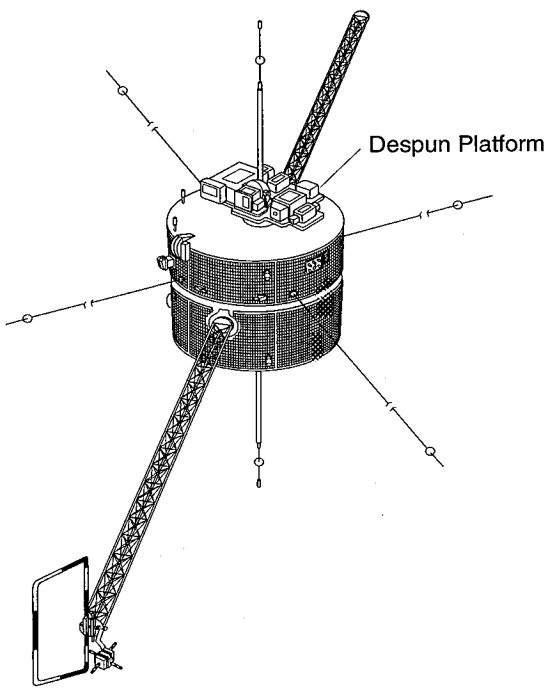

The Polar laboratory.

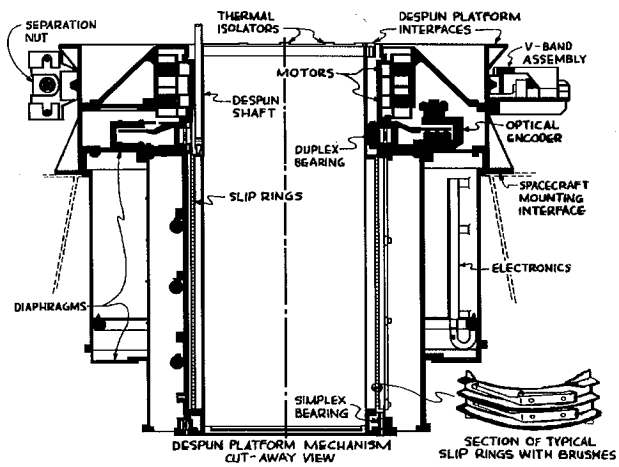

Despun platform mechanism.

Early in the program, it was recognized that the originally proposed single-protoflight-unit-approach was high risk. More test hardware would be needed to prove viability of design and assembly techniques, and to verify that lifetime requirements could be met. As a result, an Engineering Development Model (EDM) and a Life Test Unit (LTU) were added. Both of these units were fully utilized and paid major dividends by bringing to light design weaknesses before completion of protoflight DPM integration and testing.

During environmental testing of the EDM, some stiction and high torques at start-up were recorded at ambient conditions and at -30°C in vacuum. After careful

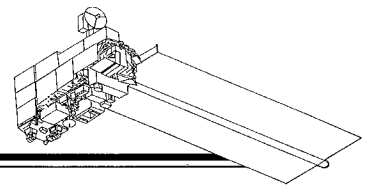

disassembly, some Teflon toroids, placed around every other ball in the duplex bearing for spacing, were found to have been damaged. The problem was traced to an out-of-round bearing race caused by preload and fit-up effects. This condition, in turn, made the toroids jam, producing ball speed variations. A combination of these speed variations and contamination found in the races then produced excessive toroid wear. Tests were performed to determine minimum required preload consistent with DPM pointing requirements. Drag torques were reduced significantly. In addition, several bearing design modifications were evaluated to reduce potential for wear. A segmented phenolic retainer, impregnated with a lubricant, was finally used to keep the 120 ball bearings equally spaced. Subsequent EDM testing proved highly successful, and these changes were incorporated directly into the protoflight unit. Upon delivery to the spacecraft prime contractor, Martin Marietta, the EDM performed another critical role. It was used for closed-loop testing in both spinning and despun modes in order to check proper end-to-end operation with a simulated spacecraft and early versions of flight software. Operational modes included DPM position, rate, maneuver, and calibration.

Another problem arose during accelerated life testing. Plans called for an LTU, consisting of the basic housing, shaft, and flight-like slip ring/brush block assemblies, to be run continuously in a vacuum at ambient temperature. Spin rates of 10 and 30 rpm would be imposed in order to obtain the equivalent of 3 years of operation. Evaluation of slip ring/brush wear was the primary objective. After the first month of operation, electrical shorts started to develop. Inspection of this unit revealed that the brushes were scratching slivers of silver off the slip rings and that the debris was falling across adjacent brush tangs. The desired isolation from one brush to the next was thus affected. Although initially judged to be the right material for light brush pressure (4.5 psi) applications, the soft silver surface applied to the slip rings proved to be incompatible with DPM geometry and speed. As a corrective measure, the slip rings were coated with hard (or coin) silver. In addition, all brush tangs were conformally coated to eliminate the potential for shorts caused by metallic debris. Life testing was resumed at 10 rpm and terminated after 1 year. Final disassembly and inspection showed no undue wear and verified that these changes were effective in resolving this issue.

Problems with the optical encoder also occurred. EDM data demonstrated that alignment of the optical encoder with the duplex bearing assembly was critical. Misalignments caused several scratches in the glass encoder disk. An optical encoder anomaly also arose on the protoflight unit. After vibration and during cold thermal-vacuum testing, optical encoder drop-outs were evident. These were eventually traced to some debonding of the encoder disk and to debris inside the lens barrel assemblies. Small-scale tests showed that the lenses were free to rotate during vibration and generated debris. This debris blocked the optical path from the light emitting diode to the read-out station on the other side of the encoder. A clamp was developed to stabilize the optical encoder disk from further debonding, and a new retention scheme was devised for the lens barrel assemblies. After these modifications were made, the protoflight DPM successfully passed all remaining tests and has now been integrated with the Polar Laboratory.

These and other lesser difficulties, not recounted here, provided a significant set of technical challenges during the development of this very complex mechanism. It is particularly important for designers of similar hardware to recognize the importance of materials selection and to institute strict quality control at each step in the build-up process. Attention to the smallest detail is mandatory to assure ultimate performance at the highest level of assembly.

Contact: Paul Caruso (Code 406)
301-286-8019

Sponsor: Office of Space Science

Mr. Paul Caruso is the GGS Observatory Manager for the Wind and Polar Laboratories and played an active technical management role in the development of the Despun Platform Mechanism. He earned a BS in Engineering Physics from Loyola College in Baltimore, Maryland and an MS in Aeronautical Engineering from the Pennsylvania State University. He has been employed by GSFC for 27 years.

REAL-TIME SOLAR WIND EXPERIMENT TO FLY ON ADVANCED COMPOSITION EXPLORER MISSION

THE ADVANCED COMPOSITION Explorer (ACE) mission is scheduled to be launched in late 1997. It is a spin-stabilized satellite that will orbit the L1 libration point while being pointed toward the Sun, for at least 2 years while its nine science instruments take measurements. Three of those instruments, the Magnetometer (MAG), Solar Wind Electron, Proton and Alpha-Particle Monitor (SWEPAM)-Ion sensor, and the Energetic Electron, Proton and Alpha-Particle Monitor (EPAM) will demonstrate ACE to be an effective platform for providing Real-Time Solar Wind (RTSW) data that could be used to forecast solar and geomagnetic storms.

The possibility of providing RTSW data was studied by GSFC as part of the ACE Phase B effort. The study was initiated in 1989 at the request of the NASA Headquarters Space Physics Division. During this period, the National Oceanic and Atmospheric Administration (NOAA) expressed an interest in this matter, as did other agencies. In December 1992, NOAA requested that NASA consider flying a NOAA-supplied RTSW monitoring package as a secondary payload on ACE. The data supplied by this hardware would, among other things, be used to provide a 1-hour warning of geomagnetic disturbances to satellite operators and power companies. A detailed study of the NOAA proposal was made and tentatively approved by NASA Headquarters.

The RTSW secondary payload consisted of a data processing unit (DPU), that would accept input from the three instruments mentioned earlier, and an X-band transmitter with parabolic antennae. The instrument data would be processed in the DPU using algorithms developed by the instrument developers and NOAA. The processed data would then be broadcast continuously over the X-band radio frequency link and would be captured by NOAA-provided ground stations located around the world. The cost of the RTSW package, its accommodation on the ACE spacecraft, and the necessary algorithm development at coinvestigator sites was estimated to be about $6.4 million.

In February 1994, NOAA concluded that, because of funding constraints, it would not be able to continue with the RTSW experiment as planned. NOAA indicated that it "...still has a strong need for real-time solar wind data from ACE..." and requested that NASA try to find some other way of providing some or all of these data. The Explorers Project at GSFC was asked to identify and provide cost figures for alternate methods of providing RTSW data. The results of that study and current RTSW implementation are described here.

Any acceptable, alternate design approach had to meet three important constraints. It had to be (1) affordable to NOAA (i.e., it had to be simple, yet capable of allowing the data to be retrieved by ground stations having 9- to 10-meter-diameter antennae); (2) simple enough so that it would not cause significant design impact to the spacecraft, and specifically the Command and Data Handling (C&DH) component; and (3) compatible with ACE link budgets for transmitted data bit rate. The simplest approach was to use what we already had, so we decided to explore the possibility of creating an additional data format within the C&DH component. This approach was taken and has proven itself superbly suited to the task.

During normal operations, ACE will be approximately 1.5 by 10^6 km from the Earth. To transmit RTSW data to a 10-meter-diameter antenna on the ground, we were constrained to a maximum bit rate of approximately 700 bits per second (bps). However, this would have required considerable change in the ACE clock and countdown circuits. With concurrence from the scientists involved, we created a new, commandable data mode at an ACE standard bit rate of 434 bps. This mode's format contains data from the three instruments mentioned earlier. This format was successfully designed into the C&DH component and is just like all the other low-data-rate formats. It is designed to be compatible with Consultative Committee on Space Data Standards (CCSDS) requirements and contains all of the overhead required for it to be processed by the NOAA ground stations or the ACE Mission Operations Center (MOC).

To provide continuous RTSW data, the ACE S-band transmitter, which was to be turned on only for regularly scheduled Deep Space Network (DSN) contact, will be left on at all times. As it turns out, this is beneficial to ACE, in that it enables us to maintain a stable thermal environment on the spacecraft lower deck without having to resort to heaters that would otherwise have been required. NOAA ground stations will have access to the RTSW data for 21 hours per day; the remaining 3 hours are reserved for ACE contacts with DSN ground stations. However, since the data in the RTSW format is also in the

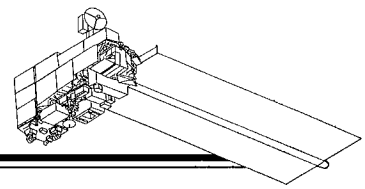

normal operational format, it is possible to provide raw ACE data to NOAA, in real time, to extract and process the needed data. The cost to implement and operate the change described herein is approximately $470K, a considerable reduction from the cost estimate given earlier. NOAA has agreed to provide funding for this change and has already transferred part of the required funding. Algorithms needed to process the data at NOAA facilities will be developed by NOAA and the instrument manufacturers.

Contact: John Thurber (Code 410)
301-286-8360

Donald Margolies (Code 410)
301-286-8984

Sponsor: Office of Space Science

Mr. John Thurber is the Observatory Manager for the Advanced Composition Explorer (ACE). He earned his BS in Electrical Engineering from the University of Illinois in 1960, and has 9 years of experience at GSFC.

Mr. Donald Margolies is the Associate Project Manager for ACE in the Explorers Project. He received his BEE from Rensselaer Polytechnic Institute in 1959 and earned an MSE and MEA from the George Washington University. Mr. Margolies has been at GSFC for 31 years and is the recipient of the NASA Exceptional Service Medal and the GSFC Outstanding Service Award.

THE FIRST FLIGHTS OF THE SMALL EXPENDABLE DEPLOYER SYSTEM: LONG TETHERS IN ORBIT

IN SPACE SCIENCE, it is all too often true that the ability to do an experiment or make a measurement is determined by the available transportation. The classical launch limitations of mass, volume, and electrical power are treated in any good design. The limitations imposed by other factors, such as orbital mechanics and atmospheric drag are, perhaps, less-well-appreciated. For example, in measuring the characteristics of the atmosphere/magnetosphere boundary or the change in plasma properties over distances of a few tens of kilometers over the entire planet, there are formidable technical challenges inherent in conventional transportation technology. Timing of common-radius observations, different orbits, and the need for engine fuel to make up for atmospheric drag are just two of the problems that must be dealt with. Design studies have suggested that spacecraft connected by long (2 km or more) tethers would at least lessen the severity of some of these difficulties. However, only within the past 3 years has the state-of-the-art been sufficient for flight demonstrations of the utility of long tethers. One example of a proof-of-concept experiment flight is described here.

At 03:40 Universal Time (UT) on the night of March 10,1994, a Delta 2 Expendable Launch Vehicle (ELV) lifted off from pad 17-B at the Cape Canaveral Air Force Station. The main purpose of this mission was to orbit the final satellite of the Global Positioning System (GPS). Some 62 minutes later the GPS satellite was successfully placed into orbit via its third stage motor, and the second stage of the Delta began its secondary mission. After GPS operations, the second stage was in a 375-km circular parking orbit with its nose in the direction of travel. Now the autopilot commanded maneuvers which put the stage in a slightly nose down attitude, with a group of small modules on the guidance ring pointed Earthward.

At 66 minutes, the autopilot activated the secondary payload. First, the computer within the uppermost pair of modules (the SEDS, consisting of the tether canister and electronics box; see the figure) was powered up and began to transmit data through the Delta telemetry system. Exactly 60.02 seconds later, explosive bolts attached to the clamp holding the lowermost module (subsatellite) to the Delta second stage fired. Four springs inside the clamp extended, forcing the subsatellite away from the Delta at

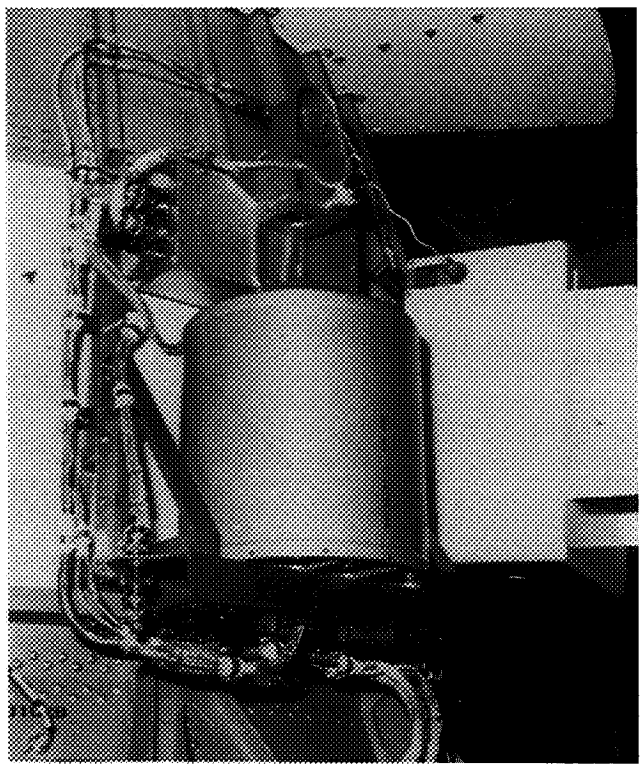

The Small Expendable Deployer System on Delta II.

a velocity of 1.5 meters per second. At ejection, the subsatellite data system powered up and began sending data on its dynamics behavior as it moved away from the Delta, while pulling the tether out from the tether canister. The second full mission of the Small Expendable Deployer System (SEDS-2) had begun.

By the time data acquisition ended 10 hours and 53 minutes later, the Deployer (which remained with the Delta second stage) had delivered the subsatellite, with tether attached, to a position 20 km directly beneath the Delta with no residual deploy rate (much less than 1 cm per second at the end of tether), and with librations less than 1°. The final dynamic state of the subsatellite was measured as a normal pendulum with a period of 52 minutes and amplitude of 1.5°, and a pure torsional pendulum (rotation), with a period of 1.5 days and a peak rotation rate of 4 rpm. Such dynamics are easy to control by simple pointing systems. Over the next months, the experiment team received reports from numerous visual observers that

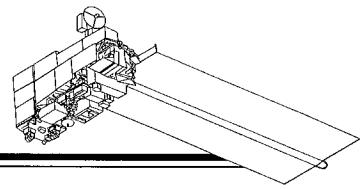

the 0.7 millimeter diameter tether was clearly visible to the ground observers without any optical aid. The braided tether, composed of eight Spectra 1000 polyethylene fibers, is a very effective scatterer of sunlight, especially when the angle between the Sun, object, and observer is near 90°.

SEDS-2 was the third unmanned tether experiment using SEDS technology. The first experiment, SEDS-1, flew on March 30, 1993 and was the first successful deployment of a long tether in orbit. In addition, this mission demonstrated the ability to precisely control the location of atmospheric entry of a payload by timing the cutting of the 20 km of tether attaching the subsatellite to the deploying body. The second mission, the Plasma Motor-Generator experiment, flew on June 26, 1993. This mission used the SEDS control computer, electronics module, and deployer sensor system with a 500-meter conducting tether to validate a new means of electrical contact with the magnetoplasma, and to show the exchange of energy between the magnetoplasma and currents flowing in the tether.

Unlike the Tethered Satellite System (TSS), which flies on the shuttle, the SEDS is a deploy-only transportation system; it provides no payload services beyond deployment under closed-loop control. The TSS could be thought of as the tether equivalent of a multiexperiment spacecraft which provides considerable support services to the on-board instruments. By contrast, SEDS is a small, quick-reaction, single-experiment system that can ride on a vehicle of opportunity.

The fourth SEDS mission (planned for November 1996) will demonstrate the SEDS system as a payload of opportunity on the shuttle, and will move a Microsat (a small, but fully functional satellite) from the shuttle orbit to an orbit with a 5- to 6-year predicted lifetime, using only momentum exchange mediated by a 20-km tether.

The experiment teams include members from of Marshall, Langley, Goddard, Johnson, and Lewis Space Centers. The project is managed by James Harrison of Marshall (overall Project and Deployer), and Kenneth Crumbly, of Langley (subsatellite).

Contact: William Webster, Jr. (Code 920.2)
301-286-4506

Sponsor: Office of Space Systems Development
(Advanced Programs)

Dr. William Webster, Jr. is the data manager and a member of the Investigator's Working Group for the Small Expendable Deployer System flight demonstration program. Dr. Webster earned a PhD in Astronomy from Case-Western Reserve University in 1970. He has been at GSFC for 23 years and is affiliated with the Computing Systems Office of the Laboratory for Terrestrial Physics.

EXPERT SYSTEM FOR DIAGNOSING SPACECRAFT ANOMALIES

OPERATIONAL EXPERT SYSTEMS capable of real-time monitoring and fault isolation of spacecraft problems have been in existence for some time. These software tools perform fault isolation functions on the hardware, which help the satellite operators to take appropriate action to safeguard the spacecraft until a solution can be found. Spacecraft Environmental Anomaly Expert System (SEAES) is an advanced rule-based software tool that will complement the operational expert systems now in existence by adding a capability for diagnosing those anomalies that are induced by the interactions of the spacecraft with the space environment, including such phenomena as high-energy proton events and geomagnetic storms (see the figure).

The knowledge base incorporated in the new system is based on facts rather than just algorithms. Before the advent of this enhancement, controllers would have to determine the cause of the anomaly by contacting experts from diverse locations by phone or fax, losing time to arrive at a decision. A system based on the concept described here could allow controllers to make important operational decisions quickly and eventually reduce the number of personnel required to operate large programs and missions.

Expert systems developed with SEAES will:

- Use lessons learned—the facts and rules are based on the experience of specialists familiar with environmental interaction with spacecraft and the anomalies caused by these interactions.
- Use heuristics as well as algorithms—"thinking" like a human expert, the system works by approximate reasoning and inference and is able to attack problems which are not rigidly defined.
- Use real-time information—unpredictable events such as magnetic storms and solar proton events can cause serious environmental interactions with spacecraft. If advance notice is given on the emergence of these

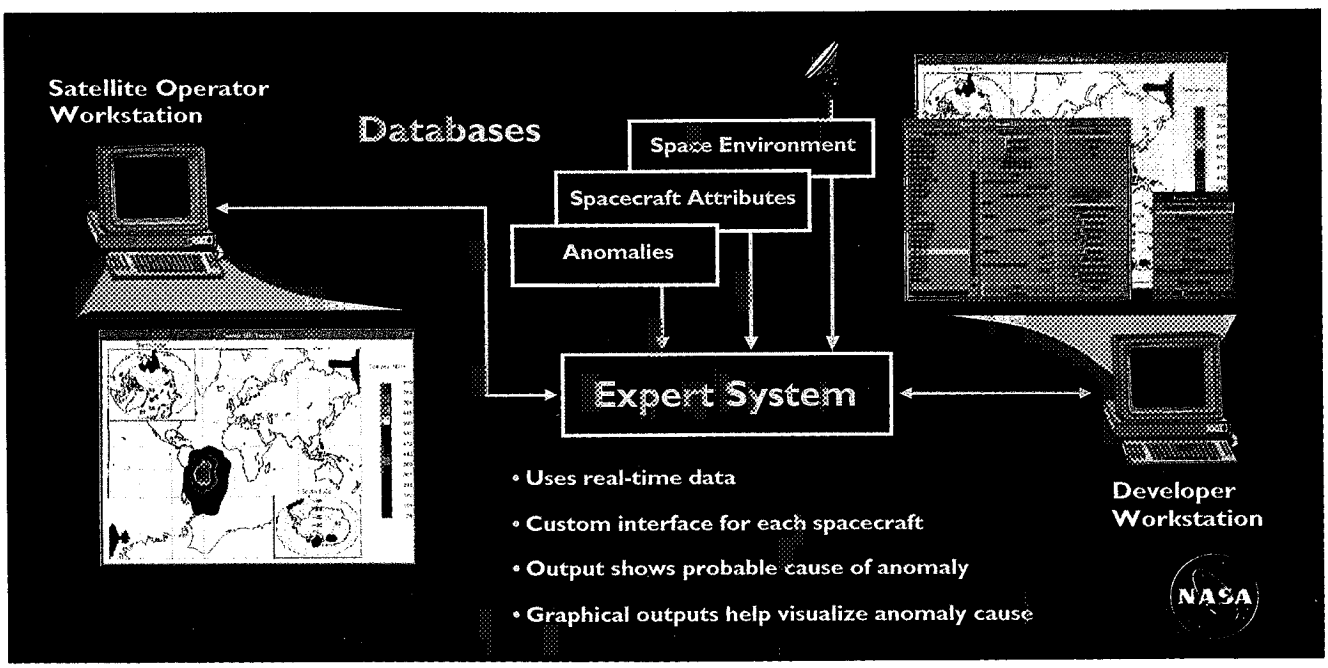

SEAES system showing the EnviroNET workstation, used to develop the graphical user interfaces and define expert system rules, and the operator's workstation, showing an output of scientific data. Single event upsets from protons which occurred in the RAM SSR of the Solar Magnetospheric Explorer (SAMPEX) mission as it orbited over the South Atlantic Anomaly.

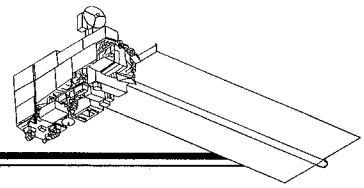

events, operators can be prepared to protect the spacecraft. NOAA's Space Environmental Laboratory Data Acquisition and Display System (SELDADS) can communicate alerts and forecasts, and can drive the real-time databases of the SEAES. The incorporation of real-time or quasi-real-time data will facilitate resolution of causes of anomalies.

- Provide highly graphical output—the SEAES system is X-Window-based, with an interface for graphical displays. Graphical outputs are provided for the user using Interactive Data Language (IDL). Histograms can reveal patterns of local time and seasonal occurrences of anomalies so that operators are prepared for these events before they occur.

- Provide transparent access to models and archives—expert system users can also seamlessly connect to EnviroNET's space environment information set of on-line models, tools, and text archives for analyzing the space environment. Hypertext links make the navigation of SEAES windows user-friendly.

- Provide customized interfaces—each spacecraft can have its own individualized system, set of input screens and users' guide, simplifying the system for operators.

SEAES relies on a fact base, a set of rules, and an inference engine. The fact base is quite extensive and consists of databases in three fields. The first is NOAA's Satellite Anomaly database from the National Geophysical Data Center, which contains information on approximately 300 historical anomalies. The second database provides space environment information, including the occurrences of X-class solar X-ray flares and the severity of magnetic storms within the Earth's magnetosphere, using the Kp planetary magnetic index. The third database gives launch and orbital information for a set of 35 satellites. Options include near-real-time linkups with NOAA's Space Environments Services Center and EnviroNET's interactive space modeling facilities.

The knowledge base consists of over 200 rules that consist of "if...then" statements that have been verified by historical case studies. For example, a typical rule states that "If the anomalies recur at the same local time repeatedly, then the cause of the anomalies is definitely (100 percent probable) not total radiation dose." The expert system is presently able to diagnose anomalies from four causes: bulk charging, surface charging, single-event upsets, and total radiation dose. The inference engine is constructed in a manner that other causes could be diagnosed with the addition of new rules.

The expert system's inference engine links the knowledge base and the rules, prompting the user for only the information needed to make the diagnosis. SEAES focuses on the high-probability causes of the anomaly. The user assigns high confidence levels to inputs that are well known and low confidence levels to inputs that are guesses. The system uses these levels of confidence as part of its probabilistic analysis. The output of a typical anomaly diagnosis inquiry is a statement such as: "The cause of the anomaly is bulk charging (75 percent probability) and not total radiation dose (80 percent probability)."

In operation, the EnviroNET workstation, based on UNIX architecture, is used as the expert system developer. It is used to develop the graphical user interface using the X-Window system, and to define the rules taken from knowledge engineers. The operator's workstation has a user interface designed for the specific satellite orbit, such as geosynchronous, low-Earth orbit, polar, or elliptical.

Additional databases and rules can be added to the system. Orbital debris, recognized as a threat, is being incorporated into the system. As more real-time and near-real-time data are made available to the expert system, anomalies will be diagnosed before or while they occur, not after-the-fact.

The new SEAES system, now on-line, is available for test purposes through EnviroNET at GSFC. EnviroNET is a node on the Internet and World Wide Web.

The development of SEAES was performed as a joint effort with Harry Koons and Dave Gorney of the Aerospace Corporation, and Mark Raincik of Presearch, Inc.

Contact: Michael Lauriente (Code 400.1)
301-286-5690

Sponsor: Office of Safety and Mission Assurance

Dr. Michael Lauriente is Manager of EnviroNET, the space environment information service. He earned a BS and an MS from Michigan Technological University and a PhD in Engineering from The Johns Hopkins University in 1955. He has been at GSFC for 12 years.

SYNTHETIC APERTURE RADAR RESEARCH FOR SEARCH AND RESCUE

THE SATELLITE-BASED COSPAS-SARSAT distress alerting and locating system, developed and improved through GSFC research, is very effective when emergency beacons are operational after an aircraft crash. Unfortunately, only about 25 percent of general aviation aircraft crashes are marked with functioning beacons. Thus, visual searches are necessary in the majority of crash investigations. Many times visual searches are impeded or delayed by inclement weather, rough terrain, heavy foliage, or lack of light.

To address this problem, the Search and Rescue Mission of the METSAT Project has been conducting aircraft wreckage detection experiments with the Jet Propulsion Laboratory (JPL) Airborne Synthetic Aperture Radar (AIRSAR) since 1989. These experiments have shown that low-frequency (L- and P-band) radar can detect aircraft wreckage that is otherwise invisible beneath foliage. Flying at high altitudes, the radar penetrates inclement weather as well as foliage, and can be used at night. In wreckage-detection experiments, salvaged parts from light planes are positioned to simulate crash scenes in forested areas. These areas are overflown by a radar-equipped aircraft, which captures and records multipolarized radar returns. The recorded data are then processed to create images.

Raw radar data must be rapidly processed into imagery if a synthetic aperture radar system is to be used during a search and rescue emergency. The SAR processing, presently done by JPL, is intended to serve the needs of the science community and does not routinely produce images in L- and P-bands that meet the time availability requirements of search and rescue applications. Algorithms to perform image processing optimized specifically for search and rescue requirements were designed and coded by GSFC in 1994. This software, referred to as Synthetic Aperture Radar Data Processing Software (SARDPS), is fully compatible with the three frequency (C-, L-, and P-band) quad-polarization raw data tapes produced by the JPL AIRSAR. The SARDPS is presently used on the CRAY C98 processor at GSFC. The CRAY's speed facilitates realistic demonstrations and applications development. However, SARDPS will ultimately be capable of operation with minimal adaptation on smaller, dedicated digital signal processing hardware located near rescue operations. The SARDPS is capable of producing images of 1- by 6-m resolution of 12- by 12-km target areas in only a few minutes, while performing speckle reduction via prefiltering, phase, and amplitude correction by applying user-specified correction constants.

A study is in progress using conductive-skinned scale model aircraft to gain knowledge of the target signatures of very small aircraft. Data obtained from model aircraft under ideal test conditions might be scaled to provide an accurate representation of data from real aircraft. If this is the case, data can be easily collected under laboratory conditions that would be difficult and expensive to obtain from full-sized airplanes. Models chosen to be representative of three aircraft types commonly available included a Cessna 172 Skyhawk, a Beech A36 Bonanza, and a Beech A35 "V-Tail." Additionally, some simulated crash scenes using model pieces were also tested. All testing was performed both with and without a metallic ground plane. The resulting database will be used to support the Automatic Target Detection study described later.

Inverse synthetic aperture radar (ISAR) tests were performed on the models in a special test chamber. Using scaled radar frequencies, the models were illuminated from a range of aspect angles to produce an image of radar cross-section over 360° in azimuth and three elevation angles. The various configurations tested yielded 1,296 image files. An example of the results from the scale model study is provided in the first figure, where the transmit and receive waves are both horizontally polarized (HH polarization). The return from the aircraft is brightest when it is viewed towards its sides or its top. Any rotated combination of linear polarizations for transmit-and-receive radar pulses can be synthesized for the 36 image viewing angles, and video animation has been created showing the effect of rotating polarization on SAR image intensities from all of the viewing angles simultaneously. The figure is one frame from this video. The detectability of a target is a function of its radar backscatter characteristics relative to those of its background. JPL is conducting an analysis of the background characteristics of selected radar images containing test targets from the field experiments. This will be used in conjunction with the scale model data to estimate the detectability of the search subjects in various types of surroundings.

After raw SAR data have been processed into imagery, the results must be further processed to reveal the presence of likely targets for search teams to investigate.

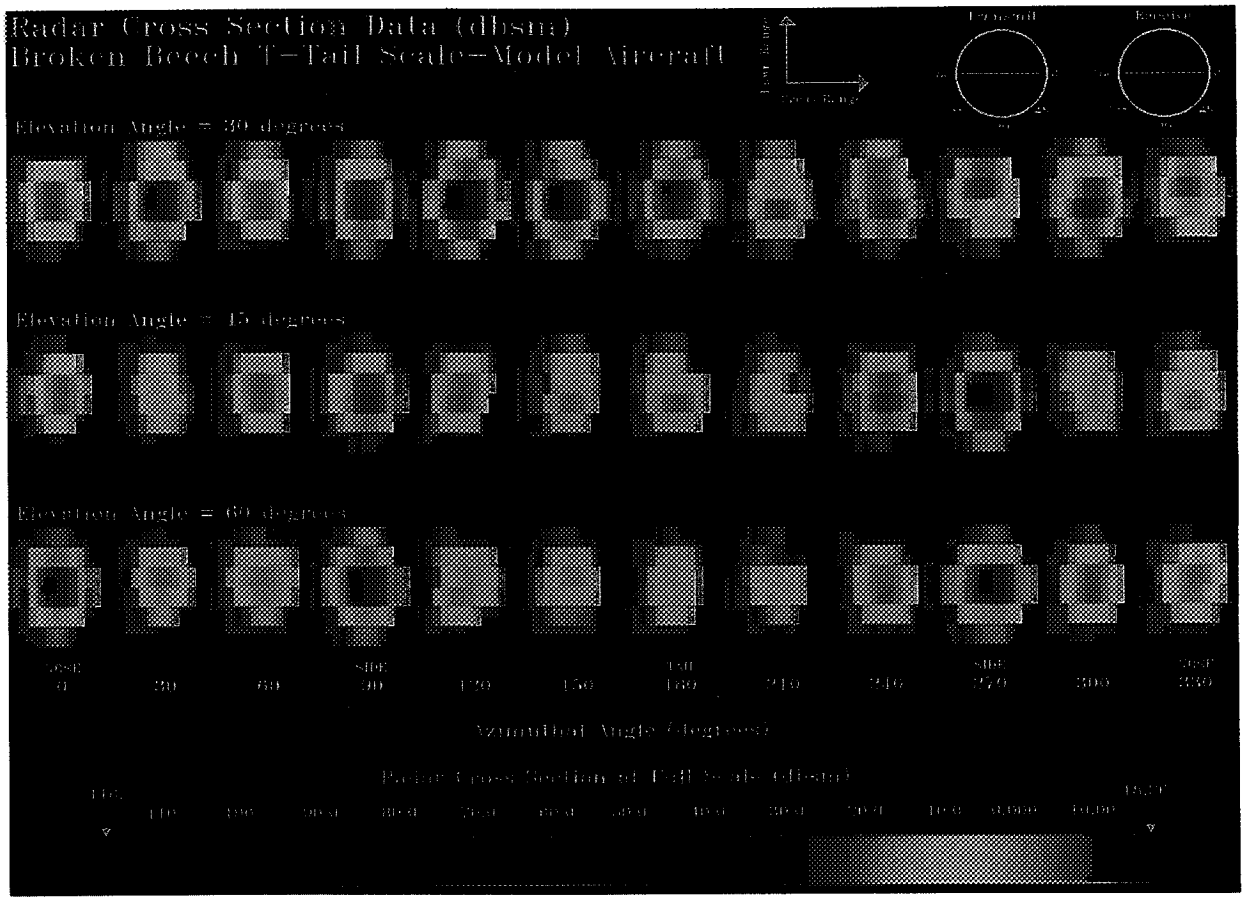

ISAR images of scale model aircraft: 36 views with HH polarization and frequency scaling to P-band.

Manual "processing" techniques are being developed using topographical maps and local knowledge of the search area, but this is arduous and time-consuming. Target detection theory originally developed for the military is being applied as part of the research initiative. A Maximum Likelihood Adaptive Neural System (MLANS) is used that estimates the parameters of a probabilistic model for the polarimetric SAR image data by using the maximum likelihood principle. MLANS is able to enhance brightness of potential target pixels that are statistical outliers relative to the pixels of the clutter background. In a process called supervised learning, where the algorithm is provided with the characteristics of known targets, MLANS is being "trained" to recognize target pixels in images of unknown scenes. During 1994 research, a subset of the ISAR scale model data was used in the MLANS supervised learning process.

During July, flight tests were conducted over the San Francisco area using the JPL AIRSAR, achieving several of our research goals. First, a series of overflights were made over mountainous central California terrain, on which there were five real crash sites. Image data from one of these crash sites is being used to support a "blind" search and rescue experiment to assess the feasibility of using manual techniques in SAR searches. High-probability targets will be determined using only area maps, SAR images, and simulated flight scenario information.

Secondly, a series of overflights were made over the Half Moon Bay area of the San Francisco peninsula. Various known targets were placed at the Half Moon Bay airport, including whole aircraft, aircraft parts, a calibration target, and a radar reflector located on a raft floating offshore. These flights accumulated image data at the same

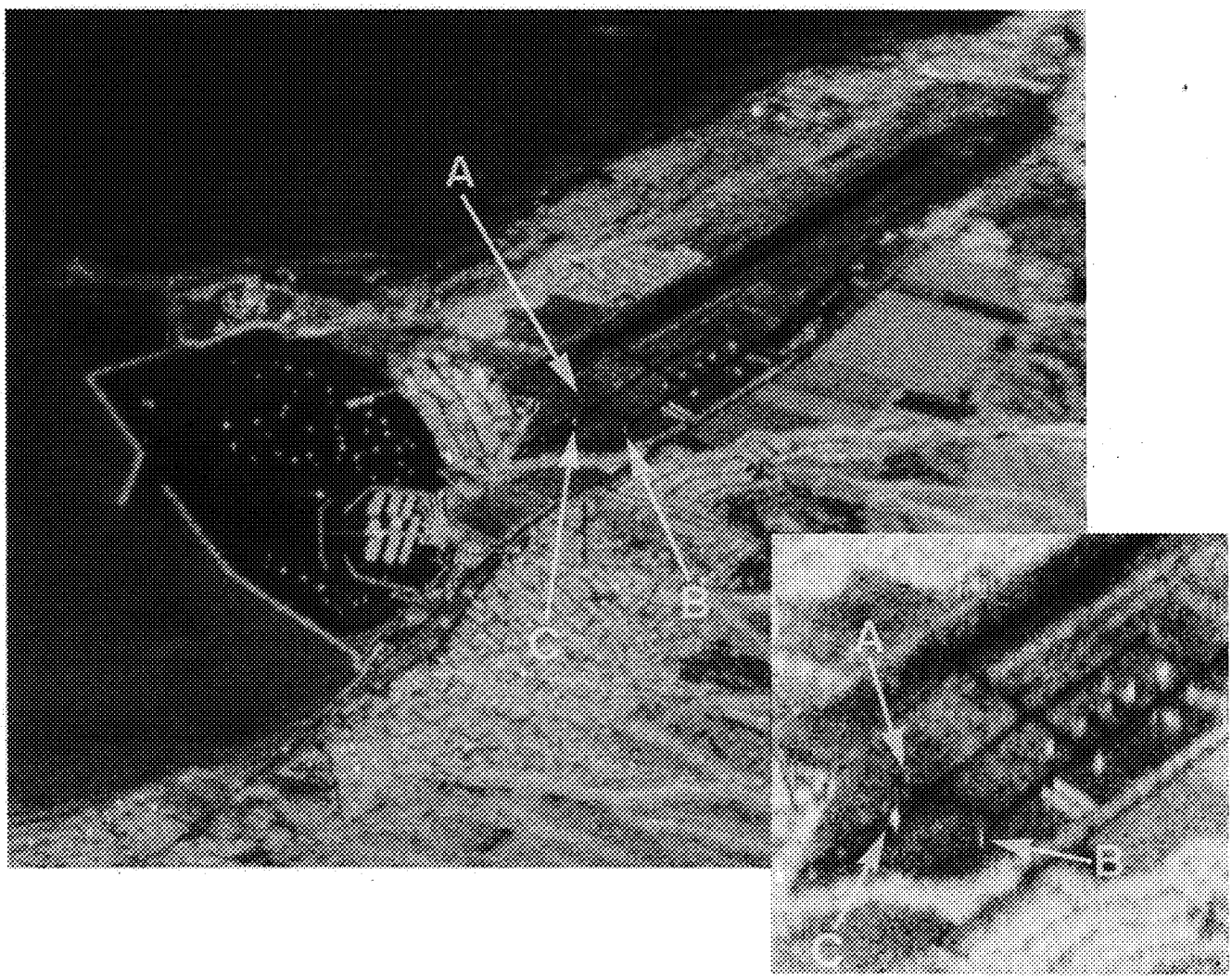

SAR image of Half Moon Bay airport at L-band with HH polarization. A: Cessna aircraft; B: Beech aircraft; C: calibration target.

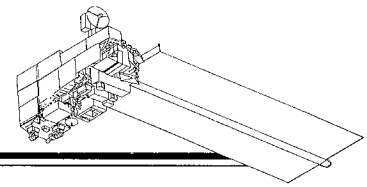

azimuthal angles as those of the scale model tests described earlier. Two of the aircraft are the same type as those used in the scale model study. Backscatter intensities of these real targets are being compared with those of the scale model study. The second figure shows the L-band, HH polarization SAR image of the Half Moon Bay airport processed at GSFC. The arrow marked "A" points to the Cessna aircraft, "B" marks the Beech aircraft, and "C" marks the calibration target.

Contact: Ronald Wallace (Code 480)
301-286-8332

Rudolph Larsen (Code 480)
301-286-5110

David Affens (Code 480)
301-286-9839

Sponsor: Office of Advanced Concepts and Technology

Mr. Ronald Wallace is SAR Mission Manager. He holds an Engineering degree from George Washington University and an MSEE from the University of Washington. Prior to his government service, he provided consulting services to NASA and DOD in the areas of communications and space systems. He has been at GSFC for 5 years.

Mr. Rudolph Larsen is SAR Systems Manager. He earned a BEE from Pratt Institute, an MS in Electrical Engineering from Johns Hopkins University, and a Masters in Engineering Administration from George Washington University. He has developed space flight components and instruments for nine GSFC flight projects. He has been with GSFC for 26 years.

Mr. David Affens is SAR Mission Support Manager. He has been with GSFC for 4 years. Prior to coming to GSFC, he worked for 21 years at the Johns Hopkins University Applied Physics Laboratory and Naval Ordnance Laboratory as a systems engineer on the TRIDENT missile program and design engineer on various submarine programs. He holds a BSEE from the University of Maryland.

ACRONYMS

ACE	Advanced Composition Explorer
ADC	Analog-to-Digital Converter
AGSS	Attitude Ground Support System
AI	Artificial Intelligence
AIT	Advanced Interconnect Technologies
AMR	Adaptive Mesh Refinement
AOS	Advanced Orbiting Systems
AOTF	Acousto-optic Tunable Filter
ASIC	Application-Specific Integrated Circuit
ASIST	Advanced System for Integration and Spacecraft Test
B-V	blue minus visual
BATSE	Burst and Transient Source Experiment
BBXRT	Broad Band X-ray Telescope
BDR	Batch Data Reduction
BPR	Business Process Redesign
bps	bits per second
BVCS	Breadboard Vapor Compressor System
C&C	command and control
C&DH	Command and Data Handling
CADC	Canadian Astronomy Data Center
CART	Cloud and Radiation Testbed
CCD	charge-coupled device
CCSDS	Consultative Committee on Space Data Systems
CD-ROM	Compact Disk-Read Only Memory
CDAW	Coordinated Data Analysis Workshop
CDF	Common Data Format
CDHF	Central Data Handling Facility
CGRO	Compton Gamma-Ray Observatory
cm	centimeter
CNES	Centre National d'Etudes Spatiales
COARE	Coupled Ocean-Atmosphere Response Experiment
COBE	Cosmic Background Explorer
COP	Coefficient of Performance
COPS	Calibrated Ancillary Data Output Processing System
COSMIC	Computer Software Management and Information Center
COSSC	Compton Observatory Science Support Center
COTS	commercial off-the-shelf
CRT	cathode ray tube
CSC	Computer Sciences Corporation
CWIT	CDF Windowing Imaging Tool
DADS	Data Archive and Dissemination Service
DDF	Data Distribution Facility
DIM	data integrity monitor
DIR	detection, isolation, and resolution
DIRBE	Diffuse Infrared Background Experiment
DMR	Differential Microwave Radiometer
DOF	degree of freedom
DPM	Despun Platform Mechanism
DPU	Data Processing Unit

ACRONYMS

DRIP	Deployable Recovery Instrumentation Package
DRS	Data Recording Subsystem
DRSL	DSTD Reusable Software Library
DSN	Deep Space Network
DSP	Digital Signal Processors
DST	Data Server Task
DSTD	Data System Technology Division
DX	Data Explorer
ECF	European Coordinating Facility
EGRET	Energetic Gamma Ray Experiment Telescope
ELV	Expendable Launch Vehicle
ElvisC	Experiment in Libraries via Incremental Schemata and Cobweb
ENSO	El Niño/Southern Oscillation
EDM	Engineering Development Model
EOS	Earth Observing System
EP	Explorer Platform
EPAM	Energetic Electron, Proton, Alpha-Particle
ERBE	Earth Radiation Budget Experiment
ESA	European Space Agency
EUVE	Extreme Ultraviolet Explorer
EVA	Extravehicular Activity
FAST	Flow Analysis Software Toolkit
FASE	Fast Auroral Snapshot Explorer
FASTRAD	FAST Real-Time Attitude Determination
FDD	Flight Dynamics Division
FDF	Flight Dynamics Facility
FE	finite element
FEA	finite element analysis
FEP	front-end processor
FFT	Fast Fourier Transform
FHST	Fixed-Head Star Tracker
FIP	First Ionization Potential
FIRAS	Far Infrared Absolute Spectrophotometer
FOC	Faint Object Camera
FOS	Faint Object Spectrograph
FOT	Flight Operation Team
FOV	field of view
FSS	Fine Sun Sensor
FUSE	Far Ultraviolet Spectroscopic Explorer
GAP	Groove Analysis Program
GAS	Get Away Special
GCM	Global Climate Model General Circulation Model
GenSAA	Generic Spacecraft Analyst Assistant
GEOTAIL	Geomagnetic Tail Laboratory
GFDL	Geophysical Fluid Dynamics Laboratory
GGS	Global Geospace Science
GHRS	Goddard High Resolution Spectrograph
GISS	Goddard Institute for Space Studies

ACRONYMS

GPS	Global Positioning System
GRIS	Gamma Ray Imaging Spectrometer
GRO	Gamma-Ray Observatory
GSA	General Services Administration
GSFC	Goddard Space Flight Center
GTAS	Generic Trend Analysis System
GUI	Graphical User Interface
HDA	HST Data Archive
HDPE	High density polyethylene
HIRS2	High-resolution Infrared Radiation Sounder 2
HLI	Host Language Interface
HPCC	High Performance Computing and Communications
HSP	High Speed Photometer
HST	Hubble Space Telescope
HUD	heads-up display
IACG	Inter-Agency Consultative Group for Space Science
IBM	International Business Machines
ICC	intelligent command and control
ICCR	Internal Configuration Changes Request
ICE	International Cometary Explorer
IDL	Interactive Data Language
IDL	Interactive Data Language
IEU	Russian Space Research Institute
IGSE	Instrument Ground Support Equipment
IKI	Russian Space Research Institute
IMF	Interplanetary Magnetic Field
IMP	Interplanetary Monitoring Platform
INS	Inertial Navigation System
IOP	Intensive Operation Period
IPD	Information Processing Division
IPD	Information Processing Division
IR	infrared
IRHS	Infrared Heterodyne Spectrometer
IRIS	Infrared Interferometer Spectrometer
IRTF	Infrared Telescope Facility
ISAR	Inverse Synthetic Aperature Radar
ISEE	International Sun-Earth Explorer
ISTP	Internationl Solar-Terrestrial Physics
ITF	Intensity Transfer Function
ITO	Indium Tin Oxide
IUE	International Ultraviolet Explorer
JPL	Jet Propulsion Laboratory
kg	kilogram
km	kilometer
L&EO	Launch and Early Orbit
LAN	local area network
LCP	liquid crystal polymers
LDB	Long-Duration Balloon
lidar	light detection and ranging

ACRONYMS

LLDPE	linear low density polyethylene
LOD	length of day
LON	local operating network
LSD	Logistics Support Depot
LTU	Life Test Unit
LZ	level zero

m	meter
MAG	magnetometer
MARA	Multimode Airborne Radar Altimeter
MCM	multi-chip module
MHD	magnetohydrodynamic
MLANS	Maximum Likelihood Adaptive Neutral System
MOC	Mission Operations Center
MOD	Mission Ooperations Division
MORTI	Modified ORSA Recovery Test Instrument
MSS	mean square slope
MSU	Microwave Sounding Unit

NASA	National Aeronautics and Space Administration
NCAR	National Center for Atmospheric Research
NCC	Network Communication Center
NCDS	NASA Climate Data Systems
NCFR	Narrow Cold Front Rainband
NDADS	NSSDC Data Archive and Dissemination Service
NDE	nondestructive evaluation
NEWSIPS	New Spectral Imaging Processing System
NFS	Network File Server
NGDC	National Geophysics Data Center
NII	National Information Initiative
NOAA	National Oceanic and Atmospheric Administration
NRL	Naval Research Laboratory
NSSDC	National Space Science Data Center
NTIS	National Technical Information Service

OBC	on-board computer
OFM	Operator Function Model
OLR	Outgoing Longware Radiation
OLS	Orbital Launch Services
ORSA	Ogive Recovery System Assembly
ORSA	Ogive Recovery System Assembly
ORU	Orbital Replacement Unit
OSC	Orbital Sciences Corporation
OSHA	Occupational Safety and Health Administration
OSI	Open System Interconnect
OVV	Optically Violently Variable

PCB	printed circuit board
PE	Polyethylene
PET	Polyethylene terphthalate
POCC	Payload Operations Control Center

ACRONYMS

PSD Power Spectral Density

PVO Pioneer Venus Orbiter

QPO quasi-periodic oscillations

QQ quasi-quadrennial

QT quasi-biennial

RAM random access memory

Re Earth Radius

ReLI Reusable Library INterface

REM Roentgen Equivalent in Man

RISC Reduced Instruction Set Code

RM Reasoning Machine

RMS Remote Manipulator System

RMS Root Mean Square

roAp rapidly oscillating peculiar-A-type spectrum

RPO revolutions per orbit

RRC Robotics Research Corporation

RSED relaxed-strain-energy density

RSI Research Systems Inc.

RTSW Real Time Solar Wind

S/N signal-to-noise

S-L9 Shoemaker-Levy 9

SAMPEX Solar, Anomalous, and Magnetic Particle Explorer

SARDPS Synthetic Aperature Raddar Data Processing Software

SAT Servicing Aid Tool

SBIR Small Business Innovative Research

SCOB sealed chip on board

SDAC Solar Data Analysis Center

SEAES Spacecraft Environmental Anomaly Expert System

SEAWARS Sea Water Activated Release Switch

SEDS Small Expendable Deployer System

SEL Software Engineering Laboratory

SELDADS Space Environmental Laboratory Data Acquisition & Display System

SEM Scanning Electron Microscope

SEPS Source/Loss Cone Energetic Particle Spectrometer

SGSE Spacecraft Ground Support Equipment

SIR-C Shuttle Imaging Radar-C

SIRM Saturation Remanence Magnetization

SMEX Small Explorer

SMM Solar Maximum Mission

SMMR Scanning Multichannel Microwave Radiometer

SOC Science Operations Center

SOHO Solar and Heliospheric Observatory

SOR Starfire Optical Range

SPOF Science Planning and Operations Facility

SPS Standard Positioning Service

SQL Standard Query Language

ACRONYMS

SRA	Scanning Radar Altimeter
SRL	Scanning Raman Lidar
SRTADS	SAMPEX Real-time Attitude Determination System
SSM/I	Special Sensor Microwave/Imager
SST	Sea Surface Topography
	Surface Skin Temperature
	Sea Surface Temperature
SSU	Stratospheric Sounding Unit
STEP	Solar-Terrestrial Energy Program
STOL	Standard Test and Operations Language
STOL	Spacecraft Test and Operations Language
STScI	Space Telescope Science Institute
SVS	Scientific Visualization Studio
SWAS	Submillimeter Wave Astronomy Satellite
SWE	Solar Wind Experiment
SWEPAM	Solar Wind Electron, Proton, Alpha-Particle Monitor

TANS	Trimble Advanced Navigation Sensor
TASS	TPOCC Advanced Spacecraft Simulator
TDM	time division multiplexed
TDRSS	Tracking and Data Relay Satellite System
TF	tension field
TGRS	Transient Gamma Ray Spectrometer
TIROS	Television and Infrared Observation Satellite
TM	Thematic Mapper
TOF	time of flight
TOGA	Tropical Ocean-Global Atmosphere
TOMS	Total Ozone Mapping Spectrometer
TOVS	TIROS Operational Vertical Sounder
TPA	Thermal Performance Apparatus
TPOCC	Transportable Payload Operations Control Center
TRMM	Tropical Rainfall Measuring Mission
TSS	Tethered Satellite System
TWT	Traveling Wavetube
TZM	Titanium/Ziroonium/Molglodenum

UARS	Upper Atmosphere Research Satellite
UIT	Ultraviolet Imaging Telescope
UKMO	United Kingdom Meteorological Office
ULF	ultra-low-frequency
USDA	United States Department of Agriculture
USE/USD	Universal Source Encoder/Universal Source Decoder
USES	Universal Source Encoder for Space
USRA	Universities Space Research Association
UT	Universal Time
UV	ultraviolet

VLBI	Very Long Baseline Interferometry
VLSI	Very Large-Scale Integration

ACRONYMS

WAN	wide area network
WFPC2	Wide-Field and Planetary Camera 2
WWW	World Wide Web
X-SAR	X-Synthetic Aperture Radar
XTE	X-ray Timing Explorer
ZP	Zero pressure

AUTHOR INDEX

AUTHOR INDEX

AUTHOR INDEX

AUTHOR INDEX

ON THE COVER:
The cover represents the current technology and methodology for reducing "raw" space data to the final product. The illustration is of TOMS data for total ozone concentration over the atmosphere of the Earth. First it is shown (1) as numbers and finally (4) depicted in the appropriate location with intensity representing ozone concentration. The dark area turned to gray represents missing data.
The back cover shows various formats of the data used for different global models.

Executive Editor:

Gerald Soffen

Editors:

Milton Halem
James Green
Kenneth Frost
Stephen Maran
Charles Boyle
Walter Truszkowski
Walter Sullivan
Howard Ottenstein

With Special Thanks To:

Sue Hart
Carol Ladd
Betty Graham
Christine Baxley

Technical and Scientific Editing, Artwork, and Production:

Brenda Vallette, Carol Smouse, Mitchell Hobish, Bob Gray, and Philip Ardanuy

Nimbus–7 TOMS Ozone

02/13/93

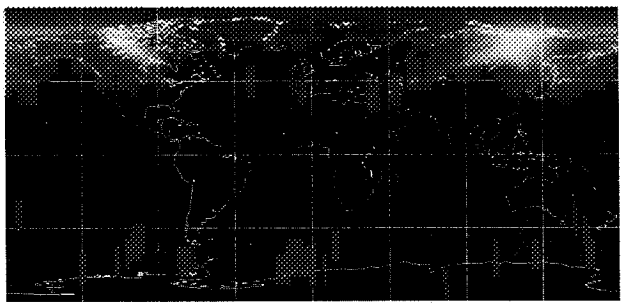

Cartesian projection

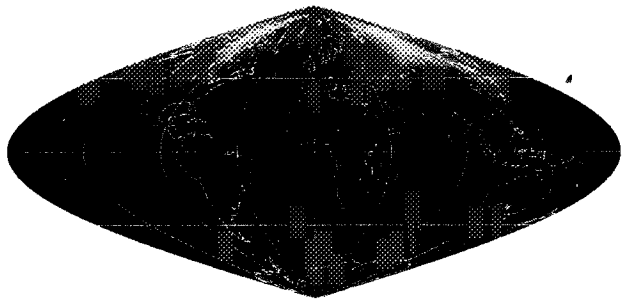

Sanson–Flamsteed projection

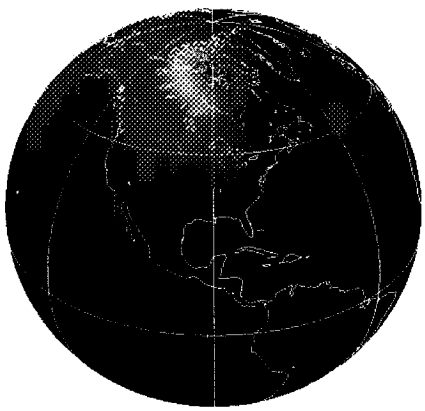

Globe projection

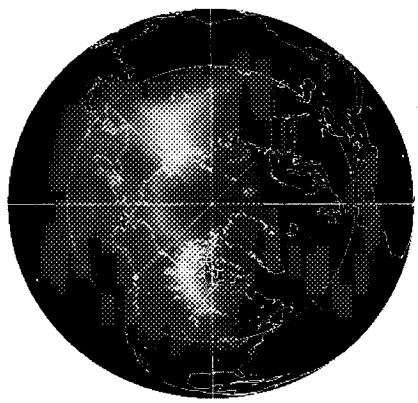

Orthographic Azimuthal projection

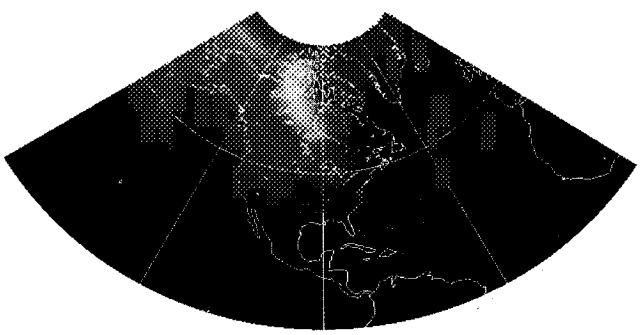

Lambert Conformal Conic projection

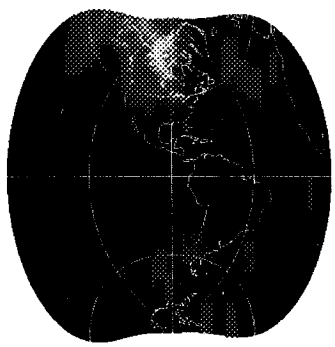

Cassini–Soldner Cylindrical Equidistant projection

Total Ozone

Dobson Units